Lib.
Copy 2
JUN 10 1933

THE PHYSICAL REVIEW

VOLUME 43 *Second Series* NUMBER 11

JUNE 1, 1933

Published for the

AMERICAN PHYSICAL SOCIETY

by the

AMERICAN INSTITUTE OF PHYSICS
Incorporated

LANCASTER, PA., AND NEW YORK, N. Y.

THE AMERICAN PHYSICAL SOCIETY

OFFICERS OF THE SOCIETY

PAUL D. FOOTE, *President*
The Gulf Companies
Pittsburgh, Pennsylvania

ARTHUR H. COMPTON, *Vice-President*
University of Chicago
Chicago, Illinois

W. L. SEVERINGHAUS, *Secretary*
Columbia University
New York, New York

G. B. PEGRAM, *Treasurer*
Columbia University
New York, New York

JOHN T. TATE, *Editor*
University of Minnesota
Minneapolis, Minnesota

L. B. LOEB, *Local Secretary for the Pacific Coast*
University of California
Berkeley, California

THE PHYSICAL REVIEW

BOARD OF EDITORS

JOHN T. TATE, *Editor*

J. W. BUCHTA, *Assistant Editor*

Associate Editors

A. J. DEMPSTER
DAVID M. DENNISON
J. C. SLATER
R. C. GIBBS
E. O. LAWRENCE
J. H. VAN VLECK
K. K. DARROW
J. C. HUBBARD
A. E. RUARK

THE PHYSICAL REVIEW, which was established in 1893, is a journal of experimental and theoretical physics. It is published for the American Physical Society by the American Institute of Physics Incorporated. There are two volumes annually with twelve issues in each volume.

Manuscripts for publication should be submitted to John T. Tate, University of Minnesota, Minneapolis, Minnesota.

Proof and all correspondence concerning papers in the process of publication, should be addressed to the Editorial Secretary, American Institute of Physics, 11 East 38th Street, New York, New York.

Subscription price $15.00 per year. Single copies $1.50 each for issues prior to July 1, 1929 (Vols. 1–33); $.75 each for issues subsequent thereto. Subscriptions and orders for back numbers should be addressed to Prince and Lemon Streets, Lancaster, Pennsylvania, or to the American Institute of Physics, 11 East 38th Street, New York, New York.

Advertising is not accepted for the *Physical Review* but attention is called to the *Review of Scientific Instruments* with *Physics News and Views*, a companion publication of the Institute, and a medium through which the field of physics can be reached most effectively. Rates and other information will be furnished on request to the Editorial Secretary.

Changes of address and complaints of failure to receive the *Physical Review*, in the case of members of the American Physical Society, should be addressed to the Treasurer; in the case of other subscribers, to the Editorial Secretary. New copies can be sent free in response to complaints of non-delivery only if notice of non-delivery is received within three months of date of issue.

The Physical Review is published semi-monthly at Prince and Lemon Streets, Lancaster, Pennsylvania.

Entered at the Post Office at Lancaster, Pennsylvania, as second class matter.

Acceptance for mailing at special rate of postage provided for in section 1103, Act of October 3, 1917, authorized September 6, 1926.

THE
PHYSICAL REVIEW
A Journal of Experimental and Theoretical Physics
VOL. 43, NO. 11 JUNE 1, 1933 SECOND SERIES

Probabilities of *K*-Electron Ionization of Silver by Cathode Rays

D. L. WEBSTER, W. W. HANSEN* AND F. B. DUVENECK, *Stanford University*
(Received April 3, 1933)

K-electron ionization by impact is treated here both experimentally and theoretically. The experimental work is on Ag in extremely thin films bombarded by cathode rays from constant potentials up to seven times the minimum ionizing potential. Ratios of probabilities of *K* ionization at different voltages are found as ratios of *K* line intensities after the latter have been corrected for minor perturbing factors. One of these is the slight retardation of the cathode rays within the film. Another is the effect of cathode-ray diffusion, in increasing the numbers of atoms penetrated. These effects occur in all films. In some of our films, which were backed with Be, there were two more corrections, both for *K* ionization of the Ag by the Be: one through rediffusion of cathode rays into the Ag, the other through continuous-spectrum x-rays. Altogether, films without backing appear more reliable at high voltages, and films with it at low voltages, though when corrected as described, the results agree well at all voltages in the range covered. An approximate empirical formula is probability = constant $\times U^{-m} \log U$, where U is the ratio of tube voltage to minimum ionizing potential, and m is about 0.78. Among the theoretical formulas in the literature, those based on wave mechanics all depend on Born's approximation, which is invalid unless U is large, so they do not apply well to these data The classical quantum theory, considered as a possible temporary approximation, requires some further development, which is given here. The formula thus obtained seems to express the principles of classical quantum theory without seriously inaccurate approximations, but it agrees with the data only in the general type of the function: the ionization probability increases from zero at $U=1$ with a finite slope, attains a maximum value, and then declines. Quantitatively, the theory is far from the facts. A strictly heuristic modification of classical theory, changing the law of repulsion between the cathode ray and the *K* electron to an inverse cube, leads to a formula

$$\text{probability} = \frac{\text{constant}}{U\{(\pi/2\cos^{-1}U^{-\frac{1}{2}})^2-1\}}.$$

This agrees fairly well with experiment, even though it contains no constant to change the shape of the graph, like the m in the other equation. But there is other evidence, as well as theoretical reason, for believing that the fundamental defect in the classical quantum theory lies not so much in any error in the inverse square law as in its dependence on contradictions of the uncertainty principle.

I. EXPERIMENTAL

A. Methods and apparatus

Regarding the above abstract as an introduction, we shall turn at once to the details of the experimental part of the research. Since the probability of ionization is to be studied as a function of the kinetic energy of a cathode ray, the first requirement is of course to have the same energy for all cathode rays in any one measurement, i.e., to use constant potentials. Up to about 100 kv these were obtained from a circuit of a type described previously by one of us[1] and shown in Fig. 1. Running on 500-cycle current, this gives a ripple of only about 4 volts

* National Research Fellow, at Massachusetts Institute of Technology, since January 1, 1933.

[1] D. L. Webster, Proc. Nat. Acad. Sci. **6**, 26 and 269 (1920); D. L. Webster and A. E. Hennings, Phys. Rev. **21**, 301 (1923).

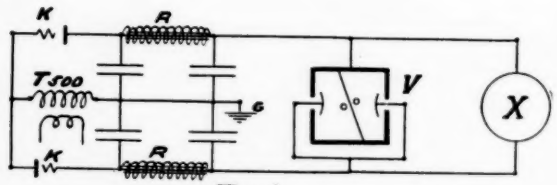

FIG 1.

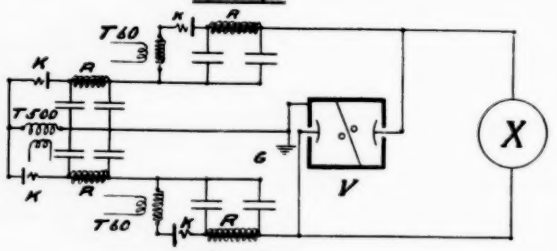

FIG 2.

FIG. 1. Circuit for use up to 100 kv. *T*500, 500 cycle transformer; *R*, reactors; *K*, kenotrons, *V*, voltmeter; *x*, x-ray tube.

FIG. 2. Circuit for use above 100 kv. *T*60, 60 cycle transformers.

at 10 m.a., as shown both by theory and by careful oscillograph measurements, for which we wish to thank Mr. H. E. Overacker, of the Department of Electrical Engineering.

Above 100 kv, we supplement this circuit with a pair of 60-cycle rectified circuits, as in Fig. 2. In adding such extra circuits, one must be very careful, on account of the oscillations of charges on the new transformers, because if these charges are drawn through the original circuit they will cause serious ripples. The preventive, of course, is very thorough electrostatic screening, not only around these transformers but between the coils of the insulation transformers feeding them, and also around the kenotrons and in their heating transformers, etc. With such screening the combined circuit is quite satisfactory, even though the flux leakage in the insulation transformers prevents the use of 500-cycle current in them and thus reduces the effectiveness of the filters. The resulting ripple at 200 kv, 1 m.a., is shown by Mr. Overacker's measurements to be about 50 volts.

Such lack of constancy as we have, therefore, is not primarily due to ripples but to slow irregular changes. These are minimized by running the 500-cycle generator and its d.c. exciter with a 3-phase motor sufficiently oversize to maintain a very constant speed at any load used. Up to 100 kv, therefore, the outfit is very steady indeed, though above 100 kv, the fluctuations of line voltage affect it through the 60-cycle transformers. Fortunately, however, the high tension voltmeter has a very short period, so that any variations of voltage due to such causes are easily detected. During every exposure of the ionization chamber to the rays, the voltage and tube current are carefully watched and controlled, the former through the field rheostat of the generator and the latter through a rheostat in the battery circuit that heats the filament. In this way up to 100 kv (that is, over the whole region of rapid change of line intensity), the variations of voltage are kept consistently less than 0.1 percent, and usually less than half that amount. For this tedious but very important part of the work, we wish to express most cordial thanks to Messrs. H. H. Baskerville, Jr., G. V. Webster, C. J. Burbank and A. W. Hackney.

The voltmeter referred to here is either of two that we have used, both designed by H. Clark. One, used for work up to 85 kv reported briefly in 1928,[2] was described in connection with earlier work on another problem.[3] The other, built for higher voltages, and used in all the later work, was described by Clark.[4] Both depend on bifilar suspensions of fine tungsten wires, and have shields around the insulators to prevent charges on them, which are unreliable, from affecting the suspended system. They are therefore very constant and reliable. They are calibrated with a series of 6 megohms of General Electric Company "copnic" voltmeter multipliers, and for the work since 1928 these have been surrounded by independently charged corona shields. Below 100 kv, the calibrations are direct; above that, the new meter is reconnected as described by Clark. These multipliers are themselves checked against standard resistances certified by the Bureau of Standards, and the current through them is measured on a Leeds and Northrup type *K* potentiometer, by using one of these standard resistances and a similarly certified standard cell.

Constant voltage gives uniformity of cathode-ray energy at the surface of the target, but for

[2] D. L. Webster, H. Clark, R. M. Yeatman and W. W. Hansen, Proc. Nat. Acad. Sci. **14**, 679 (1928).

[3] D. L. Webster and A. E. Hennings, Phys. Rev. **21**, 312 (1923).

[4] H. Clark, Rev. Sci. Inst. **1**, 615 (1930).

uniformity at all the ionizing impacts one must also make the target extremely thin. For this purpose, in all the work reported in 1928[2] and in some of the later measurements, we used films of silver deposited on beryllium by rapid distillation in high vacuum. For two beryllium targets, in the form of cylinders with holes for cooling by circulating transil oil, we wish to express our cordial appreciation of the kindness and metallurgical skill of Mr. H. S. Cooper, of the Kemet Laboratories, Cleveland, Ohio.

A point of vital importance is that the films shall be uniform enough to contain no parts so thick as to increase unduly the corrections for retardation and diffusion of the cathode rays, mentioned above in the abstract. At high voltages, this means merely that the irregularities must be not over a thousand Angstroms or so, i.e., no worse than those of a mirror good enough to reflect normally incident light without appreciable scattering. These films satisfy this condition excellently.

As the tube voltage is reduced, both corrections are increased, and a need appears for more uniformity in the films. This need arises because each correction, when considered as a percentage of the x-ray intensity, is proportional to the thickness of the film so long as the film is uniform, but for an irregular film, this thickness is replaced by (mean square of the thickness)/(mean thickness).

The most exacting requirement for uniformity, however, is in the investigation of the fine structure of the ionization probability function very near the minimum ionizing potential V_K. One of the most definite predictions of the classical quantum theory of impacts is that this function, in its increase from zero at V_K, should start with its first derivative finite. Other quantitative predictions might be changed fairly readily by changing the assumptions about the laws of force, etc., but not this one. Presumably when the wave mechanics makes any prediction about the derivative at V_K, the data on it will furnish a crucial test of that theory also.

On the experimental side, the difficulty of getting these data in reliable form arises from the correction for retardation. A finite derivative for an ideally thin target, i.e., a monomolecular film, can readily be shown to produce a zero derivative for a target of finite thickness, but the converse does not follow. In fact, if the thick target probability, at any voltage V near V_K, is proportional to $(V-V_K)^n$, that of a thin target is proportional to $(V-V_K)^{n-1}$. A finite thin-target derivative at $V=V_K$ gives n a definite value, 2, but a zero thick-target derivative says nothing so definite. And any film thicker than monomolecular becomes a thick target when V gets near enough to V_K. The problem is to make practical thin targets such that the behavior of an ideal thin target can be deduced from intensities observed with them.

To see what this requires, let $i(U)\delta x$ denote the line intensity from an ideal target of strictly infinitesimal thickness δx, with $U=V/V_K$. Then with a real target of thickness X, neglecting the other corrections, the intensity is $X\overline{i(U')}$, where eV_KU' is the kinetic energy of a cathode ray retarded from eV_KU by going a distance x in silver, and the bar denotes an average from $x=0$ to $x=X$. Neglecting second-order terms, we obtain

$$U'=U+x(dU'/dx). \tag{1}$$

Then, approximately, so long as $U'>1$ even at $x=X$,

$$X\overline{i(U')}=Xi\left(U+\tfrac{1}{2}X\frac{dU'}{dx}\right)$$
$$=Xi(U)+\tfrac{1}{2}X^2\frac{dU'}{dx}\frac{di}{dU}. \tag{2}$$

When $U'<1$ at $x=X$, of course, if di/dU is discontinuous at $U=1$, the second order terms become infinite and the whole theory must then be treated differently. Without going into detail, it is evident that the relation between the observed intensities and $Xi(U)$ is then of the type represented in Fig. 3. The test for a finite value of di/dU at $U=1$, so far as it can be made, is therefore to see whether an extrapolation like that shown in the dotted line of Fig. 3 strikes the potential axis with a finite slope; and if we had accurate data on dU'/dx we might add also a requirement that the intercept should be at the value of U noted in the figure.

If now the target is assumed to be nonuniform, the range of U over which the observed curve departs from the formula calculated above depends not on the mean thickness $\overline{X}$, but on the

maximum X_{max} as indicated in Fig. 3. To make the extrapolation of Fig. 3 possible, X_{max} must be small enough so that this range of upward curvature will be restricted to a range of U lying well within the straight portion of the corrected intensity $Xi(U)$. Consider, for example, one of our films which had $X = 280$A. The retardation in

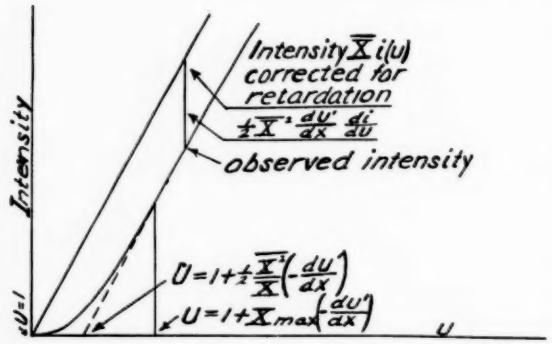

FIG. 3. Effect of retardation of cathode rays on intensities of x-rays near $U=1$.

this distance at $U=1$ is only about 0.15 kv, at least as calculated from such data on dU'/dx as we have found in the literature. Therefore with $V_K = 25.5$ kv, $XdU'/dx = 0.006$. This is so small that we can readily allow X_{max} to be several times $\overline{X}$ without seriously impairing the test.

To see whether X_{max} is within that limit, let us consider further the method of preparation of the films. The best way to secure uniform thickness was suggested to us by Joffé before our measurements of 1928, and later confirmed by the experiments of Reinders and Hamburger.[5] It is to keep the target cold with liquid air during the deposition of the film. The theory of this is that at room temperatures (at least if the real surface of the target is a nonmetallic adsorbed film) any lone silver atoms either migrate along the surface or re-evaporate; therefore permanent accumulation of silver starts only at the rare points where two lone atoms happen to come together before either of them re-evaporates. The silver that accumulates is then in the form of crystals growing around these points. At liquid air temperature, on the contrary, migration and re-evaporation are prevented, and the silver accumulates everywhere into a smooth film. Nevertheless, we were reluctant to subject our beryllium targets to such sudden changes of temperature as in using liquid air. Experimenting on copper targets first, therefore, we found that slow deposition, by sublimation from silver wires kept just below their melting point, gave matt surfaces, easily resolved by a microscope into glittering silver crystals. On the other hand, distillation from molten silver in a molybdenum trough, several hundred degrees hotter, gave perfect mirrors, especially if the trough had previously been heated in hydrogen to clean the molybdenum and silver and make good thermal contact between them. All this is exactly as expected from the above theory. We believe, therefore, that in using rapid distillation (20 to 50A thickness per second) we accomplish something of the same objective as with a cold target.

As to how uniform these films are, one line of evidence is the practically complete disappearance of the color of copper with about 50A of silver and perfectly complete with 100, which may perhaps mean complete covering of the copper surface at such thicknesses. For comparison, we have 45A, given by Reinders and Hamburger as the thickness needed for appreciable electrical conductivity in silver films on glass made by sublimation at room temperature. At 400A such films attain the very high conductivity of massive silver. This implies for 400A, not only complete connections between crystals, but also a fair approximation to the uniformity of thickness required for a minimum of resistance. Altogether it seems reasonable to assume that with fast distillation we probably had deposition practically everywhere by the time the mean thickness was 50 or 100A. From there on, as indicated by Reinders and Hamburger's theory of deposition, there should be no appreciable increase in the sizes of the irregularities. In studying the fine structure of the excitation function, therefore, we shall assume that all of these films, both those of our 1928 paper[2] and later ones, had their maximum thicknesses within a very few hundred Angstroms of their averages.

At some of our higher voltages, as noted above, we used not only silver films on beryllium, but

[5] W. Reinders and L. Hamburger, Ann. d. Physik **10**, 649 and 668 (1931); Hamburger, ibid. **10**, 789 and 905 (1931), and **11**, 40 (1931).

also other films, of silver leaf about 1800A thick, with no backing. This leaf, of course, was far from uniform, obviously porous in a strong light, and not a perfect mirror. Fortunately, however, we do not need to rely on it except at voltages so high that it can be very non-uniform without serious error.

The measurement of thickness of thin silver films can be accomplished in either of two ways. One is by the use of x-rays from a standard Coolidge tube. If these rays are sent through the film, their spectrum is given a discontinuity at the *K* limit of silver, and the thickness of the film can be found from the magnitude of this discontinuity. Practically, to make it show strongly enough with a film only a few hundred Angstroms thick, the rays must go through the films very obliquely, say at about 3°. With silver leaf, on the other hand, one may use 10 sheets or so with normal incidence. The other method of measurement is by comparison of intensities of line rays, between the thin film and a thick target, as explained in our 1928 paper. For the thickest film used then, 280A, these methods agreed as noted there, far better than one might expect. For the silver leaf used recently, 10 sheets measured by absorption gave a mean thickness of 1770A, whereas 3 measured the other way gave 1900, 1650 and 1700A according to our formulas of 1928. For the thinner films, both methods are very inaccurate, but for the thicker films the absorption method is preferable because of the uncertainties as to cathode-ray retardation involved in the other method. We are therefore basing our estimates of thickness primarily on the absorption in these thickest films, and thinner ones are estimated by ratios of their line intensities to a mean of those of the three silver leaf films.

So much for the problem of uniformity of kinetic energy of impacts. A matter of equal importance in studying any ionization probability as a function of voltage is to insure that the number of cathode rays striking the film per second shall be the same at all voltages. For our 1928 work, we approximated this condition well up to 65 or 70 kv with a tube much like a standard Coolidge tube except that the electrodes were demountable and that it was pumped during operation. (Mercury vapor was kept off the films at other times by a cock in the vacuum line at the top of the liquid air trap.) At higher voltages, however, keeping the power down to 50 watts, to retard the disintegration of the brittle beryllium targets, serious difficulties arose from field-current and positive-ion effects. To overcome these and obtain a satisfactory technique for intensity measurements at high voltages with small currents, we developed a new type of tube, described in detail in the *Review of Scientific Instruments*.[6]

To the treatment of the general problem of such measurements given there, we need add only some details on the special anodes used here. For films on beryllium, the anode was a simple cylinder, oil cooled inside, with a flat end for the target, 21 mm in diameter, perpendicular to the axis. The cathode rays struck this end normally, on a focus 6 mm in diameter, expanding to 8 mm in very much overexposed pinhole pictures, but never more; and this focus was centered to within 1 mm, so as to eliminate any danger of losing cathode rays beyond the edge of the target. To catch rediffused electrons, we mounted a cylindrical steel fence, of inside diameter equal to the diameter of the target, and of length 12 mm, coaxially with the target, with its nearer edge 5 mm in front of the target. While this fence is not of vital importance, it helps to insure accuracy in our rediffusion correction by catching most of the rediffused electrons and preventing them from being attracted back to the target face.

For using silver films without the beryllium backing, we mounted them on the end of a hollow cylinder, or tube, 21 mm o.d. like the beryllium target, and 16 mm i.d. In front of the film, to prevent the electrostatic field from tearing it to pieces, were two grids of 0.1 mm tungsten wires, threaded through holes in a sleeve that fitted over the cylinder holding the film. Two such holders were used. The first, made of copper, had the cylinder bored to a depth of 29 mm. The second was made of aluminum, to be more nearly free from rediffused rays from the bottom of the hole, and was 63 mm deep. The films were stretched very flat, giving them almost no freedom of motion and insuring

[6] D. L. Webster, W. W. Hansen and F. B. Duveneck, Rev. Sci. Inst. **3**, 729 (1932).

against wrinkles that would allow any x-rays going to the spectrometer (at 5° from the plane of the film) to suffer serious absorption.

The spectrometer is of the Bragg type, with a Seemann slit, used with the familiar precautions against errors due to changes of size or position of the cathode-ray focus. The main point here, of course, is to have all slits wide enough to include all the rays of either line of the $K\alpha$ doublet that will reflect from the crystal when it is set for the line measurement. Incidentally, the range of continuous spectrum should be limited by only one slit, the one we use for this purpose being the Seemann slit. To minimize the deduction for continuous spectrum rays, this slit is made as narrow as is consistent with certainty of including all the line rays.

The only new feature of this spectrometer is the ionization chamber, which was made in two compartments with opposing potentials to cancel natural ionization, only one compartment being exposed to the x-rays. The slight residual effect due to unavoidable inequalities is cancelled by a collector of natural ions in the pipe carrying the wire to the electrometer. Since all compensation here depends on natural ionization, this apparatus is better than the usual radium-compensated chambers, in being much less sensitive to changes in the emanation content of the air around it.

The electrometer was of the Compton type, used ballistically as explained elsewhere.[7] It was checked often with a potentiometer, to make sure there were no departures from linearity greater than one percent, and corrections were made for such departures as there were. In short exposures of the chamber to the rays, such as 10 or 20 seconds, as used with silver on beryllium, a group of electrometer readings at one setting would usually give a mean deviation of individual readings of about 0.3 percent. Deducting the continuous spectrum, the mean deviation in a line intensity measurement would be relatively greater, ranging from about 1 percent, in the neighborhood of $U=2$, to 2 or 3 percent near $U=7$. With silver leaf, the tube current had to be limited to 40 microamperes or less, giving weaker rays and requiring longer exposures, usually 60 seconds. These gave more chance for errors from zero shifts, unbalanced fluctuations of natural ionization, etc., but the deduction for the continuous spectrum was much less. So here also, 2 or 3 percent is a fair estimate for the errors.

The deduction of the continuous-spectrum intensity just mentioned can be made in either of two ways. The most obvious, graphical interpolation, was used with our first 5 films, in our work up to 85 kv reported briefly in 1928. More recently, however, we have used an analytical method, depending on a Taylor's series for the continuous spectrum intensity about the α-line glancing angle θ_α. (This angle is the middle of the short flat top of the peak given by the slit width conditions described above.) Writing the series as

$$I(\theta)=I(\theta_\alpha)+c_1(\theta-\theta_\alpha)+c_2(\theta-\theta_\alpha)^2+\cdots, \quad (3)$$

we apply it to 5 angles, equally spaced with an interval $\theta_1=0°\ 13.5'$. These angles, taken in increasing order, will be called $\theta_{-2}, \theta_{-1}, \theta_\alpha, \theta_{+1}, \theta_{+2}$.

A simple linear interpolation, $\frac{1}{2}\{I(\theta_{-1})+I(\theta_{+1})\}$, is sufficient for use with the silver leaf targets without backing, because with them the continuous spectrum is very weak. With films on beryllium, however, it is definitely incorrect if (as is usually the case) the graph of the spectrum is appreciably curved at θ_α, i.e., if the quadratic term in the series is appreciable. The next approximation, covering both the quadratic and cubic terms, is obtained by adding to the first $(1/6)\{I(\theta_{-1})+I(\theta_{+1})-I(\theta_{-2})-I(\theta_{+2})\}$. This is sufficiently accurate for all practical purposes, as shown by tests with a bare beryllium target, and probably at least as accurate as the graphical method, as well as faster—an important advantage when using perishable targets.

B. Data

Measurements were made with thirteen films, denoted here by letters a to m, the first nine being silver on beryllium and the last four free silver leaf. Films a to e were made by successive depositions of silver, with care never to touch the surface. Each one therefore included those before it, though films a to d were used so little that film e was practically fresh when first put to use. This film, however, was used for a long series of measurements, and then the tube was dismantled

[7] D. L. Webster, and R. M. Yeatman, J. O. S. A. and R. S. I. **17**, 248 (1928).

and work was started on a tube for higher voltages. Before the beryllium target was used again, therefore, the silver was removed with cyanide and the surface was ground down on a lathe, far enough to remove any minute pits into which the silver might be rubbed in cleaning. Then it was polished and tested for silver K radiation, of which no trace could be found. Then film f was deposited and used, and the same process was repeated. Film i was on a new beryllium target.

While the data from all the films were consistent, they differed in accuracy for various reasons, and we are therefore discarding the less accurate ones. These include: films a, b, c, g, which were too thin to give rays as intense as were desirable; film h, which was marred by transil oil seeping through a crack in the beryllium target; and film j, the first silver leaf without any backing, which got torn too soon to give a comparison of intensities at different voltages. The films retained differ considerably in the values of the corrections they need, and the data on which the corrections are based are not so good as we may hope for later. We are therefore presenting the most essential data here without any corrections, for use at any time when the corrections can be calculated more exactly than now.

To make the data on different films comparable, in spite of different thicknesses and different adjustments of the electrometer and other instruments, it is desirable to express all intensities for each film in terms of the intensity for that film at a standard voltage. For this we have chosen $U=2$, the integer giving a higher efficiency of line-ray emission than any other, and so giving the greatest accuracy with films on beryllium. Intensities reduced to this standard will be denoted by $j(U)$, to distinguish them from $i(U)$, the absolute intensity per unit film thickness mentioned above.

Two minor points about this reduction should be mentioned. One relates to films d and e, for which data were not taken at exactly the voltages listed here, on which most of the work on later films was concentrated. The values for d and e were therefore obtained by graphical interpolation from a graph of $(\log U)/j(U)$ against U, like that of Fig. 5, below. Values given in parentheses are inaccurate because of stray currents at the highest voltages in the tube used in 1928.

The observed intensities, reduced in this way, are given in Table I.

TABLE I. *Observed intensities, reduced to $j(U)$.*

U	*On Beryllium*				*Free Leaf*, 1932–33		
	In glass bulb tube, 1928		In steel and Pyrex tube, 1932		Copper holder	Aluminum holder	
	d, 170A	*e*, 280	*f*, 450	*i*, 1400	*k*, 1900	*l*, 1650	*m*, 1700
1.2	0.39	0.394	0.401	0.418		0.387	
1.5	0.73	0.714	0.732	0.781		0.760	
2.5	1.12	1.115	1.110	1.084		1.070	
3.0	(1.16)	(1.16)	1.176	1.110		1.078	1.074
3.5			1.203	1.116		1.079	
4			1.203	1.125	1.070	1.068	1.062
5			1.210	1.103	1.043	1.037	1.036
6			1.212	1.103	1.023	1.005	0.987
7			1.193	1.107	1.002	0.967	0.972

C. Corrections

As noted above, all these films must be corrected for such systematic errors as are inherent in the diffusion and retardation of cathode rays in any thin film. Furthermore the films on beryllium and the one on the copper holder must be corrected to eliminate the x-rays produced by cathode rays striking the films for a second time because of rediffusion. And those on beryllium need still a fourth correction, to eliminate fluorescence of the film under x-rays from the beryllium.

Two of these corrections, those for diffusion within the film and rediffusion from the beryllium, have been treated at length in a previous paper.[8] The effect of diffusion is to make each cathode ray, in its passage through the film, take a curved path and thereby go through more atoms than it would if it went straight. For a film of uniform thickness X_0, the mean length of path is a function of U which we call $X(U)$. For absolute intensities, if we could measure them, the correction would consist in multiplying the observed intensities by $X_0/X(U)$. For relative intensities reduced to unity at $U=2$, the correction factor is $X(2)/X(U)$, which we shall call c_d, the correction for diffusion.

[8] D. L. Webster, H. Clark and W. W. Hansen, Phys. Rev. **37**, 115 (1931).

The calculation of $X(U)$ involves several approximations of the type $\sec\theta = 1+\theta^2/2$, which is nearly one percent low at $\theta = 25°$, or $\sec\theta = 1.10$. Taking these approximations altogether, the error in $X(U)/X_0$ at any given value, such as this 1.10, may be two or three times as large as that in $\sec\theta$ at the same value. This makes the values of c_d for our thicker films at low voltages very uncertain. In tabulating them we are therefore using parentheses to indicate probable errors of 5 or 10 percent in $X(U)/X_0$, and square brackets for figures even more unreliable. At high voltages, however, since the excess of $X(U)/X_0$ over unity varies nearly as U^{-2}, the error in $X(U)/X_0$ decreases rapidly. c_d then approaches $X(2)/X_0$, keeping only such constant error as there may be in this ratio. The ratio of c_d at $U=4$ to that at $U=7$, for example, must be free from any serious error. With these reservations, the values of c_d are listed in Table II.

TABLE II. $100(c_d-1)$.

	On Beryllium				*Free Leaf*		
U	*d*, 170A	*e*, 280	*f*, 450	*i*, 1400	*k*, 1900	*l*, 1650	*m*, 1700
1.2	−1.7	−2.9	−4.7	[−12.4]		[−14.0]	
1.5	−0.7	−1.5	−2.3	(−5.7)		(−7.3)	
2.5	+0.5	+0.7	+1.0	+3.2		+3.7	
3.0	+0.8	1.1	1.6	5.7		6.2	6.4
3.5			2.0	6.3		7.4	
4			2.2	7.1	9.5	8.2	8.5
5			2.5	8.1	10.9	9.4	9.7
6			2.7	8.7	11.7	10.2	10.5
7			2.8	9.0	12.2	10.5	10.8

The rediffusion correction also is calculated as in our paper of 1931,[9] but with changes for more recent data on rediffusion, found by Neher.[10] Such data as were previously available had indicated that the rediffused electrons probably departed notably in their directional distribution from the simple cosine law. But Neher's data (both those in the abstract cited and others very kindly furnished us by letter) prove these departures to be actually too small to consider. In the formulas derived in our previous paper, this changes a factor called S from 2.11 to 2.00. A more important effect of Neher's data is on the value to be adopted for the so-called rediffusion constant, p. Data previously available were all on elements from aluminum to gold, for which p is practically independent of U, and extrapolation had indicated for beryllium a value $p=0.043$. Neher, however, found for beryllium 0.029 at 70 kv and 0.025 at 130, with intermediate values between. For extreme accuracy, this dependence on voltage should produce some changes in the method of calculating the correction to our data. Practically, however, since the correction is small anyway, and these changes all reduce it still further, it is sufficient for the degree of accuracy attainable to date to assume $p=0.025$. In the final values of the correction, p and S enter only in their product, which is thus changed from 0.090 to 0.050.

In our previous paper, there was considerable uncertainty in the energy distribution function for the rediffused electrons, but calculations with several alternative functions showed that changes could be made over a wide range without seriously affecting the result. It is therefore of interest to note that new data by Chylinski[11] on silver confirm the idea that this distribution function is within the range considered. These functions were of two types, chosen for integrability in connection with two empirical intensity formulas. The latter were almost equally good up to $U=3.3$, our limit in 1928, but one of them fails at higher voltages. The present corrections are therefore extended to $U=7$ on the basis of the other one, that the line intensity is

$$i(U) = \text{const} \times U^{-0.8} \log U. \qquad (4)$$

With the free films, not on beryllium, one cannot entirely neglect rediffusion, because the cathode rays must eventually strike something, and some of them can then rediffuse to the film. The first apparatus we used to hold such films, as described above, was made of copper. For this, calculations based on the cosine law of distribution and a value of 0.29 for the rediffusion constant of copper show this correction to be 0.9 as large as for films on beryllium. But with the aluminum holder used later, this factor is reduced to 0.1, making the correction negligible.

These corrections, with $pS=0.050$, are given in

[9] D. L. Webster, H. Clark and W. W. Hansen, Phys. Rev. **37**, 115 (1931).

[10] H. V. Neher, Phys. Rev. **37**, 655 (1931).

[11] S. Chylinski, Phys. Rev. **42**, 393 (1932).

Table III in terms of the factor c_r, by which the intensities must be multiplied to correct for rediffusion, still keeping the intensity at $U=2$ unity.

TABLE III. $100(c_r-1)$.

	On Beryllium	*Free Leaf*	
U	films *d*, *e*, *f*, *i*	On copper holder film *k*	On aluminum holder films *l* and *m*
1.2	+1.6	+1.4	+0.2
1.5	+1.0	+0.9	+0.1
2.5	−0.7	−0.6	−0.1
3.0	−1.2	−1.1	−0.1
3.5	−1.6	−1.4	−0.2
4	−1.9	−1.7	−0.2
5	−2.2	−2.0	−0.2
6	−2.4	−2.2	−0.2
7	−2.6	−2.3	−0.3

Turning now to the correction for retardation of the cathode rays, the main principles of this have already been stated in connection with the preparation of films, in Section IA. By Eq. (2) there, it can obviously be put into the form of a factor c_x like c_d and c_r, above, as soon as we have approximate data on $i(U)$, di/dU and dU'/dx. For the first two of these functions, the uncorrected data of Table I are sufficient, or one may use the empirical Eq. (4), above, which readily gives

$$c_x=[1+Xf(2)]/[1+Xf(U)], \tag{5}$$

where X is the thickness of the film and

$$f(U)=\tfrac{1}{2}(dU'/dx)_{U'=U}U^{-1}\{-0.8+(\log U)^{-1}\}. \tag{6}$$

For dU'/dx, the data in the literature are somewhat contradictory, but it seems to us best to use an empirical equation found by Williams[17] for light elements, modifying it slightly. In our notation, it is

$$V_K(dU'/dx)=-a\rho\beta^{-1.4} \tag{7}$$

where $\beta=v/c$ as usual, ρ is the density, and a is a nearly constant factor a few percent over 1.06 kv cm²/g. We shall take the numeric of a to be 1.1.

One modification needed for heavy elements, since retardation is done only by extranuclear electrons, is the insertion of a factor $2Z/A$, where Z and A are the atomic number and weight. This is probably not a sufficient change, since it weights all electrons alike and the tightly bound K and L electrons of silver should not be counted in full; but it is probably good enough for the present purpose.

Another modification, for convenience, is the approximation, good within 15 percent over our range of voltages, that

$$U=(\beta/\beta_K)^{2.5}. \tag{8}$$

Together, these lead to

$$dU'/dx=-(2.1\times10^3\ \text{cm}^{-1})U'^{-0.58}. \tag{9}$$

With these equations, we find corrections for our films as shown in Table IV.

TABLE IV. $100(c_x-1)$.

U	*d*, 170A	*e*, 280	*f*, 450	*i*, 1400	*k*, 1900	*l*, 1650	*m*, 1700
1.2	+0.6	+1.0	+1.6	+5.0		+5.9	
1.5	+0.1	+0.2	+0.3	+1.0		+1.2	
2.5	0.0	0.0	−0.1	−0.2		−0.3	
3.0	0.0	0.0	−0.1	−0.3	−0.4	−0.3	−0.3
5			−0.1	−0.3	−0.5	−0.4	−0.4
7			−0.1	−0.3	−0.5	−0.4	−0.4

Only one correction remains; namely, that for fluorescence of the silver films on beryllium, under continuous-spectrum x-rays from the beryllium. In our 1928 paper, we estimated values for that on the basis of equations taken from an earlier paper,[12] on thick silver, in which rays produced directly by impact ionization were compared with those produced indirectly by fluorescence. The latter were calculated by integration with respect to depth into the target. For silver films on beryllium, we took the integrand of this integral, multiplied it by the thickness of the films, and multiplied it also by 4/47 on the assumption that the continuous-spectrum rays causing the fluorescence would be simply proportional in intensity to the atomic number of the element they come from.

This assumption may hold well enough for rays emerging at large angles from the face of the target, but at small angles it is incorrect, because of absorption in the target. Although this error becomes notable only below about 5° or so, it is at exactly such angles that the silver film can absorb the largest fraction of the rays. Changing to a more detailed calculation, therefore, the fluorescence correction is increased by an un-

[12] D. L. Webster, Proc. Nat. Acad. Sci. **4**, 330 (1928).

expectedly large factor, becoming for high voltages the largest of the four corrections. It was on this account that we decided to supplement our data on films on beryllium with others on free films, at least for high voltages; and it was primarily this change in the fluorescence correction, rather than any difference between the new data and the old, that necessitated a revision of our intensity values between two recent abstracts.[13]

The integral for the intensity of fluorescent rays, assuming the film to be of infinite area, is

$$X\mathfrak{J}f(U)=\tfrac{1}{2}\int_{\nu_K}^{\nu_0}\int_0^{\pi/2} I(\nu_0,\nu)(1-e^{-\mu X_0\sec\theta})\frac{\mu_K}{\mu}\cdot\frac{\nu_\alpha}{\nu}u_\alpha\sin\theta d\theta d\nu. \tag{10}$$

Here $I(\nu_0, \nu)d\nu$ is the intensity of the beryllium spectrum in the range $d\nu$, in directions perpendicular to the cathode rays (other directions counting but little), ν_0 is the high-frequency limit, and ν_K the K limit of silver. μ is the absorption coefficient of silver at frequency ν, and μ_K the part of it due to K electrons. θ is the angle made by any ray with the normal to the target. u_α is the fluorescence yield of silver for its α-lines only.

For values of these quantities, we take μ and μ_K to be proportional to ν^{-3}, using Richtmyer's[14] values at the K limit. For u_α, we use Balderston's[15] value 0.62.

For $I(\nu_0, \nu)$ a first approximation is to call it simply proportional to $(\nu_0-\nu)$. This is in line with measurements by Wagner and Kulenkampff[16] on many elements up to 12 kv, and by Webster and Hennings[3] on molybdenum up to 70 kv, and it yields a quickly converging series for $f(U)$. But special measurements to test it here indicate that it is considerably in error at high values of ν_0/ν, the graphs of $I(\nu_0, \nu)$ against ν_0 being concave downward. To correct for this, we have plotted several such graphs for various values of ν, and modified the corrections according to them arithmetically. Fortunately, the region fairly near ν_K contributes nearly all the fluorescence rays, even at high voltages. Therefore, while we cannot claim great accuracy for it, without any direct test of $I(\nu_0, \nu)$ as a function of ν, it is probably much more accurate when calculated this way than by the simple linear formula.

Another correction to this integral is for the fact that the depths of production of the beryllium rays at high voltages are not strictly infinitesimal in comparison to the radius of the target, 10.5 mm, so the target cannot be considered as of infinite extent. At $U=7$, for example, the extreme case, Williams's[17] retardation formula for cathode rays shows a range of 0.030 mm. At half this depth, however, Bothe's[18] diffusion formula shows a most probable angle of deviation just over one radian. So the mean depth of production of x-rays will not be half the range, but something nearer a third of it. Even this, however, is appreciable, on account of the sec θ in Eq. (10), and it requires a change in the limit of integration with respect to θ, from $\pi/2$ to the angle for rays going to the edge of the target.

To use the fluorescence intensity thus calculated for correction of the line intensity, the essential point to note is that it is expressed in terms of the continuous-spectrum intensity from beryllium. It can therefore be related directly to the observed continuous intensity at the silver lines. One must of course take proper account of the fact that the ratio of electrometer readings for line and continuous rays depends on the resolving power of the spectrometer. This is easily done, however, by using the ratio of the area of the line, plotted on any scale, to the ordinate in the continuous spectrum under it, this ratio being independent of resolving power.

Altogether, this correction is not only arithmetically cumbersome but at high voltages the least accurate of the four. In tabulating it, therefore, we are indicating relatively large probable errors by parentheses. The values, in a

[13] D. L. Webster, W. W. Hansen and F. B. Duveneck, Phys. Rev. **42**, 141L (1932) and **43**, 384A (1933).

[14] F. K. Richtmyer, Phys. Rev. **27**, 1 (1926).

[15] M. Bladerston, Phys. Rev. **27**, 696 (1926).

[16] E. Wagner and H. Kulenkampff, Phys. Zeits. **23**, 503 (1922).

[17] E. J. Williams, Proc. Roy. Soc. **A130**, 310 (1932).

[18] W. Bothe, Handbuch der Physik **XXIV**, 18 (1927).

form analogous to that used for the other corrections, are in Table V.

TABLE V. $100(c_f-1)$.

U	d	e	f	i
1.2	+2.8	+2.8	+2.7	+2.0
1.5	+2.1	+2.0	+1.7	+1.4
2.5	−1.1	−1.1	−1.2	−1.2
3.0	−2.8	−2.6	−2.5	−2.5
3.5			−3.7	−3.7
4			−5.0	−4.9
5			(−7)	(−7)
6			(−9)	(−8)
7			[−11]	[−10]

D. Results

These corrections are now applied to the data of Table I. The results are tabulated for the individual films in Table VI and then averaged in the last column, "weighted average."

The weighting here is based on various considerations. These include of course the numbers of measurements at each point, and also questions of reliability, on the basis of which, for example, the data of 1928 at the highest voltages used then are discarded entirely because of stray currents in the tube. A further question of reliability relates to the corrections, especially those for fluorescence, which is large and unreliable at high voltages, and for diffusion, which becomes unreliable at low voltages in thick films. On this basis we favor the free silver leaf films at high voltages and the films on beryllium at low. However, these questions of judgment are not of primary importance, because the data of both types agree fairly well anyway.

This weighted average is taken now as the function of U to represent either the line intensity or the ionization probability, each on the arbitrary scale making it unity at $U=2$. To distinguish it from the uncorrected reduced intensity $j(U)$, of Table I, we shall call it the corrected reduced intensity, $j_0(U)$.

A graph of $j_0(U)$ is given in Fig. 4, with dotted curves for two empirical equations,

$$j_1(U)=2(m_1+2)\cdot(1-U^{-1})/(m_1+U) \quad (11)$$

and

$$j_2(U)=(2/U)^{m_2}(\log U/\log 2). \quad (12)$$

with $m_1=4$ and $m_2=0.783$.

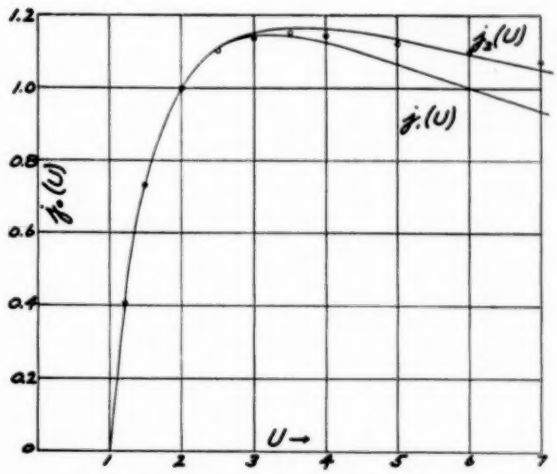

FIG. 4. Graph of corrected reduced intensity, $j_0(U)$ against U.

While $j_1(U)$ represented our 1928 data fairly well as far as they went with $m_1=3$, and it may be the more convenient function to use in some calculations, it is evidently not nearly so good as $j_2(U)$ for the whole range of U now available. In $j_2(U)$ the method of choice of a best value for m_2

TABLE VI. *Corrected reduced intensities, $j_0(U)$.*

	On Beryllium				*Free Silver Leaf, 1932–33*			
	1928		1932		On Cu holder	On Al holder		Weighted average
U	d, 170A	e, 280A	f, 450	i, 1400	k, 1900A	l, 1650	m, 1700	$j_0(U)$
1.2	0.403	0.404	0.406	[0.40]		[0.36]		0.404
1.5	0.748	0.726	0.737	(0.763)		(0.714)		0.733
2.5	1.115	1.103	1.100	1.095		1.105		1.103
3.0	(1.12)	(1.13)	1.150	1.129		1.140	1.137	1.138
3.5			1.162	1.135		1.153		1.153
4			1.145	1.134	1.148	1.149	1.146	1.145
5			(1.13)	(1.09)	1.131	1.128	1.130	1.123
6			(1.11)	(1.07)	1.115	1.101	1.085	1.099
7			[1.07]	[1.06]	1.095	1.062	1.070	1.072

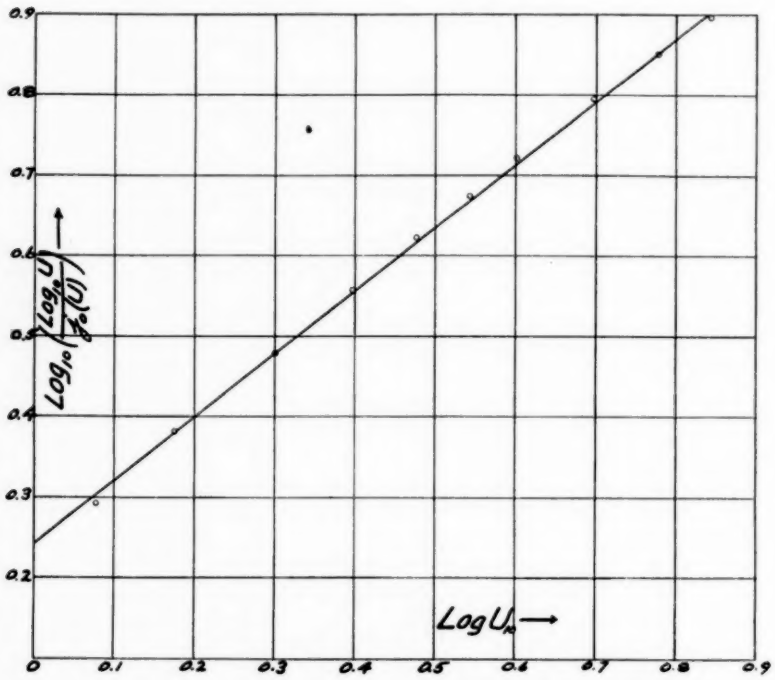

FIG. 5. The points show log $U/j_0(U)$ as a function of U; the line represents log $U/j_2(U)$ with $m_2=0.783$.

appears more clearly in Fig. 5, where the variables are chosen to make $j_2(U)$ give a straight line of slope m_2.

In addition to the data at the voltages tabulated here and shown in these graphs, we have data for film e at many other voltages. These were shown in a graph in our 1928 paper, but are not repeated here nor extended in that form, because they showed no departures beyond limits of error from a smooth curve, and there is every reason to expect the curve to be smooth, except at $U=1$.

The break at this point, however, is very significant, as noted in Section IA. It was therefore checked further with several films, and studied especially carefully with film e, with results shown in Fig. 6. Comparing this with the theoretical form for such a curve, shown in Fig. 3 above, it is evident that with a film so thin as this one, the whole region of upward curvature due to thick target effects is very small. This facilitates greatly the test for a finite slope at $U=1$, which consists, as noted above, in an extrapolation downward from a part of the curve safely above this thick-target region. Just how far one must go for this is difficult to say. The information on dU'/dx in Section IA would indicate 150 volts if the film were strictly uniform

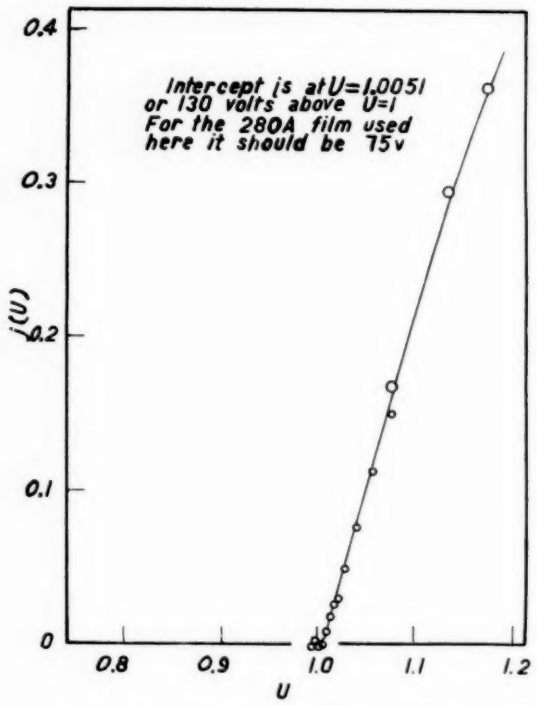

FIG. 6. Graph of $j(U)$ for film e near $U=1$.

and if it had no carbon on it. But strict uniformity is improbable, and there was enough carbon to retard cathode rays by an amount not negligible in comparison with 150 volts. At that, however, 150 volts takes us only to $U=1.006$, and one might begin the extrapolation many times as far above $U=1$ without impairing the test. It is evident that any such extrapolation proves the slope at $U=1$ to be finite and not zero.

Incidentally, the intercept of the extrapolated curve is about 130 volts above $U=1$, whereas the predicted value is 75 volts. The 55 volt difference is presumably the retardation in the carbon, and judging by our records of its color and our later measurements[6] on such films, this value is reasonable. With further study such measurements may prove useful as a means for measuring dU'/dx in films prepared for that purpose.

II. Theoretical

A. Comparison of wave mechanics with our experiments and others

The wave mechanics has been applied with considerable success to several other problems of electron impact, but relatively little has been done with it for the present problem. Elastic impacts and excitations of discrete levels have been treated by several authors, notably Massey and Mohr.[19] Ionization by electron impact has also received considerable attention from Ochiai,[20] Bethe[21] and others, even including work on the effects of relativity by a method due to Møller.[22] But so far as we have found, all the work on ionization has been done by Born's approximation, which is intended only for cathode rays of kinetic energy large compared to the ionization energy. Just how large it must be is uncertain, but one may question whether any such theory can be tested reliably with data extending only to $U=7$. This is even more questionable when, as in the present case, the data are not absolute probabilities, but only relative, because then the data even at $U=7$ acquire meaning only by comparison with data at still lower voltages.

With this understanding, however, we shall compare our data as well as we can with Bethe's[21] theory, which seems nearest to our conditions. This theory, like most, predicts an absolute probability of ionization by a cathode ray, rather than either our relative probability $j_0(U)$ or even the x-ray line intensity, which depends also on events subsequent to ionization. The absolute probability is defined most conveniently, not in terms of a path length Δx in metal, but as (probability of ionization) ÷ (number of atoms per unit area of target). This identifies it as the cross-section area of each atom effective for ionization. As applied to the present case of K electrons, by neglecting relativity, Bethe's value for this may be written as

$$\Phi_B(U)=(\pi e^2/V_K^2)\cdot(2b/U)\ln(4U/B), \quad (13)$$

where b and B are constants for any given element and shell, and the 2 comes from the number of electrons in the shell to be ionized.

Values are given for b for typical elements, including hydrogen and beryllium, for which it is 1, and silver, 0.32. B is described, for elements in which the K shell is well buried, as of the order of magnitude of unity. For hydrogen it becomes 0.638 for a cross section for ionization and excitation put together, but only 0.048 for ionization alone; and for valence electrons in general the corresponding constant is probably more of the order of 0.1 than 1. Beyond these qualitative statements, however, there is no value predicted for B.

To get what information is available about it, before comparing the theory with our data, one should examine such data as are available on thin targets at voltages so high that the approximations of the theory are justified. The best data of this sort are on gases, in which the data are obtainable directly from ionization measurements, rather than x-ray intensities. Helium is the best, being the only gas but hydrogen with only one shell to ionize, and fortunately this is a K shell. For helium, data have been taken by Hughes and Klein[23] Compton and Van Voorhis,[24]

[19] H. S. W. Massey, Proc. Roy. Soc. **A129**, 616 (1930); H. S. W. Massey and C. B. O. Mohr, ibid. **135**, 258 and **136**, 289 (1932), and **139**, 187 (1933).

[20] K. Ochiai, Proc. Phys. Math. Soc. Japan **11**, 43 (1929).

[21] H. Bethe, Ann. d. Physik **5**, 325 (1930).

[22] C. Møller, Zeits. f. Physik **70**, 786 (1931); Ann. d. Physik **14**, 531 (1932).

[23] A. L. Hughes and E. Klein, Phys. Rev. **23**, 450 (1924).

[24] K. T. Compton and C. C. Van Voorhis, Phys. Rev. **26**, 436 (1925) and **27**, 724 (1926).

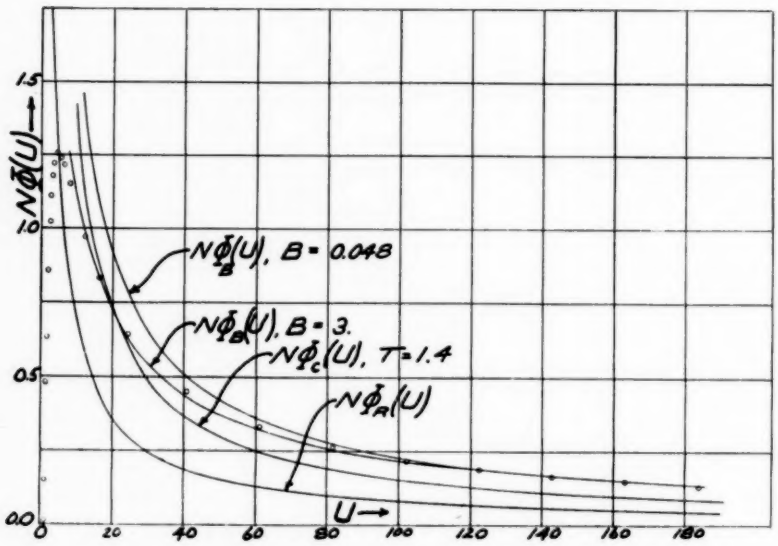

FIG. 7. Comparisons of Bethe's theory and others with Smith's data on helium. The functions $\Phi_B(U)$ and $\Phi_C(U)$ are explained in the next section.

and Smith.[25] They differ somewhat in detail but their graphs are all of the same general character as ours for silver, so far as our graph goes. Smith's data, the most recent, place the maximum at $U=$about 4.5, fairly near ours, though with a higher value of $j(U)$ there. His data extend to 4.5 kv or $U=183$. This is so high as to give the best evidence of all on the value of B. Furthermore his data are not merely comparisons of probabilities at different voltages, but absolute measurements. As such, they check b as well as B.

Multiplying $\Phi_B(U)$, with $b=1$ and $B=0.048$ (as for hydrogen), by the number of atoms per unit volume to which Smith reduced his data, the relation of this theory to helium is as shown in Fig. 7.

If these values of b and B are indeed the best, it would seem likely that Bethe's theory is accurate for values of U up in the hundreds, but that as U is reduced the theory becomes completely inapplicable long before reaching our upper limit $U=7$. Because of the approximations in the theory, however, it is possible that these values of b and B are not the best. We are therefore including also in Fig. 7 a graph for Bethe's theory with $b=1.75$ and $B=3$. These values were selected to fit the data as well as possible, by Professor W. V. Houston, to whom we wish to take this occasion to express our heartiest thanks for many very interesting conferences on this subject.

The fact that an increase of B from 0.048 to 3.0 makes it possible to fit the helium data so much farther down toward the low values of U will be recalled later in connection with our data, which are fitted best with $B=6$.

In the meantime, however, there are other data at high U's to be considered, taken by Lorenz[26] with aluminum. Lorenz used aluminum leaf, 8000A thick, and estimated the low-voltage limit for regarding this as a thin target at about 15 kv (about $U=10$) where the Thomson-Whiddington law would make the retardation only 1 kv. But this estimate does not allow for diffusion of the cathode rays. Bothe's diffusion formula, used in our calculations of the correction for diffusion in Section IC, gives the most probable deflection of a cathode ray under these conditions as 56°, making the increase in effective thickness 48 percent. Under such conditions, as noted with our Table II, the approximations used in the theory of the correction are very inaccurate, and the correction is probably greater than its calculated value. Practically, therefore, it seems difficult to interpret these data below about 25 or 30 kv, or $U=15$ to 20. From there up to Lorenz's limit, $U=33$, the

[25] P. T. Smith, Phys. Rev. **36**, 1293 (1930).

[26] E. Lorenz, Zeits. f. Physik **51**, 71 (1928).

data can be corrected reasonably well by this formula. For this calculation, we have read the experimental values from his Fig. 8, and cor-

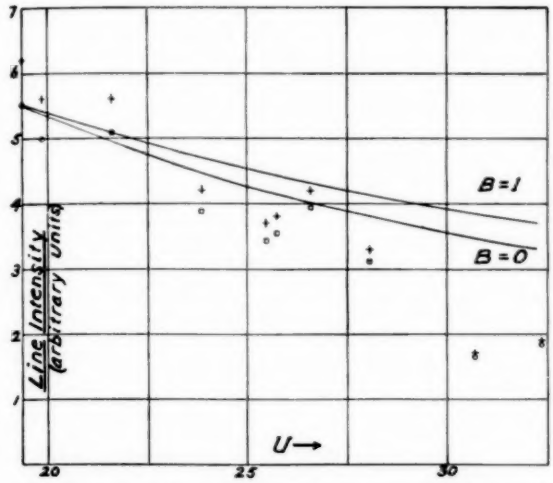

FIG. 8. Comparison of Lorenz's data on aluminum with Bethe's theory. Crosses, data as observed; circles, as corrected for diffusion.

rected them for diffusion, with results shown in our Fig. 8. Since the data are in an unknown unit, we have plotted the graph of Bethe's formula on arbitrary scales, chosen to fit the corrected intensity at 30 kv, both with $B=0$ and with $B=1$. Evidently the theory and the data would agree better if B could go below zero, but at least they are qualitatively alike, and zero is the best value for B here.

Returning now to our own data, with the conflicting evidence on B reviewed above, we shall treat B as a purely arbitrary constant. Since our data, like Lorenz's, are in an unknown unit, we have used arbitrary scales for Bethe's probabilities, with $B=4$, 6 and 8, and plotted the results in Fig. 9. Remembering that the theory is not intended for voltages near $U=1$, there is no reason to expect the theoretical curve to strike the U axis there, and it is evident that the best value of B for our data is about 6.

High as this value of B is, it seems probable that others of the same sort may be found. Preliminary measurements here by Webster, Kirkpatrick and Pockman on the $L\alpha$ and β_1-lines of gold at $U=7$ to 14 indicate that the decline of intensities is very slow, much as one might expect from extrapolation of our data on silver. This suggests high values of B for the gold L_{22} and L_{21} electrons, respectively. The L_{11} electrons are not easy to test in gold because of the proximity of their strongest lines to those of the other sub-series. But Coster and van Zuylen[27] have used thin films of tungsten on beryllium, to compare the intensities of lines of the L sub-series. Up to $U=3.3$ for L_{11}, they find a rise in the ratio of the intensity of β_3 (of L_{11}) to β_1 (of L_{21}) or β_2 (of L_{22}), fast enough to indicate a considerable difference in the ionization probability functions. This suggests that the maximum of the function for L_{11} must occur at a higher value of U than those of L_{21} or L_{22}, and thus indicates a value of B for L_{11} even higher than for L_{21} or L_{22}.

(*Note added in proof:* It might be supposed that the slowness of this decline is due to the rise of L ionization produced indirectly, as a result of $K\alpha$ transitions. One line of evidence against this comes from the V_K^2 in the denominator of each of the theoretical ionization functions, because this predicts that the number of such indirect L ionizations is small. Other evidence is the absence of any noticeable breaks in graphs of the observed L intensities at the K ionization potential, which was included in the measurements, to test this point, even though it was excluded in the report made above, because of cathode-ray diffusion. The slowness of

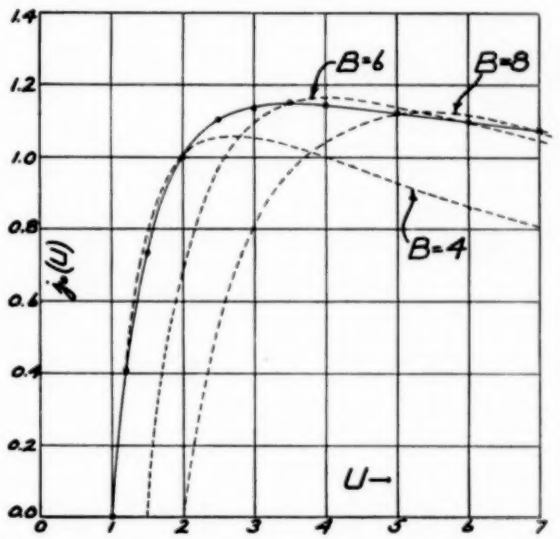

FIG. 9. Comparisons of Bethe's theory with our data on silver.

[27] D. Coster and J. van Zuylen, Nature **129**, 942 (1932).

the decline of intensity therefore depends primarily on the direct L ionization, as assumed above in deducing the high values of B for the L electrons.)

It must be remembered, however, that any use of Bethe's equation for these low values of U is a severe strain on the approximations on which the theory is based. The use of his equation with large values of B, either in helium, silver, gold or tungsten, is therefore really on a semi-empirical basis. It is evident that the next step in testing the applicability of wave mechanics to the range covered by our data must be the development of a theory not limited to high values of U.

B. Nonrelativistic classical quantum theory

While the classical quantum theory is so badly out of date that we habitually discard it, the conclusion of the last section reminds us that the equations of classical theory are after all not bad as first approximations in many cases. In the present status of wave mechanics for this case, therefore, the classical theory should be tested as a temporary substitute.

Three theories of the classical type are at hand. The first, devised by Davis[28] in 1918, was based on the simplest model of an impact, namely the impact of hard elastic spheres. One of these was the cathode ray, the other something about the atom, not defined. Further hypotheses were equivalent to taking the mass of the atomic sphere as that of an electron and assuming that ionization would occur whenever classical mechanics indicated a transfer of energy as great as the ionization energy, but never otherwise. This theory predicted a value for $\Phi_0(U)$ given by

$$\Phi_D(U) = D(1 - U^{-1}), \tag{14}$$

where D is an arbitrary constant.

The next theory, developed for ionization of gases by Thomson, and applied to x-rays by Rosseland,[29] was exactly like Davis's except that the spheres were electrons with the classical inverse-square repulsion. He predicted

$$\Phi_R(U) = (\pi e^2/V^2_K)\cdot 2\cdot(1 - U^{-1})/U, \tag{15}$$

where the constant factors are the same as in Bethe's theory with $b=1$. Its relation to Bethe's theory and Smith's data is shown in Fig. 7.

Thomas[30] introduced two innovations into Rosseland's theory: (1) that the atomic electron, which had been treated as at rest, is in motion, with the speed of Bohr's K electron; (2) that the cathode ray, just before its encounter with the K electron, has a speed greater than it had before entering the atom, because it has been attracted by the nucleus. The result was

$$\Phi_T(U) = \frac{\pi e^2}{V^2_K}\cdot 2\cdot\frac{1 - U^{-1} + (2T/3)(1 - U^{-2})}{1 + T + U}, \tag{16}$$

where T is the ratio of the orbital kinetic energy to the ionization energy, which for silver is 1.278.

To express the classical theory still more completely, we have recently[31] introduced another innovation, discussed in more detail in the next section of this paper. This is the deflection of a cathode ray by nuclear attraction within an atom, before it reaches the K electron it is to ionize. Since the K electrons are very near the nucleus and this deflection is always toward it, the effect must be an increase in the chance a cathode ray has of coming near a K electron. The change in the ionization probability is by a factor $(1+T+U)/U$. Thomas's calculations take account of all other important factors, so far as we can see, with no seriously inaccurate approximations except the neglect of relativity. Therefore we believe the application of this factor to his value for the ionization probability must give a reasonably complete and logical expression of the prediction of nonrelativistic classical quantum theory. With the subscript C for classical this gives

$$\Phi_C(U) = \frac{\pi e^2}{V^2_K}\cdot 2\cdot\frac{1 - U^{-1} + (2T/3)(1 - U^{-2})}{U}. \tag{17}$$

This formula, like Rosseland's and Bethe's, makes a prediction about the absolute value of the ionization probability. As Smith pointed out, and as Fig. 7 shows, the Thomson-Rosseland formula predicts ionization probabilities at high U's much too low to fit his data. The $(2T/3)$

[28] B. Davis, Phys. Rev. **11**, 433 (1918).
[29] G. Rosseland, Phil. Mag. **45**, 65 (1923).
[30] L. H. Thomas, Proc. Camb. Phil. Soc. **23**, 829 (1927).
[31] D. L. Webster, W. W. Hansen and F. B. Duveneck, Phys. Rev. **43**, 384A (1933).

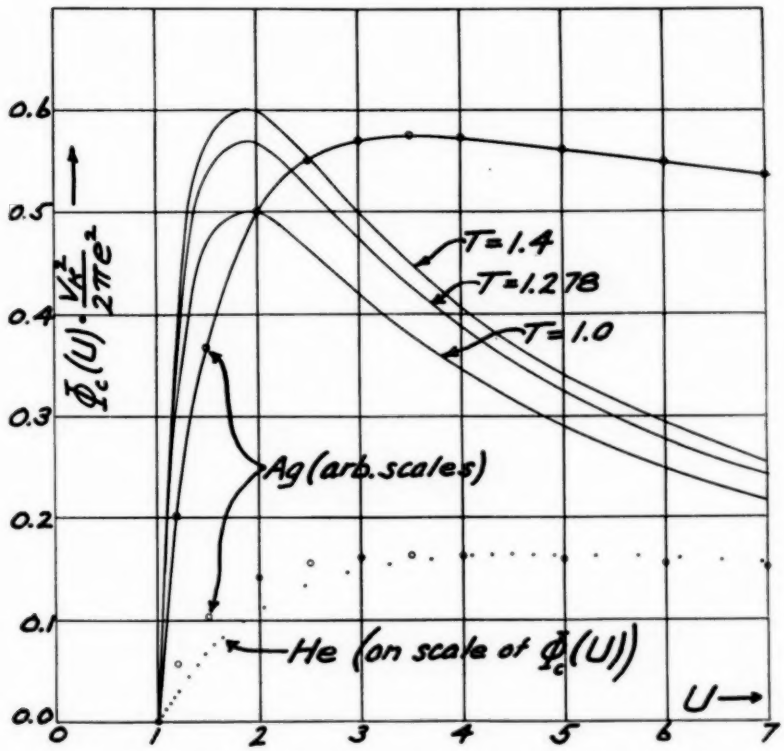

FIG. 10. Comparison of classical theory with data on silver and helium.

term introduced in this theory helps to reduce this discrepancy, as shown in Fig. 7. (*Note added in proof:* Here T is assumed to be 1.4, as given by strictly classical theory, though it might be better to use 1.6, as indicated by the observed ionization potentials.) At that, however, the theory is only an approximation, even at high voltages, not nearly so good as Bethe's.

To compare the classical theory with our data on silver, expressed in an unknown unit, $\Phi_C(U)$ must be in an arbitrary unit. Presumably this scale should be chosen to fit the curve to our data over as wide a range as possible. The fact is, however, it simply will not fit either silver or helium well on any scale, as shown in Fig. 10.

Turning to the data on other electrons discussed in Section IIA, which are also in unknown units, Lorenz's data on aluminum have about the same relation to this theory as to Bethe's with $B=0$, shown in Fig. 8. For L electrons, the classical theory for those with circular orbits is of course just like the theory for K electrons, and it would not fit our preliminary data on gold. For elliptical orbits (L_{11}) the only modification of the theory is that the constant T becomes an average around the orbit. This leaves it still practically unity, and gives no good way to account for the difference in the L ionization functions found by Coster and van Zuylen.

Evidently, even though the classical theory is a moderately good first approximation, though no more than that, for high values of U in helium, it is practically useless with $U<10$, even as a temporary substitute for a theory, for any element yet tested.

C. Theory of deflection of a cathode ray before an ionizing impact

It is indeed surprising that the classical quantum theory should depart from the data quite so badly as is shown by Fig. 10. Before accepting this conclusion, therefore, one may wish for more proof than our simple statement above, that the factor by which the probability of ionization is increased by the deflection of cathode rays really is $(1+T+U)/U$. The purpose of this section is therefore to give such a proof.

The essential basis for this proof is a feature of

classical ionization theory pointed out by Thomas: for a cathode ray to transfer to a K electron enough energy for ionization, it must approach the K electron to a distance so small compared to that of either of them from the nucleus that their relative motion is practically like that of two free electrons. More specifically, in an atom of atomic number Z, this distance must be of the order of $1/Z$ of the radius of the K orbit, which we shall call a. Ionizing collisions occur therefore only in a thin shell, with a mean radius a and a somewhat indefinite thickness of the order of a few times a/Z. With no irreparable loss of rigor, this thickness will be treated as if it were definite (calling it b), and the value of any function of the distance r from the nucleus will be taken for any point in this shell to be the same as at $r=a$.

If a K electron is considered as exposed to impacts of an atmosphere of cathode rays (very rarefied, of course), all of one speed, the probability that it will be ionized in a time dt is evidently proportional to the density of this atmosphere. The present problem is therefore to find the factor by which the density of cathode rays in the K shell just defined differs from their density outside the atom. Considering this problem now as if the density were great enough to speak of a group of many cathode rays found in that shell all at any one instant, the ratio of densities is the reciprocal of the ratio of the volume of the shell to the volume which this group of cathode rays must have occupied before they entered the atom. This may be found by treating their paths like stream lines of a fluid, with a typical tube of flow as shown in Fig. 11. This tube may be described in spherical coordinates r, θ, ϕ, with the polar axis $\theta=0$ pointing at the cathode; and its cross section on a plane perpendicular to this axis, outside the atom, will be given in a plane polar coordinate system R, ϕ as $Rd\phi dR$. Considering the electrons in this stream that are found at any one instant crossing the K shell as defined above, their length along the stream there is $b \sec i$, where i is their angle of incidence on that shell. Outside the atom, therefore, the group must have had a length

$$B=(v_0/v_1)b \sec i, \tag{18}$$

where v_0 is their speed out there and v_1 their speed at the K shell. Although v_1 is the same for all such tubes of flow, i is not. B evidently increases with R, becoming infinite at $R=A$, the value of R for a path tangent to the K sphere. The volume to be calculated is therefore that of a sort of concave lens, of radius A and thickness B.

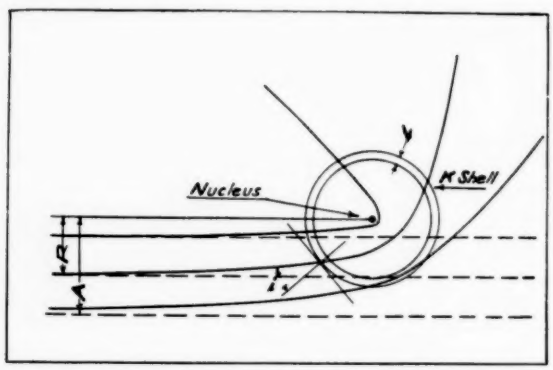

FIG. 11. Cathode-ray paths approaching a K shell.

Calling the densities outside the atom and in the K shall n_0 and n_1, respectively, and counting in n_1 the outgoing cathode rays as well as the incoming ones, it follows that

$$\tfrac{1}{2}n_1 \cdot 4\pi a^2 b = n_0 \int_0^A 2\pi RBdR. \tag{19}$$

If the electrostatic screening in the atom were too strongly concentrated near certain radii, this analysis might break down because it would be impossible to find a path from infinity tangent to the K shell. In any real atom, however, this does not happen, and it is easy to prove without any more specific assumptions about the field, that

$$n_1/n_0 = A/a = v_1/v_0 = [(1+T+U)/U]^{\frac{1}{2}}. \tag{20}$$

A part of this change of density, however, is due to the change of speed, which would make (n_1/n_0) exactly the reciprocal of this value, if it acted alone without the deflection. This is one of the effects included by Thomas in his calculation of $\Phi_T(U)$, and here it is combined with the deflection effect. To avoid correcting for it twice, therefore, we must divide it out before multiplying by the ratio of Eq. (20). In other words, $\Phi_T(U)$ must first be divided by (v_0/v_1) and then multiplied by (v_1/v_0). Altogether,

$$\Phi_C(U)=\Phi_T(U)\left(\frac{v_1}{v_0}\right)^2=\Phi_T(U)\frac{1+T+U}{U}, \tag{21}$$

this last fraction being the point to be proved.

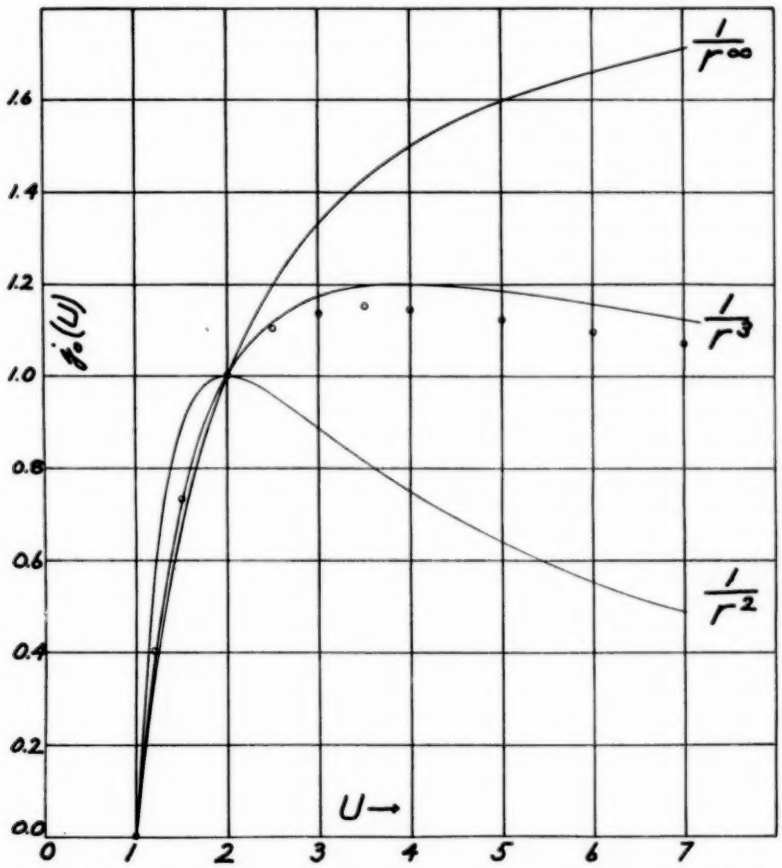

FIG. 12. Comparison of simple inverse-power theories with experiment: $j_R(U)$, inverse-square; $j_3(U)$, inverse-cube; $j_D(U)$ Davis's inverse infinity-power.

D. Modifications of classical quantum theory

Returning to the conclusion of Section IIB, that the nonrelativistic classical quantum theory was practically useless for silver K ionization even as a temporary approximation, and on the other hand remembering that nonrelativistic wave mechanics is very similar to classical theory in the well tested impacts of alpha-ray scattering, one may well question whether the change from classical theory to wave mechanics, without relativity, is likely to give a much better approximation. Then there is the question, how much difference relativity is likely to make. In classical orbit theory, as is well known, the effect of relativity is in the same direction as the effect that would be produced by changing the law of force from the inverse-square to a slightly higher inverse power. Is that, then, the sort of change we need here?

For a preliminary survey on this question, the easiest case to try is an inverse-cube law. Since Rosseland's theory differs but little from the more complete classical theory in its prediction for $j_0(U)$, even though they differ considerably on the absolute probability $\Phi_0(U)$, a rough test can be made on Rosseland's basis. With all assumptions exactly like his except on the force between the cathode ray and the K electron, the inverse-cube law there gives

$$j_3(U)=6/U\{(\pi/2\cos^{-1}U^{-\frac{1}{2}})^2-1\}. \quad (22)$$

This equation is compared with our data in Fig. 12.

While we cannot take the agreement of $j_3(U)$ with our data too literally as evidence for any such fantastic law of force, it is of interest to note that the difference between this function and the inverse-square function $j_R(U)$ is in line with the evidence on low-voltage ionizations also. Among these we may recall the ionization of

helium reviewed in Section IIA. In fact, as noted there, while the maximum probability for helium occurs at $U=4.5$, near ours for silver, the intensities around $U=2$ are relatively lower. In other words, the change from classical theory needed for helium is even greater than for silver. Furthermore, even with silver, using voltages up to 180 kv, it is asking a good deal of relativity to change the effective law of force as much as this; and in the corresponding range for helium, up to 180 volts, such large effects of relativity seem quite impossible. For helium, a more important point may be the fact that Thomas's condition as to distances, that enabled him to treat the electrons as free, does not hold with $Z=2$. The more complicated 3-body analysis needed for this case may give results quite different from $\Phi_C(U)$. In either silver or helium, however, the change required by experiment must be something more or less equivalent in its results to a change in the exponent of the force law from -2 to about -3.

E. Derivatives at $U=1$

There is one prediction on which all the classical theories agree. This is on the slope of the graph of $j_0(U)$ at $U=1$: regardless of changes in assumptions, either about laws of force between electrons, motions of K electrons, or attractions by nuclei, this slope must be finite and not zero. This prediction is verified by experiment, both for silver and for helium.

For double ionization, however, the classical theory fails even here. The basis for this statement is the theory of x-ray satellites developed from Rosseland's theory by Wentzel and Druyvesteyn.[32] According to this theory, if U is now defined by reference to the minimum energy for double ionization, rather than single, then when U is but little greater than 1, the probability of double ionization should not vary as $(U-1)$, but as $(U-1)^2$, giving a graph with a zero slope at $U=1$. Experiment, however, contradicts this prediction flatly: Bleakney,[33] working with helium, finds a finite slope at $U=1$ for the double ionization probability, much like Smith's for single ionization.

This fact seems especially significant, because of the reason for the $(U-1)^2$ prediction, which is that double ionization is regarded in this theory as a succession of two ionizing impacts by the same cathode ray during its passage through one atom. These two impacts are related only by the condition that the first impact must not deprive the cathode ray of so much energy as to preclude ionization at the second impact. Otherwise they are separate events, each with its own probability of occurrence. The resulting probability of double ionization is therefore a product of the two single-ionization probabilities. It is this idea, in slightly more rigorous mathematical form, that accounts for the prediction of the exponent 2 in $(U-1)^2$.

The verdict of experiment, therefore, seems to be that double ionization shall not be regarded as a succession of two events, but as a single event. It seems reasonable to assume that it would be regarded so in the wave mechanics. The defect of the classical mechanics here, as in many cases of interaction between electrons, is then that it is too specific: it contradicts the uncertainty principle. In the case of double ionization at least, therefore, it seems reasonable to expect great changes when the wave mechanics is applied to the problem. So perhaps we may hope for similar improvement in the theory of single ionization also, despite the lack of notable changes in the theory of the simpler two-body impacts.

[32] G. Wentzel, Ann. d. Physik **66**, 437 (1921); M. J. Druyvesteyn, *Dissertation*, Universiteit te Groningen, 1928. The equations from which these statements are deduced are in this dissertation, pp. 18–19.

[33] W. Bleakney, Atlantic City Meeting, Phys. Rev. **43**, 378A (1933).

Secondary Effects in Ionization by Hard Gamma-Rays

E. J. WORKMAN,* *California Institute of Technology*

(Received January 28, 1933)

The observations presented in this paper show that the ionization produced in a counting chamber by gamma-rays from a given source depends in a complicated way upon: (a) the nature (atomic) and thickness of the walls of the chamber; (b) the nature, amount, and distribution of matter in the neighborhood of the chamber. When the walls are sufficiently thick to stop the secondary beta-particles (the actual effective ionizing agencies) the secondary influences from the outside are greatly reduced, and the uncertainties involved among measurements with different thicknesses of the same wall material may be no more than a few percent. The results emphasize the effects of nuclear scattering of the secondary beta-particles. This action is effective in any material from which beta-rays may pass to the gas of the chamber, and consequently, the atomic properties of any such materials must be considered in interpreting ionization measurements. The following effects of nuclear scattering are discussed in their relation to ionization measurements: (1) equilibrium conditions between primary and secondary radiation with attention to the effects of "filtering"; (2) reflection of the secondaries by the wall material; (3) the dependence of the "stopping power" for electrons, of the wall on the atomic number of the material. In the second part of the paper, the front and back wall effects are treated separately. Transition effects between different materials on the front wall are shown. These transition curves are discussed in connection with "stopping power," equilibrium conditions, and photoelectric conversion of the gamma-radiation. The bearing of these phenomena on measurements of gamma-radiation with different counting chambers is discussed.

INTRODUCTION

THE following represents the first results of a research program initiated by R. A. Millikan to obtain a better experimental understanding of the effects of walls upon the ionization produced within ion-collecting chambers by rays of large penetrating power. The results were obtained prior to June, 1932, and partial reports have appeared in earlier papers.[1]

The ionization of a gas by gamma-rays is due in the main to electrons ejected from matter in the occasional close encounters between the gamma-quanta and atoms. Secondary electrons such as are produced by gamma-rays from radioactive processes, may have a path length of several meters in standard air or one to five mm in the metal wall of the counting chamber. Most of the secondary particles which produce ions in ordinary counting chambers with thick walls are produced by encounters within the wall itself, while with very thin-walled chambers the ionization within the chamber is almost wholly due to secondary electrons which were produced outside the chamber and often at a considerable distance from it. Thus, with thin-walled chambers the ion count depends upon the nature and distribution of surrounding materials as well as upon the energy flux of the primary radiation.

When the walls of the chamber are thick enough to exclude all secondary action from without, the ionization for a given chamber will be determined by the atomic properties of its walls.

A great amount of work has been done by way of determining the sensitivity of particular electroscopes to a given state of gamma-radiation. In nearly all instances, however, these investigations were preliminaries to other work, and, although they served their purpose, they are not sufficiently related to one another to give a general picture of the action. The investigations of Eve,[2] Moseley and Robinson,[3] and, more recently, Reitz[4] on the total ionization, in free air, because the gamma-rays from a unit mass of radium are of particular interest in this problem. These investigations show that the

* National Research Fellow.

[1] Workman, Phys. Rev. **40**, 1055A (1932); **41**, 264A (1932).

[2] Eve, Phil. Mag. **22**, 551 (1911); **27** (1914).

[3] Moseley and Robinson, Phil. Mag. **28**, 327 (1914).

[4] Reitz, Zeits. f. Physik **69**, 259 (1931).

activity in a volume of air in the vicinity of a sample of radium is influenced by a great number of conditions which give rise to secondary beta-particles which pass through the gas of the chamber producing the ions observed. Mayneord[5] has made an extended study of the relative sensitivity of small ionization chambers, lined with various metal foils and animal tissues, when irradiated by beams of x-rays and gamma-rays of a different mean wave-length.

The first part of the present paper is devoted to a description of results obtained when the ionization on account of various states of gamma-ray activity is measured with an electroscope having walls of variable thicknesses of iron or aluminum. The source of gamma-rays was a small plaque of radium from which the natural beta-rays were removed by filters.

Apparatus and Method

At the outset of this work, it was planned to use electroscope chambers differing widely in size and shape as well as of different wall materials. In order to facilitate this program, it seemed necessary to make some improvements in electroscope assembly; accordingly, a compact deflecting element was mounted on the end of the observing microscope in such a way that the various walls could be interchanged without making uncertain changes in the electrical capacity of the instrument or the charge calibrations on the micrometer eyepiece. The assembly is shown in Fig. 1. The deflection element

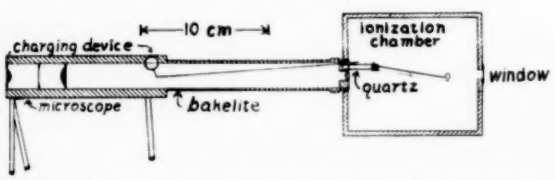

Fig. 1. Scale drawing of ionization chamber showing assembley of electrical and optical systems.

consisted of a quartz fiber strung parallel to a slender quartz rod as shown. The fiber and quartz rod from which the fiber was repelled were made conducting by a thin film of gold. The quartz insulating support was mounted on the end of the microscope, and a small cross fiber (0.3 mm long), mounted on the longitudinal fiber, served as an indicator. The charging device which is schematically shown was placed inside the barrel of the microscope. With this arrangement of the essential parts of the radiation meter, the walls were of simple cylindrical form with a 15/16 inch hole at one end and a cover glass window at the other end. They could quickly and easily be interchanged and could range in size from several inches in diameter to a chamber of the diameter of the microscope barrel. With a chamber 10.5 cm long and 630 cc volume, the electrical capacity of the instrument was 0.93 cm.

The electroscope assembly was supported by a light frame which held the chamber approximately 80 cm above and near the edge of a laboratory table. The radium was placed in metal boxes (filters of uniform wall thickness) at various distances from the chamber, on a line perpendicular to the axis of the chamber. These boxes were held 170 cm from the floor by a light wooden stand.

A mean ion-collecting potential of 300 volts was used. The ion current measurements were made by observing the time required for a given change of potential on the indicating element. The usual precautions to avoid errors due to polarization of the quartz insulator were observed. The "natural leak" with each wall in place was observed, and appropriate corrections were made for the results obtained with gamma-rays.

Filters

Since the gamma-ray spectrum of radium in equilibrium with its products consists of a great number of lines of different wave-length, screens of different thicknesses would be expected to change the relative hardness of the transmitted rays; while screens of different materials might give rise to different qualities in the resultant beam. Accordingly, different thicknesses of either iron, lead, or aluminum were used as filters. The air between the source and chamber will contribute to the supply of secondary electrons when thin walls are used. In order to study this feature, readings were taken with the radium at three different distances (25, 50, and 100 cm) from the axis of the chamber.

[5] Mayneord, Proc. Roy. Soc. **A130**, 63 (1931).

Results

Table I gives results for a cylindrical ionization chamber, 10.5 cm long with a volume of 630 cc, and aluminum walls of different thickness. Table II gives data for iron walled chambers of the same size. In these tables, the number of ion pairs per cubic centimeter per second has been multiplied by the square of the distance (D) from the source. These products are given in the tables according to distance, the wall thickness, and the filter. The results given under "zero" wall thickness were obtained by using a wall of tissue paper, made conducting by a coat of India ink. The thickness of this wall was 0.03 mm, and no supporting materials were used. The results thus obtained represent ionization measurements which are, to a close approximation, independent of any wall effects. These data, as well as all others given in this paper, refer to air at normal pressure and 20°C.

TABLE I. *Aluminum walls.*

		Ion pairs/cc/sec. $\times D^2 \times 10^{-4}$ given under the description of filter used								
Wall	D	Lead			Aluminum		Iron			None
(mm)	(cm)	3.18	6.35	12.7	12.7	25.4	6.35	12.7	25.4	0 mm
Paper	25	841	561	332	937	781	830	652	403	——
"	50	869	631	359	1001	867	882	715	445	——
"	100	928	700	449	1113	938	975	793	522	——
0.025	25	858	588	344	——	820	854	678	409	——
	50	873	637	390	——	885	919	729	461	——
	100	935	706	454	——	971	1013	826	526	——
.05	25	911	625	377	——	858	896	711	441	——
	50	920	666	416	——	911	948	763	482	——
	100	972	725	471	——	993	1037	843	598	——
.20	25	926	704	461	1095	954	1002	822	528	——
	50	933	710	471	1108	974	1014	832	547	——
	100	938	743	501	1157	1029	1069	890	582	——
.30	25	946	729	498	1140	991	1045	858	564	——
	50	932	727	502	1143	1005	1043	872	574	——
	100	948	745	524	1188	1047	1085	910	601	——
.51	25	942	746	520	1142	1024	1060	884	592	——
	50	935	748	522	1144	1020	1051	885	595	——
	100	943	756	534	1164	1052	1096	911	614	——
.87	25	961	766	556	1180	1045	1077	916	622	——
	50	945	764	551	1160	1045	1079	913	634	——
	100	952	776	554	1180	1063	1088	941	633	——
1.17	25	961	784	571	1179	1066	1104	947	640	——
	50	959	782	565	1189	1072	1100	955	646	——
	100	958	779	557	1192	1078	1106	956	647	——
1.58	25	959	770	560	1160	1048	1076	928	638	——
	50	931	757	557	1158	1052	1080	933	636	——
	100	933	763	556	1168	1070	1097	941	643	——
3.18	25	913	753	556	1132	1027	1054	915	626	——
	50	886	774	547	1134	1027	1058	910	626	——
	100	908	752	546	1157	1056	1071	924	634	——
6.34	25	896	744	547	1128	1024	1041	900	617	——
	50	891	732	535	1116	1011	1036	897	616	——
	100	896	742	540	1123	1024	1044	909	625	——
12.70	25	874	720	533	1095	993	1018	876	602	1176
	50	868	717	524	1084	985	1017	871	599	1170
	100	867	716	525	1091	994	1025	890	600	1184
18.93	25	834	680	512	1060	942	971	851	577	1113
	50	838	697	502	1038	945	978	844	580	1125
	100	841	688	511	1043	954	981	847	581	1129

TABLE II. *Iron walls.*

		Ion pairs/cc/sec. $\times D^2 \times 10^{-4}$, given under the description of filter used								
Wall	D	Lead			Aluminum		Iron			None
(mm)	(cm)	3.18	6.35	12.7	12.7	25.4	6.35	12.7	25.4	0 mm
Paper		Same as in Table I.								
0.05	25	988	726	471	1322	1175	1114	910	599	——
	50	995	750	484	1357	1205	1155	956	622	——
	100	1038	798	534	1472	1327	1268	1050	693	——
.13	25	1053	820	562	1435	1275	1261	1054	707	——
	50	1054	832	572	1451	1324	1273	1069	718	——
	100	1095	864	599	1532	1395	1355	1145	711	——
.254	25	1085	876	622	1460	1335	1285	1113	748	——
	50	1074	865	614	1465	1345	1299	1120	781	——
	100	1098	884	626	1535	1398	1356	1170	770	——
.381	25	1068	866	628	1440	1328	1245	1113	754	——
	50	1092	885	622	——	——	——	——	——	——
	100	1072	881	625	1499	1372	1343	1160	780	——
.635	25	1048	852	626	1421	1308	1268	1100	756	——
	50	1030	848	622	1435	1305	1291	1118	764	——
	100	1072	863	624	1460	1362	1326	1146	776	——
1.170	25	1022	859	616	1373	1271	1263	1096	746	——
	50	1023	844	616	1382	1280	1267	1084	744	——
	100	1051	863	617	1423	1318	1301	1124	761	——
1.575	25	972	808	576	1304	1180	1195	1032	701	——
	50	976	806	582	1305	1202	1200	1046	710	——
	100	992	811	582	1345	1238	1242	1065	723	——
3.165	25	946	782	572	1235	1152	1168	1005	692	——
	50	950	784	577	1240	1153	1184	1013	689	——
	100	965	790	572	1265	1164	1190	1019	690	——
6.35	25	902	736	541	1128	1042	1071	928	634	1237
	50	989	732	535	1128	1038	1067	924	631	1244
	100	885	730	535	1128	1031	1059	923	623	1253
12.7	25	735	610	448	913	818	866	743	505	972
	50	722	601	442	887	805	848	723	500	977
	100	712	599	432	875	799	835	721	492	969

The tabulated results reveal the following features:

(1) As the wall thickness increases the ionization first increases, reaches a maximum, and then decreases.

(2) The percentage of increase is greater for iron walls than for aluminum walls.

(3) As the distance of the source increased the maximum becomes relatively less pronounced.

(4) When the chamber walls are thin the increased air distance increases the ionization—the inverse square law being taken into account. This effect vanishes when the walls are sufficiently thick to stop the secondary beta-radiation from the intervening air.

(5) The increase in air distance is similar in effect to increase in wall thickness.

(6) Filters of heavier materials transmit to the

chambers less secondary beta-radiation relative to the number of gamma-quanta passed. Evidence for this action exists in the relative ionization for paper and thin walls when compared to that for walls thick enough to stop the secondaries originating in the respective filters.

The effect of different filter material on the equilibrium conditions (indicated under 6 above) is discussed at length later in this paper. Here, however, it is well to anticipate that discussion in order to explain why iron walled chambers show a greater wall effect than do aluminum chambers. The increased nuclear scattering of the secondary electrons in the materials of greater nuclear charge causes these materials to have a greater stopping power for the beta-particles for a given surface density. This nuclear scattering gives rise to reflection of the fast electrons on the inside surface of the chamber wall and also enhances the chance of a secondary generated in the side wall (with respect to the source) to enter the chamber. As a result, iron walled chambers may show a greater beta-ray activity even though the actual number of secondaries which enter from the wall in direct line with the source may be less than in the case of materials of lower atomic number. *This complicated action must be considered when dealing with the relative sensitivity of chambers differing in (1) shape and size, (2) manner of incidence of the radiation on their walls, or (3) nature and density of gas in the chamber.*

Although the above results are direct and show quite definitely what may be expected when apparatus of this type is used, they do not yield sufficient information on the individual effects involved. The principal complications arise from: (a) variable wall thickness as seen by the primary gamma-rays; (b) contribution of the side wall to secondary and reflected particles; (c) scattering from the walls of the room; (d) wide angle scattering of gamma and secondary beta-rays from the filter. In view of these complications, it appeared advisable to forego investigations with different sized chambers and to use new apparatus designed to eliminate some of the uncontrolled features inherent in the first method. Furthermore, it seemed necessary to deal separately with the front and back wall effects and to study composite walls: transition effects.

Second Apparatus

A sectional drawing of the apparatus is shown in Fig. 2. The gamma-rays are canalized by the large lead block (*A*) and directed along the axis of the cylindrical ionization chamber (*F*). The front wall (*G*) and back wall (*H*) were of aluminum foil 0.0005 cm in thickness. These thin windows were permanently fixed and served to define the volume of the ion chamber. Any additional wall to be studied was placed in contact with the windows and supported by the ledges shown in the figure. Filters could be inserted in any of the positions shown—*B*, *C*, and *D*. The lead bushing (*E*) was removed when changing filter (*D*) or (*C*), and the steel bar (*O*) could be removed for the purpose of changing filter (*B*). The lead plug

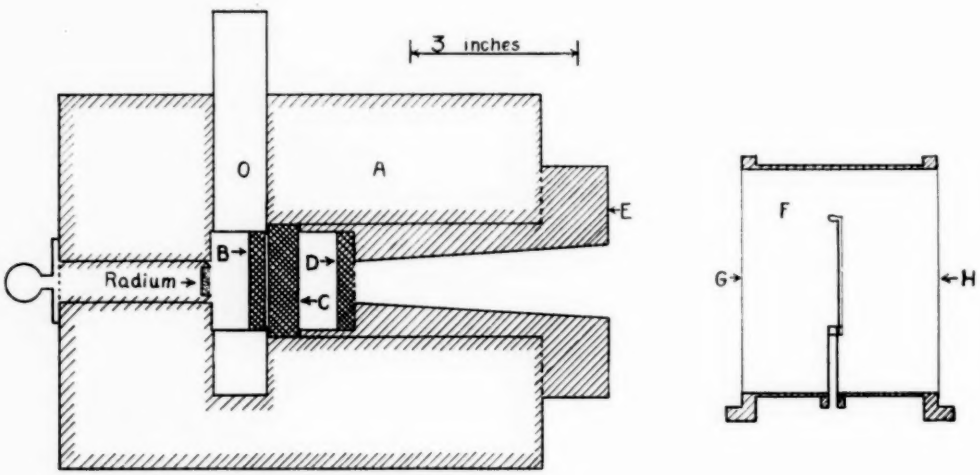

Fig. 2. Scale drawing of second apparatus.

in which the radium plaque was securely mounted could be withdrawn when measuring the leak and residual ionization of the electroscope.

The ionization chamber is formed by a Bakelite tube of approximately 1.5 mm wall thickness and is lined with foil like that used for the windows. In the early part of this work a single fiber deflecting element was used, but later, when greater sensitivity and faster action became desirable, another type, described elsewhere,[6] was used. The electrical capacity of this instrument was not measured but was of the order of 0.5 cm. The ionization in arbitrary units was deduced in the same manner as in the first experiments except that greater precautions were observed to avoid errors due to polarization and leakage on the thin quartz insulator. Since it was impossible to seal this electroscope, the surface of the quartz was covered with a thin film of ceresine. This treatment provided a non-hygroscopic insulator which remained sensibly constant over a great range of humidity.

Discussion and Results

Attention will be directed first to results obtained when plates of various thicknesses of lead, tin, iron, aluminum, or graphite were placed on the back wall (H) of the chamber. A 12.7 mm lead filter was used at position D in the gamma-ray gun.

Curves are given in Fig. 3 showing the back wall effect. The thicknesses of the material, in

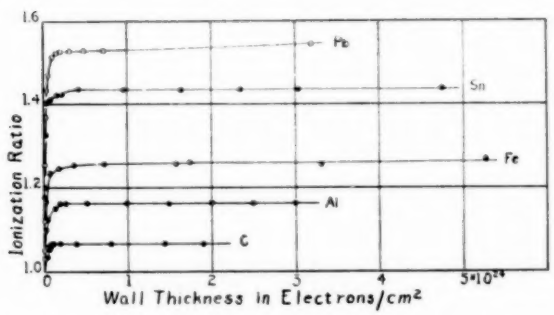

FIG. 3. Showing increase in ionization because of reflection from the back wall.

electrons per square centimeter, are plotted as abscissae, and the ratios of the ionization when the material is used to that when only the thin windows are used are given as ordinates. *The denominator of this ratio will be a constant for any given filter arrangement.* The ratio is plotted merely to facilitate comparison and to reduce all readings to the same scale. We see that the addition of material on the back causes the ionization to increase rapidly until it reaches a value beyond which no further increase takes place. This is what we would expect because the secondary beta-particles which strike this wall cannot emerge again after they have penetrated beyond a certain depth in a given material.

If we consider percentage of increase in ionization to represent the relative amount of reflection of the rays and plot this quantity against the atomic number of the material, we obtain a curve which agrees, almost perfectly, with that obtained by Schonland[7] and others, for the reflection of beta-particles. It will be noted, when plotting these points, that the point for lead falls too high to agree with pure reflection data. This is seen to be due to the existence of photoelectrons ejected backwards from the lead by the gamma-rays. When the filter thickness is increased to give relatively harder gamma-rays, this affect disappears, as shown in Fig. 7. It should be pointed out that the agreement of the data for the back wall effect with reflection data may be over emphasized because the conditions of experiment are by no means analogous. We have compared these results with results obtained by measuring reflection from a beam of electrons normally incident with the surface. Although our case is not one of random incidence, there is good reason to assume that the relative reflection should be considerably greater than in the *normal* case. It is to be emphasized, however, that the ionization which we were actually measuring depended upon the total length of beta-particle tracks within the chamber, and it is likely that some compensation arose, from the fact that a few of the reflected particles crossed only a part of the chamber before they were absorbed in the walls.

A somewhat more detailed study of the back wall effect was made by taking amply sufficient thicknesses of the materials on the back wall and

[6] Workman and DeVore, Phys. Rev. **41**, 262A (1932).

[7] Schonland, Proc. Roy. Soc. **A104**, 235 (1923); **108**, 187 (1925).

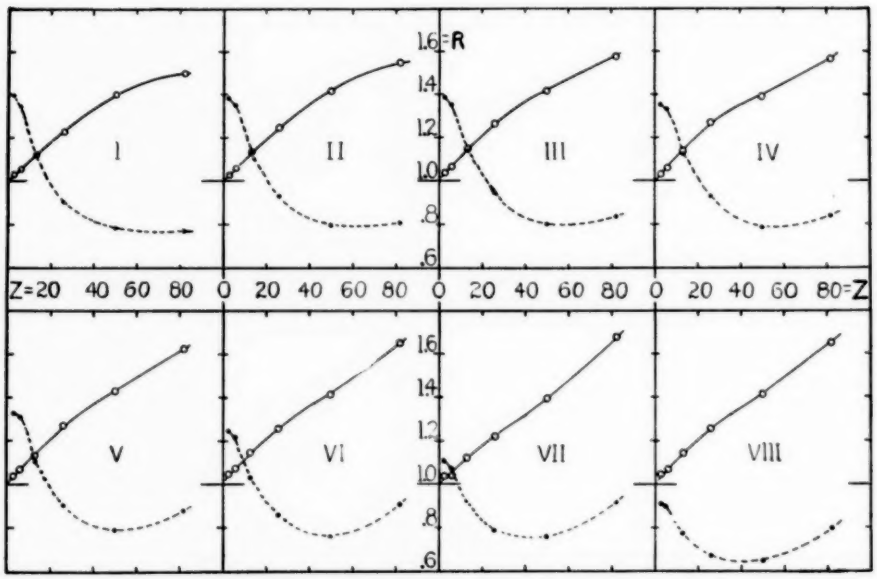

FIG. 4. Ionization ratios for front wall (broken lines) and back wall (full lines) plotted against atomic number of the material. Each material of thickness—0.2×10^{24} electrons/cm². Lead filter thickness in mm as follows: I—32.0; II—25.2; III—19.3; IV—13.2; V—7.24; VI—3.56; VII—0.89; aluminum: VIII—3.10.

measuring the ionization ratios with different thicknesses of lead filter in the "gun." The thickness of wall materials for this test was 0.2×10^{24} electrons per cm². The results are shown in the solid lines of Fig. 4. These curves show in a striking manner the photoelectric response of lead to this radiation. In passing from curve I to VII a marked increase in the effect of lead is observed. The increase follows the decrease in filter thickness: i.e., the increase in effective wave-length of the radiation. It is of interest to note here, that, aside from variations brought about by the photoelectric effect, the back wall effect is practically independent of the wave-length of the radiation; i.e., the probability of reflection of the beta-particles is, as expected, independent of their energy over this range. Moreover, the relative back wall effect, exclusive of photoelectric action, was shown by other tests to be quite independent of the equilibrium between the primary and secondary radiations incident on the electroscope. This is in accord with the view that we were dealing only with the secondaries and the action of the back wall upon them. By the same tests, that part which has been attributed to the photoelectric effect, is caused to stand out as a result of the gamma-radiation incident on the back wall.

The dotted curves of Fig. 4 show the front wall effect. They were determined in the same manner as the above discussed back wall curves. At this point reference will be made only to the behavior of lead relative to the other elements. An increase is observed at the lead end of the curve which corresponds to a similar increase on the solid lines. There can be little doubt that this contribution to the ionization is from beta-particles resulting from the photoelectric absorption of the gamma-rays in the lead wall. There may be a slight indication of the same effect in tin, but the probability of such absorption depends upon a too high power of the atomic number to give any appreciable effect when observed in this way.

In passing the discussion of the back wall effect, it may be well to point out that some of the electrons which were scattered back into the chamber from the back wall actually originated in the wall. If, for example, a Compton or photoelectric encounter were to give rise to a beta-particle among the surface (inside) atoms of the back wall, it will have the same chance of being scattered back as any other particle going in the same direction. Some thickness of material is required, however, for an appreciable number of such encounters, and the probability of the

resultant particle entering the chamber will vanish rapidly with the depth of its origin. It appears that the magnitude of the effect should have the same dependence upon the atomic number of the material as the *true* reflection.

The Front Wall Effect

The effect on the ionization in the electroscope of adding material to the front wall is shown in Fig. 5. Here, as before, the *ionization ratios* are

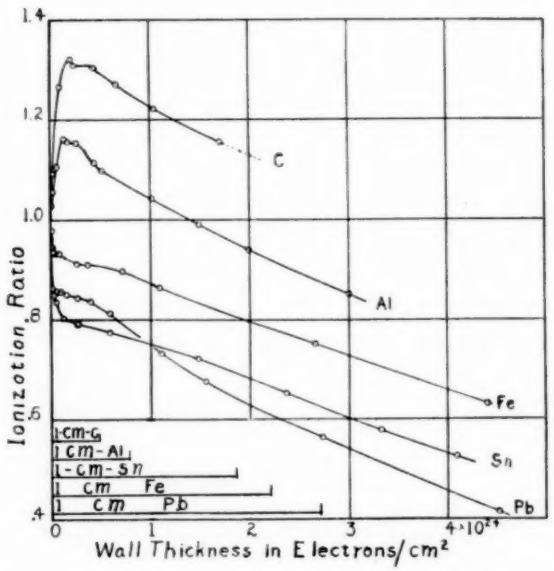

Fig. 5. Ionization ratios, *vs.* wall thickness showing effect of material on the front wall.

plotted against the thickness of the material in electrons per square centimeter. *These points represent the actual ionization currents observed, as no absorption corrections were made in their deduction.*

Any material placed on the front of the chamber will, of course, decrease the quantity of gamma-radiation which passes through it, but it is certain that for all points given on Fig. 5 the ratio of secondary beta-ray activity to transmitted gamma-radiation is greater than when no material is on the front wall. Indeed, for limited thicknesses of carbon and aluminum the actual beta-ray activity is greater than when no front wall exists. In general, it can be said that the relative positions of the curves are determined by the atomic properties of the materials, while the position of the group as a unit depends upon the state of equilibrium existing between the gamma-radiation and its secondaries at the electroscope. When, for example, the lead filter (12.7 cm in this case) is placed in position *B* (Fig. 5) where it is irradiated more strongly by the gamma-rays, the effect is to decrease all of the ratios given in Fig. 8 by about 12 percent. Here the geometry of the beam is such as to allow a relatively greater number of secondary beta-particles from the filter to fall upon the electroscope. This will have the effect of increasing the *zero wall* ionization and decreasing the ratios. Such action has been demonstrated by experiment, and there is good reason to believe that, if only gamma-rays were present in the beam, all of the materials would yield a ratio greater than unity for, at least, limited thicknesses. This ideal condition could not be realized without removing the air from in front of the electroscope and deflecting the particles which originate in the filter and canals from the beam. With even these precautions we would still have a few secondary gamma-quanta with reduced frequency due to Compton encounters in the filter and canals. With all of the apparent complications there is, nevertheless, a rather simple explanation of the general features of the curves in Fig. 5.

If the scattering and absorbing mechanisms for primary and secondary radiations were the same for all the materials and depended only on the number of extranuclear electrons per cm^2 in the path of the beam, we should expect all of the points on Fig. 8 to fall on one curve. This simple interpretation is obviously untrue for it must be said that, when equivalent thicknesses of the various elements are used, the secondary beta-ray activity in the chamber decreases as the atomic number of the material increases—except in the case of lead of thickness below 3.6 mm. If Compton encounters only are considered, it is apparent that there will be as many beta-particles generated in one material as in the other when the same thickness in electrons is taken. The velocity spectrum of these electrons will be sensibly the same for each material, and if, once started, they encountered no nuclear scattering, about the same number would emerge from each material. *Such scattering does take place*, and because of it the actual path length of

an electron in penetrating to a depth of N electrons per unit of area will be "longer" as the atomic number of the material is greater. The heavier elements thus show, progressively, a greater stopping power in proportion to the number of Compton electrons generated. This, of course, is in accord with observations on the back wall effect, for there we were observing particles which were turned completely in their courses.

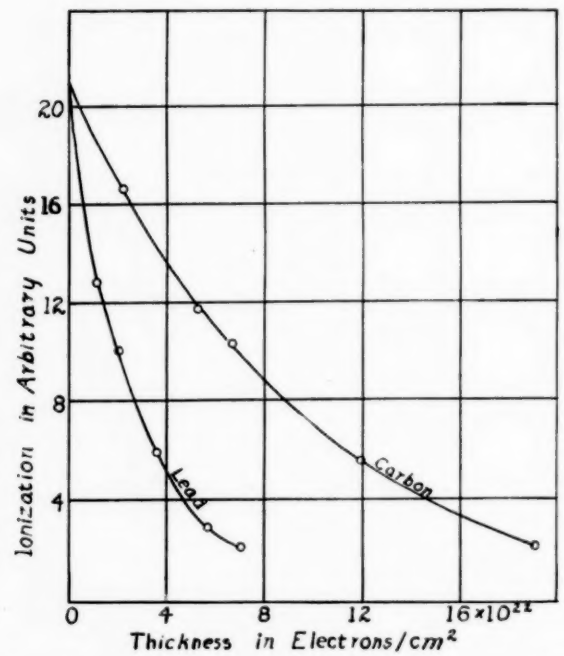

FIG. 6. Curves showing the relative "stopping power" of carbon and lead.

The effect of variable scattering of the secondary particle on the equilibrium conditions existing between the primary and secondary radiations appeared of such general importance that further proof of the correctness of the above interpretation was sought in the following test. The gamma-ray gun (Fig. 2) was moved back to a distance of about a meter from the ionization chamber and was pointed up at such an angle that no primary gamma-rays entered the chamber. Tests were made showing that all of the resultant activity in the chamber was due to secondary beta-rays which entered through the thin window. With these conditions, the relative stopping power of the wall materials for the electrons could be determined by placing sufficient material on the front wall to reduce the activity of the chamber to that given by the natural leakage. This was done in gradual steps for carbon and lead. The results are shown graphically in Fig. 6. It is shown that, in order to stop a given fraction of the beta-particles more than three times as much surface density of carbon as of lead is required. The apparent constancy of this ratio for the different ionization rates indicated as ordinates, is of interest because approximately the same net result is obtained for slow as for fast electrons. Further study along this general plan would doubtless lead to many interesting features of the response of counting chamber to ordinary gamma radiation and the ultra-penetrating or cosmic radiation.

Composite Walls and Transition Effects

A thickness of one to five mm is sufficient to stop all of the secondary electrons in these materials. If, then, the character of the transmitted gamma-rays is determined only by the thickness in electrons, of the front wall, we should expect the response of the electroscope to be determined only by the inside layers of the wall: i.e., when a thickness of material sufficient to stop the secondaries is on the front wall, the ionization should be the same when an equivalent thickness of *any material* is added.—Perhaps the tertiary x and gamma-radiation should be considered in this connection. These radiations resulting from impacts of the beta-rays and the filling of levels disturbed or left vacant by them would be relatively efficient in the production of ions as a consequence of their low energies. The actual quantity of such radiation is small, however, and its effect will be determined completely by an appropriate thickness of inside wall material.

Fig. 7 shows the curves given before in Fig. 5 with the addition of ionization ratios obtained for composite walls. In most cases the thickness of one of the materials is varied to show the transition from one material to another. The broken lines show the various transition effects. The indicated ionization ratios which define these lines were obtained by placing different thicknesses of the indicated material in contact with the chamber and immediately back of other

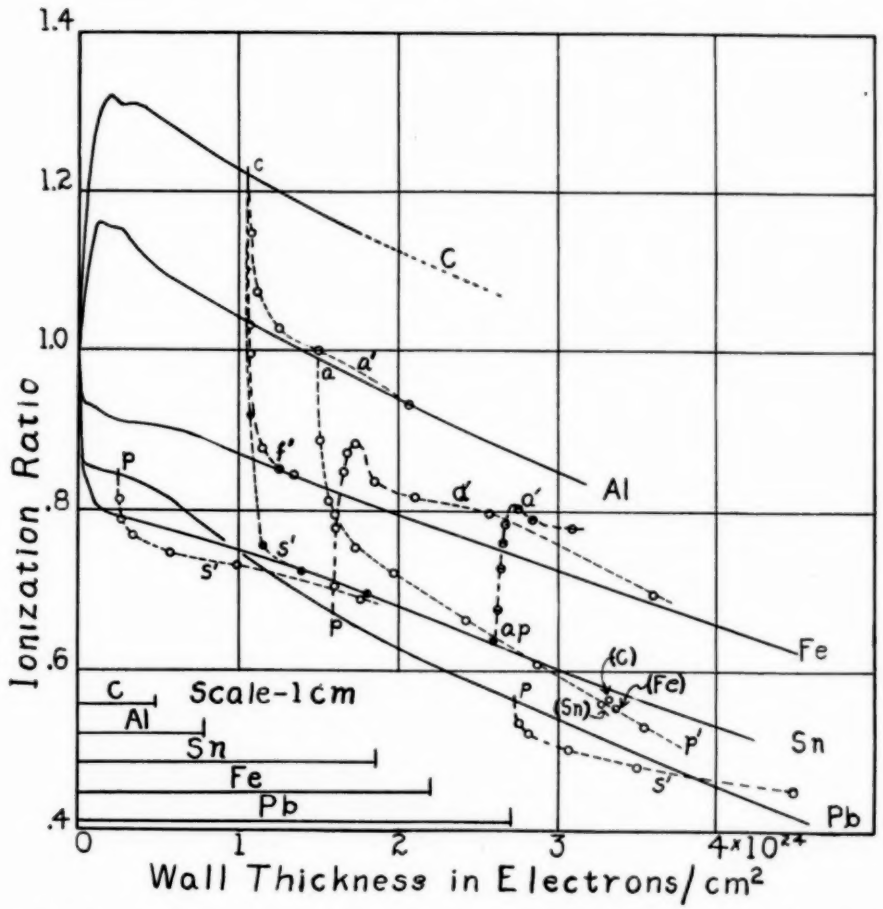

FIG. 7. A tracing of the curves given in Fig. 8, with the addition of curves showing transitions from one wall material to another.

material of thickness given by the point where the curves start. They are listed as follows:

c–a'..graphite to aluminum	*p–s'*..lead to tin (two curves)
c–f'..graphite to iron	*p–a'*..lead to aluminum
c–s'..graphite to tin	*ap–a'*..a double transition-aluminum to lead to aluminum
a–p'..aluminum to lead	

Except where different thicknesses of lead are used, the transitions shown in Fig. 7 are all complete and certainly indicate that the mechanism of absorption and scattering of the gamma-rays are the same in all these elements except lead. It seems also that it would be difficult to find a better unit for measuring the thickness of the absorbers than the number of extra-nuclear electrons per unit of area. At least some property proportional to this number should be used.

Where transitions involving lead are considered, we see that certain peculiarities exist. In fact, the curve representing the front wall effect, alone, for lead is peculiar in the manner in which it crosses the curve for tin, and does not take its expected position on the graph until a considerable thickness of lead has been added. This excess in the ionization for thin lead walls must result from the photoelectric conversion of some of the softer gamma-rays and the consequent passage of the fast moving electrons through the gas of the chamber. This conversion of the gamma-rays, which becomes relatively efficient for softer radiation compared to the usual Compton scattering, will become less important as the thickness of the lead wall is increased: i.e., as the effective filter becomes thicker and gamma-radiation transmitted to the layers from which photoelectrons may escape to the chamber becomes harder.

With this action in mind, it is clear why a metal such as tin, if placed between the lead and the window, decreases the ionization by way of *stopping* the photoelectrons from the lead "faster" than *effective* Compton electrons are produced in the tin. The two transitions marked p–s' show this effect. The lead to aluminum combination given by transition p–a' shows an increase from lead because of the greater number of effective Compton electrons produced in the aluminum. It should be noted that this transition (p–a') is by no means complete. This was expected because we have approximately 1.6×10^{24} electrons per cm² of lead between the aluminum and the source which has abstracted gamma-radiation from the beam by photo-electric absorption. Such absorption did not occur, of course, in the front wall effect for aluminum to which curve the transition would have otherwise gone. Similar action is observed in all transitions from lead. The first transition p–s' nearly approaches the tin curve, because here the amount of lead, to the point p, is small and little photo-absorption has taken place. The second transition of this type would, by similar reasoning, be expected to have a greater interval between it and the lead curve. The curve showing the change from aluminum to lead (a–p') is of special interest because we see a gradual approach to the lead curve as the amount of lead for the curve a–p' becomes comparable to the amount for the curve showing the front wall effect for lead. Of even more significance, perhaps, is the fact that the abundance of material in front of the electroscope has served to "harden" the radiation to the extent that the effect of photoelectric conversion is no longer felt at the chamber: i.e., the gamma-rays of frequency suitable for photoelectric conversion have been almost completely absorbed regardless of any special mechanism.

The points indicated by (C), (Fe), and (Sn) on the a–p' curve indicate respectively the transitions:

1.70×10^{24} electrons/cm² of graphite to 1.63×10^{24} electrons/cm² of lead

1.57×10^{24} electrons/cm² of iron to 1.79×10^{24} electrons/cm² of lead

1.49×10^{24} electrons/cm² of tin to 1.79×10^{24} electrons/cm² of lead

The positions of these points, on or near the a–p' transition curve, are very significant because they indicate that complete transition curves of the type indicated doubtless would pass along the a–p' curve in this region. Such curves would, therefore, bear the same relation to the front wall curve for lead as the a–p' curve.

Although it appears that the photoeffect in lead is adequate to produce the above results, it should be pointed out that from the results given it cannot be said that other mechanisms do not exist in lead for absorbing or modifying the primary radiation. Any action of this kind would show its effects along with the rather complicated response to photoelectric absorption. By the same reasoning, one hesitates to say that the results for the other materials, *as a group*, could not arise, at least in part, from other processes than the Compton scattering of gamma-quanta and nuclear scattering of beta-particles.

The Effect of Wave-Length

When using a complex radiation of the type given by radium in equilibrium with its products, it is difficult to specify the spectral energy distribution given by the most simple arrangement of filters. It is possible, nevertheless, to characterize the radiation as having a relatively longer mean wave-length when the amount of filtering is small. Another consequence of the complexity of the primary radiation is the fact that a true state of equilibrium, with the secondaries, will never exist regardless of the amount of material through which the radiation may pass. Although these factors will limit our interpretation of the results, it is of interest to examine further the effects of filter thickness when the chamber has plates of different materials on the front or on the back.

Fig. 8 shows the actual ionization obtained for the materials, *viz.*, paraffin, graphite, aluminum, iron, tin and lead, as a function of filter thickness. These results represent ionization currents for thickness of 0.2×10^{24} electrons per cm² of the materials as used in the two positions. The curves indicated by "zero" are identical and refer to values obtained by using no wall except the thin aluminum windows. The position and shape of the curves for zero wall are subject to secondary

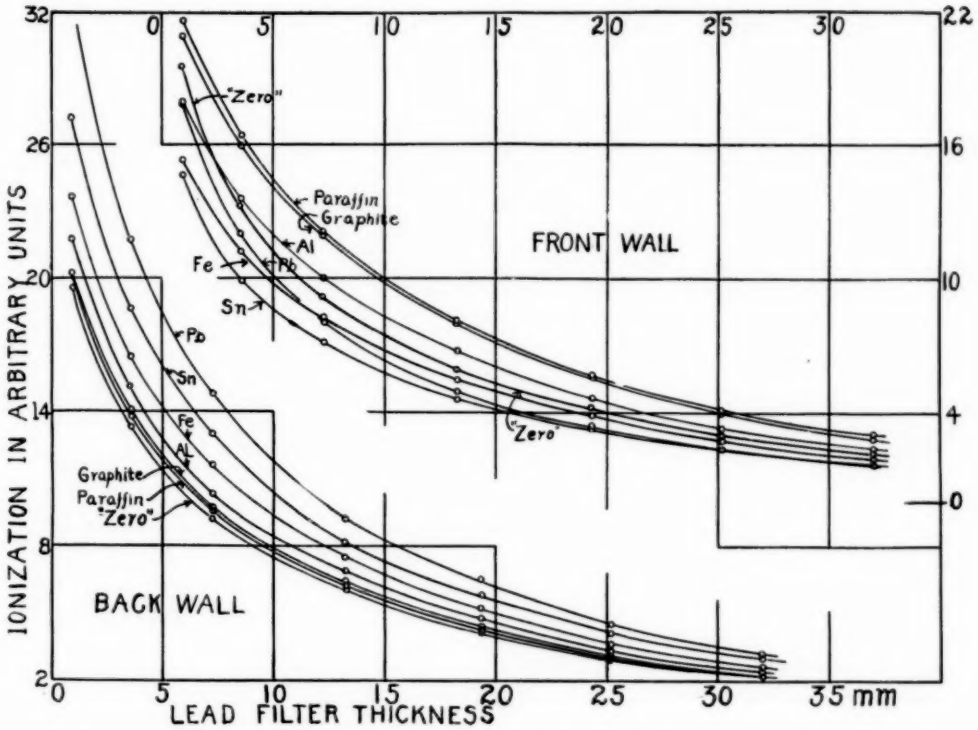

FIG. 8. Ionization currents as a function of lead filter thickness. Each material of thickness—0.2×10^{24} electrons per cm^2.

radiations from the "gun" and the air between it and the chamber, as well as those originating in the chamber. The ratio of secondary to primary gamma-activity will change with changes in wave-length; as a result, we do not expect the "zero" curves to be consistent with the strength of the gamma-rays. The curves for the back wall are, of course, influenced by the same secondary particles, but their relation to the zero readings and to each other are significant because they represent responses to the same states of radiation.

The front wall curves given in Fig. 8 call for a different treatment because they are not influenced by secondary beta-particles originating outside the walls of the chamber. The indicated ionization currents represent the action of the gamma-rays on the respective walls and, therefore, have little direct meaning relative to the values for zero wall. In these curves, we observe the same arrangement according to atomic number as in Fig. 5, except that in the present case the photoeffect in lead is sufficient to cause the lead curve to turn upward and cross the one for iron as well as that for tin.

When pictured in this way, there is evidence for the photoeffect in tin at the extreme left of the upper group.

Even though the front wall materials are sufficiently thick to stop the beta-particles as well as the softer secondary x-rays or gamma-rays, the curves given in Fig. 7 differ enough in character to give a variety of conflicting absorption coefficients for lead if, such methods were to be used for their deduction. Here it appears that it would be interesting to obtain similar curves when filters of different materials are used. With this additional information, some separation could be made between scattering and true absorption effects. For work of this kind, however, smaller canals should be used and consequently a much larger radium source would be necessary.

While this work was in progress Schindler's[8] excellent paper on transition effects in cosmic

[8] Schindler, Zeits. f. Physik **72**, 635 (1931).

rays appeared. The similarities in the results are very striking, considering the great difference in the energy of the primary radiations. The enormous difference in energy is appreciated when one considers that the thickness of lead required to stop the "fastest" secondary electrons from gamma-rays of radium (approx. 2.5×10^6 volts) is about 0.3 mm, whereas from Schindler's results one obtains a stopping thickness of about 100 mm. It is of further interest to note that the transition curves for cosmic rays are all complete, indicating no type of absorption of the primary radiation peculiar to one or a part of the materials which were used.

General Considerations

In concluding this paper, it appears desirable to point briefly to some important observations which, though substantiated by an interpretation of the data, may escape notice:

(1) Secondary effects have been discussed only in relation to ionization chambers. Indeed the complications may appear so numerous as to cause this useful device to yield grace to other methods of observation. Wilson cloud chambers and various adaptations of the Geiger counters furnish additional information, but it should be observed that many of the same rules hold in reasoning from the secondary or tertiary observation to the primary cause.

(2) The sensitivity of nearly all ionization chambers, thus far developed, will vary with the quantum energy of the primary radiation. That is to say, any factor used to deduce energy flux from ionization rates will vary with the hardness of the primary gamma-radiation. This variation is brought about, at least in part, by variation in extent of nuclear scattering of the secondary electrons by the wall material, and by variations in their specific ionization in the gas as well as any selective action exemplified by photoelectric conversion. Standard air chambers such as used in much hard x-ray standardization must necessarily have similar limitations. Here the relative amount of secondary radiation in equilibrium with the primary radiation will vary with the hardness of the primary radiation and conditions of intervening air and filtering materials. In hard radiation therapy where perhaps the prime interest should be in the amount of secondary beta-ray activity produced in the tissues, the walls of the chamber should be such as to be atomically equivalent to the tissues in question.

(3) Of perhaps more importance than any of the above considerations, is the question of when and under what conditions an ionization chamber or any similarly used device is designed to exclude all secondary activity originating outside its walls. Great improvements in the technique of ion counting bring emphasis to this question because many of the causes for disagreement doubtless are to be found here. One especially interested in some of the smaller deviations, amounting to several percent, may find interest in the following approach to the study of data given in Tables I and II. Consider the radiation for any two filter arrangements and observe the ionization resulting from these two states as measured with various wall thicknesses of both iron or aluminum. If ratios between corresponding ionization values (same wall thickness) be taken for two columns, deviation of several percent may be found between say a 1/8 inch steel wall and a 1/2 inch steel wall. This is not due to transmission of beta-rays through walls and must otherwise be explained.[9]

In measuring gamma-like radiation where different wave-lengths or different absorbing materials are involved, the interpretation is greatly simplified by excluding secondary beta-radiation from the outside. *The important thing to observe in this connection is the fact that the "stopping thickness" of material for the secondary beta-radiation depends very much upon the atomic number of the material and not simply upon the surface density of matter.* No simple relation exists to determine anything like equivalent stopping thicknesses for let us say, copper and lead or air and mercury. This contention will doubtless be substantiated by more exacting studies of transition phenomena.

The author takes pleasure in acknowledging the valuable help of Mr. H. B. DeVore who assisted in many departments of this work.

[9] The author is aware of possible effects resulting from a "selective" or variable nuclear conversion of the gamma-rays in the wall or filter materials and has work in progress designed to give information on these effects through transition phenomena.

Ionization of Gases by Neutrons

T. W. BONNER, *Rice Institute, Houston, Texas*

(Received April 10, 1933)

The ionization currents produced in hydrogen, helium, nitrogen, methane, ethylene and argon by the neutrons from beryllium have been measured for gas pressures from 5 to 80 atmospheres. The relative diameters of the atomic nuclei have been calculated from the relative ionizations. Assuming that the radius of the neutron is small compared to the radii of the atomic nuclei, the relative radii of the nuclei are found to be $r_H = 1.0$, $r_{He} = 1.4$, $r_N = 1.9$, $r_C = 2.8$, and $r_A = 4.1$. The target areas of the nuclei $a_H = 1.0$, $a_{He} = 2.0$, $a_N = 3.5$, $a_C = 8.0$, and $a_A = 17$, vary roughly as their atomic numbers. The pressure-ionization curves for neutrons are found to differ from the γ-ray curves in the same gases.

THE object of the experiments described in this paper was to find the relative amounts of ionization produced in different gases by neutrons. When neutrons collide with nuclei of gaseous atoms contained in an ionization chamber, energy is transferred from the neutrons to the nuclei. A recoil atom formed in this manner then produces a large number of ions in the gas.

Experiments on the relative ionization produced by neutrons in argon, nitrogen and helium containing 20 percent air have been described by Curie and Joliot[1] with an ionization chamber containing these gases at atmospheric pressure. In the present experiments the relative ionization currents due to neutrons have been determined for argon, helium, nitrogen, hydrogen, methane and ethylene over a range of pressure of from 5 to 80 atmospheres.

The diagram of apparatus (Fig. 1) shows the ionization chamber B, the inside dimensions of which were $5 \times 5 \times 10$ cm. The iron walls of the ionization chamber were one cm thick. The electrode was insulated by amber with a guard ring which was so arranged that the insulators were not in the electrical field across the ionization chamber. The chamber was made pressure tight with sealing wax between the metal and amber surfaces. A Lindemann electrometer C operated at a sensitivity of 50 divisions per volt was used to measure the currents. In order to eliminate insulation leakage a null method employing a potentiometer and a compensating condenser (D in Fig. 1) was used. Thus the electrometer needle was always kept at zero potential by changing the potential on the condenser. A potential of 400 volts supplied by "B" batteries was applied across the ionization chamber.

A two-inch lead shield surrounded the ionization chamber, except on the top side, to cut down the ionization due to local radioactivity. This shield also increased the number of neutrons entering the chamber, since a considerable number of the neutrons are scattered into the chamber from the lead.

The polonium, used as a source of alpha-particles, was deposited on a silver disk 9 mm in diameter. The silver disk is shown in Fig. 1 directly above the ionization chamber. The polonium had an activity of roughly 15 millicuries. A thin slab of beryllium was mounted on a slide (A in Fig. 1) so that it could be put either just under the source of polonium or out of the range of the alpha-particles. 4 mm of lead was interposed between the source of neutrons and the ionization chamber.

The pressure in the chamber was measured by a Heise pressure gauge E which could be read accurately to 2 lb. per sq. in.

The ionization chamber was thoroughly flushed out by successively filling to 70 atmospheres and emptying it three times. The gases were slowly passed through a P_2O_5 drying tube and a length of tubing containing glass wool before they were

[1] I. Curie and F. Joliot, J. de Physique et le Radium **4**, 1, 21 (1933).

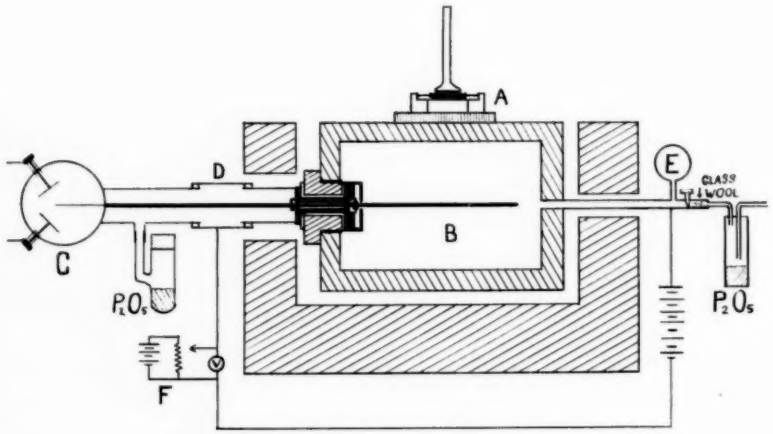

FIG. 1. Diagram of ionization chamber.

admitted to the ionization chamber. Measurements were made first at 80 atmospheres and then at the lower pressures.

In determining the ionization due to the neutrons, the ionization produced when the beryllium was out of the range of the alpha-particles was measured first, and then the ionization when the beryllium was directly under the polonium. The ionization in the first case was that due to γ-rays from the polonium source, cosmic rays, and radioactivity of the chamber. To determine the ionization due to the neutrons the first current was subtracted from the second. In these experiments the ionization due to the neutrons was several times that due to the other radiations.

The variation of the current with the potential applied to the ionization chamber was determined with different gases at 80 atmospheres. It was found that when the potential was changed from 200 to 400 volts there was an increase in the ionization current of only a few percent. In the subsequent measurements alternate readings were made with the chamber at a potential of $+400$ volts with respect to the electrode and then -400 volts and the mean of the two currents was used.

The capacity of the system was determined by comparing it with that of the compensating condenser and was found to be 9.6 e.s.u. The number of ion pairs per cc per second was

$$(9.6\times 12)/(50\times 300\times 4.77\times 10^{-10}\times 250\times t)$$

where 250 cc was the volume of the chamber; 12, the number of divisions deflection of the electrometer; 50, the sensitivity of the electrometer in divisions per volt; and t, the time in seconds required for this deflection.

Under the given experimental conditions the ionization by the less penetrating γ-rays,[2] emitted along with the neutrons was found to contribute only a small percentage of the total ionization. This was shown by getting the ionization in CH_4, H_2, and N_2 with an additional lead absorber of 2.2 cm thickness. The 2.2 cm of lead cut down the amount of ionization by 23 ± 5 percent in CH_4, 26 ± 5 percent in H_2, and 30 ± 5 percent in N_2. If the γ-rays produced a considerable part of the total ionization, then the apparent absorption coefficient would have been much larger when using CH_4 and N_2 than when using H_2 in the chamber.

Fig. 2 shows the ionization currents produced at different pressures by the neutrons in CH_4, C_2H_4, A, H_2, N_2, He. Similar data given in Table I show the relative ionization in these

TABLE I. *Ionization due to γ-rays in arbitrary units.*

Gas	10 atmospheres	20	40	80	$\frac{80}{10}$ for γ-rays	$\frac{80}{10}$ for neutrons
N_2	1.00	1.76	2.56	3.55	3.55	3.78
He	0.223	0.438	0.774	1.27	5.70	2.02
H_2	0.184	0.342	0.544	0.850	4.61	3.32
A	1.64	3.15	5.49	8.91	5.44	6.16
CH_4	0.956	1.60	2.38	3.64	3.81	2.16
C_2H_4	1.42	2.29	3.52	—	—	—

[2] Becker and Bothe, Naturwiss. **20**, 41, 757 (1932).

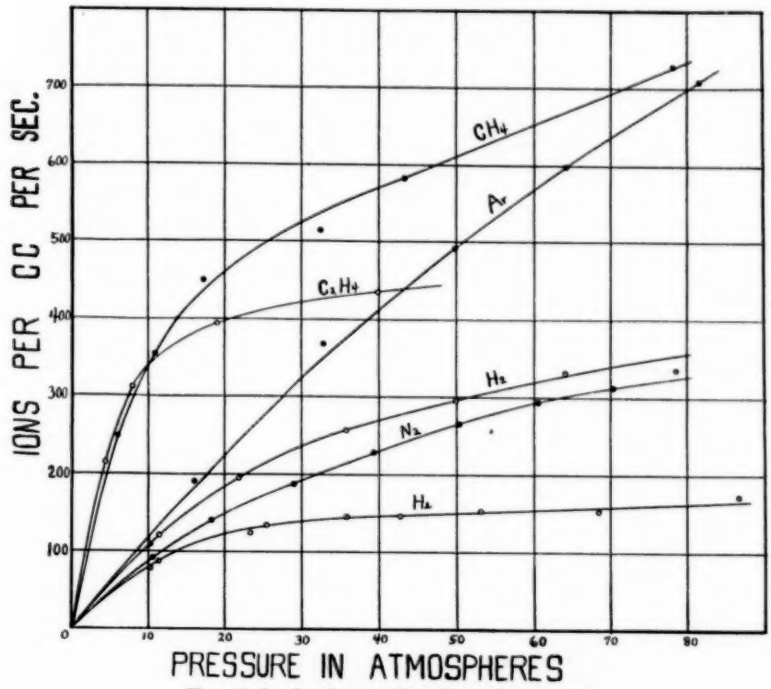

FIG. 2. Ionization as function of pressure.

different gases by the γ-rays from 10 milligrams of radium placed several meters from the chamber and filtered by 5 cm of lead. The ionization produced by the neutrons in H_2 is a little larger than that in N_2, while there is approximately four times as much ionization due to γ-rays in N_2 as in H_2. In the case of H_2, He, C_2H_4, and CH_4 the ratio of ionization currents, due to the neutrons, at 80 atmospheres to the currents at 10 atmospheres is less than that for γ-rays. Now when the ionization currents are not proportional to the pressure of the gas, it means that there is a lack of saturation. Since neutrons collide with atomic nuclei, which in turn produce ions in short thick tracks, we might expect these ions to recombine more easily and thus be harder to saturate. This agrees with the data for H_2, He, CH_4, and C_2H_4, but in A and N_2 it appears that it is slightly easier to saturate the ions produced by recoil atoms than those produced by γ-rays.

Since the neutron collides only with the nuclei of the atoms, a comparison of their sizes can be obtained. We have $I=k_1naAE/R$ where I denotes the number of ion pairs produced per unit time; n, the number of neutrons passing through the chamber per unit time; a, the number of atoms per cc in the chamber; A, the collision area between neutron and nucleus; E, the average energy given to the nucleus per collision; and R, the average energy spent in the production of a pair of ions by the recoil nucleus;—k_1 being a constant. In the case of a gas containing two different kinds of atoms $I=I_1+I_2$ where I_1 and I_2 are the ionizations due to the two different kinds of recoil atoms. In this case $I=k_1na_1A_1E_1/R+k_1na_2A_2E_2/R$. Since no data were available as to the average energy required to form an ion pair by the different recoil atoms in the six gases used, the average energy spent by an alpha-particle in producing an ion pair in each gas[3] was employed in these calculations.

If we assume that the collisions made with nuclei by neutrons are perfectly elastic, we have for a head-on collision $v=2MV/(m+M)$ where v is the velocity given to the nucleus; M, the mass of the neutron, which is taken to be 1.00 in these calculations; V, the original velocity of the neutron; and m, the mass of the nucleus. Thus the relative amounts of energy given to the various nuclei are $E_H=1.00$, $E_{He}=0.64$, $E_N=0.250$, $E_C=0.284$, and $E_A=0.095$. For col-

[3] Rutherford, Chadwick and Ellis, *Radiations from Radioactive Substances*, p. 82.

TABLE II. *Ionization due to neutrons.*

Gas	I	R_1	IR_1	I_1R_1	I_2R_2	$k\frac{I_1R_1}{a_1}$	$k\frac{I_2R_1}{a_2}$	Gas	E_1	A	Atomic No.	Atomic Weight
He	80.6	27.8	2240	2240	——	2240	——	N	0.250	3.5	7	14
H_2	106	33.0	3500	3500	——	1750	——	He	0.640	2.0	2	4
A	113	25.4	2870	2870	——	2870	——	H	1.00	1.0	1	1
CH_4	436	27.9	12200	7000	5200	1750	5200	A	0.095	17	18	40
C_2H_4	468	26.8	12600	7000	5600	1750	2800	C	0.284	8.0	6	12
N_2	87.1	35.0	3050	3050	——	1525	——					

I = ionization currents at 10 atmospheres (except for CH_4 and C_2H_4).
R_1 = average energy spent per ion pair for alpha-particles.
E_1 = relative energies given to nuclei.
a_1 = relative number of atoms of type 1 in chamber.
a_2 = relative number of atoms of type 2 in chamber.
A = relative collision area between neutron and nucleus.

lisions other than head on, the ratios of energy given to the various nuclei are the same as in the case of head-on collisions.

The values of the ionization I in Table II are those at 10 atmospheres where very nearly all the ions formed are drawn to the electrodes. But for CH_4 and C_2H_4 twice the value of I at 5 atmospheres is given instead. Table II gives these data on ionization and energies and the calculated value of the collision area A between the neutrons and nuclei. If we assume that the neutrons and nuclei are spherical we have

$$\pi(r_n+r_{He})^2/\pi(r_n+r_H)^2=2.0$$

and $(r_n+r_{He})/(r_n+r_H)=1.4$, where r_n is the radius of the neutron and r_{He} and r_H are respectively the radii of the helium and hydrogen nuclei. If the size of the neutron is small compared to that of the nuclei $r_{He}/r_H=1.4$, $r_N/r_H=1.9$, $r_C/r_H=2.8$, and $r_A/r_H=4.1$. The relative target areas $a_H=1.0$, $a_{He}=2.0$, $a_C=8.0$, $a_N=3.5$, and $a_A=17$ are roughly proportional to the atomic numbers. This suggests that the nucleus may be regarded as a group of separate protons and neutrons so that its target area is proportional to the number of protons it contains.

If we take the value 3.5×10^{-13} cm obtained by Chadwick[4] as the radius of the carbon nucleus, then we get for the radii of the nuclei $r_H=1.3\times10^{-13}$ cm, $r_{He}=1.8\times10^{-13}$ cm, $r_C=3.5\times10^{-13}$ cm, $r_N=2.4\times10^{-13}$ cm and $r_A=5.1\times10^{-13}$ cm. Although the neutron is probably considerably smaller than a proton, it seems worth while to consider what sizes are obtained for the nuclei if we assume that the radius of the neutron is equal to that of the proton. Using this hypothesis we get $r_H=0.76\times10^{-13}$ cm, $r_{He}=1.4\times10^{-13}$ cm, $r_N=2.1\times10^{-13}$ cm, $r_C=3.5\times10^{-13}$ cm, and $r_A=5.5\times10^{-13}$ cm.

I am endebted to Dr. L. M. Mott-Smith for the use of the ionization chamber used in these experiments. I also want to thank Professor F. J. Hodges of the University of Michigan Hospital, Mr. C. B. Braestrup of the New York City Cancer Institute, and The State Institute for the Study of Malignant Disease, Buffalo, N. Y., for their gifts of old radon tubes. My thanks are due to Professor H. A. Wilson for the interest he has taken in this work and for many valuable suggestions.

[4] J. Chadwick, Proc. Roy. Soc. **A136**, 703 (1932).

Elastic Electron Scattering in Neon

A. L. HUGHES* AND J. H. MCMILLEN, *Washington University, St. Louis, Missouri*

(Received April 13, 1933)

The *distribution in angle* of electrons having energies ranging from 10 to 800 volts scattered by *neon* atoms was measured over a range from 7° to 150°. For the higher energies, above 600 volts, the scattering curves fall monotonically with increasing angle. For smaller energies, an increase of scattering with increasing angle in the large angle region becomes more and more accentuated as the energy is reduced to 35 volts. Below this the curves flatten out. The position of the minimum in the scattering curves shifts steadily to smaller angles as the electron energy is increased. The *elastic cross section* obtained by integration of the scattering coefficient multiplied by the sine of the scattering angle is computed for electron energies between 10 volts and 800 volts, and is compared with direct absorption measurements. Mott's formula is inadequate to describe the scattering curves even at the highest voltage, a result in accordance with a criterion set up by Morse. The low-voltage curves can be fitted satisfactorily to a formula of the type developed theoretically by Allis and Morse.

INTRODUCTION

SEVERAL investigations on the elastic scattering of electrons by atoms of neon have been published in the last few years. Arnot[1] studied the elastic scattering, by neon atoms, of electrons having energies between 29 and 412 volts over a range from 10° to 120°. (Results were also given for 830 volt-electrons over a more limited angular range, 10° to 40°.) He found that the scattering fell off sharply with increasing angle up to a certain angle somewhere between 90° and 120° beyond which the scattering increased, especially for the lower electron energies. Bullard and Massey[2] investigated the scattering within the energy range 6 to 30 volts, and within the angular range 30° to 130°. Ramsauer and Kollath[3] devised an experimental method considerably different from that employed by other workers in the field to measure the scattering over the angular range 15° to 167° for electrons having energies between 0.61 and 15.9 volts. Recently Mohr and Nicoll[4] published a paper giving curves for the scattering of 50, 84, and 150 volt-electrons between 20° and 155°. The foregoing investigations were made over different angular ranges and different energy ranges. The agreement, when they overlap, is not always satisfactory. The present investigation was undertaken because it is desirable to have accurate experimental data, taken under identical conditions, over as wide a field as possible, in order to test quantitatively advances which are being made in the theoretical treatment of electron scattering.

APPARATUS AND METHOD

The apparatus is the same as that used in our recent work on helium but which was not described in the published paper.[5] In our earlier work on hydrogen and argon,[6] the apparatus was constructed of metal, made air-tight by sealing wax, and therefore could not be outgassed by heating. It was found that slow electrons (energies below about 50 volts) would not pass through narrow slits in such an apparatus, possibly because of adsorbed gases on surfaces near the slits. To permit some degree of outgassing by heating, the present apparatus (Fig. 1) was so designed that all of it could be enclosed in

* The investigation was made possible by assistance to the first named author from a grant made by the Rockefeller Foundation to Washington University for research in science.

[1] F. L. Arnot, Proc. Roy. Soc. **A133**, 615 (1931).

[2] E. C. Bullard and H. S. W. Massey, Proc. Roy. Soc. **A133**, 637 (1931).

[3] C. Ramsauer and R. Kollath, Ann. d. Physik **12**, 837 (1932).

[4] C. B. O. Mohr and F. H. Nicoll, Proc. Roy. Soc. **A138**, 469 (1932).

[5] A. L. Hughes, J. H. McMillen and G. M. Webb, Phys. Rev. **41**, 154 (1932).

[6] A. L. Hughes and J. H. McMillen, Phys. Rev. **39**, 585 (1932).

a glass tube 5.5 inches in diameter. A small electrostatic analyzer[7] containing the deflecting plates P and R (radius 19 and 21 mm) was made of Monel metal. Only those electrons travelling within a small angle with the normal to the slit S_1 could enter the analyzer and reach the collector E. This small angle was determined by the slit S_1 and the distance apart (2 mm) of the plates P and R. For most of the small angle scattering, increased resolution was secured by the addition of slit S_2, so that S_1 and S_2 now defined the angle of entry. The apparatus was erected on a flat

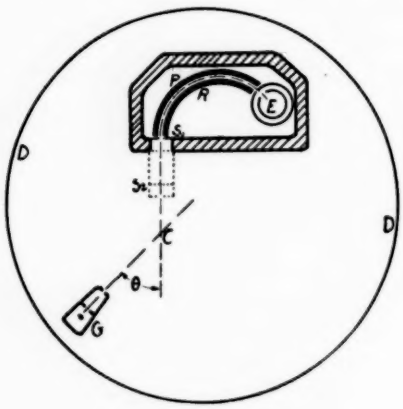

FIG. 1. Apparatus.

brass base plate through which all the necessary wire connections and gas, pump and gauge tubes passed. The electron gun G was rotated by means of a ground glass joint mounted in the base plate. To outgas the apparatus, a furnace was lowered over the glass tube and extended sufficiently far down to allow heating the analyzer and gun. The setting, θ, of the electron gun could be changed from 0° to ±150°. At very small angles, however, the results were unsatisfactory, partly because some of the electrons could pass straight into the analyzer from the gun. Another source of error in the scattering measurements at small angles arises from the fact that, though above a certain small angle, no primary electrons can pass directly from the gun into the analyzer, yet the finite angular width of the electron beam from the gun may cause it to straddle the slit S_2 and so prevent parts of the electron beam from contributing to the electrons scattered into the analyzer. For reasons such as these we do not consider that our apparatus measures satisfactorily the scattering at angles less than about 7°. (This was determined by measuring the width of the electron beam in a subsidiary experiment, in which the beam was swept across a fine slit and the number of electrons passing through it measured for different setting of the gun.)

For any given electron energy, scattering curves were obtained by taking observations at small angular intervals, usually 4° or 5°. To get the scattering coefficient, each observation was multiplied by $\sin\theta$ to correct for the change in length of the scattering path effective at the different angular settings. Then to make all the values strictly comparable with each other, the scattering coefficients were measured at one angle (30°) for all the electron energies selected for investigation. Thus the results for all angles and for all energies are given in terms of the same unit. It was not possible to make a satisfactory experimental determination of the absolute value of the scattering coefficient, although, in principle, this could be found from the geometry of the apparatus, nor could we follow the procedure we used in our helium paper.[8]

EXPERIMENTAL RESULTS

The scattering coefficients measured in this investigation are given in Table I. The results in all columns are strictly comparable with each other.

The scattering curves are shown in a series of separate figures (Figs. 2–6) as it would be too confusing to plot them all on the same diagram. The only curves which show a regular diminution in the scattering coefficient with increasing angle are those for 800 and 625 volts. For all the others

[7] A. L. Hughes and J. H. McMillen, Phys. Rev. **34**, 291 (1929); A. L. Hughes and V. Rojansky, Phys. Rev. **34**, 284 (1929).

[8] We found for helium that, when the electron energies exceeded 400 volts, the experimental curves fitted perfectly the theoretical curves given by Mott's theory. It was then *assumed* that Mott's theory not only gave the shape of the curve, but also its absolute magnitude. Since the relative values of the curves for all energies were measured, it was possible to compute their absolute values. Such a procedure was not possible for neon, since within the range of energies used by us, no agreement between an experimental curve and the corresponding theoretical curve could be found.

TABLE I. *Scattering coefficients for electrons scattered elastically by neon atoms (arbitrary units).*
θ = angle. V = energy of electrons in volts.

θ \ V	10	15	25	35	50	75	100	150	225	300	400	625	800
5.0°	..	..	..	..	(3827.0)	(6792.0)	(4695.0)	(6040.0)	(6855.0)	....	....	(5021.0)	....
7.5°	..	..	..	..	(2798.0)	(5330.0)	(4010.0)	(4640.0)	(4535.0)	(3158.0)	(4400.0)	(3610.0)	(3200.00)
10.0°	..	..	..	1423.5	(2363.0)	3782.0	3283.0	3358.0	3392.0	(2552.0)	(2958.0)	2560.0	1994.00
12.5°	..	..	..	1289.0	2161.0	2730.0	2539.0	2382.0	2385.0	1895.0	1957.5	1850.0	1301.00
15°	..	..	..	1198.0	1878.0	2341.0	2057.0	1977.0	1774.0	1491.0	1463.0	1424.0	918.00
20°	419.0	524.6	..	1044.0	1434.0	1720.0	1488.0	1345.0	1164.0	893.5	836.0	769.3	502.50
25°	417.0	535.0	863.0	910.0	1150.0	1273.0	1072.0	988.8	803.0	587.0	491.0	431.8	308.30
30°	414.0	524.0	731.0	800.0	951.0	956.2	796.6	682.1	514.4	401.2	298.8	250.3	187.20
35°	413.9	527.0	682.0	719.0	795.0	730.0	605.5	479.2	330.8	260.7	195.7	156.7	125.25
40°	428.0	533.0	636.0	664.0	675.0	566.3	506.6	351.0	243.7	160.8	140.6	108.4	87.08
45°	432.8	530.8	593.0		577.7	436.8	326.3	255.3	173.0	113.7	99.2	81.6	65.60
50°	432.8	526.4	570.5	566.5	468.5	359.0	240.6	189.3	128.6	88.8	69.7	64.2	52.81
55°	419.8	506.2	544.4		398.0	290.8	188.3	150.3	97.4	65.5	49.3	50.6	41.95
60°	407.8	498.3	515.5	474.0	344.2	245.5	151.6	116.3	76.3	50.8	41.0	38.7	34.27
70°	367.3	444.0	434.2	383.5	241.2	165.0	90.9	74.6	55.3	39.9	35.2	27.2	20.84
80°	307.7	360.0	344.8	292.0	177.3	96.6	47.4	49.8	47.4	32.9	29.3	23.8	15.44
90°	244.6	266.2	261.2	182.4	104.1	44.2	25.1	44.8	41.4	29.9	24.2	21.1	13.13
100°	184.7	193.0	181.4	118.2	63.3	28.1	24.5	46.4	42.2	28.6	21.2	18.2	11.24
110°	136.1	135.2	147.3	84.0	60.8	44.9	41.1	63.0	48.3	29.5	20.9	16.0	9.41
120°	101.9	103.8	144.2	127.8	107.4	102.4	74.7	88.3	55.3	31.5	20.3	13.6	8.10
130°	80.2	95.5	177.4	230.0	196.4	185.6	128.0	112.9	63.9	33.5	19.4	12.3	7.29
140°	75.4	110.5	306.8	347.0	288.9	283.0	187.7	138.0	73.2	41.6	19.2	11.3	6.65
150°	74.8	124.6	380.5	569.0	353.0	348.8	236.3	157.5	77.6	64.0	20.2	10.7	6.24

a more or less pronounced minimum develops in the region 90° to 135°. It will be noticed that relatively high values of small angle scattering persist down to 50 volts (Fig. 6), while below this value, the small angle scattering tends to become of the same order as that at much larger angles. The *increase* in the scattering coefficient with *increasing angle*, at large angles, first becomes clearly noticeable at 300 volts (Fig. 3) and becomes most marked at 35 volts (Fig. 5). For still smaller energies the curves in the large angle region flatten out once more. Attention is called to a definite, though small, maximum at 50° for 10 volt-electrons and one at 45° for 15 volt-electrons (Fig. 5). A hump on the 25, 35 and 50 volt curves in the vicinity of 70°, suggests the superposition of a maximum on a steeply falling curve (Fig. 5).

The position of the minimum shifts in a regular way with the primary energy of the electrons as shown in Fig. 7.

On comparing our results with those of previous investigators in the regions where they overlap, we find good agreement in several cases, poor in other cases. By "good agreement" is meant that, if two curves are fitted together at some arbitrary point, they do not deviate

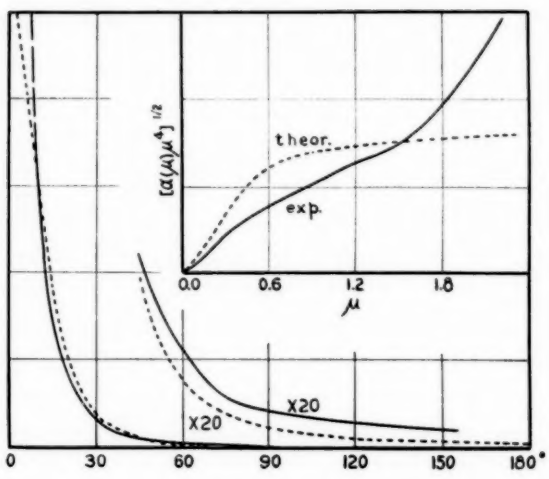

FIG. 2. Scattering of 800 volt-electrons: *continuous line*, experimental values; *broken line*, theoretical values. *Inset*. Comparison of the experimental and theoretical values of $[\alpha(\mu)\cdot\mu^4]^{\frac{1}{2}}$.

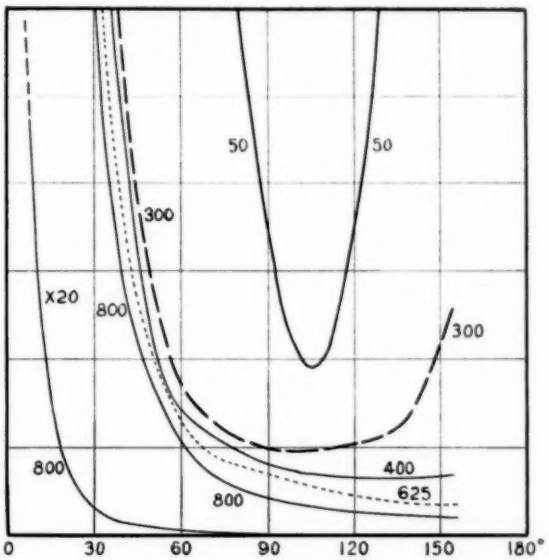

FIG. 3. Scattering of 800, 625, 400, 300 and 50 volt-electrons.

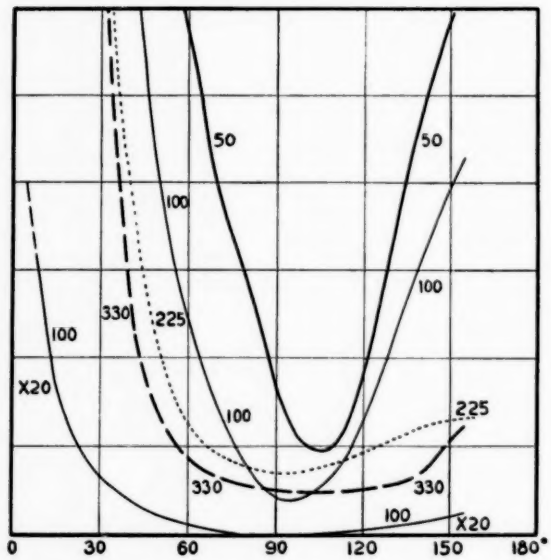

FIG. 4. Scattering of 300, 225, 100 and 50 volt-electrons.

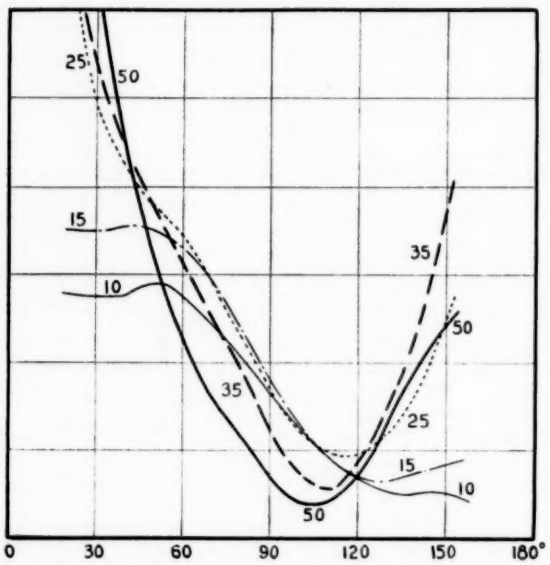

FIG. 5. Scattering of 50, 35, 25, 15 and 10 volt-electrons.

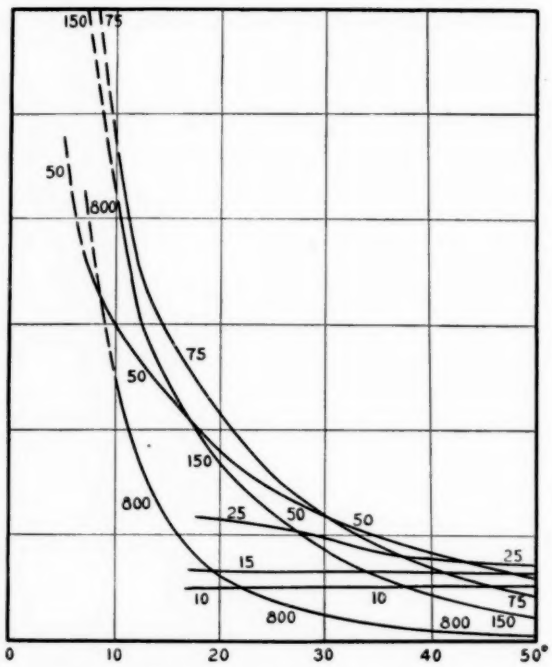

FIG. 6. Small angle scattering of 10 to 800 volt-electrons.

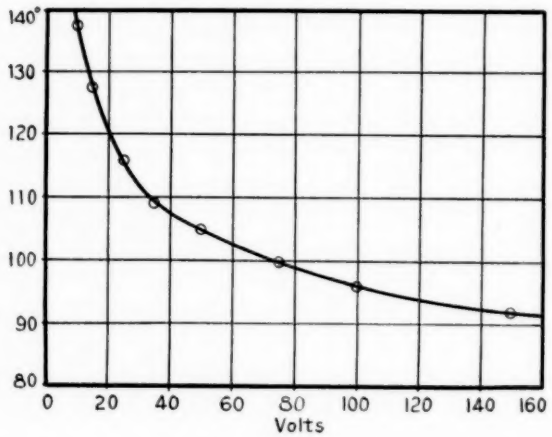

FIG. 7. Change in position of the minimum scattering with electron energy.

from each other anywhere by more than 10 percent. Our 10 volt curve shows good agreement with that of Bullard and Massey, but only fair agreement with that of Ramsauer and Kollath. The agreement between our 50 volt curve and that of Mohr and Nicoll is fair, that between our 150 volt curve and theirs is good. Our 50 volt curve agrees well with that of Arnot. We find only fair agreement between our 404 volt curve and his 412 volt curve.

DISCUSSION

The first approach to a theoretical treatment of the scattering of electrons by atoms is to suppose that the effect of the electrons within the atom on the incoming electron may be neglected. The problem then becomes one of the interaction between an electron of charge, $-e$, and a nucleus of charge, $+Ze$. This leads, as is well known, to a Rutherford scattering distribution, according to which the scattering coeffi-

cient is proportional to $\text{cosec}^4(\theta/2)$, where θ is the angle of scattering. Such a formula did not represent the experimental facts, and it became evident then that the modification in the interaction forces between the atomic electrons and the incoming electrons must be taken into account. The problem has been attacked from the point of view of wave mechanics by several investigators. The formulas given by Mott,[9] using a method first advanced by Born,[10] for the scattering coefficient of electrons, colliding elastically, are

$$\alpha(v, \theta) = [(e^2/2mv^2)(Z-F)\ \text{cosec}^2(\theta/2)]^2 \quad (1)$$

and

$$\alpha(\mu) = [(e^2m/2h^2)(Z-F)(1/\mu^2)]^2 \quad (2)$$

where e, m, and v are the charge, mass and velocity of the scattered electron, Z the atomic number of the atom, θ the angle of scattering, and $\mu = \sin(\theta/2)/\lambda$, where $\lambda = h/mv$. F, which is a function of μ, or of v and θ, is the atomic structure factor and measures the contribution of the atomic electrons to the scattering. Its value has been calculated by James and Brindley.[11] In Fig. 2, we have plotted the value of $\alpha(v, \theta)$ as given by Eq. (1) together with the experimental values. If we make the curves fit together at $\theta = 10°$, we see that the experimental curve is steeper than the theoretical curve at small angles ($<20°$) and less steep at large angles ($>40°$). This is precisely the kind of departure which occurs between the corresponding curves for the scattering by helium atoms when the speed is not high enough to give a perfect fit.[12]

The failure of Mott's theory to represent the scattering of 800 volt-electrons is shown more clearly in the following way. According to Eq. (2), $\mu^2[\alpha(\mu)]^{\frac{1}{2}}$ should, when plotted as a function of μ, give a graph of $Z-F$ and therefore of F. In the inset in Fig. 2, we have plotted $\mu^2[\alpha(\mu)_{exp.}]^{\frac{1}{2}}$ in arbitrary units, where $\alpha(\mu)_{exp.}$, the *experimental* scattering coefficient, is calculated from the 800 volt column in Table I. We have also plotted $Z-F$, using James and Brindley's values for F. It is evident that there is no similarity in shape between the theoretical and experimental curves. The conclusion to be drawn is that the simplifying assumptions made in deriving the above equations do not hold for collisions between neon atoms and electrons with energies as low as 800 volts. Morse[13] gives a curve for $Z-F$ for neon and shows that Arnot's scattering coefficients for 412 volt-electrons fit on it. The reason for this apparent agreement is that only a few points corresponding to small angle scattering were taken. On examining the inset in our Fig. 2, it will be seen that if we adjust the experimental curve to coincidence with the theoretical curve at $\mu = 0.7$, then the two curves will practically coincide for *all* values of μ less than 0.7, but will diverge tremendously for greater values. From $\mu = 0$ to $\mu = 0.45$ (on allowing for the fact that Morse's μ is 4π times ours) is just the limited region over which Morse found agreement between Arnot's results and theory. Morse[14] gives as a criterion of the minimum energy at which one would expect the formulas given in Eqs. (1) and (2) to hold, a value of 50 Z^2 volts. (This value comes from the fact that the approximations made in deriving the formula are satisfactory only when the distance of closest approach of the particle to the scattering center is much smaller than the wave-length associated with the electron.) For the inert gases this leads to the values in Table II.

TABLE II.

Gas	Z	$50Z^2$	Experimental
He	2	200 volts	>350 volts, <500 volts
Ne	10	5000 "	>800 volts
A	18	16,200 "	?

The results in the "Experimental" column for helium are taken from our previous paper, and those for neon, from this paper. It would be

[9] N. F. Mott, Proc. Roy. Soc. **A127**, 658 (1930).

[10] M. Born, Zeits. f. Physik **38**, 803 (1926).

[11] R. W. James and G. W. Brindley, Phil. Mag. **12**, 81 (1931). See also D. K. Froman, Phys. Rev. **36**, 1339 (1930).

[12] It is to be admitted that there is a certain degree of arbitrariness in selecting a point at some distance from either end of the experimental range for fitting the curves together. Had either end point been chosen, the curves would not have crossed a second time. In view of the trend observed in the comparison between the experimental and theoretical curve for helium, it was reasonable, however, to look for a similar trend in the neon curves.

[13] P. M. Morse, Rev. Mod. Phys. **4**, 597 (1932); Fig. 9.

[14] P. M. Morse, *Private communication.*

interesting to carry out experiments with neon up to 10,000 volts, to see if Morse's criterion holds also for this gas. Considerable modification in our apparatus would be necessary to enable us to use voltages higher than about 800. It is evident then that Mott's formula is not adequate to describe the scattering of electrons of energies of the order of 800 volts in neon.

The formulas given by the Born-Mott theory are approximate, because, in deriving them, it has been assumed that the waves representing the electrons are not distorted by the atomic field. Only when the electron wave is sufficiently short is the assumption justified by agreement between theory and experiment. This distortion of the electron wave is not neglected in another method used by Mensing,[15] Allis and Morse,[16] Faxen and Holtzmark.[17] The method is similar to that used by Mie and Debye[18] in the problem of the scattering of ordinary light waves by very small particles, where the distribution in angle of the scattered light contains maxima and minima which move in towards small angles as the wave-length is diminished. Allis and Morse find that the angular distribution of the scattered electrons is given by the expression

$$\frac{d\omega}{k^2}\sum_{\lambda,\,\lambda'=0}^{\infty}(2\lambda+1)(2\lambda'+1)P_\lambda(\cos\theta)P_{\lambda'}(\cos\theta)\sin\gamma_\lambda\sin\gamma_{\lambda'}\cos(\gamma_\lambda-\gamma_{\lambda'}),$$

where $d\omega$ is the solid angle, θ the angle of scattering, k^2 is the kinetic energy of the electrons, λ and λ' are integers, the P's are Legendre polynomials, and the γ's are certain angles. These angles, γ_λ and $\gamma_{\lambda'}$, are the shifts in phase of the wave representing the electron when in the field of force of the atom. The above expression is exact as it stands. Before anything can be done with it, however, the γ's must be calculated for a given electron wave-length and for the potential field representing the atom. This is where an approximation has to be made, for the calculation has been carried out only for very simple types of field. Morse calculates the γ's for the case of an atom represented by a nucleus Ze surrounded by a spherical shell of charge $-Ze$ and having a radius r_0. On inserting these into the formula, it is possible to compute the scattering coefficients for various angles and for various electron energies. The results, however, do not agree with our experimental values. We therefore attempted to use the expression as an empirical formula for electron scattering. Expanding the formula as far as the first three terms, we get, for the scattering, a quantity proportional to

$$(1/v^2)(\sin^2\gamma_0+6\cos\theta\sin\gamma_1\sin\gamma_0\cos(\gamma_1-\gamma_0)+9\cos^2\theta\sin^2\gamma_1)$$

where v is the velocity of the particle. The γ's were determined, for each velocity, from the scattering at two arbitrarily chosen angles. Then with the γ's so determined (Fig. 8*A*) the complete curves were computed by means of the above expression. The results are shown in Fig. 8. It will be seen that, if we ignore the small angle scattering ($<30°$), the agreement between the experimental and theoretical curves is fairly good. The curves shown in Fig. 8 are all plotted on the same scale, i.e., the experimental and theoretical curves have not been separately fitted together in each of the plots *C*, *D* and *E*, except insofar as the γ's in plot *A* are determined for each electron speed at some arbitrarily chosen angle. (Mohr and Nicoll[4] have already shown that certain large angle scattering curves resemble in shape some of the Legendre coefficients.)

Massey and Mohr[19] have developed a theory of electron scattering in which the distortion of the electron wave by the atom and electron exchange are taken into account. Unfortunately they have

[15] L. Mensing, Zeits. f. Physik **45**, 603 (1927).

[16] W. P. Allis and P. M. Morse, Zeits. f. Physik **70**, 567 (1931); see also P. M. Morse, Rev. Mod. Phys. **4**, 578 (1932).

[17] H. Faxen and J. Holtzmark, Zeits. f. Physik **45**, 307 (1927).

[18] See M. Born, *Optik*, p. 275 (Springer, 1933).

[19] H. S. W. Massey and C. B. O. Mohr, Proc. Roy. Soc. **A136**, 289 (1932).

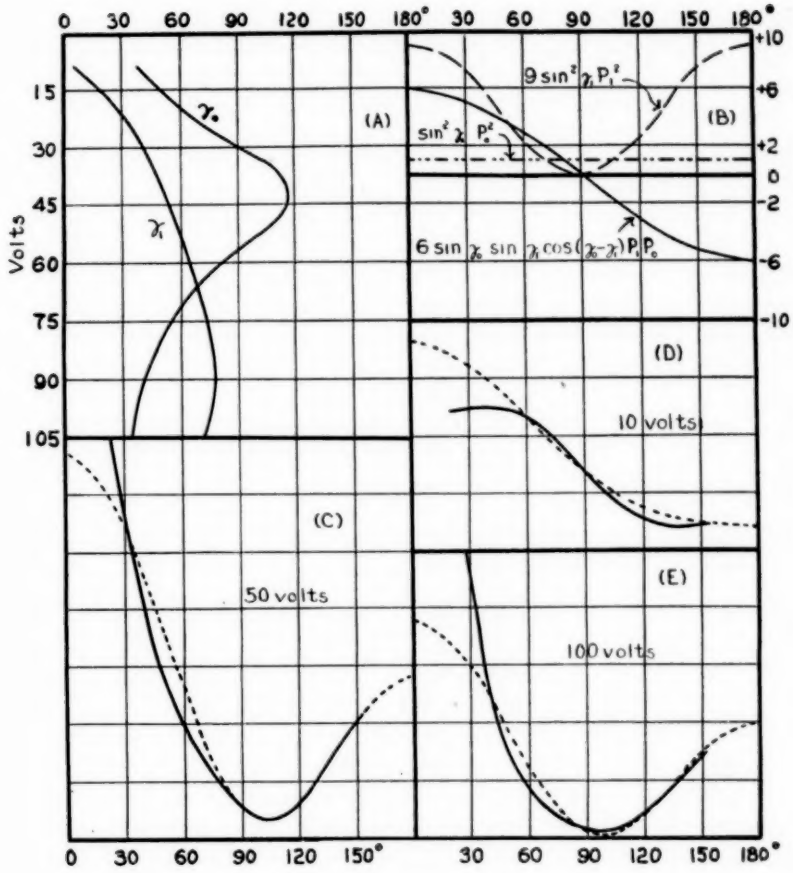

FIG. 8. Comparison of experimental with theoretical scattering curves: *A*, phase angles, γ_0 and γ_1. *B*, Legendre coefficients. *C*, *D* and *E*, *continuous lines*, experimental values for 10, 50 and 100 volt-electrons; *broken lines*, theoretical values.

not computed numerical results for neon which could be checked by our experimental values.

The absorption coefficient of a gas for electrons is frequently interpreted in terms of the "cross section" of the atom for interception of the electrons. If a single atom be placed on an area 1 cm², and if that area be bombarded by a beam of electrons uniformly distributed over the area, then the ratio of the number of electrons diverted from the original direction to the total number measures the cross section of the atom. (Another type of cross section would involve, in addition, the number of electrons losing speed but not changing direction on passing through the atom. This does not concern us here.) The cross section includes the "elastic cross section" and the "inelastic cross section." The former refers to the number of electrons diverted from the beam without loss of energy, while the latter refers to those diverted and losing energy. It is possible to use our scattering curves to compute the elastic cross section. Since the number of electrons scattered down a solid angle $d\omega$ is proportional to $d\omega \cdot \alpha(v, \theta)$, by the definition of the scattering coefficient $\alpha(v, \theta)$, then the number deviated from the main beam of electrons, through an angle larger than a certain small angle $\delta\theta$, by elastic scattering, is proportional to

$$\int_{\delta\theta}^{2\pi} \alpha(v, \theta) \cdot 2\pi \sin\theta d\theta.$$

This integral can be evaluated graphically from the values given in Table I after each value is properly multiplied by $\sin\theta$. According to theory, the value of $\alpha(v, \theta) \cdot \sin\theta$ goes to zero, as θ

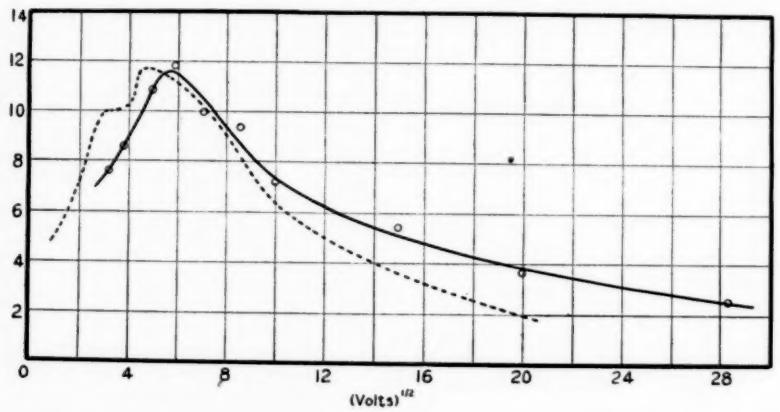

FIG. 9. Elastic cross section. *Continuous lines*, experimental values; *broken line*, calculated from Normand and Smith's results.

changes from a small angle to zero angle. This tendency was very evident in our curves, even though the smallest angles at which measurements were made was usually 7°. Consequently an obvious extrapolation of our curves to $\theta=0°$ gives us the total number of electrons scattered between the extreme limits $\theta=0°$ and $\theta=180°$. It is believed that the elastic cross section, so computed, is more accurate than any values which can be inferred from direct measurements of absorption of electrons in gases, for it has been found[20] that the total cross section depends considerably on the geometry of the apparatus, which is another way of saying that the effective minimum angle, $\delta\theta$, through which the electrons must be deviated in order to be counted, is not small enough to have no effect on the measured cross section. The elastic cross sections so calculated for different energies are plotted as a heavy line in Fig. 9. A comparison with direct measurements of the absorption coefficient can be made in this way. Normand[21] measured the absorption coefficient for electrons in neon, which gives us the total cross section. If we make the assumption that the inelastic cross section is accounted for chiefly by collisions resulting in ionization, thus neglecting the inelastic collisions resulting in excitation, then, on subtracting the ionization yield from the total absorption, both in the proper units, we should get a quantity proportional to the elastic cross section. Smith[22] has determined the ionization yield. The dotted curve is that obtained by subtracting the ionization yield from the total absorption. It will be seen that there is fairly satisfactory agreement between the shape of the elastic cross-section curve determined by the proper integration of the elastic scattering coefficients and that obtained from total absorption and ionization experiments. The nature of the deviation between the two is accounted for qualitatively when we remember that, as the energy of the electrons is diminished, the relative number of inelastic excitation collisions increases. This is the factor which was left out of consideration in computing the dotted curve, as we have no quantitative data available as to the relative number of collisions leading to excitation.

[20] R. R. Palmer, Phys. Rev. **37**, 70 (1931).

[21] C. E. Normand, Phys. Rev. **35**, 1217 (1930).

[22] P. T. Smith, Phys. Rev. **36**, 1293 (1930).

The Infrared Absorption Bands of Acetylene

G. B. B. M. SUTHERLAND, *Trinity College, Cambridge, England**

(Received March 30, 1933)

The present interpretations of the overtone bands in the infrared spectrum of acetylene are unsatisfactory in that they either do not fulfill the known selection rules or else fail to give satisfactory numerical agreement between calculated and observed band positions. A new arrangement of the complete infrared spectrum of acetylene is given which is in accord with the selection rules and yields consistent numerical results. Several of the anharmonic and interaction constants are thus determined for the five fundamental frequencies. It is remarked that there is probably a direct connection between the magnitudes of these anharmonic constants and the intensities of the overtone bands.

IT has been known for some time that the form of the acetylene molecule is linear and symmetrical. This was proved by the work of Levin and Meyer[1] and of Mecke and others[2] on its infrared absorption bands. Such being the case, it must possess five fundamental frequencies and it should be possible to interpret all of the observed infrared bands in terms of the allowed overtone and combination bands of these five fundamentals, the physical character of which is illustrated in Fig. 1. Several attempts have now

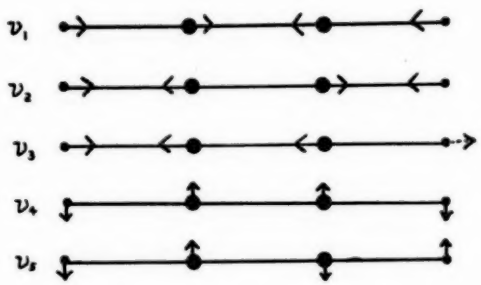

FIG. 1.

been made to do this,[3] but none of them can be regarded as satisfactory. Those of Mecke, and of Lueg and Hedfield may be immediately disregarded since the selection rules given by Dennison[4] are fulfilled by neither of them, while that of Lochte-Holtgreven and Eastwood leads to flagrant discrepancies between the observed and calculated values of several combination frequencies.

There is actually little doubt about the assignment of the five fundamental frequencies; these have been given their approximate values by Mecke, *viz.*

$$\nu_1 = 1975\ \text{cm}^{-1}, \quad \nu_2 = 3370\ \text{cm}^{-1}, \quad \nu_3 = 3277\ \text{cm}^{-1},$$
$$\nu_4 = 729\ \text{cm}^{-1}, \quad \nu_5 = 600\ \text{cm}^{-1},$$

and we need not go into the arguments which show that this is the only possible choice. The difficulty comes in combining those to yield the other observed frequencies while conforming with Dennison's selection rules. The latter are given in Table I where n_3, n_4, n_5 are quantum numbers (taking any integral values) in the general expression for an overtone or combination band, *viz.*

$$\nu = n_1\nu_1 + n_2\nu_2 + n_3\nu_3 + n_4\nu_4 + n_5\nu_5.$$

TABLE I. *Dennison's selection rules.*

	Parallel Bands		Perpendicular Bands	
n_3	odd	even	even	odd
n_4	even	odd	odd	even
n_5	even	odd	even	odd

* Commonwealth Fund Fellow at the University of Michigan.

[1] Levin and Meyer, J. Opt. Soc. Am. **16**, 137 (1928).

[2] Childs and Mecke, Zeits. f. Physik **64**, 162 (1930); Hedfield and Mecke, Zeits. f. Physik **64**, 151 (1930); Mecke, Zeits. f. Physik **64**, 173 (1930).

[3] Mecke, Zeits. f. physik. Chemie **B17**, 1 (1932); Hedfield and Lueg, Zeits. f. Physik **77**, 446 (1932); Lochte-Holtgreven and Eastwood, Zeits. f. Physik **79**, 450 (1932).

[4] Dennison, Rev. Mod. Phys. **3**, 280 (1931).

TABLE II. *Observed bands and interpretations.*

Frequency observed (cm^{-1})	Arrangement		
	Mecke	Hedfield and Lueg	Lochte-Holgreven and Eastwood
730	ν_4	ν_4	ν_4
1326	$\nu_4+\nu_5$	$\nu_4+\nu_5$	$\nu_4+\nu_5$
2643	$\nu_2-\nu_4$	$\nu_2-\nu_4$	$\nu_2-\nu_4$
2670	$\nu_3-\nu_5$	$\nu_3-\nu_5$	$\nu_3-\nu_5$
2683	?	?	?
2702	$\nu_1+\nu_4$	$\nu_1+\nu_4$	$\nu_1+\nu_4$
3288	ν_3	ν_3	ν_3
3898	$\nu_3+\nu_5$	$\nu_3+\nu_5$	$\nu_3+\nu_5$
4092	$\nu_2+\nu_4$	$\nu_2+\nu_4$	$\nu_2+\nu_4$
4690	$\nu_2+\nu_4+\nu_5$	$\nu_2+\nu_4+\nu_5$	$\nu_2+\nu_4+\nu_5$
5250	$\nu_3+\nu_1$	$\nu_3+\nu_1$	$\nu_3+\nu_1$
6500	$\nu_3+\nu_2$	$2\nu_3$	$\nu_3+\nu_2$
8450	$\nu_1+\nu_2+\nu_3$	$\nu_1+\nu_2+\nu_3$	$\nu_1+\nu_2+\nu_3$
9641	$3\nu_3$	$3\nu_3$	$3\nu_3$
9835	—	$3\nu_3$ "ohne verstimmung"	$\nu_3+2\nu_2$
10400	—	$2\nu_3+2\nu_1$	$2\nu_3+2\nu_1$
11599	$3\nu_3+\nu_1$	$3\nu_3+\nu_1$	$3\nu_3+\nu_1$
11783	—	$4\nu_3-\nu_4$	$\nu_3+3\nu_2$
12676	$4\nu_3$	$4\nu_3$	$3\nu_3+\nu_2$
15600	—	$5\nu_3$	$3\nu_3+2\nu_2$
18430	—	$6\nu_3$	$3\nu_3+3\nu_2$

The observed bands together with the existing interpretations of them are given in Table II. Of these bands the positions of the last eight are known with great accuracy, since these have been observed photographically under very high dispersion.[5] The positions of the preceding four are not known with any accuracy, while the first nine are correct to within about one wave number.

Since the appearance of overtone and combination bands is due to an anharmonicity in the vibrational motions of the molecule the simple formula

$$\nu = n_1\nu_1+n_2\nu_2+n_3\nu_3+n_4\nu_4+n_5\nu_5$$

will only give the positions of the bands very approximately and to obtain accuracy we must introduce anharmonic correction terms depending on the second powers of the quantum numbers. Thus we write

$$\nu = n_1\nu_1+n_2\nu_2+n_3\nu_3+n_4\nu_4+n_5\nu_5+x_{11}n_1^2 + x_{22}n_2^2+x_{33}n_3^2+x_{44}n_4^2+x_{55}n_5^2+x_{12}n_1n_2 + x_{13}n_1n_3+\cdots+x_{45}n_4n_5$$

and the observed fundamentals are no longer ν_1, ν_2, ν_3, ν_4 and ν_5 but ν_1+x_{11}, ν_2+x_{22}, etc. If now there exists a series of combination bands of, say, the two fundamental frequencies ν_2 and ν_3, then three of those will be sufficient to determine x_{22}, x_{33} and x_{23}; the positions of the others may then be predicted with great accuracy and the resulting agreement forms a test of the correctness of the assignment. This was the method employed by Lochte-Holtgreven and Eastwood whose results are summarized in Table III. The agreement between calculated and observed values is seen to be most unsatisfactory. It will now be shown that an alternative arrangement of the bands exists which yields very consistent results.

TABLE III. *Results of Lochte-Holtgreven and Eastwood.*

$\nu_2 = 3285n_2-56n_2^2$; $\nu_3 = 3308.4n_3-31.6n_3^2$; $x_{23} = -65.6\ cm^{-1}$

	$\nu_3+\nu_2$	$\nu_3+2\nu_2$	$\nu_3+3\nu_2$	$3\nu_3+\nu_2$	$3\nu_3+2\nu_2$	$3\nu_3+3\nu_2$
Frequency						
Calculated	6440	9492	12,431	12,673	15,593	18,401
Observed	6500	9835	11,782	12,675	15,600	18,430

The essential point in this new interpretation is that the very strong band at 9641 cm^{-1} is no longer taken to be $3\nu_3$ but to be $\nu_3+2\nu_2$. While this may seem surprising at first sight the arguments for such an assignment are very strong for in addition to yielding consistent values for the anharmonic constants it explains several qualitative features which seemed rather puzzling on the old interpretation. For instance, it seemed surprising that if $3\nu_3$ (i.e., 9641 cm^{-1}) were so intense, no sign of $5\nu_3$ should be observed, but on the new arrangement $3\nu_3$ (i.e., 9835 cm^{-1}) is already a weak band and so one would not expect $5\nu_3$ to be observed. Again if $3\nu_3$ is an intense band one would expect to find signs of $3\nu_3+\nu_5$ since $\nu_3+\nu_5$ is quite a strong band (cf. $\nu_3+\nu_1$ and $3\nu_3+\nu_1$ which appear on either assignment). This is fulfilled by the new, but by none of the old arrangements. Another satis-

[5] Lueg and Hedfield, reference 3.

TABLE IV. *New assignments of bands.*

$\nu_1 = 1974$ cm^{-1}; $\nu_2 = 3372$ cm^{-1}; $\nu_3 = 3288$ cm^{-1}; $\nu_4 = 730$ cm^{-1}; $\nu_5 = 605$ cm^{-1}.

Frequency observed cm^{-1}	Character† observed	Character predicted	Assignment	Frequency predicted cm^{-1}
730	Perpendicular	Perpendicular	ν_4	—
1326	Parallel	Parallel	$\nu_4+\nu_5$	—
2643	Perpendicular	Perpendicular	$\nu_2-\nu_4$	2642
2670	?	—	Overlapping bands	—
2683	Perpendicular	Perpendicular	$\nu_3-\nu_5$	—
2702	"	"	$\nu_1+\nu_4$	—
3288	Parallel	Parallel	ν_3	—
3882	Perpendicular	Perpendicular	$\nu_3+\nu_5$	3880
3910	Parallel (?)	Parallel	$3\nu_4+3\nu_5$	—
4092	Perpendicular	Perpendicular	$\nu_2+\nu_4$	—
4690	?	Parallel	$\nu_2+\nu_4+\nu_5$	—
5250	?	"	$\nu_3+\nu_1$	5253
6500	?	"	$\nu_3+\nu_2$	6513
8450	?	"	$\nu_3+\nu_2+\nu_1$	8435
9641*	Parallel V.S.	"	$\nu_3+2\nu_2$	9641
9835*	" S.	"	$3\nu_3$	9835
10,400*	? V.W.	Perpendicular	$3\nu_3+\nu_5$	10,400
11,599*	Parallel S.	Parallel	$\nu_3+2\nu_2+\nu_1$	11,599
11,783*	" M.	"	$3\nu_3+\nu_1$	11,783
12,676	" S.	"	$\nu_3+3\nu_2$	12,668
15,600	" M.	"	$\nu_3+4\nu_2$	15,598
18,430*	" M.	"	$\nu_3+5\nu_2$	18,430

* Abbreviations for intensity of photographed overtones: V.S. = very strong, S. = strong, M. = medium, V.W. = very weak.

† A "perpendicular" band possesses a Q branch while a "parallel" band possesses no Q branch.

factory feature of the new arrangement is that it explains the very weak band at 10,400 cm^{-1} which seemed to contradict Dennison's selection rules even in Lochte-Holtgreven and Eastwood's arrangement. It is unfortunate that its extreme weakness seems to have prevented even a determination of the general character of this band.

Table IV gives the new assignment. The experimental values are taken from Levin and Meyer (for the first nine frequencies), from Mecke (for the next four) and from Hedfield and Lueg (for the last eight). The values for the frequencies ν_1 and ν_2 are taken from the measurements of Bhagavantam[6] on the Raman spectrum of the gas; these are probably correct to within less than 2 cm^{-1}.

Six frequencies (marked with an asterisk) were required to determine the anharmonic constants x_{12}, x_{13}, x_{22}, x_{23}, x_{33} and x_{35} giving the values

$$x_{12} = -3 \text{ cm}^{-1}, \qquad x_{23} = -146.8 \text{ cm}^{-1},$$
$$x_{13} = -9 \text{ cm}^{-1}, \qquad x_{33} = -5 \text{ cm}^{-1},$$
$$x_{22} = -49.2 \text{ cm}^{-1}, \qquad x_{35} = -13 \text{ cm}^{-1}.$$

These constants then permitted a calculation of the positions of six other bands formed by combinations of the fundamentals ν_1, ν_2, ν_3 and ν_5. The agreement between calculated and observed positions is very satisfactory, considering the uncertainty with which some of the bands are known[7] and the assumptions involved in such a calculation. It is interesting to notice the variations in magnitude of these constants. The fact that x_{23} and x_{22} are so large compared with the others is in accordance with the observed intensity of the series of overtones $\nu_3+\nu_2$, $\nu_3+2\nu_2$, $\nu_3+3\nu_2$, $\nu_3+4\nu_2$ and $\nu_3+5\nu_2$. A similar phenomenon has been found by Adel and Dennison[8] in the overtone bands of carbon dioxide.

As regards the bands between 1300 cm^{-1} and 5000 cm^{-1} some modifications of Mecke's arrangement are proposed. The difference band

[6] Bhagavantam, Indian J. Phys. **6**, 319 (1931).

[7] It is important that the bands at 6500 cm^{-1} and 8450 cm^{-1} be reexamined under high dispersion as a confirmation of the above assignments. Professor Imes of Fisk University informs me that he intends to undertake this work very shortly.

[8] Adel and Dennison, Phys. Rev. **43**, 716 (1933).

$\nu_3-\nu_5$ is associated with the frequency 2683 cm^{-1} instead of 2670 cm^{-1} yielding an accurate value for ν_5 of 605 cm^{-1}. When this is used along with the value of x_{35} determined from the band at 10,400 cm^{-1} to predict the position of the band $\nu_3+\nu_5$ we obtain a calculated value of 3880 cm^{-1}. This seems to fit the weak maximum observed at 3882 cm^{-1} much better than the strong one at 3898 cm^{-1}. Accordingly we take the latter to be the P branch of a parallel band with center at 3910 cm^{-1} and interpret it as $3\nu_4+3\nu_5$. The anomalously high intensity of the P branch is probably due to its having superimposed on it the R branch of the 3882 cm^{-1} band. The fact that, in the corresponding band at 1326 cm^{-1}, due to $\nu_4+\nu_5$ the convergence was in the P rather than the R branch, is important since a slight exaggeration of this effect in the "overtone" at $3\nu_4+3\nu_5$ would also tend to make the unresolved P branch appear stronger than the R branch.[9] If Mecke's assignment is correct then the accurate value of ν_5 is 618 cm^{-1} and the calculated position of $\nu_3+\nu_5$ is 3888 cm^{-1} (with $x_{35}=-18$ cm^{-1}). Since this seems to agree with neither of the maxima we would have to assume that the interpretation of the band at 10,400 cm^{-1} as $3\nu_3+\nu_5$ is wrong. A careful reexamination of the bands at 2670 cm^{-1}, 2683 cm^{-1}, 3882 cm^{-1}, 3898 cm^{-1} and 10,400 cm^{-1} would be very desirable in order to discriminate between these assignments.

Some of the other interaction constants may be determined from the remaining bands. Thus we obtain;

$$\text{from that} \quad \begin{aligned} \nu_4+\nu_5 \quad & x_{45}=-9\ cm^{-1}, \\ \nu_4+\nu_1 \quad & x_{14}=-2\ cm^{-1}, \\ \nu_4+\nu_2 \quad & x_{24}=-10\ cm^{-1}, \\ \nu_4+\nu_2+\nu_5 \quad & x_{25}=+2\ cm^{-1}. \end{aligned}$$

These values cannot be verified until more bands have been observed, the positions of which depend on them, but (with the exception of x_{25}) we may assume that the error is not more than one or two wave numbers. To determine x_{25} with this accuracy the position of the band at 4690 cm^{-1} requires to be known with a corresponding accuracy.

While the correct assignment of the overtone and combination bands in an infrared spectrum such as that of acetylene is of considerable interest as a verification of theoretical selection rules the question arises whether it will lead to further results of importance. We feel that this is the case since it allows a determination of the anharmonic constants x_{ij} which describe the behavior of the potential energy for amplitudes of vibration which are not infinitesimally small. It seems quite probable that these will prove to be of major importance in eventually furnishing the molecule with a potential function valid over a large range of the coordinates. Some progress has already been made in this direction by Adel and Dennison[9] in their study of the carbon dioxide molecule. The acetylene molecule being somewhat more complex, the necessary analysis has not as yet been made. One qualitative feature has already appeared however, for, as we have pointed out, there exists a direct connection between the magnitude of the anharmonic constants and the intensities of the combination bands.

I would gratefully acknowledge the benefit of much helpful discussion of this problem with Professor D. M. Dennison. I am also indebted to him and to Mr. Adel for permission to use their results on carbon dioxide before publication.

[9] Cf. *The Infrared Spectrum of Carbon Dioxide, Part II* by Adel and Dennison (to appear shortly in The Physical Review) where it is shown that, when no resonance degeneracy exists, the factor giving the convergence of the rotation lines in a fundamental band has to be multiplied by three for the convergence in the second overtone.

Hyperfine Structure and the Polarization of Resonance Radiation. II. Magnetic Depolarization and the Determination of Mean Lives

ALLAN C. G. MITCHELL, *Department of Physics, New York University, University Heights*

(Received April 3, 1933)

Breit has derived formulae giving the polarization $P(H)$ and the angle of maximum polarization θ of a resonance line showing hyperfine structure, as a function of a weak magnetic field applied in the direction of observation of the resonance radiation. The formulae give a means of estimating the effect of hyperfine structure on the calculation of the mean life τ of an excited atom from experiments on the magnetic depolarization and rotation of the plane of polarization of resonance radiation. The calculation has been carried through for the case of the resonance line of Cd(λ3261) and that of Hg(λ2537), and it is found that the differences between the value of τ calculated from hyperfine structure data and that calculated from $\tan 2\theta$ by the usual non-hyperfine structure method lie well within the experimental error. $P(H)/P_0$ is found to be practically the same whether hyperfine structure is taken into account or neglected. This is due to the fact that the greatest contribution of the polarization in these cases comes from the isotopes having no nuclear spin and the g-value for the upper state of these isotopes is larger than any other upper hyperfine structure state involved. The mean lives of the 7^3S_1 state of mercury have been recalculated from Richter's data on the polarization of stepwise radiation. The values of τ obtained by this method of calculation are 7.2×10^{-9} for λ4047, 1.69×10^{-8} for λ4358 and 1.53×10^{-8} for λ5461. A discussion of Richter's results is given.

INTRODUCTION

RECENTLY, the writer[1] has given a general method for the calculation of the polarization to be expected for any resonance or fluorescence line showing *hfs*[2] if the *hfs* of the line in question is known. Breit[3] has derived expressions for the polarization, $P(H)$, in weak magnetic fields, oriented along the direction of observation, as a function of the field, and also for the angle of maximum polarization θ. It is the purpose of this paper to carry through the calculation for certain resonance and fluorescence lines and to compare the results with the observed experimental data. Since the expressions for $P(H)$ and θ contain the mean life, τ, of the excited state giving rise to the radiation as a parameter, this quantity may be calculated.

In making the calculation for a line showing *hfs* one must make use of quantities related to the polarization of the line in zero magnetic field discussed in I. Consider an element consisting of various isotopes α, of nuclear spin i_a and relative abundance N_a. Let the lowest gross state of such an isotope be denoted by a, having a quantum number j_a and various hyperfine levels f. By absorption of radiation of a suitable frequency from an exciting arc, atoms are raised to various hyperfine levels φ of an upper state b having a quantum number j_b. Atoms may return to a by the emission of resonance radiation ab or to another state $c(h, j_c)$ by the emission of line fluorescence (bc). (See Fig. 1 of I.)

Suppose that the resonance tube, containing the gas to be investigated, is situated at the origin of a rectangular coordinate system in which the exciting light is progressing along the Y-axis and the direction of observation is along the Z-axis. Let a magnetic field of strength H be placed anywhere in the XY plane such that the angle between the electric vector of the exciting light and the field is Θ. The chance of reaching a magnetic sublevel μ of φ by the absorption of a suitable *hfs* component of the line ab is therefore

$$\frac{CN_aI_\nu}{(2j_a+1)(2i_a+1)}\left[A_\pi^{\varphi\mu a}(a)\cos^2\Theta+\tfrac{1}{2}A_\sigma^{\varphi\mu a}(a)\sin^2\Theta\right], \qquad (1)$$

[1] A. C. G. Mitchell, Phys. Rev. **40**, 964 (1932). Hereafter referred to as I. See this paper for references to calculations by other authors.

[2] The term hyperfine structure will be designated by *hfs*.

[3] G. Breit, Rev. Mod. Phys. **5**, 91 (1933).

where $A_\pi^{\varphi\mu\alpha}(a)$ is the transition probability for a π component between the magnetic sublevels $\mu(\varphi, j_b)$ and $m'(f, j_a)$ of the lower state (equivalent to γ of I); and $A_\sigma^{\varphi\mu\alpha}(a)$ is the sum of σ transition probabilities from $\mu(\varphi, j_b)$ to $j_a(\Gamma$ of I). The quantity $(2j_a+1)$, being the same for all *hfs* components of a given line, may be absorbed into the constant C as may also I_ν if we limit our considerations to exciting sources in which all *hfs* components have equal intensity (broad line source). If $X(\varphi\alpha)$ and $Y(\varphi\alpha)$ are the contributions to the intensity of the line bc, from the level φ, which are polarized along and perpendicular to the field, respectively, we have

$$\left.\begin{aligned} X(\varphi\alpha) &= \frac{CN_\alpha}{(2i_\alpha+1)} \sum_\mu \frac{A_\pi^{\varphi\mu\alpha}(c)}{A_\pi^{\varphi\mu\alpha}(c)+A_\sigma^{\varphi\mu\alpha}(c)} [A_\pi^{\varphi\mu\alpha}(a)\cos^2\Theta+\tfrac{1}{2}A_\sigma^{\varphi\mu\alpha}(a)\sin^2\Theta], \\ Y(\varphi\alpha) &= \frac{1}{2}\cdot\frac{CN_\alpha}{(2i_\alpha+1)} \sum_\mu \frac{A_\sigma^{\varphi\mu\alpha}(c)}{A_\pi^{\varphi\mu\alpha}(c)+A_\sigma^{\varphi\mu\alpha}(c)} [A_\pi^{\varphi\mu\alpha}(a)\cos^2\Theta+\tfrac{1}{2}A_\sigma^{\varphi\mu\alpha}(a)\sin^2\Theta], \end{aligned}\right\} \quad (2)$$

where $A_\pi^{\varphi\mu\alpha}(c)$, $A_\sigma^{\varphi\mu\alpha}(c)$ are the sums of the transition probabilities from the magnetic sublevel $\mu(\varphi, j_b)$ to all $m'''(h, j_c)$ for π and σ components, respectively.

Let us denote the contribution to the polarization of the line bc from the hyperfine level φ by $P(\varphi, \alpha)$ defined by the relation

$$P(\varphi\alpha) = \frac{X(\varphi\alpha)-Y(\varphi\alpha)}{\sum_\alpha\sum_\varphi (X(\varphi\alpha)+Y(\varphi\alpha))}. \quad (3)$$

The total polarization of the line will then be given by

$$P = \sum_\alpha \sum_\varphi P(\varphi\alpha). \quad (4)$$

The expressions for $P(\varphi\alpha)$ may be brought into the form

$$P(\varphi\alpha) = \frac{[N_\alpha/(2i_\alpha+1)]\{3\sum_\mu A_\pi^{\varphi\mu\alpha}(a)A_\pi^{\varphi\mu\alpha}(c) - [(2\varphi+1)/3]A^{ab}A^{bc}\}(3\cos^2\Theta-1)}{\sum_\alpha[N_\alpha/(2i_\alpha+1)]\{\sum_\varphi\sum_\mu A_\pi^{\varphi\mu\alpha}(a)A_\pi^{\varphi\mu\alpha}(c)(3\cos^2\Theta-1) + [(2j_b+1)(2i_\alpha+1)/3]A^{ab}A^{bc}(3-\cos^2\Theta)\}} \quad (5)$$

by using the relations

$$A_\pi^{\varphi\mu\alpha}(a)+A_\sigma^{\varphi\mu\alpha}(a) = A^{ba}, \qquad \sum_\mu A^{ab} = (2\varphi+1)A^{ba}, \qquad \sum_\mu A_\pi^{\varphi\mu\alpha}(a) - \tfrac{1}{2}\sum_\mu A_\sigma^{\varphi\mu\alpha}(a) = 0, \quad (6)$$

which express respectively the fact that: The total chance of leaving the sublevel μ of φ is A^{ba}; there are $(2\varphi+1)$ magnetic sublevels of φ; and all *hfs* components coming from φ are unpolarized if the level is isotropically excited. Similar relations hold for the fluorescence line bc.

In making the calculation for resonance lines the same procedure is adopted as in I, namely that the transition probabilities are so chosen that the chance of leaving any magnetic sublevel of any upper hyperfine state is the same for all such states. This makes A^{ba} directly calculable. In the case of fluorescence lines the transition probabilities for the line ab are left unchanged and the total transition probability from $\mu(\varphi)$ to all levels $h_1, h_2, \cdots$ etc., is called A^{bc}. The relative transition probabilities from $\mu(\varphi)$ to $h_1, h_2, \cdots$ etc., must be adjusted to be in accord with the sum rule for intensities. If the line ab is resolved spectroscopically from bc it is convenient to choose A^{ab} equal to A^{bc}.

If the resonance tube is in a zero magnetic field and the exciting light is polarized with its electric vector parallel to X, then from spectroscopic stability we may place $\Theta=0$ in Eq. (5). Throughout the article we shall use the notation $P_0(\varphi\alpha)$ for the value of the expression at $\Theta=0$. If we are dealing with resonance rather than fluorescent light it is, of course, to be understood that one takes $c=a$ in (5). Furthermore, if $P_{\|}$ and $P_\perp$ be the polarizations observed with the electric parallel or perpendicular to the magnetic field, it follows from (5) that $P_\perp = P_{\|}/(P_{\|}-2)$.

Magnetic Depolarization

1. Theory

It is well known that if a small magnetic field is directed along the Z-axis (direction of observation) the degree of polarization decreases as the field increases and the plane of maximum polarization is rotated through an angle θ with respect to its original direction. If the polarization $P(H)$ is measured by observing the intensity of light polarized parallel to X and Y respectively, then according to Breit,[3] $P(H)$ is given by

$$P(H)=\sum_\alpha\sum_\varphi \frac{P_0(\varphi\alpha)}{1+[(eH/mc)g_\varphi(\alpha)\tau]^2}, \quad (7)$$

where $g_\varphi(\alpha)$ is the *hfs* Lande g-factor for the state φ. In making the calculation it is assumed that τ is the same for all hyperfine states of the gross state b. Similarly the angle θ is given by

$$\tan 2\theta=\frac{\sum_\alpha\sum_\varphi P_0(\varphi\alpha)\sin(2\theta)_{\varphi\alpha}\cos(2\theta)_{\varphi\alpha}}{\sum_\alpha\sum_\varphi P_0(\varphi\alpha)\cos^2(2\theta)_{\varphi\alpha}}, \quad (8)$$

where the angle $(2\theta)_{\varphi\alpha}$ is given by

$$\tan(2\theta)_{\varphi\alpha}=(eH/mc)g_\varphi(\alpha)\tau. \quad (9)$$

2. Comparison with experiment

(*a*) *Mercury resonance radiation* λ*2537*. With the methods outlined above the values of $P(H)$ for mercury resonance radiation (λ2537) were calculated for different values of the magnetic field H, by using for the mean life[4, 5] $\tau=1.08\times10^{-7}$ sec. The values of $P_0(\varphi\alpha)$ and $g_\varphi(\alpha)$ for the various upper *hfs* states of the line are given in Table I for reference. The results of the calculation are shown by the full curve in Fig. 1, in which $P(H)$ is plotted as ordinate and

Table I.

State (isotope, i, φ)	$P_0(\varphi\alpha)$	$g_\varphi(\alpha)$
(even, 0, 1)	0.754	3/2
(199, 1/2, 1/2)	0.000	...
(199, 1/2, 3/2)	0.058	1
(201, 3/2, 1/2)	0.000	...
(201, 3/2, 3/2)	0.016	2/5
(201, 3/2, 5/2)	0.020	3/5
$P_0=$	0.848	

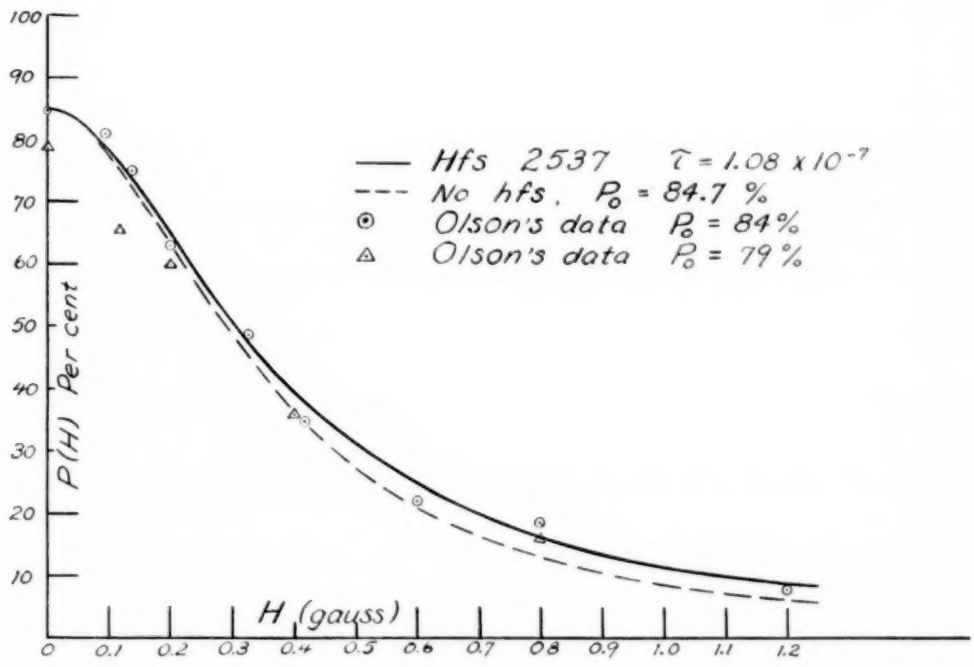

Fig. 1.

[4] W. Zehden and M. W. Zemansky, Zeits. f. Physik **72**, 442 (1931).

[5] P. H. Garrett and H. W. Webb, Phys. Rev. **37**, 1686 (1931).

H as abscissa. The broken curve is a hypothetical curve obtained on the assumption that the λ2537 line is due to isotopes having no nuclear spin with a g-value for the 6^3P_1 state of 3/2, but that for some unknown reason the degree of polarization in zero field is 84.7 percent instead of 100 percent, as would be expected in such a case, i.e., calculated by

$$P(H)=P_0/(1+[(eH/mc)g\tau]^2)$$

with $P_0=84.7$ percent. Some experimenters have made exactly this assumption in calculating τ for mercury from a curve showing $P(H)$ as a function of H. Comparison of the two curves shows that the error in such a procedure is within the limits of experimental measurement. The reason for this is two-fold. In the first place the greatest contribution to the polarization comes from the non-spin isotopes (70 percent of the mixture), and secondly these isotopes have the largest g-values for the upper excited state, so that they contribute relatively more to the depolarization in weak magnetic fields than do the other isotopes. A similar situation arises in the case of the resonance line of cadmium λ3261.

Olson's[6] experimental points are also plotted on Fig. 1. He made two sets of experiments. In the series represented by the circles in the figure, the exciting mercury arc lamp was run at low current density, and it was found that the degree of polarization in zero field attained the theoretically predicted value of 84 percent. In the other set of experiments represented by the triangles, the exciting source was operated at higher current density and the degree of polarization obtained in zero magnetic field was found to be 79.5 percent, considerably lower than that predicted from the theory. It will be seen from Fig. 1 that the observed points from the first group of experiments fit the theoretical curves admirably. The data from the second set of experiments deviate from the theoretical curve, especially in the region of low fields. The cause of the deviation in the second case is not exactly clear but it is possible that at the high current densities used the vapor pressure in the exciting source was high enough to cause a relatively greater self-reversal in the strong (non-spin) components than in the weaker components. The distribution of intensity over the various *hfs* components in the exciting source probably did not correspond to the assumption of a "broad line" exciting source on which the calculation is based. It is interesting to note that Olson, without introducing considerations of *hfs*, calculated a value for the mean life τ of the 6^3P_1 state of 0.98×10^{-7} sec., whereas when one takes into account *hfs*, his data appear to be in good accord with the value $\tau=1.08\times10^{-7}$ sec.

The result of the calculation of the angle of maximum polarization, θ, as a function of the magnetic field in the case of mercury resonance radiation is given in Fig. 2, in which tan 2θ is

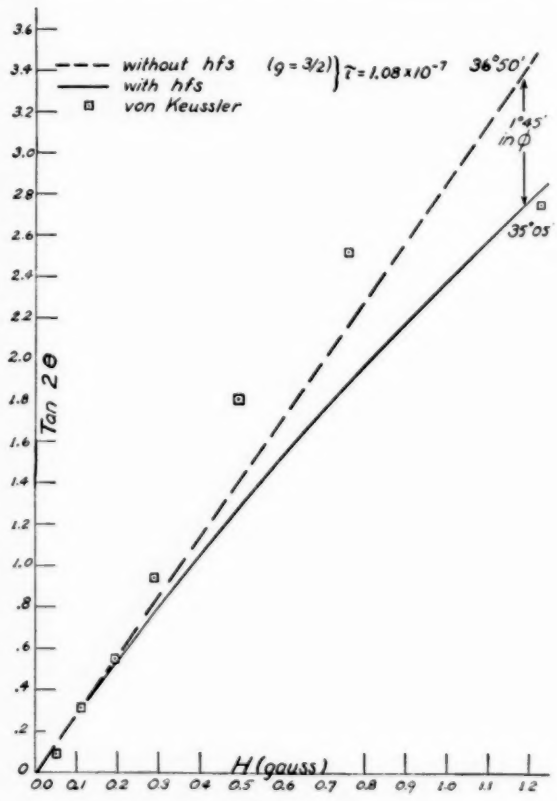

FIG. 2.

plotted as a function of the magnetic field. The full curve gives the result of the present calculation whereas the broken curve represents the results to be expected if mercury resonance radiation consisted of lines from the non-spin isotopes alone. Here again the difference between the two curves is probably within the limit of experimental error of present experiments. The

[6] Olson, Phys. Rev. **32**, 443 (1928).

observations of von Keussler[7] are represented by the squares on the diagram and it will be seen that the agreement is, in general, not good. The reason for the discrepancy is at present not clear. It should be pointed out that the value of τ obtained by von Keussler from these measurements was 1.13×10^{-7} sec.

Recently Mrozowski[8] has been able to excite individual *hfs* components of the mercury resonance line as resonance radiation, and to measure the angle of maximum polarization of this resonance radiation as a function of weak fields in the direction of observation. Two sets of experiments are of interest to us in these calculations. He was able to excite as resonance radiation either (a) the 0.0 and +11.5 mA components together, or (b) the −25.4 mA component separately. The first two components are due to the non-spin isotopes (see Fig. 3) the

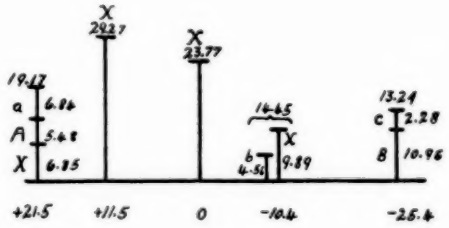

FIG. 3.

upper state of which shows $g=3/2$. The −25.4 mA component, on the other hand, is made up from components B and c from the isotopes of mass 199 and 201, respectively. The component c is, however, unpolarized under all circumstances and hence contributes nothing to the angle of maximum polarization. The upper state of the component B shows $g=1$. From Eq. (8), therefore, a plot of tan 2θ against H should yield straight lines for the case a and b, respectively. Furthermore, if the mean life τ is the same for the two upper *hfs* states of the two isotopes, the ratio of the slopes of the straight lines obtained in the two cases should be that of their respective g-values of the upper states; namely, 3/2 : 1. A plot of Mrozowski's data does indeed yield straight lines for tan 2θ plotted against H and the ratio of the slopes of the two lines is 1.5 as expected. This would appear to be evidence in favor of the usual view that the mean life of any *hfs* state of any gross level j is the same for all such *hfs* states.[9]

(*b*) *Cadmium resonance radiation* (λ*3261*). A calculation similar to that for mercury resonance radiation has been made for the case of cadmium resonance radiation (λ3261). The polarization of this line has already been calculated by Mitchell[10] and Ellett and Larrick[11] on the assumption that the line is made up of contributions from isotopes of even atomic weight (having no spin) and isotopes of odd atomic weight with a spin of 1/2. Table II gives the values of $P_0(\varphi\alpha)$ and $g_\varphi(\alpha)$

TABLE II.

State (isotope, i, φ)	$P_0(\varphi\alpha)$	$g_\varphi(\alpha)$
(even, 0, 1)	0.765	3/2
(odd, 1/2, 1/2)	0.000	···
(odd, 1/2, 3/2)	0.102	1
$P_0=$	0.867	

necessary for carrying out the calculations for the polarization $P(H)$ in weak magnetic fields parallel to the direction of observation. The values are computed for broad line excitation using the value of $\gamma=2.53$ (the ratio of even to odd isotopes) given by Ellett and Larrick. By using the value $\tau=2.5\times10^{-6}$ sec., as determined by Koenig and Ellett,[12] the value of $P(H)$ was computed as a function of the magnetic field H. The results of the calculation are given by the full curve of Fig. 4. The circles in the figure represent experimental points obtained by Solleillet[13] who used, however, unpolarized exciting light. Strictly speaking, experiments ob-

[7] V. von Keussler, Ann. d. Physik **82**, 793 (1927).

[8] S. Mrozowski, Bull. Acad. Pol. p. 491 (1930).

[9] The value of the mean life of the 6^3P_1 state obtained from these curves is 1.67×10^{-7} sec., not in agreement with other values. Such a discrepancy might arise if the value of the applied magnetic field was calculated from the current flowing in a coil of given dimensions. The actual field in the resonance tube might thus differ from that calculated by a constant multiplier. This would leave the ratio of the slopes of the two curves a and b the same but might account for the abnormally large calculated value of τ. This point should certainly be tested.

[10] A. C. G. Mitchell, Phys. Rev. **38**, 473 (1931).

[11] A. Ellett and L. Larrick, Phys. Rev. **39**, 294 (1932).

[12] Koenig and Ellett, Phys. Rev. **39**, 576 (1931).

[13] P. Solleillet, Comptes Rendus **185**, 198 (1927); **187**, 212 (1928).

tained using unpolarized exciting light are not comparable with a theoretical curve based on the assumption of polarized exciting light. Unfortunately, no data are available for the case in which polarized exciting light is used.

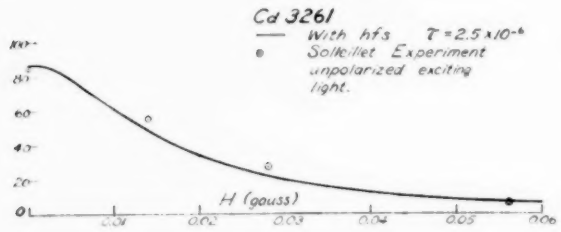

FIG. 4.

THE MEAN LIFE OF THE 7^3S_1 STATE OF MERCURY

If a mixture of nitrogen and mercury vapor is irradiated by the full spectrum of the mercury arc, the visible triplet (λ4047, 4358, 5461) and diffuse triplet (λ2967, 3131, 3663) of mercury, together with other mercury lines, are found to be emitted as fluorescence. A discussion of this effect and the method of calculating the degree of polarization of the lines for various orientations of electric vector of the exciting light and applied magnetic field are given in I. Because of the fact that the sum rule for intensities of the various *hfs* components was not correctly applied, the values of the polarization for the lines λ4358, 5461, 3131 and 3663, given in I are in error. When the sum rule is correctly applied, in order to obtain correct values of $A_{\pi}^{\varphi\mu\alpha}(c)$, as explained in the introduction, the values of P_0 given in Table III are obtained by the use of (4) and (5). These values are arrived at on the assumption that the incident light shows "broad line" characteristics and that it is polarized in a direction at right angles to the observation direction. The degree of polarization to be expected for other orientations of electric vector and magnetic field may be calculated from (5).

TABLE III.

	Polarization			*Mean Life*	
Line	Obs.	Calc.	θ (Obs.)	τ (Richter)	τ (Calc.)
4047	72±6	84.7	17°	4.8×10^{-8}	7.2×10^{-9}
4358	−49±6	−67.0	29°	4.6×10^{-8}	1.69×10^{-8}
5461	13±1	8.6	29.5°	1.7×10^{-7}	1.53×10^{-8}
2967	67±7	84.7			
3131	−29±7	−67.0			
3663	42±4	8.6			

The minus sign (−) indicates that the line is polarized with its electric vector at right angles to the electric vector of the incident light

Richter[14] has made observations on the angle of maximum polarization θ for the various lines of the visible triplet for several different values of a magnetic field parallel to the direction of observation. From these values of θ he attempted to calculate the value of the mean life of the 7^3S_1 state giving rise to the three lines in question. With an applied magnetic field of 2.81 gauss and at a nitrogen pressure of 1.75 mm, he found the values of θ given in column 4 of Table III for the three lines in question. In making the calculation of the mean life of the upper state from the observed angle, he did not consider the effect of hyperfine structure. Furthermore, the formulae he used relating tan 2θ and τ are incorrect. Moreover, there appears to be a mistake of a factor of 2π in the calculation since his formulae contain the quantity $eH/2\pi mc$ instead of eH/mc usually occurring in such formulae. The values obtained by Richter are given in column 5 of Table III.

With the angles θ given by Richter for the three lines λ4047, 4358 and 5461, the value of τ for the 7^3S_1 state has been computed from Eqs. (8) and (9) by using the hyperfine structure data for the lines in question. The results of the calculation are given in column 6 of Table III. As might be expected, they do not agree with those calculated by Richter.

One should point out here that Richter believed his results to be a confirmation of the results of Randall[15] obtained by an entirely different method. Randall found that the mean life of the 7^3S_1 state of mercury appears to depend on the line which is used to measure it. Richter's calculation seemed to show that the value of the mean life of this state obtained from measurements on the line λ5461 was four times as long as that obtained from measurements on λ4047, and λ4358 in agreement with Randall. The present calculation shows, however, that the values of τ, calculated by the present method, are no longer in agreement with those of Randall. Indeed, it appears, from the values given in the

[14] E. F. Richter, Ann. d. Physik **7**, 293 (1930).

[15] R. H. Randall, Phys. Rev. **35**, 1161 (1930).

table, that Richter's measurements on the two lines λ4358 and 5461 give equal mean lives for the 7^3S_1 state, while the measurement on the line λ4047 leads to a value of the mean life about half as large as that obtained by measurements on the other two.

At the present writing it seems futile to speculate on the meaning of the results obtained for the mean life of the 7^3S_1 state of mercury. In the first place the values of the polarization obtained by Richter in zero magnetic field do not agree with the theoretical values; and in the second, the effect of the nitrogen is a disturbing factor. The writer is repeating Richter's experiments with an improved apparatus, and preliminary results on the polarization of the λ4358 line in zero magnetic field yield a value more nearly in agreement with the theoretical value than that obtained by Richter. It is to be hoped that these new experiments will help to clear up the perplexing difficulty of the mean life of the 7^3S_1 state of mercury.

Anomalies in Hyperfine Structure

S. GOUDSMIT AND R. F. BACHER,* *University of Michigan*

(Received April 13, 1933)

The deviations from the interval rule in the hyperfine structure of two of the energy states in mercury can be explained satisfactorily as due to perturbations arising from their proximity. The forbidden line Hg I λ2967.5 ($6s\,6d\ ^1D_2 - 6s\,7p\ ^3P_0$) and its hyperfine structure are also explained by these perturbations. The hyperfine structure ascribed to the $3s\,4f$ levels of ionized aluminum which has seemed to be in contradiction with the theory, can be shown to belong partially to the $3s\,ng$ levels and to come out in agreement with theoretical expectations.

THE difficulties encountered in the interpretation of hyperfine structure can be divided into two classes. The first class contains those which are due to our lack of knowledge of nuclear structure. The main questions are why certain nuclei possess the observed mechanical and magnetic moments and why they cause the observed amount of isotope shift. The second class of difficulties is connected with the interaction of the nucleus with the surrounding electrons. Assuming that the hyperfine structure is due to nuclear spin, the observed splitting of the levels does not always agree with this hypothesis. For example, the values of the nuclear magnetic moments calculated from different levels of the same atom were not always the same. Similar discrepancies seemed to exist for isotope shifts. It has been shown by various workers[1] that these difficulties do not mean that the hypothesis of nuclear spin is incorrect, but that they arise from neglect of important relativity corrections or from the approximate nature of certain numerical calculations.

In two more or less isolated cases no satisfactory explanation of discrepancies has been given up to the present. They are a deviation from the interval rule for the hyperfine structure of a level in neutral mercury (Hg I) and a discrepancy in the magnitude and number of components of the hyperfine structure of a few levels in ionized aluminum (Al II). It is hoped that this paper will clarify these difficulties.

MERCURY

In Fig. 2 the crosses represent the $6s\,6d$, $^3D_1$ and $^1D_2$ levels of Hg I with their hyperfine structure as given in the interpretation by Schüler and his coworkers.[2] The isotopes of even atomic weight show no splitting up and also no observable isotope shift. The latter means that the isotope shift for initial and final levels of the investigated lines is practically the same, in agreement with expectations. Isotope 199 has a nuclear moment $\frac{1}{2}$ and a negative g-value, isotope 201 has a moment $1\frac{1}{2}$ and a positive g-value. From other levels the ratio of the g-values is found to be $g(199)/g(201) = -2.70$. Using this ratio and the interval rule one may find that the total hyperfine structure separation of a level of Hg^{199} with $J=1$ is 1.01 times larger than that of Hg^{201}. For levels with $J=2$ the total separation of Hg^{199} is 0.90 times that of Hg^{201}.

Schüler and Jones point out that the interval rule is violated in Hg^{201}, the separation of the lowest two levels being too small. They notice moreover that the center of gravity of the hyperfine splitting of the odd isotopes does not coincide with the position of the levels for the even isotopes and that the ratio of the total separations is also in disagreement with expectations. Schüler and Jones ascribe these deviations to a mutual perturbation between these two neighboring levels, which causes an apparent repulsion between levels with the same

* Alfred Lloyd Fellow.

[1] Breit, Phys. Rev. **42**, 348 (1932). Racah, Zeits. f. Physik **71**, 431 (1931). Goudsmit, Phys. Rev. **43**, 636 (1933).

[2] See especially Schüler and Jones, Zeits. f. Physik **77**, 801 (1932).

quantum number F. We shall show that this supposition is for the most part correct.[3]

The perturbation in this case is similar to a beginning Paschen-Back effect since the hyperfine separation is of the same order as the distance between the two levels. It can be treated quantitatively in the same manner as the transition from one scheme of vector coupling to another. It is possible to write down simple expressions for the energy levels in the two extreme cases where the hyperfine structure is much smaller and where it is much larger than the distance between the two levels. This knowledge is sufficient to obtain the level pattern for all intermediate cases. We shall assume that the nuclear moment interacts with the 6s electron only and shall neglect its interaction with the 6d electron which is estimated to be more than a hundred times smaller. We shall also neglect perturbations due to levels farther away as it is too complicated to take them into account. Such perturbations are expected to be small but may perhaps explain why we do not find exact agreement between observed and calculated levels.

The distance between the two levels in case there is no hyperfine structure is denoted by X and is found from the even isotopes to be approximately 3.0 cm^{-1}. The exact value is not necessary for our purpose. The interaction of the nuclear moment with the 6s electron is of the form (1).

$$E = A\,Is\cos(I, s) \qquad (1)$$

I and s are the nuclear spin and the spin of the s electron, respectively. From the hyperfine structure of other states in Hg I it is found that A is approximately 1.20 cm^{-1} for Hg^{199} and -0.445 for Hg^{201}.

[3] The perturbation in this case is not quite similar to that brought forward by Langer (Phys. Rev. **35**, 649 (1930) and applied by Russell and Shenstone (Phys. Rev. **39**, 415 (1932)) as was stated by Schüler and Jones. In that case the perturbations arose from the large non-diagonal matrix elements in the electrostatic energy matrix. Here, rather, it is a change of coupling due to the close proximity of levels with different J values. This allows one to consider only F the total angular momentum as a constant of the motion, and no longer J. That it also causes a repulsion between levels of the same total quantum number is not particularly characteristic, as this is common to all quantum mechanical perturbations.

In order to use the sum relations two extreme cases will be considered, first with the ordinary multiplet structure large compared to the hyperfine structure ($X \gg A$) and second with the hyperfine structure large compared to the ordinary multiplet structure ($X \ll A$). In the latter case we shall pass to the limit and take $X = 0$ which means (j, j) coupling. By using the strict validity of the interval rule for $X \gg A$ and the sum rule in passing from one extreme to the other, it is possible to find the energy values for the extreme cases. These energies, referred in each case to the largest F-value as zero, are given in Table I and plotted in Fig. 1. The two isotopes must, of course, be treated separately. In comparing Fig. 1 and Table I it must be noted that for Hg^{201}, A is negative.

TABLE I. *Energies of $^3D_1$ and $^1D_2$ in extreme coupling schemes.*

Hg^{199} $I=\frac{1}{2}$	$A \ll X$	$X=0$	
$F=2\frac{1}{2}$	$E=0$	$E=0$	reference level
$F=1\frac{1}{2}$	$E'=-\frac{3}{8}A$ $E''=X-\frac{3}{8}A$	$E'=0$ $E''=-A$	
$F=\frac{1}{2}$	$E=X$	$E=0$	
Hg^{201} $I=1\frac{1}{2}$	$A \ll X$	$X=0$	
$F=3\frac{1}{2}$	$E=0$	$E=0$	reference level
$F=2\frac{1}{2}$	$E'=-\frac{7}{8}A$ $E''=X-\frac{9}{8}A$	$E'=0$ $E''=-2A$	
$F=1\frac{1}{2}$	$E'=-\frac{3}{2}A$ $E''=X-\frac{1}{2}A$	$E'=0$ $E''=-2A$	
$F=\frac{1}{2}$	$E'=-1\frac{5}{8}A$ $E''=X-\frac{1}{8}A$	$E'=0$ $E''=-2A$	

TABLE II. *Calculated and observed levels of $^3D_1$ and $^1D_2$.*

		Hg^{199}			Hg^{201}	
	F	calc.	obs.	F	calc.	obs.
$^3D_1$	$\frac{1}{2}$	0.300 cm^{-1}	0.329 cm^{-1}	$2\frac{1}{2}$	0.226 cm^{-1}	0.260 cm^{-1}
	$1\frac{1}{2}$	−0.051	−0.056	$1\frac{1}{2}$	−0.055	−0.065
				$\frac{1}{2}$	−0.258	−0.260
$^1D_2$	$2\frac{1}{2}$	0.300	0.301	$\frac{1}{2}$	0.480	0.460
	$1\frac{1}{2}$	−0.549	−0.559	$1\frac{1}{2}$	0.277	0.279
				$2\frac{1}{2}$	−0.007	−0.022
				$3\frac{1}{2}$	−0.337	−0.335

The information given in Table I is sufficient to write down quadratic equations,[4] the roots of which will give the positions of the levels for any intermediate value of A and X. These equations are given in (2) and (3).

[4] Goudsmit, Phys. Rev. **35**, 1325 (1930).

$$
\begin{aligned}
&\mathrm{Hg}^{199} \quad I=\tfrac{1}{2}\\
&F=2\tfrac{1}{2} \quad E=0\\
&F=1\tfrac{1}{2} \quad E^2-(X-A)E-\tfrac{5}{8}XA=0\\
&F=\tfrac{1}{2} \quad E=X\\
&\text{Center of gravity } G=\tfrac{3}{8}X+\tfrac{3}{4}A
\end{aligned}
\qquad (2)
$$

$$
\begin{aligned}
&\mathrm{Hg}^{201} \quad I=1\tfrac{1}{2}\\
&F=3\tfrac{1}{2} \quad E=0\\
&F=2\tfrac{1}{2} \quad E^2-(X-2A)E-\tfrac{7}{8}XA=0\\
&F=1\tfrac{1}{2} \quad E^2-(X-2A)E-\tfrac{3}{2}XA=0\\
&F=\tfrac{1}{2} \quad E^2-(X-2A)E-\tfrac{15}{8}XA=0\\
&\text{Center of gravity } G=\tfrac{3}{8}X+\tfrac{1}{4}A.
\end{aligned}
\qquad (3)
$$

The level schemes in Fig. 2 give the positions of the levels calculated from (2) and (3), taking $X=3.0$ cm^{-1}, $A(199)=1.20$ cm^{-1} and thus from the known g ratio $A(201)=-0.445$ cm^{-1}. The crosses indicate the observed positions of the levels. Not only is there good agreement within each isotope, but the relative position of the levels of the two odd isotopes and their relation to those of the even isotopes fits very well. The outside level scheme of the figure indicates the hypothetical position of the levels calculated from Table I if there were no perturbation. The small discrepancies which remain may well be due to perturbations by other levels or perhaps may be attributed to some uncertainty in the measurements of the highly complicated line patterns. Table II gives the calculated and observed levels referred to the position of the even isotopes.[5]

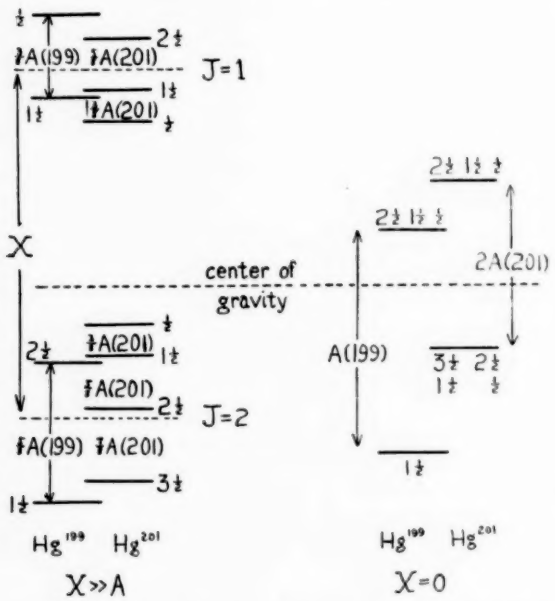

FIG. 1. Positions of $6s\,6d\ ^3D_1$ and $^1D_2$ levels of Hg I for $X \gg A$ and for $X=0$. For convenience the distance X at the left is not drawn to scale. It should be much larger than it is drawn in the diagram.

Perturbations of the type discussed here are always accompanied by anomalies in intensities and the occurrence of "forbidden" transitions. In cases where there are only two levels of the same total quantum number F which perturb each other, the intensity change is given by a simple expression. Let δ denote the displacement of the level from the ideal position which it would have had without the perturbations and let Δ be the distance of this level from the other one with the same quantum number F, also in the ideal case. Then the ratio of the intensity of the forbidden transition I_1 to that of the allowed one I_0 is given by (4)

$$I_1/I_0=\delta/(\Delta+\delta). \qquad (4)$$

This can be derived by considering the secular determinant which gives rise to quadratic equations like those given above. One must expect therefore that for the odd mercury isotopes, transitions can occur from $6s\ 6d\ ^1D_2$ to odd levels with $J=0$ and from $^3D_1$ to odd levels with $J=3$. An example is the transition $^1D_2-6s\ 7p\ ^3P_0$, $\lambda 2967.5$. Fig. 3 represents the expected transitions and indicates the intensities as obtained from (4). One sees that one can expect two or perhaps three components to have been observed. Cardaun[6] indeed gives two components 0.76

[5] Professor Breit has called our attention to the fact that our treatment of these mercury lines is really mathematically identical with the calculations of Casimir (Zeits. f. Physik **77**, 811 (1932)). We believe, however, that our method is considerably simpler. Casimir concludes that there is grave disagreement between theory and experiment because he considers only the *ratio* of the displacements from the ideal positions. This ratio is too sensitive to small errors to justify Casimir's conclusion. He does not calculate the theoretical positions of the levels. Casimir's calculations are connected with ours by observing that his quantity $D=\frac{1}{4}A$. Using the values of A given above, Casimir's formulas give the same final results as ours.

[6] Cardaun, see Kayser and Konen, Vol. VII, page 674.

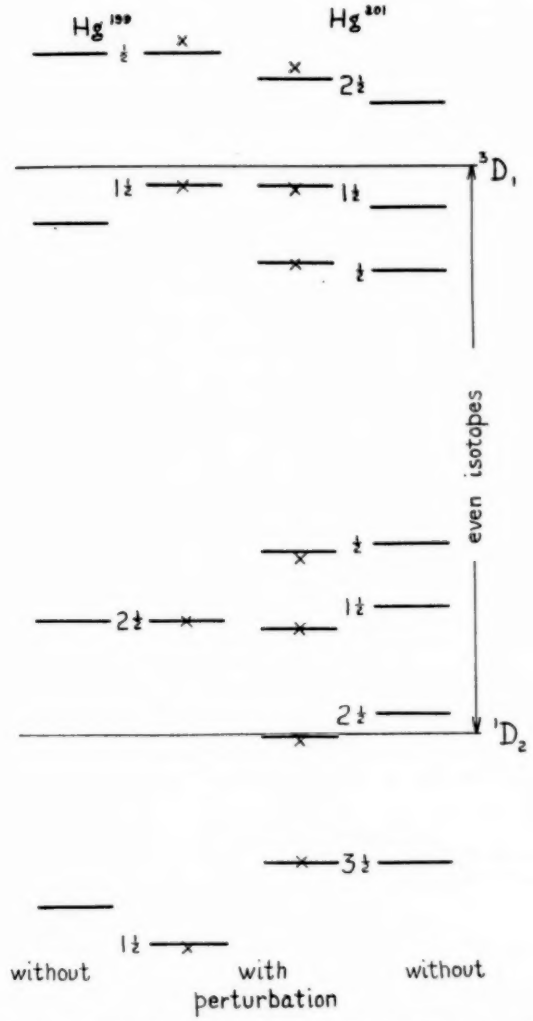

FIG. 2. Level diagram of $6s\,6d\,{}^3D_1$ and $^1D_2$ of Hg I calculated with and without perturbation. The crosses indicate the observed levels. The distance $^3D_1-{}^1D_2$ is drawn about half its actual size, for convenience.

cm^{-1}. apart. Wendt[7] also has observed two components ($\Delta\nu=0.70$), but his reproduction shows clearly that the one with larger frequency is broadened.

ALUMINUM

In his work on the classification of the spectrum of ionized aluminum Paschen[8] found that the $3s\,4f\,{}^3F_4$, $^3F_3$, $^3F_2$ and $^1F_3$ levels show hyperfine structure in combination with higher members of the $3s$ ng series. Since the separations were all nearly the same the structure was attributed to the hyperfine structure of the $3s\,4f$ levels alone. This hyperfine structure was at first entirely impossible to understand as no other levels in Al II were known to show any separation. Recently, however, Ritschl[9] has discovered the presence of hyperfine structure in other levels of Al II and Al I and has determined the nuclear spin to be $\frac{1}{2}$. From the hyperfine structure found by Ritschl one can conclude that the $3s\,4f$ levels must have a hyperfine structure of the order of magnitude of that assigned by Paschen. Nevertheless this structure is in disagreement with the theory and fails to explain why the $3s\,4f$ terms do not show the same hyperfine structure in other combinations. In Al II the hyperfine structure is caused almost entirely by the deeply penetrating $3s$ electron present in most of the electron configurations. In such a case one expects Eq. (5) to hold.[10]

$$A=\tfrac{1}{2}a(g-1). \tag{5}$$

A is the separation factor for a given level and a that of the s electron. This expression is strictly valid only for Russell-Saunders coupling, g being the Landé g-factor. The total width of the

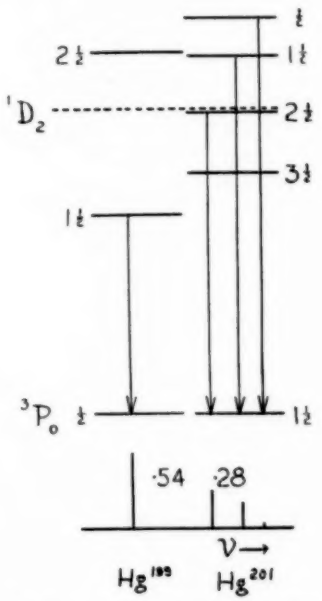

FIG. 3. Calculated structure of the forbidden line λ2967.5 ($6s\,6d\,{}^1D_2-6s\,7p\,{}^3P_0$) of Hg I.

[7] Wendt, Ann. d. Physik **37**, 545 (1912).

[8] Paschen, Ann. d. Physik **71**, 537 (1923). See also Sawyer and Paschen, Ann. d. Physik **84**, 1 (1927).

[9] Ritschl, Nature **131**, 58 (1933).

[10] Goudsmit and Bacher, Phys. Rev. **34**, 1501 (1929).

splitting of the $3s\ 4f$ levels should be therefore

$^3F_4 : 9a/20,\ ^3F_3 : 7a/48,\ ^3F_2 : -5a/12,\ ^1F_3 : 0.$

The observed hyperfine structures are 0.10, 0.49, 0.25, 0.49 cm^{-1}. The value for a derived from Ritschl's data is about $a=0.50$ cm^{-1} and one would expect therefore

$^3F_4 : 0.23, ^3F_3 : 0.07, ^3F_2 : -0.21, ^1F_3 : 0\ cm^{-1}.$

Though the levels of the $3s$ nf series in aluminum are greatly perturbed by other levels, these perturbations cannot be the reason for the irregularities in the hyperfine structure of the $3s$ $4f$ state. The perturbing states do not contain a $3s$ electron and possess themselves no appreciable hyperfine structure.

The discrepancy can be removed entirely if one considers first that the $3s$ ng states also must possess a hyperfine splitting due to the $3s$ electron. The data indicate the interesting fact that for these states the hyperfine structure is larger than the multiplet splitting of the ^3G as well as the singlet triplet distance from ^3G to ^1G. We have here an extreme coupling in which the nuclear spin is more strongly coupled to the $3s$ electron than the latter is to the g-electron. The hyperfine structure in this case will be that of the $3s$ electron, as if the g-electron were absent, and will thus be equal to a. The upper part of Fig. 4 gives the level scheme for this case. It will be the same for all higher members of the $3s$ ng series.

Special attention must be given to the selection and intensity rules for the transition from this extreme coupling to the other extreme of the F-states. Though it is possible to set up the intensity formulas, we believe that it is not necessary for this case to go into such complicated derivations. We shall restrict ourselves to simple correspondence considerations to find out which transitions will be strongest. In both extreme couplings the interaction between the orbit of the electron which makes the transition and the nuclear spin as well as that between the orbit and s-electron will be negligible compared to the other interactions. Therefore only such transitions may occur in which the position of the spin of the s-electron with respect to the nuclear spin is not altered. In the upper level of the G-state these spins are parallel, in the lower they are opposite. For the upper hyperfine levels of $^3F_4$

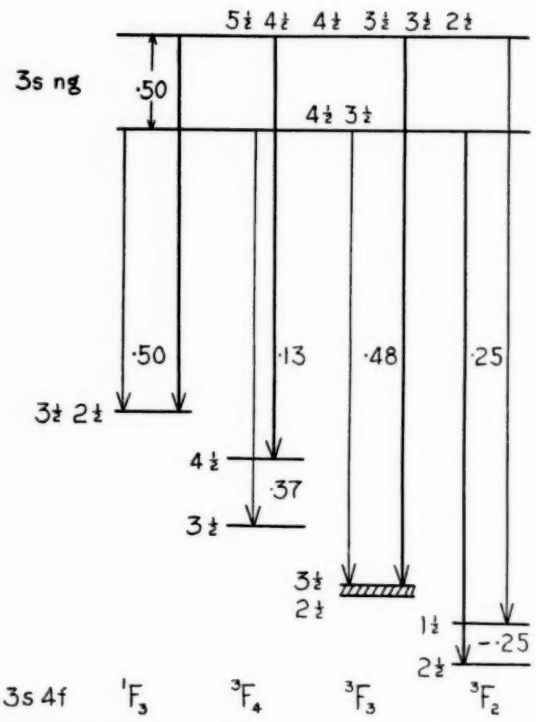

FIG. 4. Interpretation of hyerpfine structure of the transitions $3s$ $ng-3s$ $4f$ in Al II.

and $^3F_2$ they are also parallel and these levels will therefore combine principally with the upper of the G-levels. The same reasoning shows that the lower G-level gives transitions to the lowest levels of $^3F_4$ and $^3F_2$ as shown in Fig. 4. For the other states nothing can be said with certainty from such simple considerations, but because of the fact that the $^3F_3$ and $^1F_3$ separations are expected to be so small, only two lines are observed anyway. For the relative intensity of the lines which are found, one would expect, from the intensity sum rules looking only at the lower levels $^3F_4$ and $^3F_2$, that those lines to the $F=4\frac{1}{2}$ and $F=2\frac{1}{2}$ would be stronger. For $^3F_3$ and $^1F_3$ there is no criterion of this sort from the lower levels but it might be expected that the stronger components will be those to the upper G state as it has greater degeneracy. For the transition to $^3F_2$ it will thus be the component of smallest frequency, for the others it will be that of largest frequency.

These considerations together with the expectation that the $^1F_3$ should have no observable hyperfine structure leads to the interpretation of the observations given in Fig. 4. The $3s$ ng

states are split up into two unresolvable groups about 0.50 cm^{-1} apart. The separations of the $3s\ 4f\ {}^3F_4$, ${}^3F_3$, ${}^3F_2$ and ${}^1F_3$ are about 0.37, ~ 0, -0.25, and 0 cm^{-1}, respectively. The separation of the ${}^3F_4$ state is still considerably larger than expected, but this may well be due to the approximate nature of our considerations in which we neglect entirely a possible further splitting of the $3s$ ng states.

In support of this interpretation it can be said that the hyperfine structure has only been resolved in the transitions from the $3s$ $8g$, $3s$ $9g$ and $3s$ $10g$ levels. The $3s$ $7g$ shows a further splitting up which causes the pattern to become too complicated and the lines are not resolved but denoted as "diffuse." The value obtained for a is furthermore in good agreement with that from the preliminary data of Ritschl.

Appendix

Since this paper was written, an article by Professor F. Paschen[11] has been received in which he treats qualitatively some of the questions considered here and which contains valuable new data on aluminum. He points out that the forbidden transition $6s\ 6d\ {}^1D_2 - 6s\ 7p\ {}^3P_0$, λ2967.5, in Hg I is due to hyperfine structure perturbations similar to a Paschen-Back effect and should occur only for the odd isotopes. Furthermore Professor Paschen discusses again the hyperfine structure of the $3s$ $4f$ levels in Al II and shows that his previous interpretation must be altered in order to take into account the hyperfine structure of the $3s$ ng series, which he finds to be larger than the ordinary multiplet structure and singlet-triplet distance.

The results of Professor Paschen on Al II do not quite agree with those given here, as he supposes the separation of the $6s$ ng levels to be 0.35 cm^{-1}. For the forbidden transitions in mercury it might be mentioned that the lines $6s\ 7d\ {}^1D_2$ and $6s\ 8d\ {}^1D_2 - 6s\ 7p\ {}^3P_0$, λ2536.04 and λ2379.46 are difficult to explain since for these levels the perturbations are much smaller than for $6s\ 6d$.

[11] Paschen, Sitz. Ber. Preuss. Akad. 1932.

Fine Structure of Electron Diffraction Beams from a Gold Crystal and from a Silver Film on a Gold Crystal

H. E. FARNSWORTH, *Brown University*

(Received March 31, 1933)

A study of the diffraction of low-speed electrons from a gold crystal has been made under the same conditions as those previously used for a silver crystal to determine the extent to which the previously observed fine structure characteristics depend on the nature of the atoms composing the crystal. For normal incidence there are many differences in the positions, structure, and relative intensities of the corresponding beams from the two crystals. *Intensity measurements as a function of angle of incidence* show some similarities in these characteristics for the two crystals, but there are many more differences. Results for a thin silver film on a gold crystal are in general the same as those for a massive silver crystal so that the different results for the two crystals appear to be real and not due to differences in surface irregularities. Differences are noted in the deviations from the surface grating formula during growth and decay of diffraction beams from the gold crystal and from the silver film on the gold crystal. This makes it appear unlikely that the number of atom lines in the elementary grating is the only determining factor. Beams which deviate from the surface grating formula may follow one of two depth grating formulas. Some dependence of this characteristic on angle of incidence is noted. Since no beams characteristic of a surface gas lattice on the gold crystal were observed when gas was known to be present, the gas layer must be noncrystalline.

INTRODUCTION

EXPERIMENTAL results reported in a recent paper[1] showed that for a silver crystal the number of experimental maxima in the low-voltage range is considerably greater than that to be expected from simple theory; and further that these additional maxima may, in general, be grouped as components of fine structure of the main diffraction beams. It was pointed out that a comparison of results for silver and gold crystals should be of value in determining the cause of this fine structure since the lattice constants of these crystals are the same to within 0.4 percent and both lattices are face-centered cubic. Thus a possible dependence of the fine structure on the lattice constant of the crystal should not be responsible for any appreciable differences in the characteristics of the corresponding diffraction beams from the two crystals, and hence any remaining differences must result from the different types of atoms.

The apparatus and method of procedure are the same as that described in detail in the former paper. In the investigations of a silver crystal two different experimental procedures were used. In one of them the characteristics of the diffraction beams were obtained as a function of primary voltage and angle of incidence which varied from zero (measured from the normal) to several degrees either side of the normal. The diffraction beams correspond to reflections from various sets of atomic planes in the crystal *not* including the one parallel to the crystal face. The other procedure was that of regular reflection from the set of planes parallel to the crystal face and with angles of incidence other than normal. This is the same as that used by Davisson and Germer[2] when they observed what they called "anomalous dispersion." In the present experiments only the first procedure was used since it is possible with the results of this method to associate the fine structure characteristics with the individual diffraction beams with greater certainty.

[1] H. E. Farnsworth, Phys. Rev. **40**, 684 (1932).

EXPERIMENTS WITH A GOLD CRYSTAL

Preparation of crystal

The crystal was made from proof gold of purity 0.99995 obtained from the U. S. Mint. The method was the same as that used for making copper and silver crystals.[1] The dimensions and

[2] C. Davisson and L. H. Germer, Proc. Nat. Acad. **14**, 619 (1928).

TABLE I. *Diffraction beams for normal incidence.*

Beam and order numbers*	Plane of reflection	Silver Lattice				Gold Lattice			
		Experimental voltage	Theoretical voltage	Voltage difference	Uncorrected relative intensity	Experimental voltage	Theoretical voltage $V=150/\lambda^2$	Voltage difference	Uncorrected relative intensity
		(100) Azimuth					*(100) Azimuth*		
1–1	(210)	46.1	56.3	10.2	100	58.0	56.8	−1.2	100
1–1	(210)	55			78				
2–1	(310)	75.7			3.5				
2–1	(310)	93.5	100.2	6.7	5	101.5	100.9	−0.6	23
3–1	(410)	141.0	162.8	21.8	21	136.0	164.0	28.0	17
4–1	(510)	229.5	243.8	14.3	7	247.0	245.6	−1.4	21
5–1	(610)	335.5	343.0	7.5	6				
1–2	(320)	152.5	169.3	16.8	4	171.0	170.5	−0.5	4
2–2	2(210)	206.5	225.4	18.9	19	191.0	227.1	36.1	9
3–2	(520)	280.5	303.3	22.8	7	303.0	305.5	2.5	11
		(111) Azimuth					*(111) Azimuth*		
1–1	(311)	20			22				
1–1	(311)	27			35	27.5			73
1–1	(311)	34.0	30.3	−3.7	70	32.0	30.5	−1.5	86
2–1	(511)	56.0	65.7	9.7	78	55.0			39
2–1	(511)	62.0			70	64.0	66.2	2.2	48
3–1	(711)	115.0	119.6	4.6	16	117.0	120.5	3.5	22
4–1	(911)	168.3	191.7	23.4	4				
4–1	(911)	175.5			3.5				
1–2	(211)					70.0			26
1–2	(211)	77.5	81.1	3.6	9	78.5	81.7	3.2	29
2–2	2(311)	112.5	121.2	8.7	16	120.0	122.1	2.1	8
3–2	(411)	158.5	182.6	24.1	9	163.0	183.9	20.9	15
3–2	(411)	173.0			6				
4–2	2(511)	250.5	262.9	12.4	9	256.0	264.8	8.8	11

* The notation is the same as that in Table I of former article.[1]

mounting of the single crystal piece used in the experimental tube were also the same as those for the previous experiments with copper and silver. The surface to be studied was cut parallel to a (100) set of planes, and mounted so that it could be rotated about an axis perpendicular to the (100) azimuth as in the case of one of the silver crystals. A smooth etched surface parallel to the (100) set of planes is much more difficult to obtain on a gold crystal than on silver. The face was etched in potassium cyanide dissolved in hydrogen peroxide. The solution was renewed every few minutes until the desired etching was obtained. *Aqua regia* was found to etch only parallel to (111) planes.

Diffraction beams for normal incidence

Table I shows the positions and relative intensities of the beams for normal incidence. The corresponding results for a silver crystal are included for comparison. When there are more than one component they are listed separately, but the differences between theoretical and experimental voltages are given for only the strongest component of each beam. There is no close correspondence in the relative intensities of the corresponding diffraction beams from the two crystals.

Curves showing the growth and decay of some first and second order beams in the (100) azimuth of a gold crystal are shown in the upper part of Fig. 1. These curves were obtained by varying the primary voltage in small steps, and measuring the current to the Faraday collector, whose angular position was adjusted for the maximum of the beam at *each* reading, while the total primary current was held *constant* for the entire set of observations. The corresponding curves for a silver crystal are shown directly beneath those for gold.

From these results it is clear that there are many differences in the positions, structure and relative intensities of the corresponding beams from the two crystals for normal incidence.

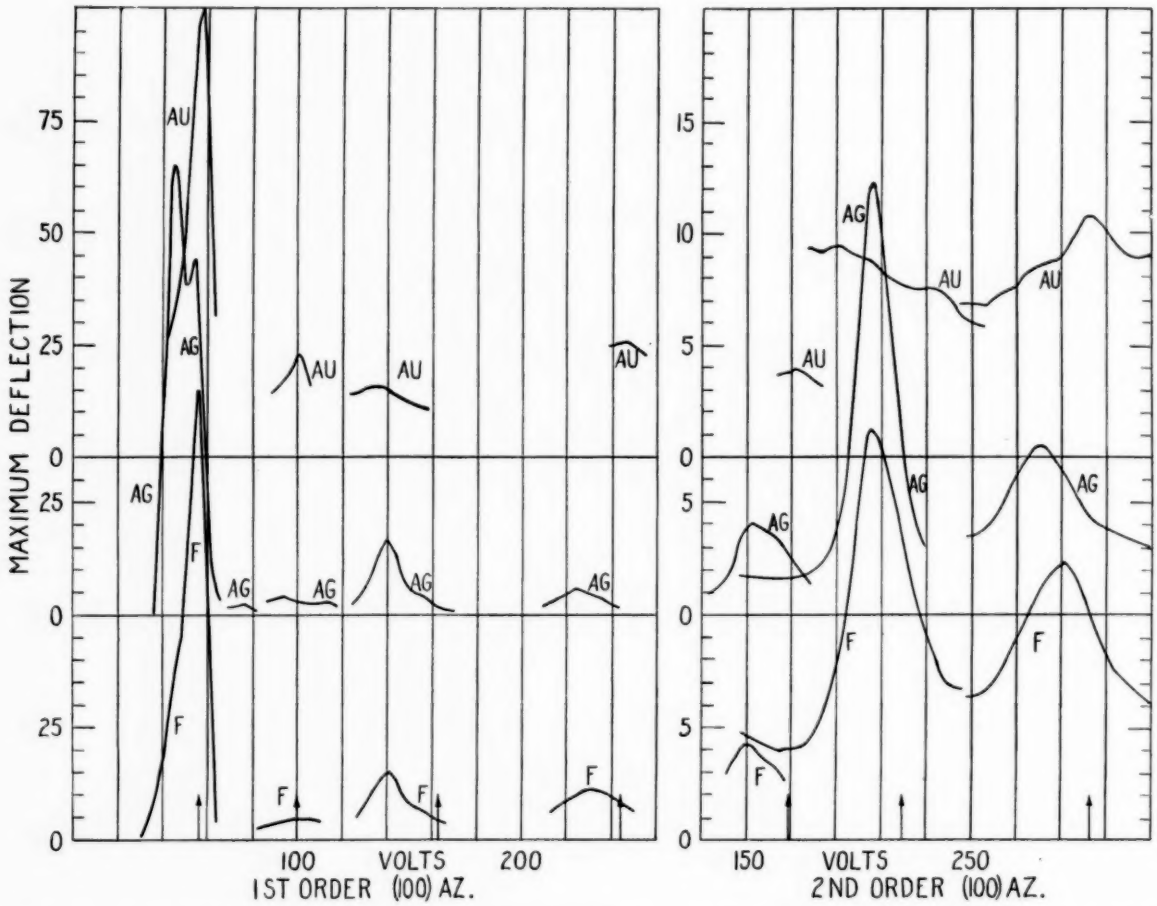

FIG. 1. Curves showing maximum deflection as a function of primary voltage for a gold crystal (Au), a silver crystal (Ag), and a silver film on a gold crystal (F). The colatitude angle is adjusted for maximum deflection for all points of the curves. Arrows indicate positions of theoretical beams for refractive index of unity.

Gas beams for gold

A search was made for beams due to a surface gas lattice at positions corresponding to half-order reflections but none was found even when the crystal surface was known to be covered with a considerable layer of gas, the presence of which results in a decrease of the intensity of the diffraction beams characteristic of the gold lattice. Thus gas does not always form in a simple lattice on the surface of a single crystal as it does in the cases of copper, silver and nickel.

Intensity measurements as a function of angle of incidence

Fig. 2 shows the relative intensities of various beam components as a function of angle of incidence. These curves were obtained by the same method as that previously used for silver crystals[1] and are to be compared with the curves for the corresponding beams from a silver crystal reproduced in Fig. 3 for comparison. This comparison of the curves for the corresponding beams from the gold and silver crystals shows both similarities and differences. Taking the 1st beam, 1st order, corresponding to reflection from the (210) set of planes, we note that there are four components in each case with considerable similarity in their distribution in angle of incidence. However, the voltages of the strongest component in the two cases are noticeably different. For the 2nd beam, 1st order, we also note the similarity that both of the strongest components increase rapidly as the angle of incidence varies from zero to negative values. However, many more weaker components of this beam were observed for silver than for gold. In

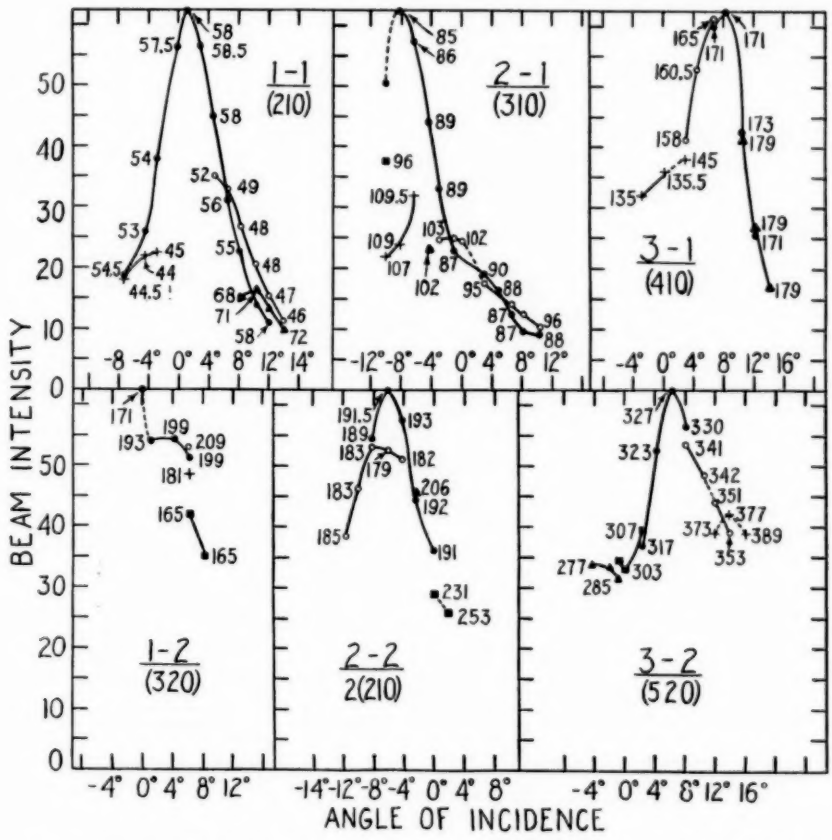

FIG. 2. Results for a gold crystal. The curves show relative intensities of beam components as a function of angle of incidence for the (100) azimuth (uncorrected for background scattering). Plane of reflection is in the (100) azimuth. Designation of beam 3–2 signifies third beam in the second order as per notation in Table I. Values of corrected voltages are given for several of the points.

the case of the 3rd beam, 1st order, there appears to be no correspondence for the two crystals. The number of components for the silver crystal is much the greater and the few components for the gold crystal do not closely resemble any of those for silver. Comparisons of three beams in the second order show no close resemblance. In each case the number, position, and form of the components are different.

EXPERIMENTS WITH A SILVER FILM ON A GOLD CRYSTAL

Although there are some similarities in the above characteristics for gold and silver crystals, the results show many differences. In comparing such characteristics for crystals of different substances it is essential to eliminate possible surface effects which may introduce differences apparently characteristic of the substance composing the crystal. By considering various surface irregularities it is possible to account for certain additional maxima, as recently discussed by Rupp.[3] The etched surface of the gold crystal was known to be much more irregular than that of the silver crystal, and it is natural to suppose that the nature of the irregularities, the size of the elementary lattices, and the mosaic structure of the two crystals may be quite different. However, a thin film of silver deposited on the surface of a gold crystal may be expected to possess the same irregularities and roughness as the underlying crystal, and consequently the corresponding results for such a silver film should furnish the desired information.

To carry out such measurements, the experimental tube was so altered that silver could be deposited on the gold crystal by evaporation in a

[3] E. Rupp, Ann. d. Physik **13**, 101 (1932).

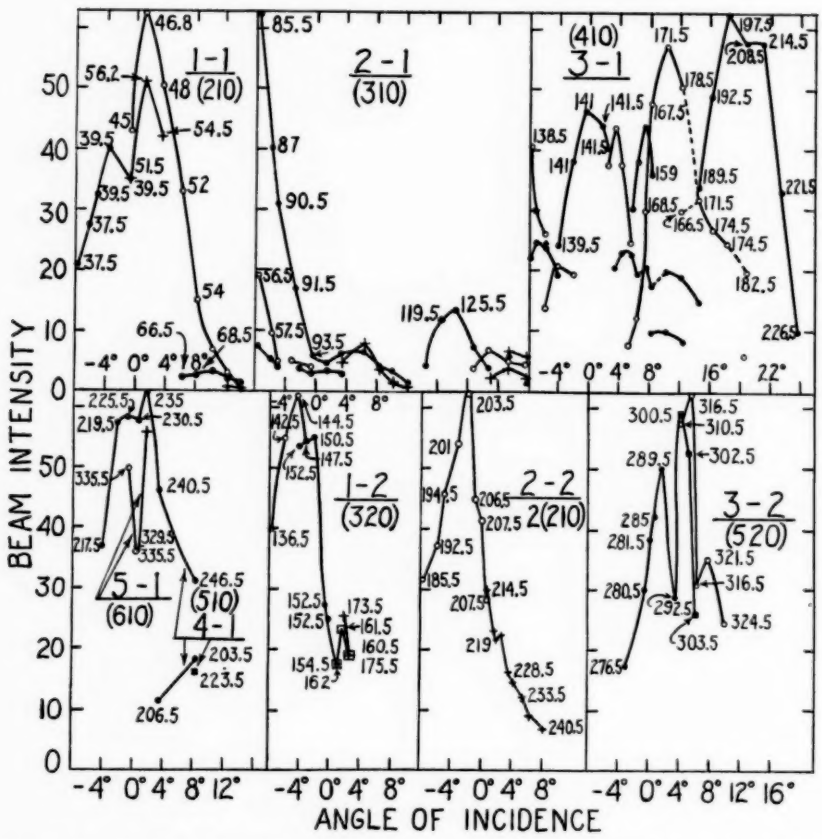

FIG. 3. Results for a silver crystal corresponding to those for a gold crystal shown in Fig. 2 with the same notation.

high vacuum and measurements were taken on the film immediately following the deposit. This was accomplished by withdrawing the gold crystal into a side tube where the front face was exposed to silver vapor coming from a pure silver mass held at dull red heat by electron bombardment from the rear. The usual order of procedure was to outgas the silver mass at red heat with the gold crystal concealed. The gold crystal was then outgassed at red heat, after which it was placed four or five cm from the dull red silver for from 1 to 10 min. The process was repeated several times by evaporating off the film on the gold crystal and then redepositing, with the same experimental results. The silver film forms in a crystalline structure whose orientation is determined by that of the underlying gold crystal. The film thicknesses were not known but were too thin to be visible.

The lower curves in Fig. 1 show the results obtained in the (100) azimuth for a silver film on a gold crystal when using normal incidence. As for the case of the other curves in the figure, we are plotting the maximum deflection of the beams for various voltages, the collector angle being adjusted for each reading. The arrows indicate the theoretical positions of the beams. The first four beams of the 1st order, and the first three beams of the 2nd order are shown. The relative intensities and positions of the beams are quite different for the silver and gold crystals. It is seen that the results for a silver film are quite closely in accord with those for a silver crystal, the chief difference being in the 1st beam, 1st order. For silver, this beam has two components, the low voltage one being more intense, while for the silver film there is an indication of a second component with the higher voltage one being much more intense. The voltage for this component is also approximately the same as that for the corresponding beam from the gold crystal. There is also some

difference in the 3rd beams of the 2nd order, but in general it is clear that the results for the film are very nearly in accord with those for a massive silver crystal. Observations on the film were also taken for various angles of incidence and curves plotted similar to those in Figs. 2 and 3 for several beams. These curves are not shown but were found to be closely in accord with those for the silver crystal. In particular, the complicated structure of the 3rd beam, 1st order, for the silver crystal was accurately reproduced for the silver film. Hence the differences between the results for silver and gold crystals appear to be real and not due to differences in irregularities of a secondary nature. Further results are required to determine the cause for the above-mentioned differences in the results for the film and for the silver crystal. In particular, measurements on thinner films of known thickness should be of value.

Deviations from the surface grating formula

It was first observed by Davisson and Germer that, during the growth and decay of a particular diffraction beam, the variation of the colatitude angle with the primary voltage was not in general such as to keep $V^{\frac{1}{2}} \sin\phi$ constant as is required by the plane grating formula. This condition was found to obtain best for the lowest voltage beams and not at all for higher voltage beams. This was interpreted to mean that the diffracting system was not a single lattice, but a collection of many small lattices of not more than five or ten atom lines in width, similarly oriented, but otherwise unrelated.

Fig. 4 shows a plot of $\sin\phi$ against $(150/V)^{\frac{1}{2}}$. The straight lines are surface grating lines given by $n_1\lambda=(a/2)\sin\phi$, and the curved lines are depth grating lines given by $n_2\lambda=a/2+a/2^{\frac{1}{2}}\cos(\phi+45°)$, and $n_3\lambda=a/2(1+\cos\phi)$. The rows of atoms corresponding to the various grating

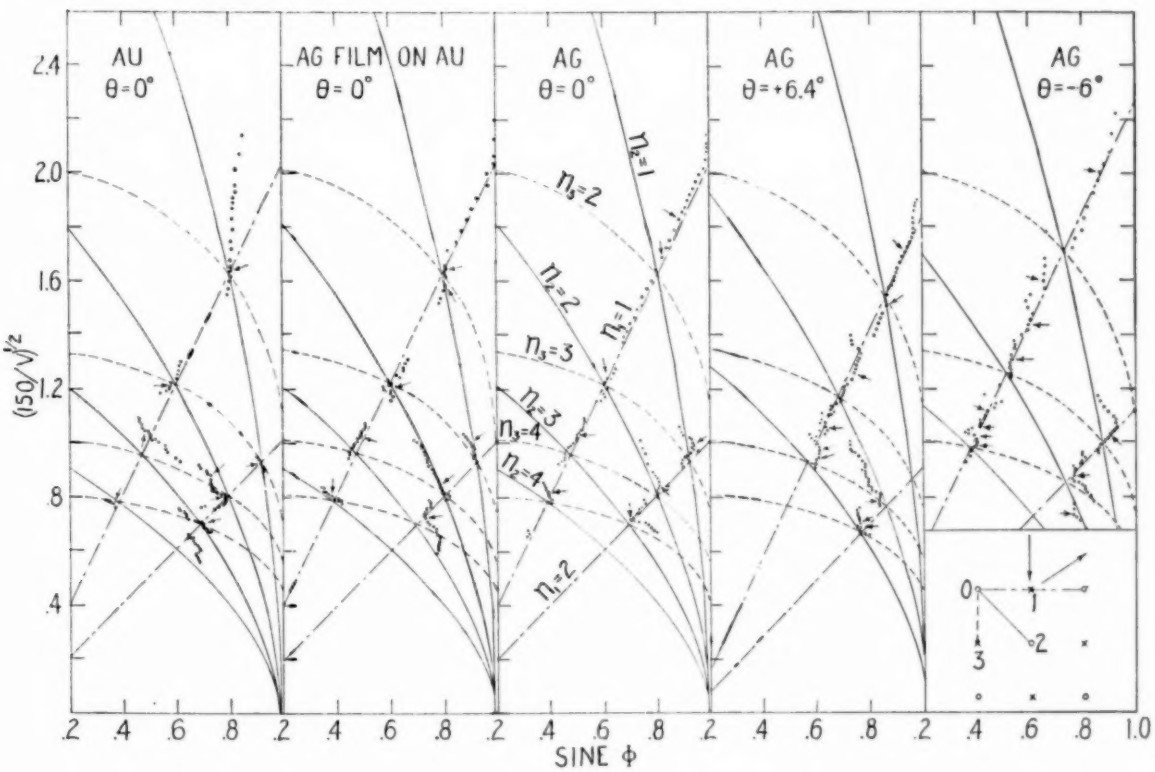

FIG. 4. Plots of $\sin\phi$ against $\lambda=(150/V)^{\frac{1}{2}}$. ϕ = colatitude angle measured from the normal. θ = angle of incidence of primary beam. The points are experimental observations, and the arrows indicate which ones correspond to maxima. The lines are obtained from grating formulas obtained by considering the corresponding rows of atoms as indicated in the lower right corner.

formulas are indicated in the lower right corner of the figure. Experimental points are given not only for voltages corresponding to maximum intensities, but at small voltage intervals over the range for which the beams can be detected during their growth and decay. It is seen that in general the surface grating formula is more nearly followed for the low-voltage beams, while a depth grating formula is a better approximation for the higher-voltage beams. But, in addition, it is to be noted that while the 3rd beam, 1st order, (3–1), follows the depth grating for the gold crystal, this beam follows the surface grating for both the silver crystal and the silver film on the gold crystal. Hence, if we grant that the grating irregularities and consequently the number of lines in the diffracting lattices are the same for the gold crystal and the silver film on the gold crystal, it appears necessary to conclude that some other factor is responsible for the difference in the behavior of this beam in the case of gold and silver crystals. One possibility is that the deviations from the surface grating formula result from the same mechanism as the fine structure of the diffraction beams. If this is the case there should be some correlation between fine structure and deviation from the surface grating formula. Both have been found to change with changes in the angle of incidence, but changes in fine structure characteristics are not always accompanied by changes in the deviation from the surface grating formula.

The two sets of curves at the right in Fig. 4 show the results for two different angles of incidence in the case of the (100) face of a silver crystal. It is to be noted that the experimental points for some of the beams follow one grating formula for one angle of incidence and a different grating formula for another angle of incidence. This is, however, not true for all of the beams. It is also seen that some of the experimental points for a beam may follow one grating formula while the remainder of the points for the same beam may follow another grating formula. These results suggest that under certain conditions some one direction in the crystal is more effective in producing constructive interference than other directions, a condition which might be realized by an unsymmetrical distribution of the potential in the outer regions of the atoms. One must, however, not overlook the possibility that if a portion of the surface is etched parallel to a set of atomic planes other than the one coinciding with the geometric boundary, this may be expected to cause the portions of the beam reflected from this surface to follow a grating formula for this surface.[4] But, it is not easy to see why all of the diffraction beams should not be equally affected. From the observations available this view does not appear sufficient to account for all of these characteristics. More observations are being made on this point.

The results of this investigation clearly show that the fine structure of the diffraction beams are determined at least to some extent by the nature of the atoms composing the crystal. It would seem that an extension of Morse's treatment[5] with fewer approximations is required to account for these results.

The purchase of the gold and some of the apparatus was made possible by a Grant-in-Aid from the National Research Council.

Messrs. K. P. Page and E. C. Bray have aided in taking the numerous observations.

Note added in proof: W. T. Sproull has now published a more detailed account of his investigation than that referred to above, and the writer is submitting some comments in a separate communication.

[4] W. T. Sproull has recently reported results [Phys. Rev. **42**, 904 (1932)] from the (112) surface plane of a tungsten crystal. In the azimuth perpendicular to the cube diagonals beams which obey a depth grating formula corresponding to rows of atoms in the (011) plane were found at every primary voltage tried. In all probability this is because the etched surface facets of the crystal are parallel to the (011) plane rather than the (112) plane. Etching parallel to the more densely populated (011) plane would result from evaporation by prolonged heat treatment even though the etched surface was originally parallel to the (112) plane. This, of course, must be taken into account in evaluating the inner potential from such observations.

[5] P. M. Morse, Phys. Rev. **35**, 1310 (1930).

On a Possible Explanation of Superconductivity

J. FRENKEL, *Physics Technical Institute, Leningrad, U. S. S R.*

(Received December 27, 1932)

An attempt is made to explain the phenomenon of superconductivity by taking into account the electromagnetic (inductive) forces which the electrons exert on each other when they move in an organized way. These forces stabilize the motion against the perturbations due to the thermal agitation of the crystal lattice. They can also entail a decrease of energy which may explain the thermodynamic stability of the superconducting state at low temperatures. The theory is not carried to the point of numerical calculation.

INTRODUCTION

THERE have been many attempts—all of them unsuccessful—to give an explanation of the phenomenon of superconductivity with the help of wave mechanics applied to the usual model of conduction electrons in a metal. The failure of these attempts can be due either to the incorrectness of the model (which is after all a refinement of the model of an electron gas), or to a neglect of some type of force which under certain conditions may become important. Kronig[1] has recently proposed replacing the electron gas model by that of a rigid electron lattice, an idea advanced long ago by J. J. Thomson and Lindemann without the notion that it can be made responsible for superconductivity, which vanishes when the lattice is melted or vaporized (at the transition temperature).

I wish to point to the possibility of a different issue, which consists in taking into account the electromagnetic (inductive) forces between the electrons. These forces have been totally neglected hitherto in the electron theory of metals (appearing in macroscopic phenomena only); it is possible however, at least in principle, to trace the phenomenon of superconduction to the action of these forces without abandoning the gas model—just as it has been possible to explain certain atomic phenomena which were beyond Bohr's theory not by a change of Bohr's model of the atom, but by taking into account the electromagnetic effects of the electron spin.

[1] R. de L. Kronig, Zeits. f. Physik **78**, 744 (1932).

I.

Let us imagine a large number N of electrons all moving in exactly the same way. If their distances apart (r_{ik}; i, $k=1, 2, \cdots N$) are small, the kinetic energy of the system will not simply be equal to the sum of the kinetic energies of the separate electrons, ΣK_i: there will be in addition what may be called the "mutual kinetic energy" of the different electrons, corresponding to their mutual induction. It is just this energy (and not the relatively insignificant sum of individual kinetic energies corresponding to drift motion which is represented as the *magnetic energy* of an electric current, $\int H^2 dV/8\pi$. The mutual kinetic energy of two electrons, i and k, is equal, roughly speaking, to e^2v^2/c^2r_{ik}; i.e., to v^2/c^2 times their electrostatic energy, where v is the (common) velocity of motion.[2] The total value of the mutual kinetic energy can be obtained by multiplying the average value of this expression for different pairs of electrons by $N(N-1)/2$, or approximately $N^2/2$, and can be written accordingly in the form: $K'=N^2e^2v^2/2c^2r$ where $1/r$ is the average value of $1/r_{ik}$. The sum of the individual energies of the electrons $K^0=Nmv^2/2$ can be

[2] In order to avoid misunderstanding, it may be mentioned that the smallness of the electromagnetic energy as compared with the electrostatic energy e^2/r of the electrons alone need not mean that the former is unimportant and should be neglected. In fact, the electrostatic mutual energy of the electrons is compensated (and even overcompensated) by their electric energy with respect to the positive ions. The situation here is quite similar to that which is met with in the ordinary theory of the mutual action of electrical currents in material circuits, where the electrostatic forces may be entirely left out of account.

written in a similar form if we replace the mass m by e^2/c^2a where a is the "radius" of an electron. The ratio

$$K'/K^0 = Na/r, \tag{1}$$

can thus become very large for sufficiently large values of N, so that finally K^0 can be neglected compared with K' (which is precisely the case with macroscopic phenomena). It should be mentioned that the distance r is itself a function of N; if the average distance between the neighboring electrons is fixed, as for instance in the case of a metallic body, we can put approximately $r=\delta N^{\frac{1}{3}}$ (identifying δ with the lattice constant) and consequently

$$K'/K^0 = N^{\frac{2}{3}}a/\delta. \tag{1a}$$

II.

To the magnetic—or rather electromagnetic—mutual action of the electrons there is associated, with the energy K', an additional *momentum* G' which is given by the expression

$$G' = \sum_{i,\ k} e^2v/c^2r_{ik} \leqq N^2e^2v/c^2r \tag{2}$$

so that

$$K' = G'v/2. \tag{2a}$$

This expression can be derived from the familiar expression $\mathbf{p}_i = m\mathbf{v}_i - e\mathbf{A}_i/c$ for the total momentum of an electron i moving in an electromagnetic field with a vector potential $\mathbf{A}_i$, in connection with the formula

$$\mathbf{A}_i = -\sum_{k \neq i} e\mathbf{v}/cr_{ik}.$$

The ratio of G' to the sum $G^0 = Nmv$ of the individual momenta of the electrons under consideration is equal to the ratio K'/K^0.

Let us imagine a crowd of electrons moving in the same way (i.e., as a rigid system) through the crystal lattice of a metal. Because of the electromagnetic mutual-action of the electrons—or to put it in other words, of their mutual induction—they must have an abnormally high inertia, so that the motion of each electron will be affected by an external perturbation—such as the heat motion of the lattice, for example—to a much smaller degree than in case it moved alone with the same velocity. Indeed, if an electron is knocked out of the crowd, coming to rest, for instance, the resulting change of the total momentum of the whole crowd will not be equal to the individual mv of this electron; there will be, in addition, the term $m'v = G_N' - G_{N-1}' = 2Ne^2v/c^2r$, representing the contribution due to the mutual action of the electron in question with all of the other $N-1$ electrons, m' being the additional "electromagnetic mass." Now for sufficiently large values of N this collective term will be very large compared with mv (their ratio being obviously equal to $2K'/K^0 = 2Na/r$). So long, therefore, as the electrons in a metal move collectively as an organized crowd of sufficiently large size, their motion can remain unaffected by the heat motion of the crystal lattice, the energy and momentum quanta of the heat waves being insufficient to knock out even a single electron.

At first sight it may seem that the above argument implies a contradiction. For so long as all of the electrons with the exception of the one under consideration preserve their state of motion they will produce a *constant* magnetic field, and will therefore contribute nothing to the inertia (mass) of the single electron which is stopped. Thus it would seem that the work done in accelerating the electrons one after the other is less than when they are accelerated simultaneously, which obviously would be incorrect. The fallacy of this objection lies in the fact that it does not take into account the energy or momentum which is transferred owing to the electromagnetic impulse of the electron in question (i.e., the one which is stopped) on the remainder. If the other electrons were allowed to change their state of motion, they would be accelerated; if they are not accelerated they must transfer the energy and momentum received to the crystal lattice. This amounts to saying that in the act of being stopped the electron pushes the crystal lattice forward, and consequently must get an additional backward impulse from it, this impulse being equivalent to the additional electromagnetic momentum which is thus indirectly revealed.

One might argue further that it is not necessary to consider transitions in which an electron is completely stopped, but only transitions in which its momentum is but slightly decreased, for which the momentum of the heat waves should suffice. In fact, the total impulse, p, of each

electron is quantized in the same way for the case in which the electromagnetic interaction is considered, as in the case when such interaction is neglected, the quantum steps Δp being the same in both cases. (See Section IV.) It follows by a consistent application of Pauli's principle, however, that only such effective transitions can occur as correspond to a change of energy or momentum of the order of magnitude of the largest existing at the absolute zero of temperature.

If we compare an organized motion of the above type with a disorganized motion *having the same total energy* we find that the total momentum will be larger in the former than in the latter case. Denoting by v_d the velocity of the disorganized motion (constituted, say, by one-half of the electrons moving in one direction and the other half in the opposite direction) we have from the condition

$$Nmv_d^2/2 = (Nmv^2/2) + (N^2e^2v^2/2c^2r) \leqq N^2e^2v^2/2c^2r,$$

$$v_d/v = (Na/r)^{\frac{1}{2}} = N^{\frac{1}{2}}(a/\delta)^{\frac{1}{2}},$$

which corresponds to the following ratio of the momenta

$$G_d/G = Nmv_d/(N^2e^2v/c^2r) = N^{-\frac{1}{2}}(a/\delta)^{-\frac{1}{2}}.$$

This ratio is smaller than 1 if N is larger than 10^7, corresponding to linear dimensions of the order of 10^{-6} cm.

It should be emphasized that by an organized motion we do not mean the drift motion constituting an electric current under ordinary conditions. The velocity of such a drift motion is usually very small compared with the individual velocities of the separate electrons, these individual velocities having practically random directions.

III.

The preceding considerations seem to suffice for the explanation of superconductivity if we assume that for some reason all of the electrons in a crystal lattice move—in the absence of any electric field—in an organized manner, the electric field applied for a moment serving simply to determine the otherwise arbitrary direction of motion.

This assumption obviously implies that under certain conditions the state corresponding to such an organized motion, that is, to a non-vanishing electric current, should have a smaller energy—or more exactly, *free energy*—than the ordinary state giving no resultant current.[3] Granting that the energy W_c of the "collectivized" state is lower than that of the "individualized" state, W_i, the former must prevail at and near the absolute zero of temperature. On the other hand, it is clear that the entropy of the collectivized state, S_c, must be *smaller* than that of the individualized S_i, since entropy is a measure of disorganization. We thus arrive at the conclusion that under the condition $W_c < W_i$, the *free* energy $F_c = W_c - TS_c$ of the c-state must be smaller than the free energy $F_i = W_i - TS_i$ of the i-state only for temperatures which are lower than a certain "critical" temperature T_0 given by the condition $F_c = F_i$, that is

$$T_0 = (W_i - W_c)/(S_i - S_c). \tag{3}$$

For temperatures which are higher than T_0 the individualized state on the contrary will have a smaller free energy than will the collectivized, becoming thus the normal one. We meet here exactly the same conditions as in the transition from the crystalline (solid) to the amorphous (liquid) state, the sharpness of the transition being explained in the same way in both cases.

IV.

It now remains to see how it is that the collectivized state of motion can have (at $T = 0$) a smaller energy than the individualized one, and this in spite of its additional electromagnetic energy. In the first place one must take into account the fact that the latter can be compensated for by a general decrease of velocity, so that for example the total energy remains constant or even *decreases*, while the momentum increases (see Section II). This possibility seems at first sight to be barred by Pauli's exclusion principle (even with due regard to the increase of the effective mass on an electron because of its electromagnetic interaction with the others). Pauli's principle, when applied to an electron gas with a homogeneous distribution of all the

[3] This possibility has been pointed out by Bloch.

directions of motion gives for the maximum value of the momentum of an electron, the expression[4] $p_{max}=h(N/V)^{\frac{1}{3}}$, where V is the volume of the gas. If instead, all the electrons are imagined to move in the same direction, in a system of parallel closed stream lines, for example, we get $p_{max}=h(N/L)$, where L is the linear extension, and is approximately $V^{\frac{1}{3}}$. This would correspond to an increase of the kinetic energy if the effective mass of an electron remained the same in both cases. As a matter of fact, for sufficiently large values of N it is much larger in the latter than in the former case. Denoting it with $m^*=m+m'$ (where m' is the "electromagnetic" mass), we have $v^*_{max}=p^*_{max}/m^*=hN/Lm^*$, and $K^*=h^2N^2/2m^*L^2$. The ratio K^*/K is thus equal to $(mN^2/m^*L^2)/(N/V)^{\frac{2}{3}}=(m/m^*)N^{\frac{4}{3}}$. Now we have also $m^*/m=1+(aN^{\frac{1}{3}}/\delta)\cong(a/\delta)N^{\frac{1}{3}}$, or more exactly (if the motion takes place in closed lines) $m^*/m=(a/\delta)N^{\frac{1}{3}}\ln N^{\frac{1}{3}}$ so that

$$K^*/K=\delta N^{\frac{4}{3}}/a\ln N^{\frac{1}{3}}.$$

We thus see that the energy is tremendously increased in spite of the decrease of velocity. However, we need not consider this extreme case of a *completely* ordered motion. If, for instance, we reverse the directions of motion of one-half of the electrons so that they all have positive projections of their velocities in a certain direction, p_{max} will be multiplied by a factor 2, whereas the electromagnetic mass will be increased practically in the same ratio as before. We thus shall have in this case $K^*/K\cong 4m/m^*=(4\delta/a)N^{-\frac{4}{3}}\ln N^{\frac{1}{3}}$, which will be very small compared to unity if N is larger than 10^7 (with $\delta=10^{-8}$). Of course there will be, in this case, practically no gain in the value of the momentum p_{max}, which must be greatly increased in order to stabilize the electrons against the perturbations produced by the heat motion of the crystal lattice.

It seems that under these conditions a compromise is possible such that through a *partial* organization of the motion of the electrons in a predominant direction the momentum will be sufficiently decreased to make the transition to this partially organized state desirable at very low temperatures.

[4] Neglecting immaterial numerical coefficients of the order of magnitude of unity.

V.

Apart from the above considerations one might look for a decrease of energy associated with the organized or collectivized motion in some *quantum effects* of the same type as those met with in the case of an isolated atom. When the number of external electrons in an atom is not too large, the normal state (i.e., the state of lowest energy) is specified according to the well-known rule of Hund by the condition that the resultant spin S and the *resultant orbital angular momentum* L should both have their *largest possible values*. Now so far as L is concerned this means that the external electrons *tend to move about the nucleus in the same direction*, that is, "collectively in the above sense."

The analogy between the motion of the electrons in an atom and in a metal which is supposed to be in the collectivized; i.e., superconducting state, is made clearer if we remember that in the latter case we actually also have to do with a motion of *revolution*, since (classically speaking) the motions of electrons in order to be stationary must proceed in *closed lines*. The quantity which serves to specify this motion is not the momentum $\mathbf{G}=\mathbf{G}^0+\mathbf{G}'$, which was considered in the foregoing sections, but something akin to the moment of momentum, or angular momentum, $\mathbf{L}=\mathbf{L}^0+\mathbf{L}'$ referred to any point of the metal.

The simplest model of the latter is provided by a closed chain (or "ring") of equidistant atoms, the free electrons being allowed to move along the chain in either direction. Under ordinary conditions the state of smallest energy is specified by the vanishing both of the resultant spin and of the resultant current $\mathbf{J}$, corresponding to the angular momentum $\mathbf{L}$ (an exact equivalence between $\mathbf{L}$ and $\mathbf{J}$ is not possible so long as the electrical field which characterizes the chain of atoms is not a central field, so that $\mathbf{L}$ is not a constant of the motion, while $\mathbf{J}$ is such a constant). This means that one-half of the electrons have their spins pointing one way, and the other half the opposite way, and that furthermore each half consists of electron pairs moving in opposite directions with a velocity of the same magnitude. According to Pauli's exclusion principle, these velocities must be different for different pairs, increasing from zero for the first pair up to

a certain maximum value for the last one. An electric current can be produced under such conditions by taking a certain number Q of electrons moving in the negative direction, for example, with velocities just smaller than v_{max} and transferring them to states of motion in the positive direction with velocities just larger than v_{max}, each individual state being occupied by a single electron (with a given spin). Under normal conditions, this must be accompanied by an increase of kinetic energy proportional to Q (taking into account both individual and electromagnetic energy of the electrons we must allow for a possible decrease of velocities, corresponding to the increase of the effective electromagnetic mass). This result is quite similar to that which is found if one examines the magnetization of an ordinary metal, displaying a paramagnetism independent of the temperature. In the latter case the increase of kinetic energy is balanced by a decrease of magnetic energy due to the presence of an external magnetic field. In the former case it can be due to the presence of an electromotive force acting along the chain of atoms (the notion of energy being no longer applicable, and an ever-increasing current being produced instead of an equilibrium state).

Now in certain metals—namely those belonging to the ferromagnetic group—the magnetization is accompanied not by an increase, but by a *decrease* of energy, the latter being proportional to the square of the number of equally oriented electron spins ($2Q$), but with a negative proportionality coefficient.

It seems natural to expect that there can exist metals which are analogous to these ferromagnetic bodies in the sense that the motion of electrons in the same direction should also correspond to a *decrease* of energy proportional to Q, where $2Q$ is the number of electrons in the "collective" or "organized" crowd. Since Q is in this case proportional to the current strength J, we can write the energy as a function of this "spontaneous" current in the form:

$$\Delta W_Q = -\tfrac{1}{2}\gamma J^2, \tag{4}$$

where γ is a certain positive proportionality coefficient, analogous to the coefficient of the molecular magnetic field in Weiss' theory.

We thus see that so long as the condition $\gamma > 0$ is fulfilled, our unidimensional model of the metallic body will give a spontaneous electric current at $T=0$, without an applied electric force; i.e., will behave like a superconductor.

VI.

It is now easy to pass from our ring-model to a real three-dimensional metal. This transition will be quite similar to that which is made in Weiss' theory of ferromagnetism, from a single body spontaneously magnetized in a given direction to a metal with elements of volume spontaneously magnetized in different directions. To these spontaneously magnetized regions of a ferromagnetic body there must correspond, in a superconducting body, regions with whirl currents whose orientations, specified by their axes, vary in an irregular manner from one region to another. As a matter of fact, such regions should behave like magnets of molar dimensions except for the spin orientation of the electrons which, just as in the case of isolated atoms, can neutralize to a large extent the magnetic moment due to the motion of revolution which constitutes the electric currents. So far as can be inferred from analogy with atoms, the normal state must be characterized by an opposite orientation of the resulting orbital and spin angular momenta if the number of electrons is less than one-half of all the individual quantum states at their disposal (within a given band); if it is larger than this, the two momenta should have the same orientation.

With regard to its reaction to an external magnetic field, a metal in the superconducting state must behave like a *diamagnetic* body with a large negative susceptibility—in view of the large size of the "orbits" of the electrons in the different regions. This is quite equivalent to saying that the interior of such a body will be screened from external magnetic fields by the system of surface currents induced by the latter. The surface currents in a superconducting body can be visualized not as the result of an extreme spin effect, but in exactly the same way as the surface currents in a magnetized nonconducting body. The latter can be ascribed, as is well known, to the orbital motion of the bound electrons in the surface atoms, their strength and direction being given by the vector product of the

magnetization at the surface and the normal to the corresponding surface element. The same description can obviously be applied to the surface currents in a superconductor, the surface atoms being replaced by the surface whirl regions.

This treatment of free electrons in whirl regions as bound electrons moving in definite orbits needs, of course, an amendment for the case of a current flowing through a superconductor forming but a link in a circuit with an ordinary conductor of electricity. In this case electrons must enter the superconductor on one side and leave it on the other. It is natural to imagine that such a transfer of electrons is achieved by a gradual shift of the whole system of whirl currents in the superconductor, accompanied eventually by the destruction ("melting") of these whirl currents on one side and the formation of new ones on the other.

The above view easily explains the dependence of the transition temperature (from the superconducting to the ordinary state) on an external magnetic field. Since the superconducting body can be considered as highly diamagnetic, its energy must *increase* when such a field H is applied to it, by an amount proportional to H^2. Putting accordingly

$$W_c(H) = W_c(0) - \tfrac{1}{2}\chi H^2, \tag{5}$$

(where χ is the effective susceptibility of the body) in the expression (3) for the transition temperature, we get

$$T_H = T_0 - aH^2, \tag{4a}$$

where $a = \chi/2(S_i - S_c)$, the entropy being obviously unaffected by the field (to a first approximation at least).

This result is in qualitative agreement with the experimental facts, which however indicate a *linear* dependence between T and H, or more accurately, a dependence expressed by the empirical formula $T_0^2 - T_H^2 = cH$. I hope that a more exact wave-mechanical theory based on the above ideas will be able to remove this discrepancy.

Magnetic Dipole Fields in Unstrained Cubic Crystals

L. W. McKeehan, *Sloane Physics Laboratory, Yale University*

(Received February 13, 1933)

Magnetic field components in certain cubic arrays of equal parallel dipoles are computed by two methods for points on the boundary of a dipole domain and for points near a vacated dipole position. The results may be of use in theories of ferromagnetism. Characteristic constants for a nonpolar cubic array of dipoles, previously computed by Bouman, are recomputed more precisely.

THE present state of ferromagnetic theory is somewhat chaotic, but a few definite conclusions have been reached and a direction for further advances may be indicated. The high stability of saturated magnetization in crystal domains containing many atoms each is inexplicable by magnetic forces but so-called exchange forces are of the right order of magnitude to account for it. These exchange forces have been estimated from electrostatic energy associated with states in which one electron in each atom of every adjacent pair has its spin-axis parallel to that of the similar disposable electron in the other member of the pair. The argument is quasi-classical in its postulation of Coulomb electric forces between the electrons in question. It is important to notice that the energy of electrostatic forces between each magnetically disposable electron and the other electrons of the atom are supposed not to be affected by the choice of direction of the electron spin-axis. The exchange interaction may thus be thought of as depending only upon the spatial distribution of the disposable electrons and the electrostatic interaction between them. It is not yet clear how easy directions for magnetization are determined. They may be due to interactions between disposable and other electrons in the same atom, but there seems to be little evidence for a control of the orientation of completed electron-shells by crystal symmetry and such completed shells may be statistically of spherical symmetry, so as to have no resultant magnetic effect. It seems worth while, at least, to consider the hitherto deliberately neglected magnetic interaction between the disposable electrons. This is of the right order of magnitude to allow control of the direction of saturation by weak magnetic forces, and must appear in some form in the completed theory. The complete solution can be outlined as soon as we know the time-average distribution functions for the magnetic field intensity and for the occurrence of the "ferromagnetic" electrons within each atomic domain. This paper makes an attack upon the first of these distribution functions. It seems more likely to be of value because it is already known that the changes in local magnetic fields which can be produced by strain are of the right sort to account almost quantitatively for the corresponding changes in ferromagnetic behavior, and for magnetostriction.

We propose to calculate the magnetic field intensity at selected points in certain cubic arrays of equal magnetic dipoles. The four easiest cases are presented by the simple cubic lattice (S), the body-centered cubic lattice (I), the face-centered cubic lattice (F), and the array characteristic of diamond (D). The last of these is a case of (F) having two dipoles specially placed with reference to each lattice point. The magnetic field intensity $\mathbf{H}$ at any point is proportional to Pa_0^{-3} where P is the magnetic moment of each dipole and a_0 is the edge of the unit cube. For greater generality we will compute a field factor $\mathbf{h}$, independent of P and a_0 and therefore related to $\mathbf{H}$ by the equation

$$\mathbf{H}=\mathbf{h}Pa_0^{-3}. \tag{1}$$

We must therefore replace each vector moment $\mathbf{P}$ by a parallel unit vector $\mathbf{p}$ and each vector translation $\mathbf{V}$ by a parallel vector $\mathbf{v}=\mathbf{V}a_0^{-1}$.

We select any dipole as an origin of rectangular

coordinates parallel to the cubic axes. Then the position of any other dipole is fixed by a vector $\mathbf{r}$ to it from the origin. The different arrays are distinguished in Table I by selection rules for the components r_i, where the subscript i is successively 1, 2 and 3 for each dipole. If two or three components are to be referred to we use subscripts i and j, or i, j and k. An arbitrary integer, positive, negative, or zero is indicated by n_i or by n, and N is the number of dipoles per unit cube.

TABLE I. *Characterization of dipole arrays.*

N is the number of dipoles per unit cube.

Name Selection Rule	Symbol	N
Simple cubic $r_i=n_i$.	(S)	1
Body-centered cubic $r_i=n_i$, and $r_i=n_i+\frac{1}{2}$.	(I)	2
Face-centered cubic $r_i=n_i$ or $n_i+\frac{1}{2}$; $\Sigma_i r_i=n$.	(F)	4
Diamond cubic $r_i=n_i$ or $n_i+\frac{1}{2}$; $\Sigma_i r_i=n$, and $r_i=n_i+\frac{1}{4}$ or $n_i+\frac{3}{4}$; $\Sigma_i r_i=n+\frac{3}{4}$.	(D)	8

We will first suppose that all dipoles are parallel so that $\mathbf{p}$ is the same for all. The magnetic moment per unit volume,

$$\mathbf{I}=N\mathbf{p}a_0^{-3}, \tag{2}$$

corresponds to magnetic saturation. If, in calculating $\mathbf{H}$ we find a term depending on $\mathbf{I}$, the field factor $\mathbf{h}$ will depend in the same way upon $N\mathbf{p}$.

We let s_i be the three coordinates of a point, not occupied by a dipole ($\mathbf{s}\neq\mathbf{r}$), at which the h_i are desired, and put $\mathbf{r}-\mathbf{s}=\mathbf{t}$. The increment of h_i due to the dipole defined by $\mathbf{r}$ is

$$\delta h_i=(3t_i^2t^{-5}-t^{-3})p_i+3t_it_jp_j+3t_it_kp_k, \tag{3}$$

or, for abbreviation,

$$\delta h_i=\delta h_{ii}p_i+\delta h_{ij}p_j+\delta h_{ik}p_k. \tag{4}$$

In a finite crystal h_i in general depends upon the crystal boundary so that we must either sum δh_i for all the dipoles in a specimen, which is inconvenient, or resort to an artifice. One such artifice, that of Lorentz,[1] substitutes for the dipoles beyond a convenient sphere of radius $t_{\lim}$ a continuum with uniform magnetization $N\mathbf{p}$.

[1] H. A. Lorentz, *Theory of Electrons*, pp. 303–306 (1909).

The correction term to the result of summing δh_i up to $t_{\lim}$ is then calculable for some shapes of specimen. For a spherical crystal the correction term vanishes. For an infinite crystal it is $4\pi N\mathbf{p}/3$. We accordingly write for an infinite crystal

$$\mathbf{h}=4\pi N\mathbf{p}/3+\lim\Sigma\delta\mathbf{h}, \tag{5}$$

or in scalar form

$$h_i=4\pi Np_i/3+\lim\Sigma\delta h_i, \tag{6}$$

that is,

$$h_i=\{4\pi N/3+\lim\Sigma\delta h_{ii}\}p_i+\lim\Sigma\delta h_{ij}p_j+\lim\Sigma\delta h_{ik}p_k. \tag{7}$$

The approximation to the final value is slow, but this final value may be predicted with fair certainty after a manageable number of terms have been computed. It saves time and improves precision to choose a symmetrical direction for $\mathbf{s}$, for then the number of terms separately to be computed becomes much less than the number of dipoles included. The field distribution in each dipole domain is the same and $\mathbf{s}$ therefore has a limit, depending upon its direction, beyond which it is unnecessary to increase its magnitude. In general $s_{\lim}\overline{\overline{<}}3^{\frac{1}{2}}/2$.

Fig. 1 shows one unit cube in each array (that lying between the origin and the dipole at $r_1=r_2=-1$, $r_3=1$) with the positions of its N dipoles indicated by small circles and with one dipole domain outlined about the origin. Corners and other important points on the boundary of each such domain are marked, on the prolongation through them of lines from the origin, with their coordinates: $s_1s_2s_3$.

If a line be drawn from the origin to any point on the boundary of the atomic domain it is easy to see from considerations of symmetry that a given h_i varies from a maximum to a minimum, or *vice versa*, as we traverse the line. A general survey of the field is therefore most easily made by selecting points on the boundary of an atomic domain. Since the field intensities at $\mathbf{s}$ and at $-\mathbf{s}$ are always equal (and parallel) it is necessary to consider only one-half of the atomic domain in selecting such points.

Table II presents h_i for selected points of the sort marked in Fig. 1, for a series of values for $t_{\lim}$, and for two simple directions for $\mathbf{p}$, in arrays (S), (I) and (F). Each line in part C of this table

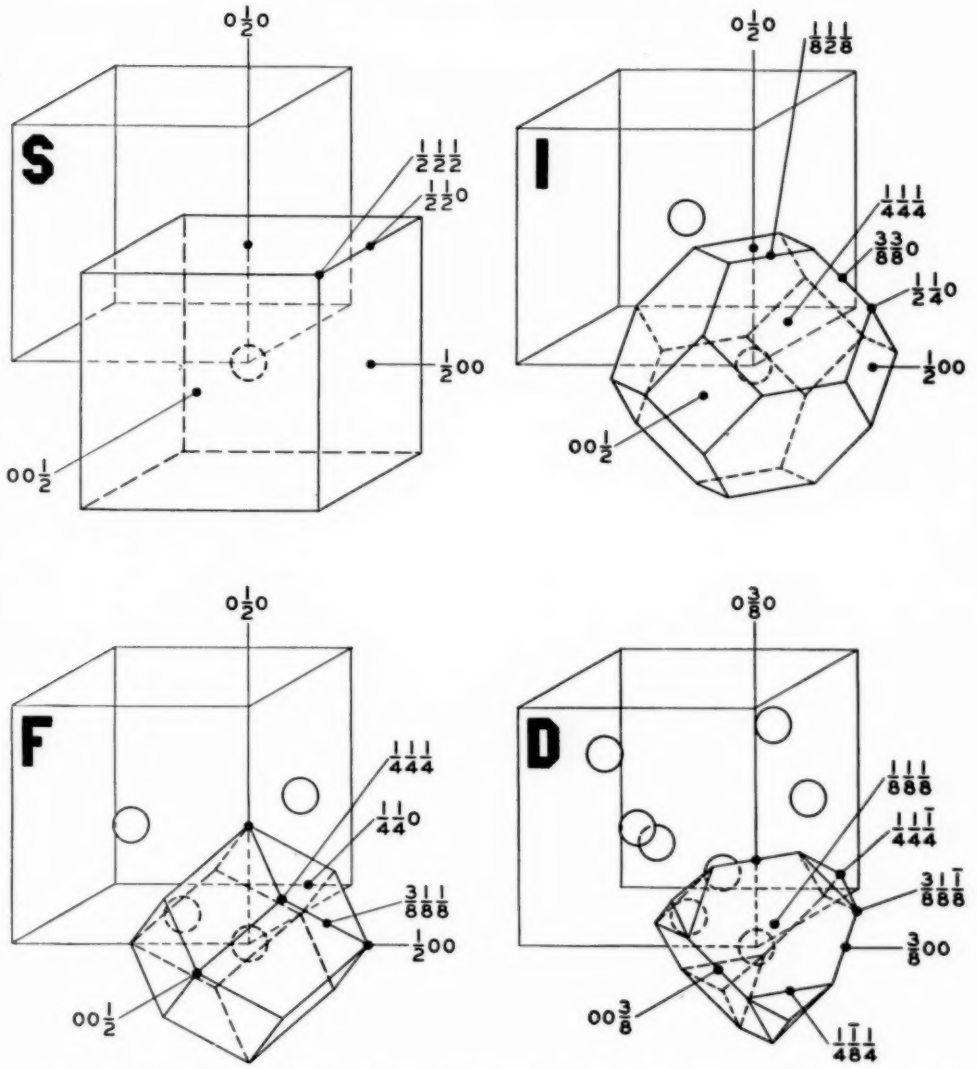

FIG. 1. Dipole domains in cubic arrays: (*S*) Simple cubic, (*I*) Body-centered cubic, (*F*) Face-centered cubic, (*D*) Diamond cubic. Coordinates $s_1 s_2 s_3$ are given in terms of the edge of the unit cube. Circles show the positions of the dipoles associated with the unit cube which is outlined.

corresponds to including an additional group of dipoles all with the same t. Since t is generally an irreducible surd t^2 is preferred as the argument. The number of dipoles, $\sum N$, included at each stage of the summation, is also recorded. It will be noted that $\sum N \sim 4\pi N t^3/3$. The term $4\pi N p_i/3$ is put last, in part A, which summarizes the results, for two reasons. In the first place it tends to smooth out those variations of the local field with which we are chiefly concerned. In the second place it is logically last because it arises from the extension of the array to infinity.

The last column in Table IIA contains values of h_i computed by a second artifice, due to Ewald,[2] applied to the present problem by Kornfeld[3] and justified in detail by Bouman.[4] We write, in analogy with (4)

$$h_i = h_{ii} p_i + h_{ij} p_j + h_{ik} p_k. \tag{8}$$

Each coefficient (h_{ii}, h_{ij}, h_{ik}) is composed of three

[2] P. P. Ewald, Ann. d. Physik [4] **64**, 253–287 (1921).
[3] H. Kornfeld, Zeits. f. Physik **22**, 27–43 (1924).
[4] J. Bouman, Archives Néerlandaises [3A] **13**, 1–28 (1931).

TABLE II, PART A. *Values of h_i for points on the boundary of a dipole domain.* Column 1: Type of array; (*S*), (*I*), or (*F*). Column 2: Components of dipole moment; $p_1p_2p_3$. Column 3: Coordinates of point; $s_1s_2s_3$. Column 4: Column number in part C where a series of values of $M\Sigma\delta h_i$ are given. A dash indicates that all values of $\Sigma\delta h_i$ are zero. Column 5: M. Column 6: Last $\Sigma\delta h_i$ here computed. Column 7: $4\pi Np_i/3$. Column 8: h_i (method of Lorentz). Column 9: h_i (method of Ewald). In columns 4 to 9 inclusive there are three entries for each entry in column 3, corresponding, in that order, to $i=1, 2, 3$.

1	2	3	4	5	6	7	8	9
(*S*)	1 0 0	1/2 1/2 1/2	–	–	0	4.18879	4.18879	4.18879
			–	–	0	0	0	0
			–	–	0	0	0	0
		1/2 1/2 0	1	2	4.39297	4.18879	8.58196	8.52266
			–	–	0	0	0	0
			–	–	0	0	0	0
		0 1/2 1/2	1	−1	− 8.78595	4.18879	− 4.59716	− 4.47894
			–	–	0	0	0	0
			–	–	0	0	0	0
		1/2 0 0	3	1	30.95208	4.18879	35.14087	34.27084
			–	–	0	0	0	0
			–	–	0	0	0	0
		0 1/2 0	3	−2	−15.47604	4.18879	−11.28725	−10.85223
			–	–	0	0	0	0
			–	–	0	0	0	0
	1/3 1/3 1/3	1/2 1/2 1/2	–	–	0	2.41840	2.41840	2.41840
			–	–	0	2.41840	2.41840	2.41840
			–	–	0	2.41840	2.41840	2.41840
		1/2 1/2 0	2	2	2.53628	2.41840	4.95468	4.92056
			2	2	2.53628	2.41840	4.95468	4.92056
			2	−1	− 5.07257	2.41840	− 2.65417	− 2.58592
		1/2 0 0	4	1	17.87019	2.41840	20.28859	19.78628
			4	−2	− 8.93510	2.41840	− 6.51670	− 6.26553
			4	−2	− 8.93510	2.41840	− 6.51670	− 6.26553
(*I*)	1 0 0	1/2 1/4 0	5	2	3.01186	8.37758	11.38944	11.41394
			–	–	0	0	0	0
			–	–	0	0	0	0
		1/4 1/2 0	5	−1	− 6.02371	8.37758	2.35387	2.30489
			–	–	0	0	0	0
			–	–	0	0	0	0
		1/2 1/8 1/8	7	1	10.02019	8.37758	18.39777	18.33361
			–	–	0	0	0	0
			–	–	0	0	0	0
		1/8 1/2 1/8	7	−2	− 5.01010	8.37758	3.36748	3.39958
			–	–	0	0	0	0
			8	1	7.21119	0	7.21119	7.14688
		1/2 0 0	12	1	21.42572	8.37758	29.80330	29.79189
			–	–	0	0	0	0
			–	–	0	0	0	0
		0 1/2 0	12	−2	−10.71286	8.37758	− 2.33528	− 2.32958
			–	–	0	0	0	0
			–	–	0	0	0	0
		3/8 3/8 0	7	−2	− 5.01010	8.37758	3.36748	3.39958
			8	1	7.21119	0	7.21119	7.14688
			–	–	0	0	0	0
		0 3/8 3/8	7	1	10.02019	8.37758	18.39777	18.33661
			–	–	0	0	0	0
			–	–	0	0	0	0
		1/4 1/4 1/4	–	–	0	8.37758	8.37758	8.37758
			14	1	21.43140	0	21.43140	21.24094
			14	1	21.43140	0	21.43140	21.24094
	1/3 1/3 1/3	1/2 1/4 0	6	2	1.73890	4.83680	6.57570	6.58984
			6	−1	− 3.47779	4.83680	1.35901	1.33072
			6	2	1.73890	4.83680	6.57570	6.58984
		1/2 1/8 1/8	9	1	5.78516	4.83680	10.62196	10.58491
			10	1	1.27080	4.83680	6.10760	6.08899
			10	1	1.27080	4.83680	6.10760	6.08899

1	2	3	4	5	6	7	8	9
(*I*)	1/3 1/3 1/3	1/2 1/8 $\bar{1}$/8	9	1	5.78516	4.83680	10.62196	10.58491
			11	−1	− 7.26900	4.83680	− 2.43210	− 2.13651
			11	−1	− 7.26900	4.83680	− 2.43210	− 2.13651
		1/2 0 0	13	1	12.37015	4.83680	17.20695	17.20036
			13	−2	− 6.18507	4.83680	− 1.34827	− 1.34497
			13	−2	− 6.18507	4.83680	− 1.34827	− 1.34497
		3/8 3/8 0	10	1	1.27080	4.83680	6.10760	6.08899
			10	1	1.27080	4.83680	6.10760	6.08899
			9	1	5.78516	4.83680	10.62196	10.58491
		3/8 $\bar{3}$/8 0	11	−1	− 7.26900	4.83680	− 2.43210	− 2.13651
			11	−1	− 7.26900	4.83680	− 2.43210	− 2.13651
			9	1	5.78516	4.83680	10.62196	10.58491
		1/4 1/4 1/4	15	1	24.74685	4.83680	29.58365	29.36734
			15	1	24.74685	4.83680	29.58365	29.36734
			15	1	24.74685	4.83680	29.58365	29.36734
		1/4 1/4 $\bar{1}$/4	–	–	0	4.83680	4.83680	4.83680
			–	–	0	4.83680	4.83680	4.83680
			15	−1	−24.74685	4.83680	−19.91005	−19.69013
(*F*)	1 0 0	1/2 0 0	–	–	0	16.75516	16.75516	16.75516
			–	–	0	0	0	0
			–	–	0	0	0	0
		3/8 1/8 1/8	–	–	0	16.75516	16.75516	16.75516
			16	1	13.35659	0	13.35659	13.49447
			16	1	13.35659	0	13.35659	13.49447
		1/8 3/8 1/8	–	–	0	16.75516	16.75516	16.75516
			16	1	13.35659	0	13.35659	13.49447
			16	−1	−13.35659	0	−13.35659	−13.49447
		1/4 1/4 1/4	–	–	0	16.75516	16.75516	16.75516
			–	–	0	0	0	0
			–	–	0	0	0	0
		1/4 1/4 0	18	2	17.57189	16.75516	34.32705	34.09064
			19	1	57.41342	0	57.41342	57.84236
			–	–	0	0	0	0
		0 1/4 1/4	18	−1	−35.14379	16.75516	−18.38863	−17.91578
			–	–	0	0	0	0
			–	–	0	0	0	0
	1/3 1/3 1/3	1/2 0 0	–	–	0	9.67360	9.67360	9.67360
			–	–	0	9.67360	9.67360	9.67360
			–	–	0	9.67360	9.67360	9.67360
		3/8 1/8 1/8	17	1	15.42286	9.67360	25.09646	25.25567
			–	–	0	9.67360	9.67360	9.67360
			–	–	0	9.67360	9.67260	9.67360
		3/8 1/8 $\bar{1}$/8	–	–	0	9.67360	9.67360	9.67360
			17	1	15.42286	9.67360	25.09646	25.25567
			–	–	0	9.67360	9.67360	9.67360
		3/8 $\bar{1}$/8 $\bar{1}$/8	17	−1	−15.42286	9.67360	− 5.74926	− 5.90849
			17	−1	−15.42286	9.67360	− 5.74926	− 5.90849
			17	−1	−15.42286	9.67360	− 5.74926	− 5.90849
		1/4 1/4 1/4	–	–	0	9.67360	9.67360	9.67360
			–	–	0	9.67360	9.67360	9.67360
			–	–	0	9.67360	9.67360	9.67360
		1/4 1/4 0	20	1	43.32741	9.67360	53.00101	53.07754
			20	1	43.32741	9.67360	53.00101	53.07754
			21	−1	−20.29027	9.67360	−10.61667	−10.34368
		1/4 $\bar{1}$/4 0	22	−1	−23.00252	9.67360	−13.32892	−13.71306
			22	−1	−23.00252	9.67360	−13.32892	−13.71306
			21	−1	−20.29027	9.67360	−10.61667	−10.34368

TABLE II, PART B. Columns 1, 2, 3: Same as in Table II, part A. Column 4: Coordinates of point, $s_1's_2's_3'$, not appearing in part A. Column 5: $h_1'h_2'h_3'$ in terms of $h_1h_2h_3$ as given in columns 8 and 9 of part A for $s_1s_2s_3$ as given in column 3. For ease in reading only the order of $h_1h_2h_3$ is given. Thus 3 1 2 means that $h_1' = h_3$, $h_2' = h_1$, $h_3' = h_2$.

1	2	3	4	5
(S)	1 0 0	1/2 1/2 1/2	1/2 1/2 $\bar{1}$/2	1 2 3
			1/2 $\bar{1}$/2 1/2	1 2 3
			1/2 $\bar{1}$/2 $\bar{1}$/2	1 2 3
		1/2 1/2 0	1/2 0 1/2	1 2 3
			1/2 0 $\bar{1}$/2	1 2 3
			1/2 $\bar{1}$/2 0	1 2 3
		0 1/2 1/2	0 1/2 $\bar{1}$/2	1 2 3
		0 1/2 0	0 0 1/2	1 2 3
	1/3 1/3 1/3	1/2 1/2 1/2	1/2 1/2 1/2	1 2 3
			1/2 $\bar{1}$/2 1/2	1 2 3
			1/2 $\bar{1}$/2 $\bar{1}$/2	1 2 3
		1/2 1/2 0	1/2 0 1/2	2 3 1
			1/2 0 $\bar{1}$/2	2 3 1
			1/2 $\bar{1}$/2 0	1 2 3
			0 1/2 1/2	3 1 2
			0 1/2 $\bar{1}$/2	3 1 2
		1/2 0 0	0 1/2 0	3 1 2
			0 0 1/2	2 3 1
(I)	1 0 0	1/2 1/4 0	1/2 0 1/4	1 2 3
			1/2 0 $\bar{1}$/4	1 2 3
			1/2 $\bar{1}$/4 0	1 2 3
			0 1/2 1/4	1 2 3
			0 1/2 $\bar{1}$/4	1 2 3
			0 1/4 1/2	1 2 3
			0 1/4 $\bar{1}$/2	1 2 3
		1/4 1/2 0	1/4 0 1/2	1 2 3
			1/4 0 $\bar{1}$/2	1 2 3
			1/4 $\bar{1}$/2 0	1 2 3
		1/2 1/8 1/8	1/2 1/8 1/8	1 2 3
			1/2 1/8 $\bar{1}$/8	1 2 3
			1/2 $\bar{1}$/8 1/8	1 2 3
		1/8 1/2 1/8	1/8 1/2 1/8	1 2 3
			1/8 1/8 1/2	1 2 3
			1/8 1/8 $\bar{1}$/2	1 2 3
			1 8 $\bar{1}$/8 1/2	1 2 3
			1/8 $\bar{1}$/8 $\bar{1}$/2	1 2 3
			1/8 $\bar{1}$/2 1/8	1 2 3
			1/8 $\bar{1}$/2 $\bar{1}$/8	1 2 3
		0 1/2 0	0 0 1/2	1 2 3
		3/8 3/8 0	3/8 0 $\bar{3}$/8	1 3 2
			3 8 0 $\bar{3}$/8	1 3 2
			3/8 $\bar{3}$/8 0	1 2 3
		0 3/8 3/8	0 3/8 $\bar{3}$/8	1 2 3
		1/4 1/4 1/4	1/4 1/4 1/4	1 2 3
			1/4 1/4 $\bar{1}$/4	1 2 3
			1/4 $\bar{1}$/4 1/4	1 2 3
			1/4 $\bar{1}$/4 $\bar{1}$/4	1 2 3
	1/3 1/3 1/3	1/2 1/4 0	1/2 0 1/4	3 1 2
			1/2 0 $\bar{1}$/4	3 1 2
			1/2 $\bar{1}$/4 0	1 2 3
			1/4 1/2 0	2 3 1
			1/4 0 1/2	2 3 1
			1/4 0 $\bar{1}$/2	2 3 1
			1/4 $\bar{1}$/2 0	2 3 1
		1/2 1/8 1/8	1/2 $\bar{1}$/8 $\bar{1}$/8	1 2 3

1	2	3	4	5
(I)	1/3 1/3 1/3	1/2 1/8 1/8	1/8 1/2 1/8	3 1 2
			1/8 1/8 1/2	2 3 1
			1/8 1/8 $\bar{1}$/2	2 3 1
			1/8 $\bar{1}$/2 1/8	3 1 2
		1/2 1/8 $\bar{1}$/8	1/2 1/8 1/8	1 2 3
			1/8 1/2 1/8	3 1 2
			1/8 1/8 1/2	2 3 1
			1/8 1/8 $\bar{1}$/2	2 3 1
			1/8 $\bar{1}$/2 1/8	3 1 2
		1/2 0 0	0 1/2 0	3 1 2
			0 0 1/2	2 3 1
		3/8 3/8 0	3/8 0 3/8	2 3 1
			0 3/8 3/8	3 1 2
		3/8 $\bar{3}$/8 0	3/8 0 $\bar{3}$/8	2 3 1
			0 3/8 $\bar{3}$/8	3 1 2
		1/4 1/4 $\bar{1}$/4	1/4 1/4 1/4	2 3 1
			1/4 1/4 $\bar{1}$/4	3 1 2
(F)	1 0 0	1/2 0 0	0 1/2 0	1 2 3
			0 0 1/2	1 2 3
		3/8 1/8 1/8	3/8 1/8 1/8	1 2 3
			3/8 1/8 $\bar{1}$/8	1 2 3
			3/8 $\bar{1}$/8 1/8	1 2 3
		1/8 3/8 1/8	1/8 3/8 $\bar{1}$/8	1 2 3
			1/8 1/8 3/8	1 3 2
			1/8 1/8 $\bar{3}$/8	1 3 2
			1/8 $\bar{1}$/8 3/8	1 3 2
			1/8 $\bar{1}$/8 $\bar{3}$/8	1 3 2
			1/8 $\bar{3}$/8 1/8	1 2 3
			1/8 $\bar{3}$/8 $\bar{1}$/8	1 2 3
		1/4 1/4 1/4	1/4 1/4 $\bar{1}$/4	1 2 3
			1/4 $\bar{1}$/4 1/4	1 2 3
			1/4 $\bar{1}$/4 $\bar{1}$/4	1 2 3
		1/4 1/4 0	1/4 0 1/4	1 3 2
			1/4 0 $\bar{1}$/4	1 3 2
			1/4 $\bar{1}$/4 0	1 2 3
		0 1/4 1/4	0 1/4 $\bar{1}$/4	1 2 3
	1/3 1/3 1/3	1/2 0 0	0 1/2 0	1 2 3
			0 0 1/2	1 2 3
		3/8 1/8 1/8	1/8 3/8 1/8	3 1 2
			1/8 1/8 3/8	2 3 1
		3/8 1/8 $\bar{1}$/8	3/8 1/8 1/8	3 1 2
			1/8 3/8 1/8	2 3 1
			1/8 $\bar{1}$/8 3/8	2 3 1
			1/8 $\bar{1}$/8 $\bar{3}$/8	1 2 3
			1/8 $\bar{3}$/8 $\bar{1}$/8	3 1 2
		3/8 $\bar{1}$/8 $\bar{1}$/8	1/8 1/8 $\bar{3}$/8	1 2 3
			1/8 $\bar{3}$/8 1/8	1 2 3
		1/4 1/4 1/4	1/4 1/4 1/4	1 2 3
			1/4 1/4 $\bar{1}$/4	1 2 3
			1/4 $\bar{1}$/4 1/4	1 2 3
			1/4 $\bar{1}$/4 $\bar{1}$/4	1 2 3
		1/4 1/4 0	1/4 0 1/4	2 3 1
			0 1/4 1/4	3 1 2
		1/4 $\bar{1}$/4 0	1/4 0 $\bar{1}$/4	2 3 1
			0 1/4 $\bar{1}$/4	3 1 2

TABLE II. PART C. Numbered columns contain values of $M\Sigma\delta h_i$ as required in part A. At the left of each group of numbered columns are two columns headed nl^2 and ΣN which give, respectively, the highest value of nl^2 and the total number of dipoles for each tabular value of $M\Sigma\delta h_i$.

$4l^2$	ΣN	1	2	$4l^2$	ΣN	3	4	$16l^2$	ΣN	5	6	$64l^2$	ΣN	7	8	9	10	11
2	4	11.31371	6.53197	1	2	32.	18.47521	5	4	9.15893	5.28791	18	3	15.64366	12.29145	9.03187	2.58053	11.61240
6	12	6.95906	4.01782	5	10	29.71026	17.15323	13	8	3.27714	1.89206	34	5	10.47852	5.45524	6.04978	.12469	6.17447
10	20	8.98292	5.18629	9	20	29.31520	16.92514	21	16	7.83745	4.52495	50	6	9.03037	7.62747	5.21369	1.79688	7.01056
14	36	9.33199	5.38783	13	28	30.78565	17.77410	29	28	5.46338	3.15428	66	10	7.87767	6.41215	4.61226	1.39593	6.00819
18	48	8.35427	4.82334	17	44	30.57081	17.65006	37	32	6.50861	3.75775	82	12	9.83861	6.86623	5.68032	1.12406	6.80438
22	56	8.63618	4.98610	21	60	29.43073	16.99184	45	48	6.05632	3.49662	98	20	10.78641	6.47849	6.22754	.62659	6.85413
26	80	8.30197	4.79315	25	70	29.72769	17.16329	53	60	6.13143	3.53998	114	24	10.87497	8.11678	6.27866	1.54689	8.03859
30	96	8.76936	5.06299	29	94	30.32121	17.50596	61	72	6.60710	3.81461	130	26	10.18411	8.64289	5.87980	2.05008	8.14291
34	112	8.95926	5.17263	33	110	31.05780	17.93123	69	88	6.45175	3.72492	146	34	9.96147	6.49599	5.75126	.87483	6.83913
38	136	8.82984	5.09791	37	118	30.79649	17.78036	77	104	6.96348	4.02037	178	38	9.21537	6.80122	5.32049	1.26644	6.79996
42	152	8.76266	5.05912	41	150	30.68947	17.71857	85	112	6.11798	3.53222	194	48	9.75842	7.48687	5.63403	1.50553	7.35259
46	168	8.20968	4.73986	45	174	30.88735	17.83282	93	120	6.22847	3.59601	210	52	9.70073	6.95810	5.60072	1.21690	7.03065
50	196	8.49569	4.90499	49	192	30.81309	17.78995	101	148	6.02371	3.47779	226	56	10.25018	7.03012	5.91795	1.09987	7.23084
54	228	8.71074	5.02915	53	216	30.79431	17.77910					242	67	9.77923	7.03517	5.64604	1.23874	7.09781
58	236	8.85563	5.11280	57	232	31.07610	17.94179					258	71	9.65281	7.40869	5.57305	1.49089	7.27697
62	268	8.87254	5.12257	61	256	30.95718	17.87314					274	77	10.32024	7.11947	5.95839	1.13123	7.30266
66	300	8.74233	5.04739	65	288	31.03233	17.91653					290	87	10.45037	7.19884	6.03353	1.13949	7.38605
70	316	8.62369	4.97889	69	320	31.07117	17.93895					306	95	10.58541	7.65646	6.11149	1.36472	7.68924
74	356	8.47424	4.89260	73	336	30.90812	17.84481					322	99	10.28380	7.21066	5.93736	1.19440	7.34478
78	372	8.63146	4.98338	77	368	30.78018	17.77095					338	100	10.20141	7.33425	5.88979	1.28954	7.39235
82	388	8.60203	4.96638	81	402	30.66801	17.70618					354	108	9.79490	6.65152	5.65509	1.01271	6.88084
86	428	8.67855	5.01056	85	418	30.87938	17.87822					370	114	9.69924	6.68302	5.59986	1.05851	6.87141
90	468	8.65356	4.99613	89	466	30.99243	17.89349					386	124	9.59500	6.97371	5.53967	1.25644	7.00914
94	500	8.75516	5.05479	93	482	30.96481	17.87754					402	132	10.01216	7.03060	5.78053	1.16886	7.16241
98	536	8.72891	5.03964	97	498	31.05045	17.92699					418	136	10.02019	7.21119	5.78516	1.27080	7.26900
102	552	8.66313	5.00166	101	554	31.10164	17.95654											
106	576	8.78595	5.07257	105	586	30.95208	17.87019											

$4l^2$	ΣN	12	13	$16l^2$	ΣN	14	15	$64l^2$	ΣN	16	17	$4l^2$	ΣN	18	19	20	21	22
1	2	32.	18.47521	3	2	24.63361	28.44444	11	3	19.13725	22.09779	2	2	45.25483	67.88225	52.25578	26.12789	26.12789
2	6	20.68629	11.94324	11	8	19.84930	22.92000	27	7	11.02742	12.73337	6	6	27.83624	59.17295	42.19915	16.07126	26.12789
5	14	18.39656	10.62126	19	14	20.58140	23.76535	43	10	13.68777	15.80528	10	10	35.93167	51.88707	40.32959	20.74516	19.58443
6	22	22.75121	13.13542	27	22	22.60885	26.10645	59	19	12.71119	14.67761	14	18	37.32797	58.17043	44.36037	21.55132	22.80906
9	32	22.35615	12.90733	35	34	21.23249	24.51717	75	26	14.25621	16.46165	18	24	33.41706	61.24329	45.00551	19.29335	25.71216
10	40	20.33229	11.73885	43	40	20.56740	23.74919	91	32	15.07286	17.40464	22	28	34.54474	58.19858	43.57317	19.94441	23.62876
13	48	21.80274	12.58782	51	52	21.02221	24.27436	107	41	12.36218	14.27462	26	40	33.20790	57.97577	43.05862	19.17259	23.88603
14	64	21.45366	12.38628	59	70	21.26636	24.55627	123	47	12.74666	14.71858	30	48	35.07746	56.41780	42.69882	20.25198	22.44685
17	80	21.23882	12.26224	67	76	21.79934	25.17171	139	56	13.17147	15.20911	34	56	35.83703	55.73418	42.52341	20.69052	21.83289
18	92	22.21655	12.82673	75	90	21.41309	24.72570	155	68	14.09582	16.27645	38	68	35.31936	58.23626	43.81854	20.39164	23.42690
21	108	21.07647	12.16851	83	108	21.17447	24.45017	171	83	13.74634	15.87291	42	76	35.05064	58.90805	44.12883	20.23650	23.89233
22	116	20.79455	12.00574	91	120	20.97031	24.21442	187	89	13.41871	15.49459	46	84	32.83874	59.22914	43.67569	18.95945	24.71623
25	126	21.09151	12.17719	99	138	20.75373	23.96435	203	101	13.88960	16.03833	50	98	33.98278	58.16474	43.39141	19.61997	23.77145
26	150	21.42572	12.37015	107	156	21.43140	24.74685	219	113	13.48275	15.56854	54	114	34.84296	57.44793	43.22587	20.11659	23.10928
								235	119	13.38477	15.45541	58	118	35.42252	58.07745	43.79125	20.45120	23.30543
								251	140	13.19241	15.23329	62	134	35.49018	56.75802	43.04901	20.49026	22.52413
								267	146	13.35328	15.41904	66	150	34.96933	57.01845	43.04901	20.18955	22.82484
								283	155	13.09677	15.12285	70	158	34.49475	57.58045	43.23648	19.91555	23.28631
								299	179	13.54985	15.64602	74	178	33.89695	57.59675	43.07332	19.57041	23.46829
								315	197	13.79930	15.93406	78	186	34.52585	58.59757	43.83252	19.93351	23.86440
								331	206	13.81086	15.94741	82	194	34.40812	58.82431	43.92961	19.86554	24.02946
								347	221	13.76224	15.89126	86	214	34.71418	58.49958	43.83049	20.04283	23.75363
								363	234	13.61234	15.71818	90	234	34.61424	57.63007	43.29962	19.98454	23.28047
								379	243	13.46239	15.54503	94	250	35.02064	57.73765	43.47905	20.21977	23.22526
								395	267	13.08594	15.11034	98	268	34.91563	57.83863	43.50704	20.15855	23.31387
								411	285	13.30033	15.35790	102	276	34.65251	57.47317	43.22008	20.00663	23.17883
								427	291	13.35659	15.42286	106	288	35.14379	57.41342	43.32741	20.29027	23.00252

convergent sums so that we may put

$$h_{ii}=h_{iit2}+h_{iit0}+h_{iiq2}, \quad (9)$$

and similar expressions for h_{ij} and h_{ik}. The sums containing t in the subscript are taken over all points of the infinite array of dipoles. The sums containing q in the subscript are taken over all points of an infinite array reciprocal to the dipole array.

In constructing the $\mathbf{q}$-array from the dipole array we start with the defining equations:

$$\mathbf{r}=\sum r_i\mathbf{a}_i, \quad (10) \qquad \mathbf{q}=\sum q_i\mathbf{b}_i, \quad (11)$$

$$\mathbf{b}_i=(\mathbf{a}_j\times\mathbf{a}_k)/[\mathbf{a}_i\cdot(\mathbf{a}_j\times\mathbf{a}_k)]. \quad (12)$$

In our cubic arrays the three fundamental translations have the same magnitude ($a_i=1$) and are at right angles so that the reciprocal array is also cubic and the $b_i=1$. We are now ready to consider the separate sums of Eq. (5) and its analogues. These are:

$$h_{iit2}=-\epsilon^5\sum t_i^2 g_2(\epsilon t), \quad (13)$$

$$h_{ijt2}=-\epsilon^5\sum t_i t_j g_2(\epsilon t), \quad (14)$$

$$h_{iit0}=h_{ijt0}=\epsilon^3\sum g_1(\epsilon t), \quad (15)$$

$$h_{iiq2}=4\pi\sum' q_i^2 q^{-2}\cos\{2\pi(q_1s_1+q_2s_2+q_3s_3)\}\exp(-\pi^2q^2/\epsilon^2), \quad (16)$$

$$h_{ijq2}=4\pi\sum' q_iq_jq^{-2}\cos\{2\pi(q_1s_1+q_2s_2+q_3s_3)\}\exp(-\pi^2q^2/\epsilon^2). \quad (17)$$

In the primed summations there is no term with $q=0$. The factor ϵ is an arbitrary parameter upon the value of which the h_{ij} do not depend. (The separate sums, such as h_{iit2}, do depend upon ϵ.) Computations for two different ϵ which give the same h_{ij} are almost certainly correct. All values here given have been checked in this way.

The functions g_1 and g_2 are defined according to the scheme:

$$\phi(\alpha)=2\pi^{-\frac{1}{2}}\int_0^\alpha \exp(-\beta^2)d\beta, \quad (18)$$

$$g_0(\alpha)=\alpha^{-1}[1-\phi(\alpha)], \quad (19)$$

$$g_1(\alpha)=\alpha^{-2}[g_0(\alpha)+2\pi^{-\frac{1}{2}}\exp(-\alpha^2)], \quad (20)$$

$$g_2(\alpha)=\alpha^{-2}[3g_1(\alpha)+4\pi^{-\frac{1}{2}}\exp(-\alpha^2)]. \quad (21)$$

Further functions of this series may be thus defined:

$$g_m(\alpha)=\alpha^{-2}[(2m-1)g_{m-1}(\alpha)+2^m\pi^{-\frac{1}{2}}\exp(-\alpha^2)]. \quad (22)$$

The probability integral $\phi(\alpha)$ is usually tabulated to 4 or 5 decimals. Values to 6 or 7 decimals, depending upon the magnitude of the argument, were found more suitable in the present work.

Eqs. (16) and (17) may be used without further modification provided that the dipole array is first divided into its N simple cubic (S) arrays in each of which a different value of $\mathbf{s}$ must be used to define the single point where the h_{ij} are wanted. The summation for each $\mathbf{s}$ is then over a simple cubic $\mathbf{q}$-lattice. Inspection shows, however, that for many $\mathbf{q}$ values the net contribution from the N sums is zero. We therefore prefer to choose one of the N values of $\mathbf{s}$ which must all be used in (13), (14) and (15) and to select the values of q_i which contribute to (16) and (17) by a rule analogous to that which selects r_i in the dipole array. Upon thus confining the summation to one $\mathbf{s}$ and to the selected q_i we may rewrite (16) and (17) as follows

$$h_{iiq2}=4\pi N\sum' f q_i^2 q^{-2}\cos\{2\pi(q_1s_1+q_2s_2+q_3s_3)\}\exp(-\pi^2q^2/\epsilon^2), \quad (23)$$

$$h_{ijq2}=4\pi N\sum' f q_iq_jq^{-2}\cos\{2\pi(q_1s_1+q_2s_2+q_3s_3)\}\exp(-\pi^2q^2/\epsilon^2). \quad (24)$$

The selection rules and the values of the auxiliary factor f are given in Table III.

The choice of ϵ fixes the number of terms dependent on t and q which must be found to attain a given precision. For a value of ϵ near unity the two series are about equally long. It is better to have rather more terms in the q series than in the t series because the functions in the

TABLE III. *Selection rules and values of the auxiliary factor f.*

Symbol	Selection Rule	f
(S)	$q_i=n_i$.	1
(I)	$q_i=n_i$; $\Sigma_i q_i=2n$.	1
(F)	$q_i=2n_i$, and $q_i=2n_i+1$.	1
(D)	$q_i=2n_i$; $\Sigma_i q_i=4n$, and $q_i=2n_i+1$.	1 1/2

former are easier to compute. The values of ϵ here chosen were 2 and 3.

At any dipole position in these infinite cubic arrays the field due to the rest of the dipoles is $4\pi N\mathbf{p}/3$. At near-by points the field due to a complete array is almost exclusively that due to the nearest dipole, and hence has little interest here. It is, however, worth while to inquire in what field a slightly displaced dipole will find itself, the rest of the array remaining undisturbed. We arrive at the desired result by computing h_i at points with small s and subtracting δh_i for the dipole at the origin.

The method of Lorentz is applicable without any special precautions and gives better approximations the smaller the value of s. Results for representative points in (I) and (F) are given in Table IV, which is similar in its general construction to Table II. The principal difference, besides the omission of one dipole, is that r^2 replaces t^2 as the argument in part C. This is now more convenient because t^2 is no longer necessarily a small submultiple of an integer and because groups for the same r, which produce zero field at the origin, produce only small field components at near-by points. Since each value of r gives rise to several values of t the number of terms separately computed is no longer equal to the number of entries in part C of the table. It is therefore reported (as $\sum T$) in a separate column for each group of $\sum\delta h_i$.

The results have again been checked by the method of Ewald, but in this work it was necessary to find $g_1(\epsilon t)$ and $g_2(\epsilon t)$ for the smallest value of the argument—ϵs—to about 10 figures, in order to justify 5 or 6 figures in the results. The terms in Eqs. (13), (14) and (15) which depend upon this argument are almost equal to the corresponding terms in (4) by which the result for a complete array must be corrected. These correction terms must also be computed to about 10 figures, but this presents no particular difficulty. Values of $\phi(\alpha)$ to 9 decimals have been reported by Burgess,[5] who also gives formulae for computing values to any desired precision. The few values here needed were so computed to 10 or more figures as an additional check upon the tabular entries.

A result of some generality may be derived from Table IV. If one dipole in an infinite lattice oscillates through its mean position it may acquire extra magnetic stability for particular directions of its line of motion. This will still be true if a compact group of dipoles oscillates as a whole. This result does not permit any generalization about the stabilizing or disturbing effect of an elastic wave which displaces layers of dipoles in succession. When we consider thermal agitation we do not see in the first place how thermal motions can be limited as to direction. Furthermore we find that if vibrations along all crystallographically equivalent directions are equally probable the average increase in stability is zero. This may be seen for a particular case in Table V.

It does not appear that the observed directions of easy magnetization in real cubic crystals, which are $<100>$ in iron (I) and $<111>$ in nickel (F), could have been predicted from the results here obtained.

A case treated by Bouman[4] falls within the scope of this paper and has been recomputed here although it is not a case of ferromagnetism. The dipole array is composed of two interpenetrating face-centered arrays in each of which separately the vectors $\mathbf{p}$ are so arranged, consistently with full cubic symmetry, that the magnetic moment per unit cube is zero. This makes the results sensibly independent of the crystal boundary. In magnetically stable arrangements $\mathbf{h}$ at each dipole must have the direction of that dipole axis, $\mathbf{p}$. Bouman shows that the h_i depend upon six constants a, b, c, d, e, f (these are A, B, C, D, E, F in his notation multiplied by the volume of a unit cube to make them pure numbers). Since $3a=2b+c=d+2e=3f=4\pi$ we need only compute c and d.

[5] J. Burgess, Trans. Roy. Soc. (Edinburgh) **39**, 257–321 (1898).

TABLE IV, Part A. Values of h_i for points near a vacated dipole position. Column 1: Type of array; (*I*), or (*F*). Column 2: Components of dipole moment; $p_1p_2p_3$. Column 3: Coordinates of point; $s_1s_2s_3\times(10)^3$. Column 4: Column number in part C where a series of values of $M\Sigma\delta h_i$ are given. A dash indicates that all values of $\Sigma\delta h_i$ are zero. Column 5: M. Column 6: Last $\Sigma\delta h_i$ here computed. Column 7: $4\pi Np_i/3$. Column 8: h_i (method of Lorentz). Column 9: h_i (method of Ewald). In columns 4 to 9 inclusive there are three entries for each entry in column 3, corresponding, in that order, to $i=1, 2, 3$.

1	2	3	4	5	6	7	8	9
(*I*)	1 0 0	100 0 0	1	−1	−0.35414	8.37758	8.02344	8.0215
			–	–	0	0	0	0
			–	–	0	0	0	0
		0 100 0	1	2	0.17707	8.37758	8.55465	8.5555
			–	–	0	0	0	0
			–	–	0	0	0	0
		70 70 0	3	−2	−0.10066	8.37758	8.27692	8.2768
			4	1	0.16628	0	0.16628	0.1682
			–	–	0	0	0	0
		0 70 70	3	1	0.20131	8.37758	8.57889	8.5792
			–	–	0	0	0	0
			–	–	0	0	0	0
		55 55 55	–	–	0	8.37758	8.37758	8.3776
			8	1	0.12421	0	0.12421	0.1249
			8	1	0.12421	0	0.12421	0.1249
	1/3 1/3 1/3	100 0 0	2	−1	−0.20446	4.83680	4.63234	4.6312
			2	2	0.10223	4.83680	4.93903	4.9395
			2	2	0.10223	4.83680	4.93903	4.9395
		70 70 0	5	1	0.03787	4.83680	4.87467	4.8755
			5	1	0.03787	4.83680	4.87467	4.8755
			6	1	0.11623	4.83680	4.95303	4.9532
		70 $\bar{7}0$ 0	7	−1	−0.15409	4.83680	4.68271	4.6816
			7	−1	−0.15409	4.83680	4.68271	4.6816
			6	1	0.11623	4.83680	4.95303	4.9532
		55 55 55	9	1	0.14343	4.83680	4.98023	4.9812
			9	1	0.14343	4.83680	4.98023	4.9812
			9	1	0.14343	4.83680	4.98023	4.9812
		55 55 $\bar{5}\bar{5}$	–	–	0	4.83680	4.83680	4.8368
			–	–	0	4.83680	4.83680	4.8368
			9	−1	−0.14343	4.83680	4.69337	4.6924
(*F*)	1 0 0	100 0 0	10	−1	−0.98009	16.75516	15.77507	15.7766
			–	–	0	0	0	0
			–	–	0	0	0	0
		0 100 0	10	2	0.49004	16.75516	17.24520	17.2444
			–	–	0	0	0	0
			–	–	0	0	0	0
		70 70 0	12	−2	−0.17342	16.75516	16.58174	16.5824
			13	1	0.52224	0	0.52224	0.5223
			–	–	0	0	0	0
		0 70 70	12	1	0.34685	16.75516	17.10201	17.1006
			–	–	0	0	0	0
			–	–	0	0	0	0
		55 55 55	–	–	0	16.75516	16.75516	16.7552
			17	1	0.21569	0	0.21569	0.2153
			17	1	0.21569	0	0.21569	0.2153
	1/3 1/3 1/3	100 0 0	11	−1	−0.56585	9.67360	9.10775	9.1086
			11	2	0.28293	9.67360	9.95653	9.9560
			11	2	0.28293	9.67360	9.95653	9.9560
		70 70 0	14	1	0.20136	9.67360	9.87496	9.8754
			14	1	0.20136	9.67360	9.87496	9.8754
			15	1	0.20025	9.67360	9.87385	9.8730
		70 $\bar{7}0$ 0	16	−1	−0.40162	9.67360	9.27198	9.2723
			16	−1	−0.40162	9.67360	9.27198	9.2723
			15	1	0.20025	9.67360	9.87385	9.8730
		55 55 55	18	1	0.24906	9.67360	9.92266	9.9222
			18	1	0.24906	9.67360	9.92266	9.9222
			18	1	0.24906	9.67360	9.92266	9.9222
		55 55 $\bar{5}\bar{5}$	–	–	0	9.67360	9.67360	9.6736
			–	–	0	9.67360	9.67360	9.6736
			18	−1	−0.24906	9.67360	9.42454	9.4250

TABLE IV, PART B. Columns 1, 2, 3: Same as in part A. Column 4: Coordinates of point, $s_1's_2's_3'\times(10)^3$, not appearing in part A. Column 5: $h_1'h_2'h_3'$ in terms of $h_1h_2h_3$ as given in columns 8 and 9 of part A for $s_1s_2s_3\times(10)^3$ as given in column 3. For ease in reading only the order of $h_1h_2h_3$ is given. Thus 3 1 2 means that $h_1'=h_3$, $h_2'=h_1$, $h_3'=h_2$.

1	2	3	4	5	1	2	3	4	5
(*I*)	1 0 0	0 100 0	0 0 100	1 2 3	(*F*)	1 0 0	0 100 0	0 0 100	1 2 3
		70 70 0	70 0 70	1 3 2			70 70 0	70 0 70	1 3 2
			70 0 $\overline{70}$	1 3 2				70 0 $\overline{70}$	1 3 2
			70 $\overline{70}$ 0	1 2 3				70 $\overline{70}$ 0	1 2 3
		0 70 70	0 70 $\overline{70}$	1 2 3			0 70 70	0 70 $\overline{70}$	1 2 3
		55 55 55	55 55 $\overline{55}$	1 2 3			55 55 55	55 55 $\overline{55}$	1 2 3
			55 $\overline{55}$ 55	1 2 3				55 $\overline{55}$ 55	1 2 3
			55 $\overline{55}$ $\overline{55}$	1 2 3				55 $\overline{55}$ $\overline{55}$	1 2 3
	1/3½ 1/3½ 1/3½	100 0 0	0 100 0	3 1 2		1/3½ 1/3½ 1/3½	100 0 0	0 100 0	3 1 2
			0 0 100	2 3 1				0 0 100	2 3 1
		70 70 0	70 0 70	2 3 1			70 70 0	70 0 70	2 3 1
			0 70 70	3 1 2				0 70 70	3 1 2
		70 $\overline{70}$ 0	70 0 $\overline{70}$	2 3 1			70 $\overline{70}$ 0	70 0 $\overline{70}$	2 3 1
			0 70 $\overline{70}$	3 1 2				0 70 $\overline{70}$	3 1 2
		55 55 $\overline{55}$	55 $\overline{55}$ 55	2 3 1			55 55 $\overline{55}$	55 $\overline{55}$ 55	2 3 1
			55 $\overline{55}$ $\overline{55}$	3 1 2				55 $\overline{55}$ $\overline{55}$	3 1 2

TABLE IV. PART C. Numbered columns contain values of $\Sigma\delta h_i$ as required in part A. At the left of each group of numbered columns are three columns headed nr^2, ΣN and ΣT which give, respectively, the highest value of r^2, the total number of dipoles and the total number of terms for each tabular value of $\Sigma\delta h_i$.

$4r^2$	ΣN	ΣT	1	2	ΣT	3	4	5	6	7	ΣT	8	9
3	8	2	0.75154	0.43390	3	0.39302	0.36162	0.09533	0.22691	0.32224	4	0.24255	0.28007
4	14	5	.32912	.19002	6	.18990	.15374	.03394	.10964	.14358	6	.11716	.13529
8	26	8	.36688	.21182	11	.20731	.17256	.03978	.11969	.15947	9	.12792	.14771
11	50	12	.33806	.19518	16	.19325	.15842	.03568	.11157	.14725	15	.11924	.13768
12	58	14	.36190	.20894	19	.20512	.17004	.03896	.11843	.15739	19	.12657	.14615
16	64	17	.34875	.20135	22	.19871	.16359	.03709	.11473	.15181	21	.12261	.14158
19	88	21	.36146	.20869	29	.20490	.16983	.03890	.11830	.15720	27	.12643	.14599
20	112	26	.35547	.20523	35	.20193	.16694	.03807	.11658	.15465	31	.12460	.14387
24	136	30	.36022	.20797	42	.20427	.16926	.03874	.11794	.15667	36	.12604	.14554
27	168	36	.35414	.20446	49	.20131	.16628	.03787	.11623	.15409	44	.12421	.14343

$4r^2$	ΣN	ΣT	10	11	ΣT	12	13	14	15	16	ΣT	17	18
2	12	3	1.26626	0.73108	5	0.48225	0.66362	0.24393	0.27843	0.52236	3	0.29928	0.34558
4	18	6	.84384	.48719	8	.27913	.45574	.18255	.16116	.34370	5	.17389	.20080
6	42	10	.99517	.57456	15	.35516	.52933	.20308	.20505	.40814	10	.22081	.25497
8	54	13	1.03293	.59637	20	.37257	.54815	.20892	.21511	.42403	13	.23157	.26739
10	78	18	.93941	.54237	28	.32678	.50231	.19568	.18867	.38434	17	.20330	.23475
12	86	20	.96325	.55613	31	.33866	.51394	.19896	.19552	.39448	21	.21063	.24321
14	134	26	.99993	.57731	41	.35659	.53192	.20417	.20588	.41004	28	.22170	.25600
16	140	29	.98678	.56972	44	.35018	.52547	.20230	.20217	.40447	30	.21774	.25143
18	176	36	.97251	.56148	53	.34314	.51849	.20030	.19811	.39840	37	.21339	.24641
20	200	41	.96652	.55802	59	.34016	.51560	.19947	.19639	.39586	41	.21156	.24429
22	224	45	.98024	.56594	66	.34693	.52231	.20139	.20030	.40169	47	.21574	.24911
24	248	49	.98499	.56869	73	.34928	.52463	.20205	.20166	.40371	52	.21719	.25079
26	320	58	.98009	.56585	87	.34685	.52224	.20136	.20025	.40162	62	.21569	.24906

The final expansions for c and d in rapidly convergent form (method of Ewald) are

$$c=-8\pi\sum A_{nc}n^{-1}x^n+128\pi\epsilon^3\sum B_{nc}n^{-1}y^n+768\epsilon\sum B_{nc}n^{-2}y^n+768\sum B_{nc}n^{-3}[1-\phi(2^{-1}\pi^{\frac{1}{2}}n^{-\frac{1}{2}}\epsilon)]$$
$$-32\epsilon\sum C_{nc}n^{-1}y^n-32\sum C_{nc}n^{-\frac{1}{2}}[1-\phi(2^{-1}\pi^{\frac{1}{2}}n^{-\frac{1}{2}}\epsilon)], \quad (25)$$

$$d=8\pi\sum A_{nd}n^{-1}x^n+8\pi\epsilon^3\sum B_{nd}n^{-1}y^n+48\epsilon\sum B_{nd}n^{-2}y^n+48\sum B_{nd}n^{-3}[1-\phi(2^{-1}\pi^{\frac{1}{2}}n^{-\frac{1}{2}}\epsilon)]$$
$$-16\epsilon\sum C_{nd}n^{-1}y^n-16\sum C_{nd}n^{-\frac{1}{2}}[1-\phi(2^{-1}\pi^{\frac{1}{2}}n^{-\frac{1}{2}}\epsilon)]. \quad (26)$$

TABLE V. *Conditions: Array (I).*

$p_1p_2p_3$	$s_1s_2s_3\times(10)^3$	$\Sigma(h_i-4\pi Np_i/3)$*
$\frac{1}{3^{\frac{1}{2}}}\frac{1}{3^{\frac{1}{2}}}\frac{1}{3^{\frac{1}{2}}}$	55 55 55	+0.4332
	$55\ \overline{55}\ \overline{55}$	−0.1444
	$55\ \overline{55}\ 55$	−0.1444
	$\overline{55}\ \overline{55}\ 55$	−0.1444
	$\overline{55}\ 55\ \overline{55}$	−0.1444
	$\overline{55}\ 55\ 55$	−0.1444
	$\overline{55}\ \overline{55}\ 55$	−0.1444
	$\overline{55}\ \overline{55}\ \overline{55}$	+0.4332
	Mean value	0

* This is here proportional to the excess negative potential energy of a dipole of moment **p** at the designated point over its negative potential energy when at the origin.

In these expansions $x=\exp(-\pi/\epsilon^2)$, $y=\exp(-\pi\epsilon^2/4)$, ϵ and $\phi(\alpha)$ have already been defined and the coefficients A_{nc}, etc., except as given in Table VI, have the value zero for all values of n.

The results, checked as usual for two values of ϵ ($2^{\frac{1}{2}}$ and $6^{\frac{1}{2}}/2$) are

$$c=-4.47894, \quad d=34.2708,$$

correct to one digit in the last figure in each. Bouman's value for $d/2$ is 17.14 which is correct as far as it goes. His value for $c/2$ is -2.20 which is not so satisfactory, but the change does not vitiate his qualitative conclusions.

TABLE VI. *Coefficients for Bouman's series.*

Note: For values of n not given the coefficient is zero.

n	A_{nc}	A_{nd}	n	B_{nc}	n	B_{nd}	n	C_{nc}	n	C_{nd}
1	1	1	6	1	1	1	2	1	1	1
2	−4	4	14	2	5	4	6	2	5	4
3	4	4	18	4	9	13	10	2	9	5
4	4	−4	22	1	13	36	14	4	13	4
5	−12	−12	26	8	17	40	18	3	17	8
6	8	−8	30	2	21	8	22	2	21	8
8	16	−16	34	4	25	61	26	6	25	5
9	−19	−19	38	11	29	172	30	4	29	12
10	−40	40	42	8	33	104	34	4	33	8
11	44	44	46	18	37	4	38	6	37	4
12	16	−16	50	8	41	144	42	4	41	16
13	20	20	54	12	45	236	46	4	45	12
14	−48	48	62	20	49	121	50	7	49	9
16	16	−16	66	28	53	204	54	8	53	12
17	−56	−56	70	18	57	296	58	2	57	8
18	20	−20	74	40	61	172	62	8	61	12
19	76	76	78	2	65	400	66	8	65	16
20	80	−80	82	16	69	392	70	4	69	16
21	−152	−152	86	29	73	40	74	10	73	8
22	−56	56	90	40	77	272	78	4	77	16
24	96	−96	94	20	81	321	82	4	81	17
25	−3	−3	98	40	85	520	86	10	85	8
					89	888	90	10	89	24
					93	200	94	8	93	8
					97	424	98	9	97	8

Magnetic Dipole Fields in Dislocated Cubic Crystals

L. W. McKEEHAN, *Sloane Physics Laboratory, Yale University*

(Received February 13, 1933)

A search is made for magnetic stability of orientation in cubic arrays of parallel dipoles subjected to dislocations of two sorts. In the first sort of dislocation cubic symmetry is lost but the dislocation is homogeneous. In the second sort, which simulates incipient or residual slip between two parts of one crystal, cubic symmetry is retained by each part separately, but the dislocation is sharply localized. Energy per dipole changes during dislocation in ways which do not account for observed directions of easy magnetization in annealed crystals of iron and nickel. Changes of magnetic behavior due to coldwork are of the proper order of magnitude to be accounted for in part at least by dislocations of the second sort.

IN a previous paper[1] we discussed the magnetic fields due to infinite cubic arrays of equal parallel dipoles. Here we abandon the perfection of arrangement there assumed in the hope of approximating better to the fields in real ferromagnetic crystals. Two considerations govern our choice of hypotheses regarding the dipole arrays to be investigated. The notation of the previous paper will be used with such additions as may be necessary.

A magnetically saturated region in a so-called cubic crystal is, at best, pseudo-cubic, because the magnetic axis is unique. If the direction of easy magnetization is a four-fold axis the symmetry is not higher than tetragonal, if it is a three-fold axis the symmetry is probably hexagonal. It is natural to consider whether the stability of direction of the magnetic axis in either case is magnetic in origin and can be ascribed to departures from a strictly cubic arrangement of dipoles which would be allowed by the lower symmetry of tetragonal and hexagonal lattices in which cubic cells may still be identified. Though it will be convenient to retain the three cubic axes for our coordinate system we must give up the crystallographic equivalence of the three cube edges, if the array is tetragonal, or of the four cube diagonals, if the array is hexagonal. If we find in the new arrangement that each dipole acquires negative potential energy (which it did not possess in the corresponding cubic arrangement) we may conclude that the assumed displacements would spontaneously occur in our simple model and that that assumed direction of magnetization would be most stable for which the negative potential energy is maximum. It should be emphasized that the model is defective in having no elasticity in dipole constraints and no thermal agitation.

A second line of attack is suggested by the occurrence in real crystals of directions in which slip most easily takes place. In such crystal-controlled slip one part of the crystal is translated with respect to the rest in a definite crystallographic direction, sometimes through enormous distances on the atomic scale. Generally the surface of separation between the two parts, which surface must, of course, include the direction of slip, is a definite crystallographic plane. If so, it is possible in cubic crystals to have more than one plane of a given form functioning as the slip plane with a single choice of slip direction. This will be made clearer by citing what is known about slip in iron and nickel.

In iron, with a body-centered cubic space-lattice (I), the slip direction is of form $<111>$. At low temperatures[2] planes of form $\{211\}$ act as slip planes. At ordinary temperatures slip planes are not easily distinguished and slip may better be described as columnar.[3] We may put this otherwise by saying that planes of forms $\{211\}$

[1] L. W. McKeehan, Phys. Rev. **43**, 913 (1933).

[2] H. Sossinka, B. Schmidt, F. Sauerwald, Metallwirtschaft **10**, 788 (1931).

[3] G. I. Taylor, C. F. Elam, Proc. Roy. Soc. **A112**, 337–361 (1926).

and {110} both function as slip planes, since any prism with a <111> axis may be thought of as bounded by planes of these two forms. Table I shows the possible slip planes of both types for the particular slip direction given at the head of each column. Since slip may be positive or negative it is unnecessary to list more than 4 of the 8 directions of form <111>.

TABLE I. *Possible slips in iron.*

Along	[111]	[11$\bar{1}$]	[1$\bar{1}$1]	[1$\bar{1}\bar{1}$]
On	(2$\bar{1}\bar{1}$)	(2$\bar{1}$1)	(21$\bar{1}$)	(211)
	(11$\bar{2}$)	(112)	(121)	(12$\bar{1}$)
	(12$\bar{1}$)	(12$\bar{1}$)	(1$\bar{1}$2)	(1$\bar{1}$2)
or (possibly) on	(10$\bar{1}$)	(101)	(110)	(110)
	(1$\bar{1}$0)	(1$\bar{1}$0)	(10$\bar{1}$)	(101)
	(01$\bar{1}$)	(011)	(011)	(01$\bar{1}$)

In nickel, with a face-centered cubic space-lattice (F), the slip direction is of form <110>, and the only known slip-plane is of form {111}. Columnar slip is not known to occur, so there is no occasion for a secondary slip plane in this case. Table II is similar in form to Table I but

TABLE II. *Possible slips in nickel.*

Along	[110]	[101]	[10$\bar{1}$]	[1$\bar{1}$0]	[011]	[01$\bar{1}$]
On	(1$\bar{1}$1)	(11$\bar{1}$)	(111)	(111)	(11$\bar{1}$)	(111)
	(1$\bar{1}\bar{1}$)	(1$\bar{1}\bar{1}$)	(1$\bar{1}$1)	(11$\bar{1}$)	(1$\bar{1}$1)	(1$\bar{1}\bar{1}$)

it will now be noted that each slip plane appears under 3 slip directions, whereas in iron the assignment was unique.

It seemed worth while to find out whether such crystal imperfections as may be described as incipient or residual slip tend to stabilize by magnetic forces those directions of **p** in iron and nickel which are known to be preferred. In iron **p** is usually a <100> direction, in nickel, a <111> direction. To prevent bias we should compare the results for both choices of **p** in each metal. Slip itself is highly localized in a real crystal and it seemed fair therefore to suppose residual or incipient slip to be even more sharply defined, especially since the case of homogeneous elastic strain is to receive special attention later.

Both lines of attack can be pursued by the same means. We modify our previous assumption —that the array of dipoles is based on a single perfect cubic lattice—in the following way. The cubic array is divided into two groups, mutually exclusive, by appropriate selection rules and one group is then translated with respect to the other by a suitable small fraction of the lattice parameter. For convenience we will call this process a dislocation. It is not a strain in any ordinary sense of that word.

The stabilizing effect of a dislocation will be estimated by the change in the magnetic potential energy of a chosen dipole. If every dipole of each of our two selected groups is similarly environed after the dislocation it will make no difference which dipole we choose. This is what happens if the combined array becomes tetragonal or hexagonal as proposed in the second paragraph. Here we can actually calculate the change in energy density which has resulted. In dislocations which simulate slip, on the other hand, there will always be a set of dipoles in each group which suffer more change in energy than any others. These will be dipoles adjacent to the surface of separation which can here be drawn as a boundary between the groups. We naturally choose one of these boundary dipoles for examination. If the surface of separation is plane we get the same result whichever side of it we make our choice. If the surface of separation is not plane but cylindrical or prismatic we will get different results depending upon which side of the boundary we consider. It is easy to see, however, from the most general reasoning, that if all the dipoles of one group are made more stable in their magnetic alignment the average effect in the other group is also stabilizing. In cases of columnar slip we avoid as much labor as possible by making one group a single row of dipoles, so that here also we need to compute the change in energy for but one dipole. The dipole considered will always be taken as the origin of coordinates.

In the perfect cubic array the dipoles were at the ends of vectors **r** from the origin and the various arrays were distinguished by selection rules for r_i. All lengths were measured in terms of the cube edge a_0 and the coordinate axes were the cubic crystal axes (four-fold rotation axes). In the dislocated array the dipoles are at the ends of vectors **r**′ from the origin and we have two selection rules, one for the undisturbed group and one for the displaced group. The vector displace-

ment of the latter group will be designated by **v**. As before all dipoles are parallel, their common direction being that of a unit vector **p**, the magnetic moment of each dipole is $\mathbf{P}=P\cdot\mathbf{p}$. The negative potential energy of such a dipole in a magnetic field of intensity **H** is $U=\mathbf{P}\cdot\mathbf{H}$ in the perfect cubic array and correspondingly in the dislocated array $U'=\mathbf{P}'\cdot\mathbf{H}'$. Putting $\mathbf{P}'=\mathbf{P}$ we see that $U'-U=\mathbf{P}\cdot(\mathbf{H}'-\mathbf{H})$ measures the excess magnetic stability due to dislocation.

To give our results maximum generality we prefer to compute $u'-u$ defined by the equation

$$U'-U=(u'-u)P^2a_0^{-3} \tag{1}$$

or, since

$$\mathbf{H}'-\mathbf{H}=(\mathbf{h}'-\mathbf{h})Pa_0^{-3}, \tag{2}$$

we may write

$$u'-u=\mathbf{p}\cdot(\mathbf{h}'-\mathbf{h}). \tag{3}$$

Since the change in energy is due entirely to changes in the local field, regardless of external form of specimen,

$$u'-u=\sum_i\{p_i(\sum'\delta h_i'-\sum'\delta h_i)\} \tag{4}$$

where $\sum'\delta h_i'$ and $\sum'\delta h_i$ are to be taken over the same limited set of dipoles, excluding the dipole at the origin. For the perfect cubic array we know already that

$$\sum'\delta h_i=0, \tag{5}$$

so that finally

$$u'-u=\sum_i\{p_i\cdot\sum'\delta h_i'\}. \tag{6}$$

It is clear that the method of Lorentz, which permits separate evaluation of the local field factor components, $\sum'\delta h_i$, is preferable to the method of Ewald. It has therefore been used exclusively in the computations here reported.

TABLE III. *Homogeneous dislocation.*

In each box of this table are 13 items of information, placed as shown in the dummy layout at the head of the table These items are as follows:

1. Serial number for abbreviated reference.
2. Character of corresponding perfect cubic array: (*I*) or (*F*).
3. Direction cosines of every dipole: $p_1p_2p_3$.
4. Components of the vector translation: $v_1v_2v_3\times(10)^3$.
5. Angle between **p** and **v**.
6. Selection rule for r_i' of the undisturbed dipoles.
7. Selection rule for r_i' of dislocated dipoles.
   Note: In 6 and 7 notice especially that n_i and n are arbitrary integers which may have a different value in each of the equations in which they appear. Thus $r_i'=n_i$, $\Sigma_ir_i'=2n$ is satisfied by $r_1'=4$, $r_2'=1$, $r_3'=1$; $\Sigma_ir_i'=6$.
8. Highest value of r^2 included in $\Sigma'\delta h_i'$.
9. Total number of dipoles, $\Sigma'N$, included in $\Sigma'\delta h_i'$.
10, 11, 12. Last computed values of $\Sigma'\delta h_1'$, $\Sigma'\delta h_2'$, $\Sigma'\delta h_3'$.
13. Stability factor, $u'-u$.

1	2	3	4	5		
	6	.....				
	7	.....				
	8	9	10	11	12	13
1	(*I*)	100	100 0 0	0°		
	$r_i'=n_i$					
	$r_1'=n_1+0.6$; $r_2'=n_2+0.5$; $r_3'=n_3+0.5$					
	6.75	168	−0.72934	0	0	−0.72934
2	(*I*)	$1/3^{\frac{1}{2}}$ $1/3^{\frac{1}{2}}$ $1/3^{\frac{1}{2}}$	55 55 55	0°		
	$r_i'=n_i$					
	$r_i'=n_i+0.555$					
	6.75	168	0.27235	0.27235	0.27235	0.81704
3	(*F*)	100	100 0 0	0°		
	$r_1'=n_1$; $r_2'=n_2$ or $(n_2+0.5)$; $r_3'=n_3$ or $(n_3+0.5)$; $\Sigma_ir_i'=n$					
	$r_1'=n_1+0.6$; $r_2'=n_2$ or $(n_2+0.5)$; $r_3'=n_3$ or $(n_3+0.5)$; $\Sigma_ir_i'=n+0.1$					
	6.5	320	−2.21452	0	0	−2.21452
4	(*F*)	$1/3^{\frac{1}{2}}$ $1/3^{\frac{1}{2}}$ $1/3^{\frac{1}{2}}$	55 55 55	0		
	$r_i'=n_i$ or $(n_i+0.5)$; $\Sigma_ir_i'=2n$					
	$r_i'=(n_i+0.055)$ or $(n_i+0.555)$; $\Sigma_ir_i'=2n+1.165$					
	6.5	320	−0.62285	−0.62285	−0.62285	−1.86854

Table III summarizes the results for a few cases in which the selected groups interpenetrate throughout, i.e., for homogeneous dislocation. The limits for $\sum'\delta h_i'$ are chosen in the perfect array so that r^2 rather than r'^2 is the appropriate tabular entry in item 8.

Three of the proposed dislocations result in magnetic instability ($u'-u$ negative). The remaining case (2) has **p** parallel to [111] in an array derived from (*I*), and therefore disagrees with experimental results for iron, which it was intended to simulate. It is concluded that this sort of dislocation is not promising enough to warrant further study.

Table IV presents results for all possible types of slip considered in Tables I and II and, in addition, for columnar slip along <111> directions in (*I*) and along <110> directions in (*F*). We will examine the results to see if **p** is preferentially stabilized when parallel to [100] in (*I*) and to [111] in (*F*).

Fig. 1 shows the individual values of $u'-u$ plotted against the angle between **p** and **v** (item 5 in Table IV). Cases in which **p** is along [100] are marked with circles; cases in which **p** is along [111] are marked with crosses. Columnar slip is distinguished by a short line at 45° to the axes of the figure. The points with common abscissa are marked near the top of each set with *I* or *F* to indicate the corresponding cubic array. The first thing to notice is that the highest stability in each array corresponds to the "wrong" direction of **p**. To get a better idea of the average degree of stabilization for a given sort of slip we must assume a reasonable distribution for slip directions in a supposedly undistorted crystal. Let us suppose that all slip directions of the allowed type, and all slip-planes for each slip direction are equally probable. We are then to find the mean value of $u'-u$, say $\overline{u'-u}$. Table V presents the findings. In array (*I*) slip of any probable sort reduces the magnetic

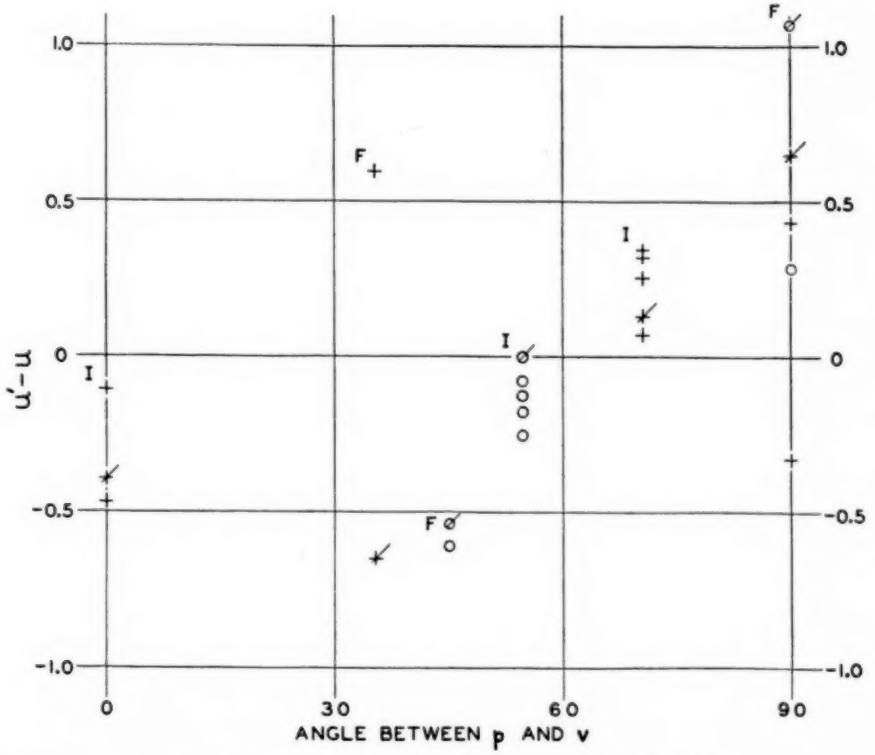

FIG. 1. Stability factor ($u'-u$) for various types of slip in body-centered cubic (*I*) and face-centered cubic (*F*) arrays, plotted against the angle between magnetization and slip direction.

TABLE IV.

In each box of this table are 15 items of information, placed as shown in the dummy lay-out at the head of the table. These items are as follows:

1. Serial number for abbreviated reference.
2. Character of corresponding perfect cubic array: (*I*) or (*F*).
3. Direction cosines of every dipole: $p_1 p_2 p_3$.
4. Components of the vector translation (slip): $v_1 v_2 v_3 \times (10)^3$.
5. Angle between **p** and **v**.
6. Miller indices of slip plane, if present.
7. Angle between **p** and slip plane, if present.
8. Selection rule for r_i' of the undisturbed dipoles.
9. Selection rule for r_i' of the dislocated dipoles.
10. Highest value of r^2 included in $\Sigma' \delta h_i'$.
11. Total number of dipoles, $\Sigma' N$, included in $\Sigma' \delta h_i'$.
12, 13, 14. Last computed values of $\Sigma' \delta h_1'$, $\Sigma' \delta h_2'$, $\Sigma' \delta h_3'$.
15. Stability factor, $u' - u$.

1	2	3	4	5	6	7
	8					
	9					
	10	11	12	13	14	15
5	(*I*)	100	55 55 55	54°–44′	$(11\bar{2})$	34°–06′
	$r_i' = n_i$ and $r_i' = n_i + 0.5$; $r_1' + r_2' - 2r_3' \geqq 0$					
	$r_i' = n_i + 0.055$ and $r_i' = n_i + 0.555$; $r_1' + r_2' - 2r_3' < 0$					
	2	26	−0.12253	0.17742	−0.05075	−0.12253
6	(*I*)	100	55 55 55	54°–44′	$(1\bar{1}0)$	45°
	$r_i' = n_i$ and $r_i' = n_i + 0.5$; $r_1' - r_2' \geqq 0$					
	$r_i' = n_i + 0.055$ and $r_i' = n_i + 0.555$; $r_1' - r_2' < 0$					
	2	26	−0.17784	−0.01544	0.06446	−0.17784
7	(*I*)	100	55 55 55	54°–44′	$(2\bar{1}\bar{1})$	54°–44′
	$r_i' = n_i$ and $r_i' = n_i + 0.5$; $2r_1' - r_2' - r_3' \geqq 0$					
	$r_i' = n_i + 0.055$ and $r_i' = n_i + 0.555$; $2r_1' - r_2' - r_3' < 0$					
	2	26	−0.25303	−0.05496	−0.05496	−0.25303
8	(*I*)	100	55 55 55	54°–44′	$(01\bar{1})$	90°
	$r_i' = n_i$ and $r_i' = n_i + 0.5$; $r_2' - r_3' \geqq 0$					
	$r_i' = n_i + 0.055$ and $r_i' = n_i + 0.555$; $r_2' - r_3' < 0$					
	2	26	−0.07558	0.06446	−0.14084	−0.07558

1	2	3	4	5	6	7
	8					
	9					
	10	11	12	13	14	15
16	(*I*)	1/3 1/3 1/3	55 55 $\bar{5}\bar{5}$	70°–32′	(112)	70°–32′
	$r_i' = n_i$ and $r_i' = n_i + 0.5$; $r_1' + r_2' + 2r_3' \geqq 0$					
	$\{r_1' = n_1 + 0.055, r_2' = n_2 + 0.055, r_3' = n_3 - 0.055\}$ and $\{r_1' = n_1 + 0.555, r_2' = n_2 + 0.555, r_3' = n_3 + 0.445\}$; $r_1' + r_2' + 2r_3' < 0$					
	2	26	0.06099	0.06099	0.20010	0.32208
17	(*I*)	1/3 1/3 1/3	55 55 $\bar{5}\bar{5}$	70°–32′	—	—
	$r_i' = n_i$ and $r_i' = n_i + 0.5$; $-r_3' = r_2' = r_1'$					
	$\{r_1' = n_1 + 0.055, r_2' = n_2 + 0.055, r_3' = n_3 - 0.055\}$ and $\{r_1' = n_1 + 0.555, r_2' = n_2 + 0.555, r_3' = n_3 + 0.445\}$; $-r_3' \neq r_2'$ if $r_2' = r_1'$					
	6.75	168	0	0	0.13188	0.13188
18	(*F*)	100	70 $\bar{7}0$ 0	45°	(111)	54°–44′
	$r_i' = n_i$ or $(n_i + 0.5)$; $\Sigma_i r_i' = n \geqq 0$					
	$r_1' = (n_1 + 0.070)$ or $(n_1 + 0.570)$; $r_2' = (n_2 - 0.070)$ or $(n_2 + 0.430)$; $r_3' = n_3$ or $(n_3 + 0.5)$; $\Sigma_i r_i' = n < 0$					
	2	54	−0.60854	0.03754	0.43898	−0.60854
19	(*F*)	100	70 70 0	45°	—	—
	$r_1' = n_1$ or $(n_1 + 0.5)$; $r_2' = r_1'$; $r_3' = 0$					
	$r_1' = (n_1 + 0.070)$ or $(n_1 + 0.570)$; $r_2' = (n_2 + 0.070)$ or $(n_2 + 0.570)$; $r_3' = n_3$ or $(n_3 + 0.5)$; $\Sigma_i r_i' = n$; $r_2' \neq r_1'$ if $r_3' = 0$					
	6.5	320	−0.53487	−0.56207	0	−0.53487

TABLE IV. *Continued.*

9	(*I*)	100	55 55 55	54°–44′	—	—
	$r_i' = n_i$ and $r_i' = n_i + 0.5$; $r_3' = r_2' = r_1'$					
	$r_i' = n_i + 0.055$ and $r_i' = n_i + 0.555$; $r_3' \neq r_2'$ if $r_2' = r_1'$					
	6.75	168	0	−0.11422	−0.11422	0
10	(*I*)	1/3 1/3 1/3	55 55 55	0°	$(2\bar{1}\bar{1})$	0°
	$r_i' = n_i$ and $r_i' = n_i + 0.5$; $2r_1' - r_2' - r_3' \geqq 0$					
	$r_i' = n_i + 0.055$ and $r_i' = n_i + 0.555$; $2r_1' - r_2' - r_3' < 0$					
	2	26	−0.20955	−0.12905	−0.12905	−0.46766
11	(*I*)	1/3 1/3 1/3	55 55 55	0°	$(1\bar{1}0)$	0°
	$r_i' = n_i$ and $r_i' = n_i + 0.5$; $r_1' - r_3' \geqq 0$					
	$r_i' = n_i + 0.055$ and $r_i' = n_i + 0.555$; $r_1' - r_2' < 0$					
	2	26	−0.07437	0.05608	−0.08773	−0.10602
12	(*I*)	1/3 1/3 1/3	55 55 55	0°	—	—
	$r_i' = n_i$ and $r_i' = n_i + 0.5$; $r_3' = r_2' = r_1'$					
	$r_i' = n_i + 0.055$ and $r_i' = n_i + 0.555$; $r_3' \neq r_2'$ if $r_2' = r_1'$					
	6.75	168	−0.13188	−0.13188	−0.13188	−0.39565
13	(*I*)	1/3 1/3 1/3	55 55 $\bar{5}\bar{5}$	70°–32′	$(1\bar{1}0)$	0°
	$r_i' = n_i$ and $r_i' = n_i + 0.5$; $r_1' - r_3' \geqq 0$					
	$\{r_1' = n_1 + 0.055, r_2' = n_2 + 0.055, r_3' = n_3 - 0.055\}$ and $\{r_1' = n_1 + 0.555, r_2' = n_2 + 0.555, r_3' = n_3 + 0.445\}$; $r_1' - r_2' < 0$					
	2	26	−0.14881	0.21871	0.00046	0.07036
14	(*I*)	1/3 1/3 1/3	55 55 $\bar{5}\bar{5}$	70°–32′	$(2\bar{1}1)$	28°–08′
	$r_i' = n_i$ and $r_i' = n_i + 0.5$; $2r_1' - r_2' + r_3' \geqq 0$					
	$\{r_1' = n_1 + 0.055, r_2' = n_2 + 0.055, r_3' = n_3 - 0.055\}$ and $\{r_1' = n_1 + 0.555, r_2' = n_2 + 0.555, r_3' = n_3 + 0.445\}$; $2r_1' - r_2' + r_3' < 0$					
	2	26	−0.14609	0.21167	0.27514	0.34072
15	(*I*)	1/3 1/3 1/3	55 55 $\bar{5}\bar{5}$	70°–32′	(101)	54°–44′
	$r_i' = n_i$ and $r_i' = n_i + 0.5$; $r_1' + r_3' \geqq 0$					
	$\{r_1' = n_1 + 0.055, r_2' = n_2 + 0.055, r_3' = n_3 - 0.055\}$ and $\{r_1' = n_1 + 0.555, r_2' = n_2 + 0.555, r_3' = n_3 + 0.445\}$; $r_1' + r_3' < 0$					
	2	26	−0.05654	0.07490	0.23654	0.25489
20	(*F*)	100	0 70 $\bar{7}\bar{0}$	90°	(111)	54°–44′
	$r_i' = n_i$ or $(n_i + 0.5)$; $\Sigma_i r_i' = n \geqq 0$					
	$r_1' = n_1$ or $(n_1 + 0.5)$; $r_2' = (n_2 + 0.070)$ or $(n_2 + 0.570)$; $r_3' = (n_3 - 0.070)$ or $(n_3 + 0.430)$; $\Sigma_i r_i' = n < 0$					
	2	54	0.28670	0.43898	−0.11700	0.28670
21	(*F*)	100	0 70 70	90°	—	—
	$r_1' = 0$; $r_2' = n_2$ or $(n_2 + 0.5)$; $r_3' = r_2'$					
	$r_1' = n_1$ or $(n_1 + 0.5)$; $r_2' = (n_2 + 0.070)$ or $(n_2 + 0.570)$; $r_3' = (n_3 + 0.070)$ or $(n_3 + 0.570)$; $\Sigma_i r_i' = n$; $r_3' \neq r_2'$ if $r_1' = 0$					
	6.5	320	1.06973	0	0	1.06973
22	(*F*)	1/3 1/3 1/3	70 70 0	35°–16′	$(1\bar{1}1)$	70°–32′
	$r_i' = n_i$ or $(n_i + 0.5)$; $\Sigma_i r_i' = n$; $r_1' - r_2' + r_3' \geqq 0$					
	$r_1' = (n_1 + 0.070)$ or $(n_1 + 0.570)$; $r_2' = (n_2 + 0.070)$ or $(n_2 + 0.570)$; $r_3' = n_3$ or $(n_3 + 0.5)$; $\Sigma_i r_i' = n$; $r_1' - r_2' + r_3' < 0$					
	2	54	−0.11957	0.23169	0.48652	0.59864
23	(*F*)	1/3 1/3 1/3	70 70 0	35°–16′	—	—
	$r_1' = n_1$ or $(n_1 + 0.5)$; $r_2' = r_1'$; $r_3' = 0$					
	$r_1' = (n_1 + 0.070)$ or $(n_1 + 0.570)$; $r_2' = (n_2 + 0.070)$ or $(n_2 + 0.570)$; $r_3' = n_3$ or $(n_3 + 0.5)$; $\Sigma_i r_i' = n$; $r_3' \neq 0$ if $r_2' = r_1'$					
	6.5	320	−0.63334	−0.63334	0.61761	−0.64906
24	(*F*)	1/3 1/3 1/3	70 $\bar{7}\bar{0}$ 0	90°	$(11\bar{1})$	70°–32′
	$r_i' = n_i$ or $(n_i + 0.5)$; $\Sigma_i r_i' = n$; $r_1' + r_2' - r_3' \geqq 0$					
	$r_1' = (n_1 + 0.070)$ or $(n_1 + 0.570)$; $r_2' = (n_2 - 0.070)$ or $(n_2 + 0.430)$; $r_3' = n_3$ or $(n_3 + 0.5)$; $\Sigma_i r_i' = n$; $r_1' + r_3' - r_3' < 0$					
	2	54	−0.58311	0.27503	−0.02037	−0.32845
25	(*F*)	1/3 1/3 1/3	70 $\bar{7}\bar{0}$ 0	90°	(111)	90°
	$r_i' = n_i$ or $(n_i + 0.5)$; $\Sigma_i r_i' = n \geqq 0$					
	$r_1' = (n_1 + 0.070)$ or $(n_1 + 0.570)$; $r_2' = (n_2 - 0.070)$ or $(n_2 + 0.430)$; $r_3' = n_3$ or $(n_3 + 0.5)$; $\Sigma_i r_i' = n < 0$					
	2	54	−0.07622	0.13994	0.36705	0.43077
26	(*F*)	1/3 1/3 1/3	70 $\bar{7}\bar{0}$ 0	90°	—	—
	$r_1' = n_1$ or $(n_1 + 0.5)$; $r_2' = -r_1'$; $r_3' = 0$					
	$r_1' = (n_1 + 0.070)$ or $(n_1 + 0.570)$; $r_2' = (n_2 - 0.070)$ or $(n_2 + 0.430)$; $r_3' = n_3$ or $(n_3 + 0.5)$; $\Sigma_i r_i' = n$; $r_3' \neq 0$ if $r_2' = -r_1'$					
	6.5	320	0.01573	0.01573	0.61761	0.64907

TABLE V. *Mean stability.*

Column 1. Character of perfect cubic array: (*I*) or (*F*).
2. Direction of **p**.
3. Direction of slip, general form $<HKL>$.
4. Kind of slip: columnar (*C*) or on planes of the specified form $\{hkl\}$.
5. Numbers of cases in Table IV which are to be included.
6. Mean stability factor $\overline{u'-u}$.

1	2	3	4	5	6
(*I*)	[100]	<111>	(*C*)	9	−0.11422
			{211}	5, 7	−0.16603
			{110}	6, 8	−0.14442
	[111]	<111>	(*C*)	12, 17	0
			{211}	10, 14, 16	0.13396
			{110}	11, 13, 15	−0.00541
(*F*)	[100]	<110>	(*C*)	19, 21	0
			{111}	18, 20	−0.31013
	[111]	<110>	(*C*)	23, 26	0
			{111}	22, 24, 25	0.32490

stability of the preferred direction of magnetization in iron. In array (*F*) the probable sort of slip, on {111} planes, has the proper sign for its stability factor. As to the magnitude of the stabilization thus afforded, it depends upon the abundance of defects and upon the magnitude of each. Even for so serious a dislocation as that here assumed the maximum excess energy for any dipole ($u'-u\sim 1$) corresponds to a controlling magnetic field of the order of $(10)^2$. The excess energy density can hardly correspond to a controlling field one-tenth as great as this unless the slip-like imperfections are improbably numerous.

In conclusion it appears that we have failed to account for magnetic stability of orientation in nearly perfect crystals as a consequence of simple sorts of dislocation in originally cubic arrays of parallel dipoles. As a by-product of the study we have discovered that local fields of the order of 10 gauss may result from possible kinds of crystal imperfection, even if magnetic saturation is strictly maintained. This may be of some value in discussing the magnetic effects of cold-work in ferromagnetic crystals.

Propagation of Large Barkhausen Discontinuities IV.[1] Regions of Reversed Magnetization

L. TONKS AND K. J. SIXTUS, *General Electric Company, Schenectady, New York*

(Received March 4, 1933)

The relations existing at a stationary boundary between saturated and antisaturated magnetic phases in a stretched NiFe wire have been investigated and a theory has been developed. Experimentally, both the minimum reversed (stopping) field required to stop the propagation of a moving discontinuity as well as the flux and magnetic pole distribution in the stopped boundary have been determined. Over the major portion of the boundary the pole field subtracted from the main field, and this demagnetizing field was found just to neutralize the excess of the applied field over the critical field. This confirmed the view that reversal in the wire proceeds only while the total field exceeds the critical field. A simple pole strength distribution which complies with this view was found to be one in which pole strength varies linearly with distance. Its demagnetizing field is approximately constant and checks the known excess fields reasonably well. Further refinement followed from recognizing that at the forward end of the boundary the pole field adds to the main field and is neutralized there by the stopping field. As a result, it was possible, given the excess field, the length of stopping coil, and the total change in induction, to calculate roughly the length of the boundary and the magnitude of the minimum stopping field. Certain details of the pole and field distribution under the stopping coil have been considered, particularly the expected sharp increase in minimum stopping field as the main field approached the starting field for the wire. When first the main field and then the stopping field was removed, the boundary was found to remain in place without any major change. The theory accounts for the escape of such a stopped boundary when the magnetic fields were reapplied. Symmetrical regions of reversed magnetization have been formed, both "spindles" and "rings," and some features of their behavior have been explained.

1. *Introduction.* Previous discussion of this subject with the exception of a short note[2] under the present title has dealt exclusively with the propagation proper of large Barkhausen discontinuities. The present paper, on the other hand, deals with the phenomena and relations involved in stopping a travelling discontinuity so that to one side of the boundary the nickel-iron untraversed by the jump is in the antisaturated phase, to the other side which has been traversed by the jump the metal is in the saturated phase.

The early observation that a self-propagating reversal of magnetization could be initiated at a point by a local adding field led to an inquiry into the effect of local opposing fields. It was thought, for instance, that by adjusting such a "stopping field" so that it was just able to halt the propagation, we might be able to ascertain the field near the front edge of the phase boundary.

2. *Experimental Method.* The coil used to produce the "stopping field" was 1 cm long and consisted of 64 turns, 0.013 cm diameter, enameled copper wire wound directly on the nickel iron wire [No. 37 (15 percent) 0.038 cm diameter] which was, as in the earlier experiments (I, p. 934) surrounded by a glass capillary. The coil leads were twisted to avoid stray fields and were brought out through the end of the capillary tube away from the side of the stopping coil on which the discontinuity was being propagated. The field strength produced by a current of i amp. in the coil is $H_{st}=80.3i$ oersted at its center. The various coils were placed along the wire in the following order: adding coil, search coil I, stopping coil, search coil II.

With the main field constant the magnitudes of the discontinuity at the two search coils were watched as H_{st} was increased. As long as the stopping field was below a certain value, both search coils indicated a full reversal of mag-

[1] K. J. Sixtus and L. Tonks, Phys. Rev. **37**, 930 (1931) will be referred to as I. II and III appeared in Phys. Rev. **42**, 419 (1932) and **43**, 70 (1933), respectively.

[2] I. Langmuir and K. J. Sixtus, Phys. Rev. **38**, 2072 (1931).

netization, but when this value was exceeded, no voltage was induced in coil II and the flux change indicated in I depended on its distance from the stopping coil. This shows that the phase boundary was halted. This value of stopping field will be called the minimum stopping field and will be denoted by H_{sto}.

3. *Minimum Stopping Field.* The minimum stopping field depends both on the length of stopping coil and the strength of the main field, as will be seen in Fig. 1 where H_{sto} is plotted

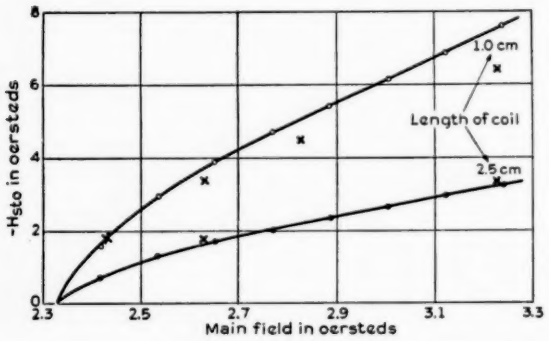

FIG. 1. Variation of minimum stopping field with main field for two stopping coils. Crosses indicate points on the theoretical curves (see Section 12).

against H for a 2.5 cm stopping coil as well as for the 1 cm coil already described. It is interesting that each curve conforms accurately to the formula

$$H_{sto}=k_l(H-H_0)^{\frac{1}{2}}, \tag{1}$$

where H_0 is, as usual, the critical field, and k_l is practically inversely proportional to the coil length. Thus

$$2.5\ k_{2.5}=8.90 \backsimeq 1.0\ k_{1.0}=8.38. \tag{2}$$

Since H_{sto} covers a distance so short that the field from the discontinuity itself can bridge it, the dependence of H_{sto} upon coil length is to be expected. On the other hand, the variation of H_{sto} with H must arise from the dependence of magnetic pole distribution upon H.

4. *Flux and Pole Distribution.* Poles occur where lines of induction leave the wire. The pole strength m per unit length is given by

$$m=-d\varphi/4\pi dx=-(a^2/4)dB/dx, \tag{3}$$

where φ is the total flux and B is the induction in the wire. Thus from a knowledge of the flux distribution one can obtain the pole distribution. The flux distribution was measured by placing the search coil at a different point along the wire for each successive passage of the boundary, observing the ballistic deflection as a function of the coil position. An alternative method, which was used in certain later cases where the

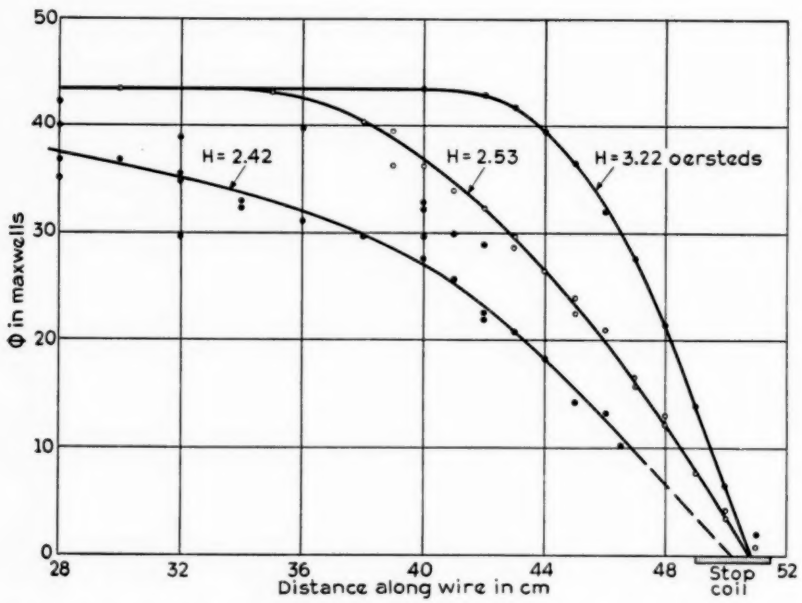

FIG. 2. Flux distribution along a stopped phase boundary with different main fields.

boundary had to remain fixed, was to move the search coil rapidly from different points over the discontinuity to a point beyond it, again observing the ballistic galvanometer deflection.

Fig. 2, obtained in the former way, gives the flux curves for three different values of main field. The curves as drawn apparently disregard experimental points near the front edge of the discontinuity. But, as has been pointed out before, the search coil, because of its finite size, gives an average value of flux over a short length of the specimen rather than the value at a point. The result is that the flux distribution, particularly at the front edge, is somewhat indefinite, so that the curves as drawn are probably not inconsistent with the experimental points.

It is evident that the region of flux change, that is, the length of the discontinuity, is longer for the smaller values of excess field ΔH. The ordinates of each curve are equal to the flux emerging from the wire between the front edge and the ordinate under consideration, so that Eq. (3) permits the calculation of the pole strength per unit length at each point along the wire from the slope at that point of the corresponding flux curve.

5. *Pole Field and Excess Field.* These poles give rise to a magnetic field H_p which will be called the pole field. It is readily seen that toward the front of the discontinuity this field, denoted by H_{pF}, aids the reversal process, while toward the rear, as a demagnetizing field, H_{pD}, it hampers reversal. On the hypothesis that reversal occurs as long as the total field at a point exceeds H_0 (II, Section II, paragraph 2), we should expect that over the major portion of the jump this demagnetizing field is equal in magnitude to the excess field, that is, that

$$H_{pD} = -\Delta H. \tag{4}$$

The empirical curves of Fig. 2 make it possible to confirm this idea, but two factors require consideration before proceeding. First, the distribution of pole strength in the cross section of the wire is unknown. The concept of the jump developed in I, Section 8, contemplated a surface distribution only. We now know (III, paragraph 6) that this picture is unsatisfactory, but calculation shows that an assumed surface distribution gives rise under the actual conditions to fields of practically the same magnitude as an assumed uniform volume distribution, so that it has been justifiable to use the former as the basis of calculation.

The second factor is the variation of H_p over

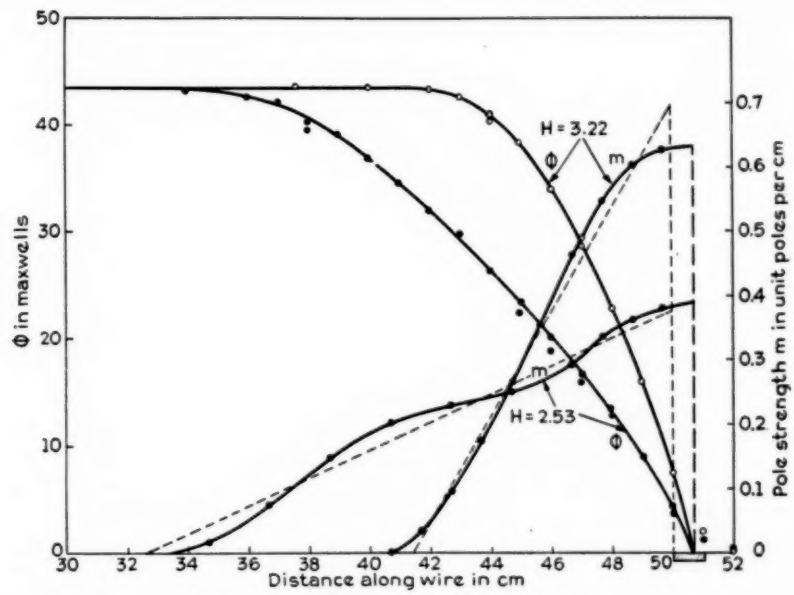

FIG. 3. Flux distributions and pole strength along a stopped phase boundary. The short dash lines show the equivalent simple pole distribution used for comparison with theory.

the cross section. Since curl H_p is zero, any systematic difference between surface and axial value of H_p would give rise to increasing radial fields along the length of the wire. It is clear that the pole distribution which we shall be led to assume cannot give rise to large radial fields, except perhaps at a few exceptional points, so that there must be essential constancy of H_p over the cross section. Accordingly, the value of H_p calculated for the axis has been used for the whole wire.

The first step in an analysis of curves of the type shown in Fig. 2[3] was to make a plot, Fig. 3, of pole-strength against distance using the slope of the curves. The field at any point was then calculated in two parts, first that arising from a triangular pole distribution whose graph would be the tangent to the actual distribution at the point; and second, the field arising from the differences between this simplified distribution and the actual one. The second field was calculated approximately by dividing the pole distribution into portions lying at different distances and adding the separate contributions. The first field was calculated exactly from the formula

$$H_1=\int_{x_1}^{x_2}\frac{mxdx}{(x^2+a^2)^{\frac{3}{2}}}, \tag{5}$$

which gives the value of H_1 at $x=0$. The assumed pole distribution was linear from $m=0$ at $x=x_1(<0)$ to m_2 at x_2.

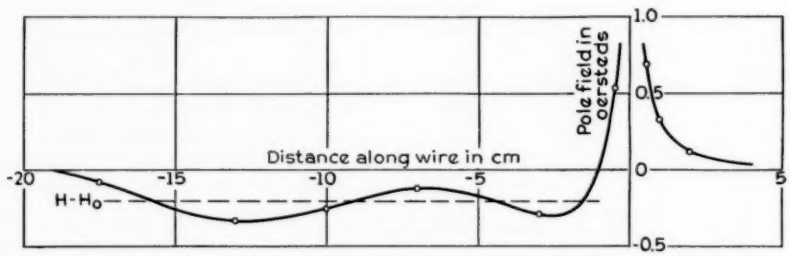

FIG. 4. Pole field along a stopped boundary calculated for the 2.53 oersted case of Fig. 3.

Fig. 4 shows the result of such a calculation for the 2.53 oersted case of Fig. 3. The curve shows a tendency toward a constant value over a considerable portion of its extent. Thus, the value of H_p in this region is not so far from ΔH that the hypothetical equality is impossible. Inhomogeneities in the wire appearing as variations in H_0 may easily contribute a large part of the observed discrepancy.

6. *Idealization of Flux Curves.* A direct examination of the curves of Fig. 2 reveals that they are significantly similar even though the excess field ΔH varies from 0.085 to 0.89 oersted in that the ratios of the displacements back from the front edge for the same value of ΔB are independent of ΔB. Further analysis shows that m_p, the pole strength per unit length, is proportional to $\Delta H^{0.43}$.

[3] Actually, the flux curves in Fig. 3 were made with a different sample from the same ingot as used for Fig. 2, and a 1 cm instead of a 2.5 cm stopping coil was used.

This checks roughly with the concept developed thus far. If we denote the length of the stopped jump by λ in order to have a distance fixing dimensions, we have $m_p \propto \lambda^{-1}$. Coulomb's law gives roughly $H_p \propto \lambda^{-2}$, whence it follows that $m_p \propto H_p^{0.5}$. Since, on our hypothesis, H_p equals $-\Delta H$, we thus expect $m_p \propto \Delta H^{0.5}$.

7. *Theoretical Pole Field Calculation.* The fact that the curves of Fig. 2 approximate rather closely parabolas gives the hint which makes it possible to develop a general theoretical treatment of the stopped discontinuity. The parabolic flux distribution implies, according to Eq.(3), a linear pole strength distribution from zero at x_1, the rear end of the jump, to a peak value, say m_2 at x_2, the front end. Formulas for magnetic field for points in the neighborhood of flux variation can be found from Eq. (5) by the proper assignment of limits. For points not too close to the ends of the pole distribution, the following formulas apply. Behind the reversal, that is, to

the left in the figure, where $x_2 > x_1 > 0$,

$$H_p = m_2[1/x_2 + (1/\Delta x) \ln x_1/x_2]; \quad (6)$$

within the reversal where $x_2 > 0 > x_1$,

$$H_p = m_2[1/x_2 + (1/\Delta x) \ln a^2/4(-x_1)x_2]; \quad (7)$$

before the reversal where $0 > x_2 > x_1$,

$$H_p = m_2[1/(-x_2) + (1/\Delta x) \ln x_2/x_1]; \quad (8)$$

where $\Delta x = x_2 - x_1$.

By using Eq. (7) the triangular pole strength distribution, shown at *A* in Fig. 6a, was found to give the pole field distribution traced by Curve *A* of Fig. 6b. The broad flat maximum demagnetizing field which extends over the major portion of the discontinuity is notable. The application of this result to the actual curves of Fig. 2 gave good enough checks between calculated and observed excess fields to confirm the view that the reversal process stops only when the total field falls to the critical value and to suggest making a more detailed analysis which would take the stopping field into account.

8. *Extension of the Phase Boundary Under the Stopping Coil.* Since the stopping coil was wound directly on the nickel-iron wire under test, the transitions in field impressed upon the wire were very sharp. This distribution of impressed field is shown by the $H + H_{sto}$ curve of Fig. 5A, where the outer light vertical lines represent the extent of the stopping coil, and the field distributions are shown shifted slightly for greater clarity. In order that the stopped discontinuity should be able to advance upon an infinitesimal reduction of the stopping field, reversal must have occurred under the coil. This conclusion is borne out by the flux curves of Fig. 2. This in turn means that in the reversed portion of the region controlled by the stopping coil, the pole field, cooperating with the main field, must exceed the stopping field H_{sto} by an amount equal to H_0. Ideally, then, the pole field can be expected to have the distribution shown by the continuous curve H_p in Fig. 5A.

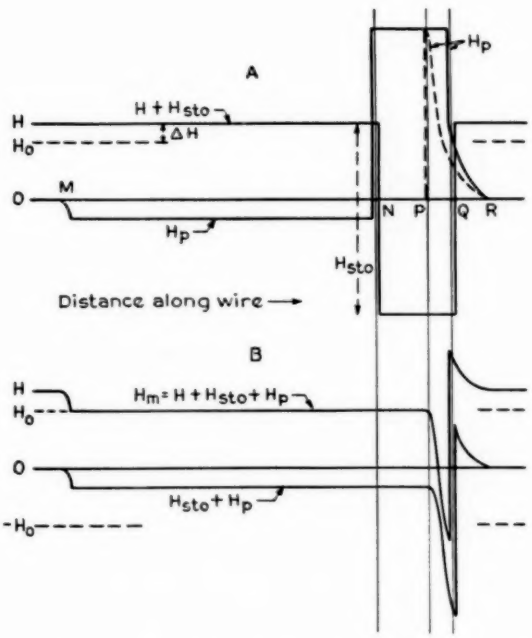

FIG. 5. Schematic field distribution including stopping and pole field.

9. *Theoretical Pole and Field Distribution in Detail.* A distribution of pole strength which would cause a field distribution approximating that of Fig. 5A is shown in Fig. 6a. For simplicity in calculation, the constants were chosen as given on the figure, namely:

$$m_2 = 1, \Delta x_A = 10 \text{ cm}, \Delta x_B = 1 \text{ cm}, a = 0.020 \text{ cm}.$$

Fig. 6b shows the fields arising from both *A* and *B* pole distributions separately as well as the combined field. The latter appears on inspection to be a fair approximation to that required theoretically. Further consideration shows that only a slight redistribution of pole strength would result in a very much closer agreement. For instance, to displace the field curve to -1 at $x = -0.5$ cm, an additional linear distribution of pole strength from zero at $x = -1$ to 0.1 m_2 at $x = 0$ would suffice, and this involves only 1 percent of the total induction change associated with the *A* region.

Although this readjustment, together with another in the *B* region near $x = 0$ may be small, the result may be an appreciable change in the values of the forward fields relative to the backward ones.

10. *Theoretical Equations for Pole Fields.* Let us, nevertheless, proceed with the simple triangular pole strength distribution, using both maximum reverse and maximum forward fields, H_{pD} and H_{pF}, respectively, for the constant pole fields which we suppose to exist over regions

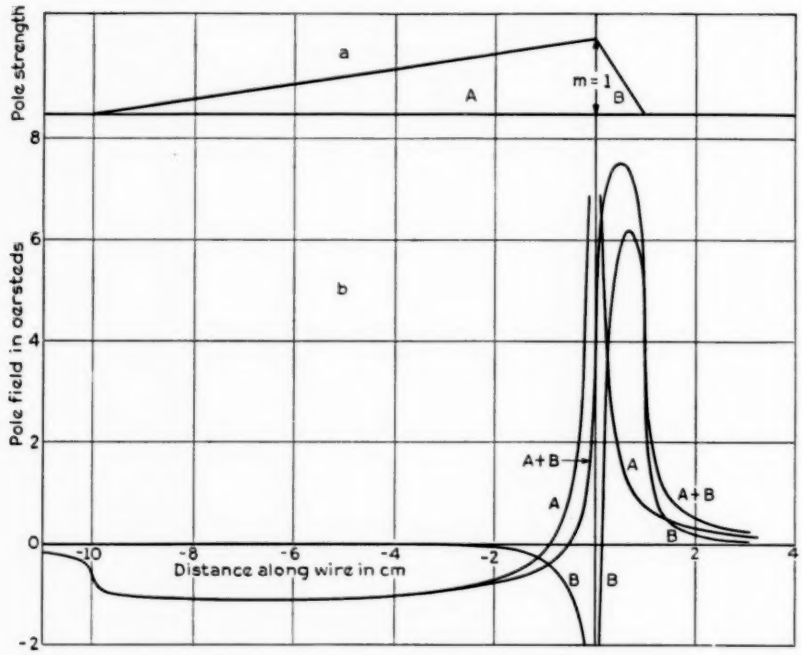

FIG. 6. Pole field distributions for idealized stopped boundary taking the stopping field into account.

A and B of Fig. 6. Our former assumption, leading to Eq. (4), may be stated in the form: At a phase boundary the sum total of all fields is H_0. This gives the equation

$$H_{pF} = -H_{sto} - H + H_0 = -H_{sto} - \Delta H \qquad (9)$$

for region B. Thus the discontinuity which was assumed in Fig. 6 is one arising in an excess field of 1.09 oersteds with a 1 cm long stopping field of $-(7.52+1.09) = -8.61$ oersteds.

The field H_{pD} was found from Eq. (7) by the ordinary method for finding a maximum, any contribution from region B being neglected since $\Delta x_A \gg \Delta x_B$. For simplicity we have substituted $m_2/a = \mu$, $\Delta x_A/a = \chi_A$, $\Delta x_B/b = \chi_B$, obtaining

$$H_{pD} = -(\mu/\chi_A)(2 \ln \chi_A - 1.603). \qquad (10)$$

The field H_{pF} is made up of two contributions, one from region A given by Eq. (8), and one from region B given by Eq. (7). The maximum of this forward field is

$$H_{pF} = (\mu\chi_B)[2 \ln \chi_B + (\chi_B/\chi_A) \ln \chi_B/(2\chi_A + \chi_B)], \qquad (11)$$

a correction of the order $\chi_B/2(\chi_A+\chi_B)$ being neglected. Finally, we note that

$$\mu = \Delta B/2(\chi_A + \chi_B). \qquad (12)$$

11. *Calculation of* Δx_A, m_2, *and* H_{sto}. Using Eq. (4) in a simultaneous solution of Eqs. (10) and (12), and neglecting $\chi_B^2/4$ in comparison with χ_A^2, one obtains

$$\chi_A = [(\Delta B/\Delta H)(\ln \chi_A - 0.8)]^{\frac{1}{2}} - \chi_B/2. \qquad (13)$$

Thus, given χ_B, which corresponds to the length of the stopping coil, as well as ΔB and ΔH, then χ_A can be calculated by successive approximations. Following in sequence, Eq. (12) yields μ, Eq. (11) H_{pF}, and Eq. (9) H_{sto}. Δx_A and m_2 follow immediately from χ_A and μ.

First let us apply these formulas to the data of Fig. 1. Here $a = 0.019$ cm, $\Delta B = 38{,}000$ and $H_0 = 2.33$. The stopping coils were 1 and 2.5 cm long, respectively, giving $1/0.019 = 52.6$ and 132 for χ_B. The theoretical results are plotted as crosses on Fig. 1. They are seen to agree as closely as can be expected in view of the approximations of the theory. The major portion of the discrepancy in the case of the 1 cm coil can be ascribed to considerations to be developed in Section 12.

The length of the boundary was not measured in these cases, but Fig. 3 presents two instances in which both Δx_A and m appear. Here a, ΔB, and H_0 were the same as before, and $\chi_B = 52.6$. The results of the calculations are shown in Table I.

TABLE I.

H	ΔH	χ_A	μ	Δx_A calc.	Δx_A obs.	m_2 calc.	m_2 obs.
2.53	0.20	1054	17.2	20.0	17.5	0.33	0.38
3.22	0.89	452	39.7	8.6	8.6	0.75	0.69

For comparison, the corresponding quantities, as nearly as they could be determined by replacing the pole-strength distribution curves of the figure by straight lines, are listed as "observed." Here, too, the check is reasonably good. The experimental results themselves were variable to almost as great an extent as the calculated and observed values differ. For instance, the $H = 2.53$ curve of Fig. 2 shows a Δx_A of 15.2 cm against a calculated 19.3, so that although this calculated value is only 3 percent less than for the almost identical condition of Fig. 3, the observed value is 13 percent less.

12. *Details of Pole and Field Distribution.* A closer analysis of the considerations which led to the pole field distribution of Fig. 5A shows that this must be modified by having reversal extend only up to P rather than to Q. In the first place, the reasonable assumption relating the progress of magnetic reversal to total field is that, once reversal has been initiated in a cross section, it proceeds continuously in such a way as to prevent the total field H_m from exceeding H_0. Neither can the total field fall below H_0, for reduction of the forward field at a point occurs only through a reversal embracing that point, and if the field is already H_0 this reversal will not occur. Reversals which do not include that point increase the forward field there. It follows that wherever any reversal has occurred, and that is wherever any magnetic poles are present, the total field has the value H_0, a view which has already been substantiated for the tail of the discontinuity in Section 7. That it is impossible to have enough pole strength extending up to Q to maintain the field at H_0 and yet not to give large fields beyond Q is seen from Fig. 6.

A possible configuration is one in which reversal extends up to some point such as P. A strictly triangular pole distribution leads, as Fig. 6 shows, to a falling of H_m below H_0 to the left of P. On the other hand, a rectangular pole distribution in this neighborhood would give a maximum value of H_m at P. Accordingly, some intermediate steepening of the pole distribution curve can well give constant $H_m = H_0$ up to P with a decrease beyond.

But a further modification in one detail is necessary. Experiments to be described in a later paper show that not only is a field larger than H_0 required to initiate reversal, but also that, once initiated, the saturated phase will not grow longitudinally unless the local field at the extremity of the boundary exceeds a value H_{sl}, greater than H_0. In the present case this means that for the boundary to have reached P, the total field *at* P must be H_{sl}, while behind P it is H_0. Literally taken, this discontinuous field distribution is impossible, for there must be limits to the sharpness of the transition required. In any event, this local requirement does not affect the general considerations which necessitate that the boundary shall not extend up to Q.

How far back from Q the extreme point P of the boundary lies is determined by the condition that at Q the sum of H_p and H shall be less than H_{sl}. Thus the greater H, the greater PQ, for the smaller must H_p be at Q. But another factor augments this effect, and that is the decrease in Δx_A and increase in m_2. The modification of the field distribution which is made necessary by the incomplete penetration of NQ by the saturated phase is shown by the broken lines of Fig. 5.

This incomplete penetration may account for the marked excess in Fig. 1 of the observed stopping field over the calculated for the case of the 1 cm coil. The distance PQ is undoubtedly a larger fraction of the 1 cm than of the 2.5 cm coil. Noting that the second term in the brackets in Eq. (11) is considerably smaller than the first, it follows that H_{pF} increases as x_B decreases so that it will be relatively greater for the 1 cm coil. It will also be true that the smaller H_{pF} is, the smaller PQ will be, and the more accurate should be the calculation of H_{sto}. This would explain the better agreement at $H = 2.43$ on the 1 cm curve

between theory and experiment than at higher values.

Since equality of total field to starting field at Q is one of the conditions for just stopping the jump, a sharp increase in H_{sto} occasioned by the necessity for keeping P further from Q is to be expected as H approaches the starting field. Yet in Fig. 1, where H at its maximum is very close to the starting value, no such tendency is to be seen. This is undoubtedly due to the fact that the starting field for the wire as a whole is the field which can reverse the most easily reversible portion, whereas the starting field at the end of the stopping coil may have been far larger than this. The expected increase was found in an experiment performed at a point for which the starting field had the minimum value. In this case the stopping *vs.* main field characteristic showed an increasing slope as the starting field was approached.

When H lies considerably below the starting field at the stopping coil, P probably lies close enough to Q so that small changes in PQ are sufficient to compensate relatively large changes in H because of the large space variation of H_p here. It follows that the magnitude of the stopping field is little affected by the value of starting field under these conditions.

13. *Special Experiments.* Some tests have been made on the effect of local changes in field strength on the shape of the stopped boundary, but these experiments have not led to any significant conclusions.

The successive removal of first the main field and then the stopping field from a stopped discontinuity left it practically unchanged so far as tests with a search coil could determine. But reapplication of these fields in reverse order resulted in its escape down the wire. The field theory which has been developed explains this behavior. Removal of the main field left the total field over most of the reversal region negative, equal to $-\Delta H$, less than H_0 in absolute value, and therefore unable to restore any of the magnetization to its original orientation. This is represented by the $H_{sto}+H_p$ curve of Fig. 5B. Only in the small unpenetrated portion PQ was $-H_0$ exceeded, but as the wire was still antisaturated here, this field, too, was without effect. Subsequent removal of the *stopping field* left H_p alone (Fig. 5A), and rendered the full excess of H_p over H_0 effective in creating new reversals beyond P. It is certain that the forward pole field caused reversals to the left of N and to the right of Q so that this field fell finally to the constant value H_0 over most of this interval. The extension of the saturated phase past Q permitted further continuous reversal when the main field was reapplied.

14. "*Frozen Spindle.*" Experiments like those already described in which the moving discontinuity is arrested have been extended in several ways.

A magnetic reversal moving from left to right was stopped near the middle of the NiFe wire by a stopping field. Another reversal was initiated in the unchanged half of the wire and it progressed from right to left until it, too, met the stopping field. This left the flux distribution to the left of the stopping coil unchanged and gave rise to a distribution of flux symmetrical about the stopping coil. Such a region is, of course, shorter, the greater the excess field. Using the picture of the phenomenon developed in **I**, p. 950, we should look upon the unreversed portion as spindle-shaped, and we shall use the term even though we may be compelled to abandon the old concept.

The spindle-shaped region just described presumably occupied almost the whole wire cross section at the stopping coil because the stopping coil was capable of completely halting the discontinuity. But if the stopping field was then reduced, further reversal occurred and the spindle shrank. Another method, and one frequently used, employed a second coil—a holding coil—which was placed to the left of the stopping coil. After the discontinuity moving to the right had been stopped, a field opposing the main field was produced in the holding coil, and then the stopping field was removed. This allowed the portion of the discontinuity between the two coils to propagate, but it left an incompletely reversed region symmetrical about the holding coil.

Fig. 7A shows the flux distribution in such a region. The positions of stopping and holding coils are shown. The asymmetry with respect to the holding coil arose from the circumstance that the holding field of 16 oersteds was considerably

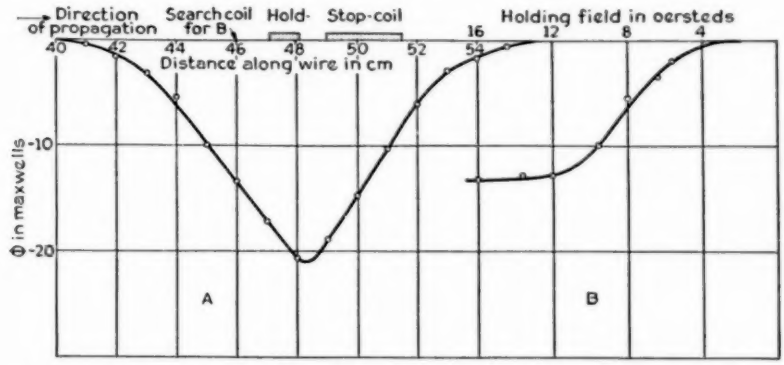

FIG. 7. A. Flux distribution in a "frozen spindle." B. Influence of holding field on the flux in the spindle.

larger than the minimum required to prevent any reversal to the left.

A rough application of the magnetic force relations to the present case along the same lines as pursued for the stopped discontinuity indicates that the flux maximum should lie within the holding coil, although it may be displaced from the center. The flux maximum is the point where the pole strength passes through zero, from north to south, with a resulting forward pole field aiding H. Consequently the holding field must embrace this point, and why it fails to do so here is not known.

It is possible, however, roughly to explain the way in which the holding power of the coil varies with its field as shown in Fig. 7B. This is a plot of the flux in the spindle cross section at 46 cm as a function of holding field. If the holding field is small, much reversal occurs when the stopping field is taken off. Only when the holding field exceeds 11 oersteds is the full discontinuity retained.

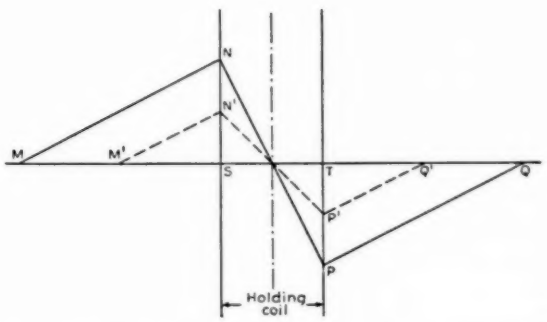

FIG. 8. Schematic pole strength distribution in a "frozen spindle."

An idealized pole strength distribution for this case is shown in Fig. 8. The demagnetizing field under the holding coil, that is, from S to T, is proportional to NS and is equal to the holding field H_h less the excess field. Thus as H_h is decreased, NS changes proportionally to $H_h - \Delta H$. As N changes position, the slope of MN remains essentially constant, since it is determined by the excess field. A new configuration for the distribution would thus be $M'N'P'Q'$. It thus appears that the area in the MNS triangle, which is practically the flux plotted in Fig. 7B, is proportional to the square of $H_h - \Delta H$. Examination of this figure yields a variation more nearly proportional to the third power, but a discrepancy in this direction is to be expected because the search coil links smaller and smaller fractions of the induction as the length of the spindle shortens.

15. "*Spindle*" *in Zero Field.* Here again the successive removal of the main field and the holding (or stopping) field leaves the spindle apparently almost unchanged. Experimentally, a readjustment of roughly 1 percent was noted and theoretically a not inconsiderable reversal decreasing the slope of NP must occur. But again this takes place over such a short length of the wire as to be almost undetected by the search coil.

16. "*Frozen Ring.*" In other experiments reversal has been initiated by a favorable local field in an opposing or zero main field to create, presumably, "ring-shaped" discontinuities, and these, too, persisted after removing all impressed fields. In this case, when zero main field was used,

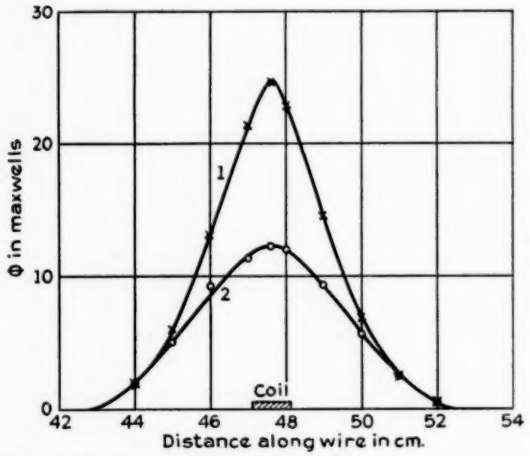

FIG. 9. Curve 1. Flux distribution in "frozen ring" with local field on. Curve 2. The same after the removal of the local field.

the reversal was concentrated in a comparatively short region, because the process of extending that portion required the maintenance at the boundary edge as it advanced of a pole field equal to the starting field. As a result, the removal of the local field allowed large demagnetizing pole fields to become operative which reduced the maximum flux change greatly, as shown in Fig. 9.

These experiments, together with one in which a moving boundary was halted in full flight by simply opening the main field circuit, were used in connection with etching tests designed to give the cross-sectional distribution of magnetic reversal. These will be dealt with in a later paper.

LETTERS TO THE EDITOR

Prompt publication of brief reports of important discoveries in physics may be secured by addressing them to this department. Closing dates for this department are, for the first issue of the month, the twentieth of the preceding month; for the second issue, the fifth of the month. The Board of Editors does not hold itself responsible for the opinions expressed by the correspondents.

The Isotope Effect in the Lyman Series of Hydrogen

By using water containing a high concentration of the hydrogen isotope H^2, six members of the Lyman series of hydrogen have been observed as close doublets. Plates were taken in the first and second orders of a 3 meter grazing incidence vacuum spectrograph. As a source we used a discharge tube similar to that designed by C. R. Jeppesen of this department (to be described in a subsequent number of this journal). In a small side tube was placed a drop of "heavy" water. Water vapor was allowed to leak through a small capillary into the discharge tube where it was dissociated by the discharge, liberating hydrogen gas. The gas diffused through the slit into the main tube of the spectrograph, but pumping speeds were great enough to maintain a pressure of 10^{-3} mm Hg in the spectrograph while the pressure in the discharge tube was several mm Hg. The discharge was excited by a 25 kv Thordarson transformer.

The first six members of the series were photographed in the first order. The first four of these were sufficiently intense to be reproduced in Fig. 1. The first member of the

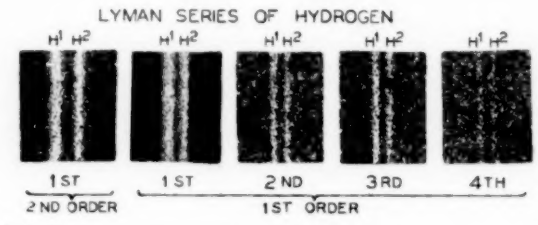

FIG. 1.

series was photographed also in the second order, against iron standards put on the plate by sending light from an iron arc through a quartz window on the end of the discharge tube. This second order doublet also is shown in Fig. 1. Microphotometer records show the H^1 component to be partially self-reversed. The relative intensity of the doublet lines is about 2 : 1, the H^1 component being the stronger. This is due to the dilution of the H^2 in the original sample of water by H^1 present in the aluminum electrodes, the walls of the tube, etc. In the original sample the ratio of H^2 to H^1 was about 2 : 1. It is interesting to notice that the H^1 component is broader than the H^2 component. This agrees with the theory of broadening of lines due to the Doppler effect, according to which the H^1 line should be 1.41 times as broad as the H^2 line.

The theoretical wave-lengths of the first six members of the series were computed following Penney.[1] Houstoun's[2] value $R(H^1) = 109{,}677.76$ cm^{-1} was used. The isotopic wave-length shifts and the wave-lengths of the H^2 lines were calculated by explicit formulas kindly furnished by Professor R. T. Birge. With Bainbridge's[3] value for the atomic weight of H^2, $R(H^2) = 109{,}707.56$ cm^{-1}. The experimental values of $\Delta\lambda$ were obtained as follows: for the first member of the series, from direct comparison with iron standards, for the other five members, from dispersion values obtained by using the computed wave-lengths of the H^1 lines as standards. All these values are listed in Table I.

TABLE I. *Wave-lengths and frequencies of lines in the Lyman series of H^1 and H^2.*

$\lambda(H^1)$ vac.	$\nu(H^1)$	$\lambda(H^2)$ vac.	$\Delta\lambda$ Calculated	$\Delta\lambda$ Observed
1215.664A	82,259.57 cm^{-1}	1215.334A	0.330A	0.330A
1025.718	97,492.71	1025.439	0.279	0.276
972.533	102,824.31	972.269	0.264	0.266
949.739	105,292.07	949.481	0.258	0.262
937.800	106,632.59	937.545	0.255	0.274*
930.744	107,440.88	930.491	0.253	0.258

Good agreement was obtained between theoretical and measured values of $\Delta\lambda$ except for one case. The fifth member of the series, marked with an asterisk, gave an experimental value of $\Delta\lambda$ larger than that predicted. This doublet was found difficult to measure, probably because of the presence of a faint line near one of its components.

We acknowledge with pleasure the generosity of Professor G. N. Lewis of the Chemistry Department in furnishing us the "heavy" water used in this work.

STANLEY S. BALLARD
H. E. WHITE

Department of Physics,
University of California,
May 3, 1933.

[1] W. G. Penney, Phil. Mag. **9**, 661 (1930).
[2] W. V. Houstoun, Phys. Rev. **30**, 608 (1927).
[3] K. T. Bainbridge, Phys. Rev. **41**, 115 (1932).

Disintegration-Experiments on Elements of Medium Atomic Number

In view of the drastic revision in the theoretical treatment of the penetration of nuclei by charged particles which is necessary if nuclei of medium and high atomic number are disintegrated by protons having energies of only a few hundred kilovolts, we have endeavored to verify the observations reported last year by Cockcroft and Walton.[1] Using a mixed beam of protons and hydrogen molecule-ions with currents exceeding 10μA to the target at voltages between 550 and 620 kilovolts (obtained with a one-meter electrostatic generator of the type devised by Van de Graaff) we have measured by means of a linear pulse-amplifier the number of alpha-particles (and protons) of range exceeding 16 mm which are emitted by targets of Al, Ni and Ag. The geometrical arrangement and dimensions of target and windows are nearly identical with those described by Cockcroft and Walton. A shutter ahead of the target and window eliminates possible spurious effects due to electrical disturbances affecting the amplifier or to radioactive contamination, all records being made in the sequence target-shutter-target-shutter with no changes in voltage, current, or other variables when the shutter is closed for the residual count. We selected Al, Ni and Ag, as representative of the heavier elements for which disintegration-counts were reported by Cockcroft and Walton (we had previously checked their later observations on Li and B).[2] Where they report (as "order of magnitude only") 135, 35 and 50 scintillation-counts per microampere per minute at 300 kilovolts we observe 0.2, 0.8 and less than 0.1 alpha-particle per microampere per minute through the window at 600 kilovolts for Al, Ni and Ag, respectively. The range of these particles was found within experimental error to be the same as that of the short-range (about 27 mm) particles observed from a boron target in the same apparatus, which gave a yield of 6600 alpha-particles per microampere per minute. The observed yields from Al, Ni and Ag can thus be explained by boron impurities of amounts 1/33,000, 1/9000 and 1/100,000 in these targets. Contamination to this extent by boron is certainly to be expected unless severe precautions are taken. The counts on Al and Ag are near the limit of detection with proton-currents of 10 to 20 microamperes. It should also be stated that a small number of very fast protons could perhaps have escaped notice, since the amplifier was set for convenient recording of alpha-particles and heavier fragments. We have no suspicion of such disintegration-protons, however. For these observations a minimum stopping-power of 16 mm was adopted, since the 600-kilovolt primary protons have a range of 12–13 mm. (It should be emphasized that roughly 10^8 protons per second are scattered 90° through the 10 mm diameter window.) The absolute yield for boron in these observations is only 1/9 of the absolute yield (one alpha-particle per 4×10^6 protons and H_2 ions) observed by us in January 1933 with the use of a stopping-power of 12 mm. The reason for this discrepancy, which in no way invalidates the comparisons for Al, Ni and Ag, is obscure, but it may be in part due to the difference in minimum stopping-power and in part to a possible overestimate of the yield in our January results, which assumed a uniform distribution of the beam over the target-area. There is thus no evidence in our observations that disintegration-protons or alpha-particles of range exceeding 16 mm are produced when Al, Ni and Ag targets are bombarded by 600-kilovolt protons. These results were reported at the meeting of the Physical Society last week, and in preliminary form were presented March 25 before the Philosophical Society of Washington.

The above data were unexpectedly obtained with targets of quite ordinary purity, although the first aluminum target used gave a somewhat higher number of counts. The observations will be extended, particularly with view to observing possible shorter-range particles (necessarily at lower voltages). Housing is under construction for our 2-meter generator, which should also enable us shortly to carry these observations up to 1400 kilovolts or higher.

M. A. Tuve
L. R. Hafstad
O. Dahl

Department of Terrestrial Magnetism,
Carnegie Institution of Washington,
May 5, 1933.

[1] J. D. Cockcroft and E. T. S. Walton, Proc. Roy. Soc. (London) **A137**, 229–242 (1932).

[2] J. A. Fleming, Science **77**, 298–300 (1933).

Occurrence of $CuAl_2$ in Duralumin

The producer of airplane propeller blade forgings as well as the manufacturer and user of propellers is vitally interested in their performance. The superiority of the aluminum alloy propeller over the wood propeller it replaced is uncontested. Failures have been relatively few, but as long as any occur, every effort must be expended to reduce their number. In the majority of instances, failure has been found to be definitely the ultimate result of progressive damage accidentally initiated some time prior to the failure. The few cases where initial mechanical damage was not evident emphasize the desirability of being able to recognize and follow such progressive damage by some nondestructive test. This desideratum prompted a hopeful and careful consideration of the observations reported by Clark and Smith.[1] Drs. Clark and Smith reported the presence of diffraction lines attributable to $CuAl_2$ in x-ray patterns from a duralumin-type aluminum alloy aircraft propeller blade. The blade had been in service for an unusually long period of time. They postulated that the presence of $CuAl_2$ lines indicated

[1] Clark and Smith, Phys. Rev. **43**, 305 (1933).

precipitation of this compound during service through the action of "the peculiar combination of forces existent in propeller blades." It is felt that attention should be called to certain factors which must be considered in evaluating Drs. Clark and Smith's observations.

Commercial heat treated forgings of 25ST alloy normally contain excess undissolved $CuAl_2$ which can be readily identified microscopically before as well as after being subjected to service conditions. Obviously this undissolved $CuAl_2$ will give rise to diffraction lines in x-ray patterns from such material. The amount of undissolved $CuAl_2$ will vary with the copper content of the alloy, with the period of time and temperature of heat treatment and with the total reduction in sectional area from ingot to finished forging. The presence of $CuAl_2$ lines in diffraction patterns from 25ST alloy propeller blades cannot, therefore, be accepted as evidence of precipitation brought about by the service conditions.

The experience in these laboratories with both microscopic and x-ray diffraction methods of examining precipitated phases indicates the former to be somewhat the more sensitive in detecting the initial stages of precipitation while the diffraction method, when sufficient precipitated phase is present, gives the most satisfactory means of establishing the identity of the phase. In the present investigation the microscopic method would seem especially applicable inasmuch as it is capable of differentiating unquestionably between precipitated and undissolved $CuAl_2$. Careful microscopic examination in these laboratories of used propeller blades as well as numerous fatigue test specimens indicate no visible structural changes as a result of extended periods of service or large numbers of stress reversals regardless of whether or not the stress was great enough to cause ultimate failure.

Diffraction lines attributable to precipitation of $CuAl_2$ from supersaturated solid solutions of copper in aluminum have been noted only after aging treatments such that the mechanical properties have been decidedly affected. It is to be expected that if service conditions are such as to bring about precipitation of $CuAl_2$ identifiable by x-ray diffraction means, the mechanical properties should show the effect of this precipitation as they do when precipitation is brought about to a similar extent at elevated temperatures. Such, however, has been found not to be the case. Determinations on a number of blades which have been in service for long periods of time indicate no change in mechanical properties at all comparable with the changes brought about by precipitation at such elevated temperatures as to render $CuAl_2$ visible by diffraction methods. It is recognized, of course, that quantitatively the effects might differ appreciably, depending on the manner of bringing about precipitation; qualitatively, however, the effects should be the same.

A method of inspection capable of detecting and following progressive deterioration of materials is exceedingly to be desired. It is conceivable that the progressive rejection of $CuAl_2$ by the supersaturated aluminum solid solution under stress, if it occurred, might form the basis of a means of following progressive changes in mechanical properties. It must, however, first be undeniably demonstrated that such precipitation does take place under the action of stress alone. Also the relationship between such effects and the various mechanical properties must be established.

L. W. KEMPF

Aluminum Research Laboratories,
Aluminum Company of America,
May 9, 1933.

The Spectrum of MgF

Two band systems are known[1] for this molecule, the heads of the 0,0 bands occurring at λ3594 and λ2689. According to Jevons, the first of these represents the $^2\Pi$, $^2\Sigma$ resonance system analogous to that known for the other alkaline earth fluorides. The second, he has suggested, may be a $^2\Pi$, $^2\Pi$ transition, having no state in common with the first system. Observations on these systems under high dispersion have been made entirely with the emission spectrum from the arc. In absorption, under low dispersion, the spectrum has been studied by Walters and Barratt,[2] who list a large number of absorption bands between λ3659 and λ3261. The strongest of these bear no relation to the λ3594 system known in emission, either in position or direction of degradation. This discrepancy has been commented on by Johnson.[3]

We have now obtained spectrograms in the first and second orders of the 21-foot grating showing the absorption of MgF vapor contained in a steel tube 80 cm long heated to 1150°C. The continuous spectrum from a hydrogen discharge tube was used. These plates show, besides a few atomic absorption lines, three band systems, two of which are those mentioned above. The third consists of a single sequence of unusual structure, with heads at λλ2276.72 (3) 2275.86 (5) 2275.29 (6) 2274.93 (10), degraded to shorter wave-lengths. Obviously the latter system cannot be definitely attributed to MgF without further study, but the fact the only other bands observed are due to MgF renders this assignment probable. We conclude that the measurements of Walters and Barratt represent chiefly bands or lines of extraneous origin.

Since the system at λ2689 comes out strongly in absorption, its lower state must be the $^2\Sigma$ normal state. Hence it appears certain that this is the analogue of the $^2\Sigma$, $^2\Sigma$ system known for CaF, SrF and BaF.[4] The spin doubling must be too small to produce a resolvable doubling of the heads.

---

[1] W. Jevons, Proc. Roy. Soc. **A122**, 223 (1929).

[2] O. H. Walters and S. Barratt, Proc. Roy. Soc. **A118**, 134 (1928).

[3] R. C. Johnson, Proc. Roy. Soc. **A122**, 199 (1929).

[4] F. A. Jenkins and A. Harvey, Phys. Rev. **39**, 929 (1932).

Some interesting modifications of the intensity distribution in the bands appear when the absorption spectrum is compared with the arc spectrum. In the λ2689 system, a distinct minimum of absorption is observed at λ2688.38, in the 0,0 band, which probably represents the band origin. The partially resolved rotational structure is simple, and of the type expected for a $^2\Sigma$, $^2\Sigma$ band. In the $^2\Pi$, $^2\Sigma$ system at λ3594, each band has three heads, and in absorption the successive bands of a sequence fall off in intensity more rapidly with increasing v than in emission. Also, the third head (λ3588.224 in the 0,0 band) is greatly strengthened in absorption relative to the first two (λλ3592.843, 3594.243). This is consistent with the interpretation of the three heads as belonging to the P_1, P_2 and Q_2 branches, in order of increasing frequency. This is analogous to the case of the BeF bands[5] except for the direction of degradation. The lower temperature conditions in absorption favor the Q_2 branch, which occurs at a low rotational quantum number. With this structure, it is evident why previous estimates of the electronic doublet separation in the $^2\Pi$ state have disagreed,[3] since they were deduced from measurements of the heads only. The 0,0 band shows in absorption a minimum at λ3592.29, which can be interpreted as the origin of the low-frequency component. The best estimate of the doublet separation we can give at present is the separation of this minimum from the Q_2 head, giving $A=-31.6$ cm^{-1}. It is hoped to obtain more quantitative results, utilizing the partially resolved rotational structure by methods similar to those applied by Harvey[6] in the case of CaF.

Magnesium has isotopes of masses 24, 25 and 26 in the abundance ratio 7 : 1 : 1. Two very faint heads have been found, at λλ2636.84, 2637.30 adjacent to the 1,0 head of the λ2689 system, which agree within the error of measurement with the positions expected for the heads of the Mg ^{25}F and Mg ^{26}F 1,0 bands. We expect to obtain plates showing stronger absorption to confirm this result. Experiments are now in progress on the absorption of BeF, in order to decide if possible the question of the existence of the isotope Be^8. The evidence for this isotope has recently been questioned, and the absorption spectrum should furnish the most sensitive test for its presence.

F. A. JENKINS
RAFAEL GRINFELD*

Department of Physics,
University of California,
May 5, 1933.

[5] F. A. Jenkins, Phys. Rev. **35**, 315 (1930).
[6] A. Harvey, Proc. Roy. Soc. **A133**, 336 (1931).
* Fellow of the Rockefeller Foundation.

The Metastable ^2D-Level of the Nitrogen Atom

The nitrogen atom (N I) has three low levels, the ^4S, ^2D and ^2P, all of which converge to the ^3P term of the N^+ ion. The first of these, the ^4S term, is the ground state and its value is known accurately; the ^2D and ^2P terms are metastable and the separation of the doublet terms in each case has been estimated[1] but not experimentally verified. Each of the three levels corresponds to an electron configuration of $2s^22p^3$. The higher ^2P term ($2p^23s$) combines with the ^2D term with the emission of a doublet at 1495 and 1492A. Since the ^2D level is a metastable one, it is possible to obtain these lines as absorption lines and through self-reversal to measure accurately the doublet separation $^2D_{2\frac{1}{2}}-{}^2D_{1\frac{1}{2}}$.

A spark of about 1 mm length was produced between metal electrodes (aluminum, copper) in flowing nitrogen at atmospheric pressure. The spark was placed from 6–10 mm in front of the fluorite window of a Hilger vacuum spectrograph whose dispersion is 2A per mm at 1500A; the exposure time varied from 1 to 4 minutes and the photographs were taken on Schumann plates made by Hilger. A photographic enlargement of the 1495–1492A doublet (Fig. 1) shows a single absorption line on the broad background of the emission line at 1495A and two absorption lines on the 1492A emission line. With the wave-length obtained from Ekefors' measurements,[1] $\lambda_1=1494.675$A, as the basis of our measurements, $\lambda_2=1492.79$A and $\lambda_3=1492.59$A. The photograph shows that the intensity of λ_3 is greater than λ_2, indicating that the ^2D term is inverted, as might be expected. The more probable transition, $^2P_{1\frac{1}{2}}-{}^2D_{2\frac{1}{2}}$, would correspond therefore to the shorter wave-length. The frequency separation of the two ^2D terms is 8.9 ± 0.1 cm.$^{-1}$ From analogy with the separation of corresponding terms in the O II spectrum, Compton and Boyce[1] estimated the probable separation as 5 cm^{-1}; the measurements of Ekefors[1] seem to indicate a separation of 7 cm^{-1}.

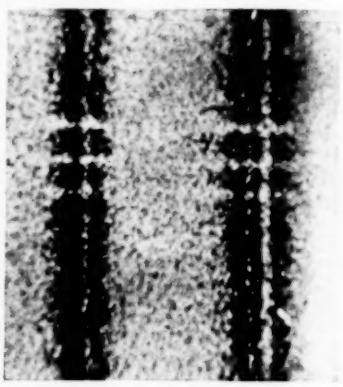

FIG. 1.

Reference to Fig. 1 shows that the line 1495 is strongly asymmetric, the middle of the emission line being shifted 0.06A or 2.7 cm^{-1} in relation to the center of the absorption line. As this shift is toward the red it cannot be explained by the appearance of the forbidden line $^2D_{2\frac{1}{2}}-{}^2P_{1\frac{1}{2}}$. It was not possible to investigate thoroughly the reason for this

[1] E. Ekefors, Zeits. f. Physik **63**, 437 (1930); K. T. Compton and F. C. Boyce, Phys. Rev. **33**, 145 (1929); S. B. Ingram, Phys. Rev. **34**, 421 (1930).

asymmetric broadening but it may be mentioned that it disappeared almost completely when a self-induction coil was put in series with the spark. The effect of the induction coil was to lower the potential of the spark as was quite evident from the decrease in intensity of the spark lines in comparison with the arc lines. At the same time, however, the total intensity of the spark became smaller so that the change may be due to the decrease in the density of the excited atoms.

The purchase of the fluorite vacuum spectrograph which was used in this investigation was made possible through a grant from the National Research Council to whom we wish to express our appreciation.

H. Stücklen
Emma P. Carr

Mount Holyoke College,
South Hadley, Massachusetts,
May 10, 1933.

Electromotive Forces Associated with Barkhausen Discontinuities

Recently the writer has described an experiment[1] in which an electric current was sent through a ferromagnetic wire, and discontinuities of the potential difference of the ends of the wire were observed when Barkhausen discontinuities of magnetization occurred. It was concluded that discontinuities of resistance were associated with the Barkhausen effect. More extended investigation has shown that this conclusion cannot be legitimately drawn from the experiment as described. As a matter of fact, subsequent work has demonstrated that intrinsic, impulsive e.m.f.'s are produced in the wire by the Barkhausen discontinuities, and these intrinsic e.m.f.'s are sufficiently large to mask any effect which may arise from discontinuities of resistance.

The cause of the impulsive e.m.f. associated with the Barkhausen discontinuity appears to be an inductive action which the magnetization change in one part of the wire exerts on another part. When a short straight nickel wire is laid parallel with a copper wire (insulated from the latter but very close to it), the large Barkhausen jumps in the nickel produce e.m.f.'s in the copper wire which can be detected with an amplifier and loudspeaker. If a nickel wire of large diameter is bent beyond the elastic limit into the arc of a circle and then thrust into a straight capillary tube it is in a state of elastic strain. When demagnetized by the bringing up of a bar magnet such a wire exhibits one large Barkhausen jump followed by several smaller ones. However, the impulsive e.m.f. due to the large jump, as detected at the ends of the nickel wire, is considerably weaker than the e.m.f. in a similar wire of small diameter. There appears to be a short-circuiting of the induced current by the extra material of the larger wire.

The production of an e.m.f. in a ferromagnetic wire by changes in the magnetization of the wire is not a new phenomenon. Matteucci[2] first observed it in the case of a twisted wire, where a circular component of magnetization was produced. Hippel and Stierstadt[3] have detected it in connection with the Barkhausen effect. The Matteucci effect appears to be well understood,[4] but the e.m.f. associated with the Barkhausen effect is yet to be explained adequately. Preliminary experiments suggest the following explanation.

The Barkhausen effect is known to have a transverse component,[5] that is, inductive jumps are observed in directions perpendicular to the magnetizing field. Suppose a filament in the wire, parallel to the length of the wire but of smaller diameter than the wire, to undergo a sudden change of transverse magnetization. The remaining filaments of the wire will then be subject to an induced e.m.f. parallel to their length. The situation is quite like that in which a bar magnet, held parallel to a straight wire, is suddenly turned to a transverse position, thus inducing an e.m.f. in the wire. On this view of the phenomenon we should expect parallelism between the transverse Barkhausen effect and the impulsive e.m.f.

Direct evidence that discontinuities of resistance are associated with the Barkhausen effect is lacking. The indirect evidence is as follows. Reversal of saturated magnetism in a wire does not alter its length or resistance, hence reversal of magnetism in a small element should produce no change, either of length or resistance. However, a Barkhausen jump can produce a change of length in a wire, hence we infer that this jump is not a pure reversal of magnetization in a small element. But in the latter event we expect a resistance change to accompany the Barkhausen jump, for the reason that transverse magnetoresistance is quite different in ferromagnetic materials from longitudinal magnetoresistance.

Further evidence is desirable in order to prove that Barkhausen jumps are not necessarily reversals of saturated magnetism. Possibly means may be discovered for reducing the magnitude of the induced e.m.f.'s till the resistance jumps can be detected. Another line of attack, which is being worked out in this laboratory, involves measurements of the simultaneous transverse and longitudinal components of a single large Barkhausen discontinuity in nickel.

C. W. Heaps

The Rice Institute,
May 11, 1933.

[1] C. W. Heaps, Phys. Rev. **43**, 763 (1933).

[2] Matteucci, Ann. chim. phys. **53**, 385 (1858).

[3] A. v. Hippel and O. Stierstadt, Zeits. f. Physik **69**, 52 (1931).

[4] Hans Ostermann and Fritz v. Schmoller, Zeits. f. Physik **78**, 690 (1932).

[5] Richard M. Bozorth and Joy F. Dillinger, Phys. Rev. **41**, 345 (1932).

On the Nature of the Primary Cosmic Radiation

The latitude effects observed by Compton and Clay call for positively charged particles as responsible for some of the primary radiation. Compton[1] has emphasized the conclusion that the facts of absorption in the atmosphere

[1] A. H. Compton, *A Geographic Study of Cosmic Rays*, Phys. Rev. **43**, 357–403 (1933).

combined with the existence of directional and latitude effects necessitate the assumption that the particles originate at least several hundred kilometers above the earth's surface in order that with the energy necessary to penetrate the earth's atmosphere they can still experience sufficient bending by the earth's magnetic field to account for the facts. If the charged particles come from distances many times the earth's radius, energies comparable with 10^{10} volts are necessary in order that, in spite of the earth's field, they may reach the earth at latitudes as low as those at which their presence is revealed by directional and latitude effects. On the other hand, as Millikan has remarked, cloud chamber measurements have given no evidence of charged particles with energies as high as 10^{10} volts, and, it is difficult to suppose that absorption of energy by the atmosphere could reduce a 10^{10} volt-particle to an energy of 10^{9} volts, such as represents about the maximum observed in cloud chamber experiments.

Many years ago the writer[2] gave reasons founded upon the classical theory, for supposing that charged particles with sufficiently high energy may be incapable of producing ions on account of the radiationary reaction resulting from the very sharp acceleration which would be necessary were an electron to be ejected from an atom by a charged particle travelling with very nearly the velocity of light, and consequently with a field highly concentrated in its equatorial plane. Recently, he has attacked the problem on a wave mechanical basis, and has obtained an equation representing the radiation reaction terms. At his request the equation was applied to the ionization problem by Dr. Bramley[3] and it appeared that on the basis of this equation ionization should become inappreciable at about 10^{10} volts. If we should accept this conclusion we have a possible explanation of the difficulties cited above. We may then suppose that the primary charged particles entering the atmosphere, generate secondaries, which continue in the direction of the primaries and so carry with them the latitude effects and the directional effects fundamentally inherent in the primaries. In other words it is not the action of the magnetic field on the secondaries which is responsible for these effects, but the action of that field on the primaries. On this view the primaries would not show themselves in Geiger counters. Their properties, however, would be exemplified by the behavior of the secondaries as above implied. It is of course to be understood that the secondaries here referred to would in general serve as primaries in the sense of producing other secondaries (or tertiaries) and so on, so that there is no inconsistency in the experiments such as those of Street and Johnson[4] in which evidence is deduced in support of the view that the rays there referred to as primaries are ionizing rays. It would indeed seem that if we accept the arguments of Millikan and Compton together, they practically demand the assumption of charged particles of a non-ionizing character in line with the ideas expressed above.

A further point bearing upon the matter concerns the fact that the directional effects above referred to have indicated that the incoming primary rays are positively charged. On the view implied in this letter, however, this would not mean that the actual rays which set off the counters are positively charged. These rays might be of either sign, and the crucial experiment would be one in which it was demonstrated that these rays which inherit from the primaries a directional effect appropriate only to a positive charge may, nevertheless, themselves involve rays with charge of either sign. Cloud chamber experiments would afford information on this matter, for, quite apart from the fact that one would have to admit that secondaries will be found in the cloud chamber, one must also admit that if the primary rays exist in the number demonstrated by the directional experiments, and if they are ionizing, they certainly should show themselves in the cloud chamber and should there reveal their true energy and the sign of their charge.

On the view that the real primary rays are non-ionizing, we have yet to admit that they may be capable of causing other atomic transitions such as are associated with the emission of secondaries with high velocity, the initiation of nuclear disintegrations, etc. The relative probability of these various occurrences is a matter whose solution awaits a more complete development of the wave mechanical theory. It may be of interest to point out that if one should accept the views here tentatively suggested, one finds in them an explanation of those peculiar phenomena found by Anderson in the cloud chamber, phenomena in which a secondary appears to be ejected from a piece of lead without the evidence of any primary having entered it.

W. F. G. SWANN

Bartol Research Foundation of
The Franklin Institute,
Swarthmore, Pennsylvania,
May 11, 1933.

[2] W. F. G. Swann, *The Absence of Ionization by Electrons with Speed Comparable with that of Light*, Phil. Mag. **47**, 306–319 (1924).

[3] W. F. G. Swann and A. Bramley, *Particle Ionization for Velocities Approaching that of Light*, J. Frank. Inst. **214**, 606–608 (1932).

[4] J. C. Street and T. H. Johnson, *Concerning the Production of Secondaries by Cosmic Radiation*, Phys. Rev. **42**, 142–144 (1932).

Erratum

Projective Relativity and the Einstein-Mayer Unified Field Theory

(Phys. Rev. **43**, 615, 1933)

Eq. (1) on page 616 should read $g_{\lambda\theta}=\delta_{\lambda\theta}$ instead of $g_{\lambda\mu}=\delta_{\lambda\mu}$.

BANESH HOFFMANN

University of Rochester.

THE AMERICAN INSTITUTE OF PHYSICS

INCORPORATED

GOVERNING BOARD

For The American Physical Society:

KARL T. COMPTON, *Chairman*
Massachusetts Institute of Technology

GEORGE B. PEGRAM, *Secretary*
Columbia University

JOHN T. TATE
University of Minnesota

For The Optical Society of America:

PAUL D. FOOTE
The Gulf Companies

LOYD A. JONES
Eastman Kodak Company

F. K. RICHTMYER
Cornell University

For The Acoustical Society of America:

H. D. ARNOLD
Bell Telephone Laboratories

HARVEY FLETCHER
Bell Telephone Laboratories

DAYTON C. MILLER
Case School of Applied Science

For The Society of Rheology:

E. C. BINGHAM
Lafayette College

WHEELER P. DAVEY
Pennsylvania State College

A. STUART HUNTER
du Pont Rayon Company

For The American Association of Physics Teachers:

HOBER L. DODGE
University of Oklahoma

PAUL E. KLOPSTEG
Central Scientific Company

FREDERIC PALMER
Haverford College

ADMINISTRATIVE STAFF

HENRY A. BARTON, *Director*
JOHN T. TATE, *Adviser on Publications*
MADELINE M. MITCHELL, *Editorial Secretary*
Office: 11 East 38th Street, New York, New York

JOURNALS

THE PHYSICAL REVIEW
REVIEWS OF MODERN PHYSICS
PHYSICS
JOHN T. TATE, *Editor*
J. W. BUCHTA, *Assistant Editor*
E. C. BINGHAM, *Rheology Editor*

THE JOURNAL OF THE OPTICAL SOCIETY OF AMERICA
THE REVIEW OF SCIENTIFIC INSTRUMENTS WITH PHYSICS NEWS AND VIEWS
F. K. RICHTMYER, *Editor*

THE JOURNAL OF THE ACOUSTICAL SOCIETY OF AMERICA
F. R. WATSON, *Chairman, Editorial Board*
WALLACE WATERFALL, *Managing Editor*

THE JOURNAL OF CHEMICAL PHYSICS
HAROLD C. UREY, *Editor*

THE AMERICAN PHYSICS TEACHER
DUANE ROLLER, *Editor*

The American Institute of Physics is a membership corporation of which five societies are the founding members. These five societies are the principal national societies devoted to pure and applied physics in America. Their names, and those of their representatives who form the Governing Board of the Institute, are given above. The principal work of the Institute is the publication of journals sponsored by the societies or by itself. The names and the editors of the journals are also listed above.

The broad purpose of the Institute is to represent, in all matters of wide or common interest, the five thousand or more members and subscribers associated with the Founder Societies and the journals. It aims to advance the science and profession of physics, and to promote cooperation between pure research, the applied sciences and the industries. To achieve these aims, it is greatly in need of an endowment and is empowered by law to administer grants and funds of any kind.

CONTENTS

PHYS. REV. 43 (1933) JUNE 1, 1933

Probabilities of *K*-Electron Ionization of Silver by Cathode Rays . . . . . D. L. WEBSTER, W. W. HANSEN AND F. B. DUVENECK 839

Secondary Effects in Ionization by Hard Gamma-Rays . . E. J. WORKMAN 859

Ionization of Gases by Neutrons . . . . . T. W. BONNER 871

Elastic Electron Scattering in Neon. .A. L. HUGHES AND J. H. MCMILLEN 875

Infrared Absorption Bands of Acetylene . . .G. B. B. M. SUTHERLAND 883

Hyperfine Structure and the Polarization of Resonance Radiation. II. Magnetic Depolarization and the Determination of Mean Lives . . . . . ALLAN C. G. MITCHELL 887

Anomalies in Hyperfine Structure . . .S. GOUDSMIT AND R. F. BACHER 894

Fine Structure of Electron Diffraction Beams from a Gold Crystal and from a Silver Film on a Gold Crystal . . . . . .H. E. FARNSWORTH 900

On a Possible Explanation of Superconductivity . . . . . J. FRENKEL 907

Magnetic Dipole Fields in Unstrained Cubic Crystals . L. W. MCKEEHAN 913

Magnetic Dipole Fields in Dislocated Cubic Crystals . L. W. MCKEEHAN 924

Propagation of Large Barkhausen Discontinuities IV. Regions of Reversed Magnetization . . . . . L. TONKS AND K. J. SIXTUS 931

Letters to the Editor:

Isotope Effect in the Lyman Series of Hydrogen . . . . . STANLEY S. BALLARD AND H. E. WHITE 941

Disintegration-Experiments on Elements of Medium Atomic Number . . . . . M. A. TUVE, L. R. HAFSTAD AND O. DAHL 942

Occurrence of $CuAl_2$ in Duralumin . . . . . L. W. KEMPF 942

Spectrum of MgF . . . . . .F. A. JENKINS AND RAFAEL GRINFELD 943

Metastable ^1D-Level of the Nitrogen Atom . H. STÜCKLEN AND EMMA P. CARR 944

Electromotive Forces Associated with Barkhausen Discontinuities. . . . . C. W. HEAPS 945

On the Nature of the Primary Cosmic Radiation . . . . W. F. G. SWANN 945

Erratum: Projective Relativity and the Einstein-Mayer Unified Field Theory. . . . . BANESH HOFFMANN 946

LANCASTER PRESS, INC., LANCASTER, PA.